UNIVERSITAT DE BARCELONA

Multi-isotopic tools for monitoring innovative remediation strategies in sites contaminated with halogenated organic compounds

Sergio Gil Villalba

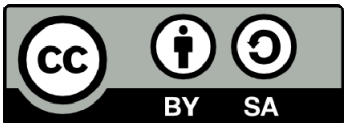

MULTI-ISOTOPIC TOOLS FOR MONITORING INNOVATIVE REMEDIATION STRATEGIES IN SITES CONTAMINATED WITH HALOGENATED ORGANIC COMPOUNDS

Sergio Gil Villalba

PhD Thesis – 2025

UNIVERSITAT DE BARCELONA

Programa de doctorat de Ciències de la Terra

Departament de Mineralogia, Petrologia i Geologia Aplicada

MULTI-ISOTOPIC TOOLS FOR MONITORING INNOVATIVE REMEDIATION STRATEGIES IN SITES CONTAMINATED WITH HALOGENATED ORGANIC COMPOUNDS

Thesis presented by

Sergio Gil Villalba

to obtain the degree of:

Doctor by the Universitat de Barcelona

This work was conducted in the MAiMA research group, SGR Mineralogia Aplicada, Geoquímica i Hidrogeologia (MAGH), under the supervision of:

Dra. Mònica Rosell Linares

Departament de Mineralogia, Petrologia i Geologia Aplicada

Supervisor

Dr. Jordi Palau Capdevila

Departament de Mineralogia, Petrologia i Geologia Aplicada

Supervisor

Dr. Albert Soler i Gil

Departament de Mineralogia, Petrologia i Geologia Aplicada

Tutor

Barcelona, May 2025

UNIVERSITAT DE BARCELONA

MAiMA ISÒTOPS ESTABLES I MINERALOGIA

Agradecimientos

Agradezco a mis directores de tesis, Mònica Rosell y Jordi Palau, por su apoyo a lo largo de este viaje, han sido unos años de aprendizaje a muchos niveles, y vuestro apoyo ha sido fundamental en muchos momentos.

Es innegable que MAiMA es un grupo de investigación muy particular, que también he visto evolucionar junto a mí. Tengo que agradecer a todos los compañeros el tiempo, aprendizaje y ayuda a lo largo de este tiempo. Especialmente a Clara Torrentó por su calidad humana y como investigadora, para mi eres la tercera directora de esta tesis, siempre disponible y dispuesta a ayudar. Martí Vinyes, mi compañero de viaje, han sido diversas experiencias (risas y lágrimas) las que nos han unido durante estos años. Albert Soler por darme la oportunidad de formar parte del grupo de investigación, estar siempre ahí de manera indirecta y disfrutar con nuestras ocurrencias. Gracias en general a todos los integrantes del grupo, Alberto del Río, Arnau, Tatiana y Pedro, por el apoyo en laboratorio, las lecciones de ornitología, los bailes prohibidos y las panettone productions.

Agradezco el apoyo de los Centres Científics i Tecnològics de la Universitat de Barcelona. Aunque a veces damos por sentado el trabajo que realizan, éste es fundamental para el desarrollo de la investigación. Gracias Anna Navarro, Asun Marin, Pilar Teixidor y Raúl Carrey.

Las estancias en otros centros de investigación han sido un estímulo para continuar y terminar esta tesis. Gracias Jesica Soder por tu alegría en los días compartidos en BIOREM (UAB), and thank you Orfan, Mirna, Nour and all the IT2 team, it was a privilege to learn from you.

No puedo dejar de lado el apoyo recibido durante la investigación vinculada al proyecto INNOTEC, donde la colaboración interinstitucional fue clave. Agradezco a los compañeros de ERM Iberia, Miguel Ángel Vallecillo, Jordi Corregidor y Andrea Tirado, así como a Marc Viñas y Miriam Guivernau del IRTA.

Mas allá del apoyo profesional, diversos personajes han marcado el desarrollo del trabajo en estos años. Encontrar a Jose Manuel Moreno y a Mónica Sánchez de IFAPA ha sido una suerte, así como compartir con ellos una feria en Córdoba. Compartir algunos cafés y ciertos puntos de vista con Josep Roqué o Roger Puig también ha sido interesante.

Hay en cambio otras personas que han tenido un profundo impacto en mí, a nivel personal y profesional, que han sido y siguen siendo ejemplos a seguir y de los cuales sigo aprendiendo

cada vez que recuerdo las experiencias juntos. Me refiero a Alex Guerra, Albert Folch y Luis Reyes.

No puedo olvidar a mis padres José y Josefa, los valores que desde pequeño me han inculcado y que han encendido la chispa de la curiosidad científica y la motivación por el estudio y la superación. ¡Gracias por habernos dado tanto siempre! Y a mi hermano Abel, desde que vimos Jurassic Park en el cine en 1993, buscábamos estrellas con el telescopio, nos pasábamos el verano buceando o íbamos a buscar fósiles a la plana de Vic, el mundo natural siempre nos ha fascinado y ha sido maravilloso crecer y aprender juntos.

Federica, gracias por tu apoyo incondicional todos estos años, sin ti jamás lo hubiera logrado. Me has abierto, además, un mundo nuevo en Barcelona, así como en el mar y en la pista de pádel. Siempre te estaré agradecido por todo lo compartido, aprendido y por haberme aguantado todo este tiempo con tanto cariño.

Abstract

Remediation strategies for groundwater contaminated with chlorinated solvents have advanced significantly in recent decades. However, understanding the complexity of factors influencing contaminant degradation and developing robust tools to evaluate remediation effectiveness under diverse conditions remain critical challenges. This thesis focuses on the application of multi-isotopic tools for the assessment of two groundwater remediation techniques targeting volatile chlorinated hydrocarbons, specifically chlorinated ethenes (CEs) and methanes (CMs).

Enhanced in situ biostimulation (EISB) using emulsified vegetable oil (EVO) as a slow-release electron donor was evaluated for CEs remediation. A combined approach, incorporating CEs carbon and chlorine compound-specific isotopic analysis (CSIA, $\delta^{13}C$ and $\delta^{37}Cl$), molecular biology tools (MBT), and hydrochemical data revealed rapid reductive dechlorination (RD) of tetrachloroethene (PCE) and trichloroethene (TCE) in both microcosm experiments and a field application. This initial degradation process led to transient cis-1,2-dichloroethene (cDCE) accumulation, which was subsequently degraded to vinyl chloride (VC). Dual-element isotope slopes ($\Lambda^{C\text{-}Cl}$), MBT results and hydrochemical parameters were consistent, confirming a successful biostimulation of the contaminated site leading to optimal conditions for reductive dechlorination of CEs, which was sustained for 12 months. However, discrepancies with previously reported $\Lambda^{C\text{-}Cl}$ values for laboratory studies using pure and mixed *Dehalococcoides* microbial populations suggest site-specific variation in reductive dehalogenases involved in cDCE RD, highlighting the need for tailored assessments. Once 2D-CSIA confirmed RD as the major degradation pathway in the field, and knowing that other degradative processes do not have a significant impact on the degradation of CEs, the microcosm-derived εC values and the carbon isotopic balance could be used to estimate the degradation extent of the contaminants in the field application and the extent of complete dechlorination of PCE to harmless ethene.

In situ chemical oxidation (ISCO) with persulfate (PS) in an alkaline interception trench (IT) was evaluated using 2D-CSIA for the remediation of CMs and CEs, but with special focus on trichloromethane (TCM). Laboratory batch experiments revealed significant variability in TCM isotopic trends under varying environmental conditions, including pH values and the presence of CO_3^{2-} ions. Under most studied conditions, PS radical-driven degradation dominated; however, alkaline hydrolysis became the main degradation process at higher pH values. While alkaline conditions seemed to favor TCM oxidation by $SO_4^{\cdot-}$ and OH· radicals, isotopic data suggested a shift toward reductive degradation pathways in CO_3^{2-}-rich environments. The results highlight the complexity underlying this remediation technique and the critical role of 2D-CSIA in

thoroughly assessing TCM fate during a PS ISCO in alkaline IT systems. Additionally, the accumulation of hexachloroethane (HCA), a higher chlorinated compound than the original contaminant was observed in the batch experiments. This finding raises significant environmental concerns, as the generation of HCA as a by-product could undermine the remediation process by introducing a compound with severe ecological implications.

Overall, this thesis demonstrates the potential of the application of $\delta^{13}C$ and $\delta^{37}Cl$ CSIA as a powerful tool for improving the understanding of contaminant transformation mechanisms under different field conditions. These findings provide key information that can support environmental consultants and contaminated site managers in selecting and optimizing remediation strategies (e.g. dosages, injection pulses) for sites contaminated with chlorinated solvents and open avenues for further research into site-specific transformation processes.

Resumen

Las estrategias de remediación de aguas subterráneas contaminadas con disolventes clorados han avanzado significativamente en las últimas décadas. Sin embargo, la comprensión de la complejidad de factores que influyen en la degradación de estos contaminantes y el desarrollo de herramientas sólidas para evaluar la efectividad de la remediación en diversas condiciones ambientales siguen siendo desafíos fundamentales. Esta tesis se centra en la aplicación de herramientas multi-isotópicas para evaluar dos técnicas de remediación de aguas subterráneas dirigidas a hidrocarburos clorados volátiles, específicamente etenos clorados (CEs) y metanos clorados (CMs).

En primer lugar, se evaluó la bioestimulación in situ mejorada (EISB, por sus siglas en inglés) con aceite vegetal emulsionado (EVO) como donador de electrones de liberación lenta para la remediación de CEs. Un enfoque combinado que incorpora análisis isotópico compuesto-específico de carbono y cloro (CSIA, $\delta^{13}C$ y $\delta^{37}Cl$), técnicas de biología molecular (MBT) y datos hidroquímicos reveló una rápida decloración reductiva (RD) del tetracloroeteno (PCE) y del tricloroeteno (TCE) tanto en experimentos de microcosmos como en la aplicación de campo. Este proceso de degradación inicial condujo a la acumulación transitoria de cis-1,2-dicloroeteno (cDCE), el cual posteriormente se degradó a cloruro de vinilo (VC). Las pendientes isotópicas de doble elemento ($\Lambda^{C\text{-}Cl}$), los resultados de MBT y los parámetros hidroquímicos fueron consistentes, confirmando una bioestimulación exitosa del sitio contaminado, generando condiciones óptimas para la RD de los CEs, durante 12 meses. No obstante, las discrepancias con valores de $\Lambda^{C\text{-}Cl}$ previamente reportados en estudios de laboratorio con poblaciones microbianas puras y mixtas de *Dehalococcoides* sugieren una variabilidad específica del sitio en las dehalogenasas reductivas involucradas en la RD de cDCE, lo que resalta la necesidad de evaluaciones específicas en cada caso. Una vez confirmada la RD como la principal vía de degradación en el campo, a través del análisis isotópico bidimensional (2D-CSIA), y dado que otros procesos degradativos no tuvieron un impacto significativo en la degradación de los CEs, se utilizaron los valores de εC obtenidos en los microcosmos y el balance isotópico de carbono para estimar el grado de degradación de los contaminantes en la aplicación de campo y la conversión completa de PCE a eteno, un compuesto no tóxico.

Además, se evaluó la oxidación química in situ (ISCO) con persulfato (PS) en una zanja de interceptación alcalina (IT) mediante 2D-CSIA para la remediación de CMs y CEs, con especial énfasis en el triclorometano (TCM). Experimentos de laboratorio en lotes revelaron una variabilidad significativa en las tendencias isotópicas de TCM bajo diferentes condiciones

ambientales, incluyendo valores de pH y la presencia de iones CO_3^{2-}. En la mayoría de las condiciones estudiadas, la degradación provocada por radicales derivados del PS activado fue predominante; sin embargo, la hidrólisis alcalina se convirtió en el proceso principal de degradación a valores de pH mayores. Aunque las condiciones alcalinas parecieron favorecer la oxidación de TCM por radicales $SO_4^{\cdot-}$ y $OH^{\cdot}$, los datos isotópicos sugieren un cambio hacia vías de degradación reductiva en entornos ricos en CO_3^{2-}. Los resultados resaltan la complejidad subyacente a esta técnica de remediación y el papel fundamental del 2D-CSIA en la evaluación detallada del destino del TCM durante un proceso de ISCO con PS en sistemas de IT alcalinos. Además, se observó la acumulación de hexacloroetano (HCA), un compuesto más clorado que el contaminante original, en los experimentos. Este hallazgo plantea implicaciones ambientales significativas, ya que la generación de HCA como subproducto podría comprometer el proceso de remediación al introducir un compuesto con implicaciones ecológicas graves en el ambiente.

En general, esta tesis demuestra el potencial de la aplicación del CSIA de $\delta^{13}C$ y $\delta^{37}Cl$ como una herramienta capaz de mejorar la comprensión de los mecanismos de transformación de contaminantes en diferentes condiciones de campo. Estos hallazgos proporcionan información clave que puede ayudar a consultores ambientales y gestores de sitios contaminados a seleccionar y optimizar estrategias de remediación (por ejemplo, dosificaciones o pulsos de inyección) en sitios contaminados con disolventes clorados, abriendo nuevas vías para futuras investigaciones sobre procesos de transformación específicos.

Resum

Les estratègies de remediació d'aigües subterrànies contaminades amb dissolvents clorats han avançat significativament en les darreres dècades. No obstant això, la comprensió de la complexitat dels factors que influeixen en la degradació d'aquests contaminants i el desenvolupament d'eines sòlides per avaluar l'efectivitat de la remediació en diverses condicions ambientals continuen sent desafiaments fonamentals. Aquesta tesi se centra en l'aplicació d'eines multiisotòpiques per avaluar dues tècniques de remediació d'aigües subterrànies dirigides a hidrocarburs clorats volàtils, específicament etens clorats (CEs) i metans clorats (CMs).

En primer lloc, es va avaluar la bioestimulació in situ millorada (EISB, per les seves sigles en anglès) amb oli vegetal emulsionat (EVO) com a donador d'electrons d'alliberament lent per a la remediació de CEs. Un enfocament combinat que incorpora anàlisi isotòpica compost-específica de carboni i clor (CSIA, δ13C i δ37Cl), tècniques de biologia molecular (MBT) i dades hidroquímiques va revelar una ràpida decloració reductiva (RD) del tetracloroetè (PCE) i del tricloroetè (TCE) tant en experiments de microcosmos com en l'aplicació de camp. Aquest procés de degradació inicial va conduir a l'acumulació transitòria de cis-1,2-dicloroetè (cDCE), el qual posteriorment es va degradar a clorur de vinil (VC). Les pendents isotòpiques de doble element (ΛC-Cl), els resultats de MBT i els paràmetres hidroquímics van ser consistents, confirmant una bioestimulació reeixida del lloc contaminat i generant condicions òptimes per a la RD dels CEs durant 12 mesos. No obstant això, les discrepàncies amb valors de ΛC-Cl prèviament reportats en estudis de laboratori amb poblacions microbianes pures i mixtes de *Dehalococcoides* suggereixen una variabilitat específica del lloc en les dehalogenases reductives involucrades en la RD de cDCE, fet que subratlla la necessitat d'avaluacions específiques en cada cas. Un cop confirmada la RD com la principal via de degradació en el camp a través de l'anàlisi isotòpica bidimensional (2D-CSIA), i atès que altres processos degradatius no van tenir un impacte significatiu en la degradació dels CEs, es van utilitzar els valors de εC obtinguts en els microcosmos i el balanç isotòpic del carboni per estimar el grau de degradació dels contaminants en l'aplicació de camp i la conversió completa de PCE a etè, un compost no tòxic.

A més, es va avaluar l'oxidació química in situ (ISCO) amb persulfat (PS) en una rasa d'intercepció alcalina (IT) mitjançant 2D-CSIA per a la remediació de CMs i CEs, amb especial èmfasi en el triclorometà (TCM). Experiments de laboratori en lots van revelar una variabilitat significativa en les tendències isotòpiques de TCM sota diferents condicions ambientals, incloent-hi valors de pH i la presència d'ions CO32-. En la majoria de les condicions estudiades, la degradació provocada per radicals derivats del PS activat va ser predominant; no obstant això, la hidròlisi alcalina es va

convertir en el procés principal de degradació a valors de pH més elevats. Encara que les condicions alcalines semblaven afavorir l'oxidació de TCM per radicals $SO_4^{\cdot-}$ i $OH^{\cdot}$, les dades isotòpiques suggereixen un canvi cap a vies de degradació reductiva en entorns rics en CO_3^{2-}. Els resultats subratllen la complexitat subjacent a aquesta tècnica de remediació i el paper fonamental del 2D-CSIA en l'avaluació detallada del destí del TCM durant un procés d'ISCO amb PS en sistemes d'IT alcalins. A més, es va observar l'acumulació d'hexacloroetà (HCA), un compost més clorat que el contaminant original, en els experiments. Aquesta troballa planteja implicacions ambientals significatives, ja que la generació d'HCA com a subproducte podria comprometre el procés de remediació en introduir un compost amb greus repercussions ecològiques.

En general, aquesta tesi demostra el potencial de l'aplicació del CSIA de $\delta^{13}C$ i $\delta^{37}Cl$ com una eina capaç de millorar la comprensió dels mecanismes de transformació de contaminants en diferents condicions de camp. Aquests resultats proporcionen informació clau que pot ajudar a consultors ambientals i gestors de llocs contaminats a seleccionar i optimitzar estratègies de remediació (per exemple, dosificacions o nombre d'injeccions) en llocs contaminats amb dissolvents clorats, obrint noves vies per a futures investigacions sobre processos de transformació específics.

TABLE OF CONTENTS

LIST OF FIGURES

LIST OF TABLES

List of Abbreviations

ARC Agència de Residus de Catalunya

B% Extent of biodegradation

CCiT-UB *Centres Científics i Tecnològics* of *Universitat de Barcelona*

C-Cl Carbon Chlorine

CHCs Chlorinated Hydrocarbons

CI Confidence interval

CEs Chlorinated ethenes

cis-DCE Cis-1,2-dichloroethene

CMs Chlorinated methanes

CSIA Compound-specific isotope analysis

CT Tetrachloromethane

DCM Dichloromethane

Dhc *Dehalococcoides*

DNAPL Dense non-aqueous phase liquid

DO Dissolved oxygen

EC Electrical conductivity

Eh Corrected redox potential

EISB Enhanced in situ bioremediation

EI Electron ionization

EVO Emulsified Vegetable Oil

FID Flame ionization detector

GC Gas chromatography

HS Headspace

IRMS Isotope ratio mass spectrometry

ISCO *In-situ* chemical oxidation

ISCR *In-situ* chemical reduction

IT Interception trench

IUPAC International of Pure and Applied Chemistry

OHRB Organo-halide respiring bacteria

PCE Tetrachloroethene

PS Persulfate

PSOX PersulfOx®

qMS Quadrupole mass spectrometry

RD Reductive dechlorination

rdh Reductive dehalogenases

RdhA Reductive dehalogenase subunit A

RdhB Reductive dehalogenase subunit B

SIM Selected/single ion mode

SPME Solid phase microextraction

TCE Trichloroethene

TCM Chloroform/trichloromethane

VC Vinyl chloride

VOCs Volatile organic compounds

VPDB Vienna Pee Dee Belemnite

Chapter I. INTRODUCTION

1. General introduction

1.1. Organochlorides and their environmental impact

The growing population, increased resource consumption, and the effects of climate change on water scarcity have elevated the importance of groundwater as a valuable drinking water resource that needs to be preserved. Preserving groundwater quality against environmental contamination is, hence, a global challenge. In this context, organochloride compounds or chlorinated solvents rank among the most concerning pollutants (ATSDR, 2022). These volatile organic compounds (VOCs) have been widely used as industrial degreasing agents, dry cleaning, and as intermediates for chemical manufacturing. While their properties make them valuable in industrial applications (Zanaroli et al., 2015), they also render these compounds quite resistant to natural degradation, allowing them to persist in soil and water systems for decades.

Improper handling, accidental spills, illegal disposal or leakage from storage tanks are the main sources of chlorinated solvents release into the environment. These contaminants are Dense non-Aqueous Phase Liquids (DNAPLs) and, because of their low solubility and higher density than water, once they reach the aquifer, they can migrate extensively downward through the saturated zone to the lower parts of the aquifer, posing risks to drinking water supplies and nearby water bodies. Furthermore, the DNAPL can distribute as small globules within the geologic matrix and form pools on low permeability lenses (Pankow et al., 1996). These properties can lead to slow release of these contaminants which become hard to detect, characterize and treat (Brusseau et al., 1999).

The general category “chlorinated solvents” refers in a broad sense to any organic compound that contains chlorine substitutions and that was developed for use as a solvent. In the strict sense of the term, “chlorinated solvents” include both chlorinated aromatic and aliphatic compounds. However, as a result of common usage, the term “chlorinated solvents” represent primarily the chlorinated aliphatic hydrocarbons (CAH) (Henry et al., 2002). The chlorinated solvents most commonly detected in groundwater include those that are (or were) most widely manufactured and used, as well as those that result from the naturally occurring biological or chemical transformation of parent compounds (Figure 1). The most frequently detected

chlorinated organic compounds are chlorinated ethenes (CEs), chlorinated methanes (CMs) and chlorinated ethanes. The research presented in this thesis focuses on the first two groups; therefore, details on CEs and CMs formulas and nomenclature are provided in Table 1.

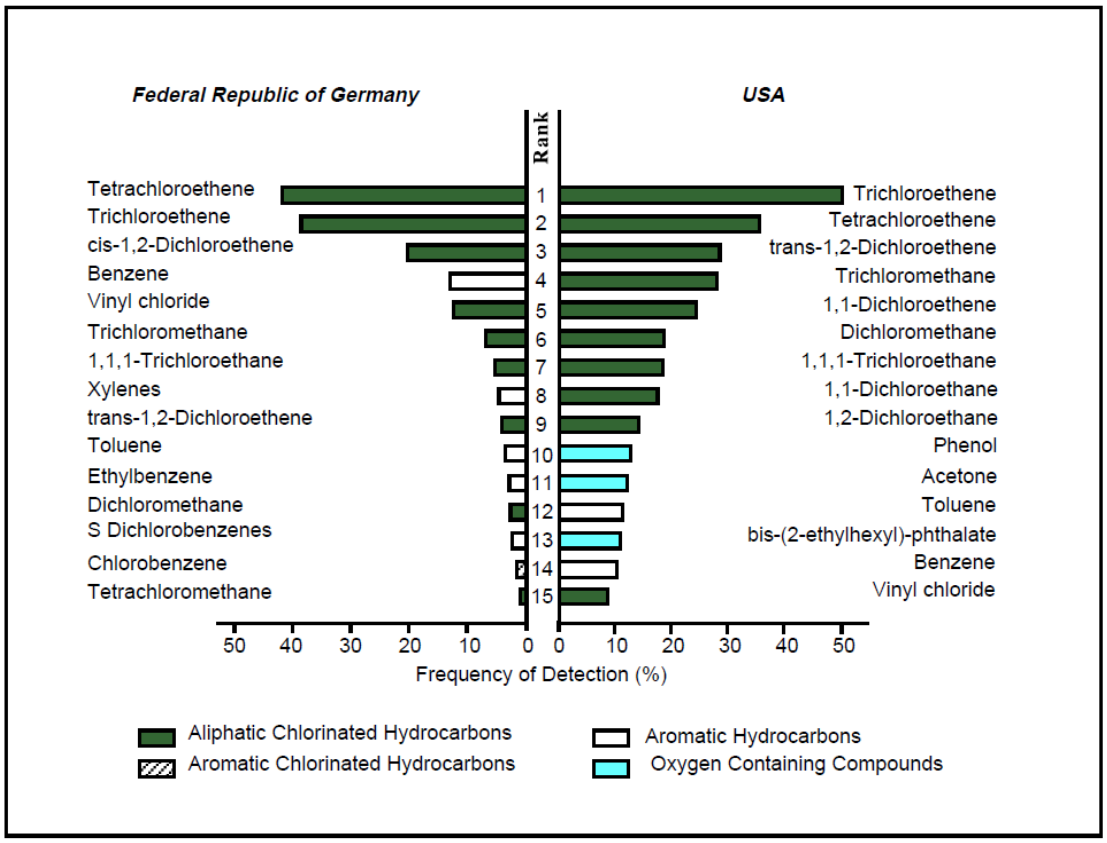

Figure 1. The 15 most frequently detected organic compounds in groundwater at waste disposal sites in Germany and the U.S. Adapted from Azadpour-Keeley et al. (2005).

Table 1. CEs and CMs nomenclature, formula and acronym.

	IUPAC name*	Common name	Formula	Acronym
Chlorinated ethenes (CEs)	Tetrachloroethene	Perchloroethylene	$CCl_2=CCl_2$	PCE
	Trichloroethene	Trichloroethylene	$CCl_2=CHCl$	TCE
	cis- 1,2-dichloroethene	cis-1,2-dichloroethylene	CHCl=CHCl	cis-DCE
	trans-1,2-dichloroethene	trans-1,2-dichloroethylene	CHCl=CHCl	trans-DCE
	Chloroethene	Vinyl chloride	$CHCl=CH_2$	VC
Chlorinated methanes (CMs)	Tetrachloromethane	Carbon tetrachloride	CCl_4	CT
	Trichloromethane	Chloroform	$CHCl_3$	TCM
	Dichloromethane	Methylene chloride	CH_2Cl_2	DCM
	Chloromethane	Methyl chloride	CH_3Cl	CM

*International Union of Pure and Applied Chemistry nomenclature of organic chemistry (Favre et al., 2013).

Globally, the reliance on groundwater as a primary resource for drinking water and agriculture underscores the critical importance of addressing this contamination. As urbanization and industrialization continue to grow, so does the potential for organochloride pollution, particularly in regions with insufficient environmental regulations or infrastructure to manage hazardous waste. Chlorinated hydrocarbons (CHCs) have been reported to be responsible for 8.3% of contaminated soils and 10.0% of contaminated groundwater bodies in Europe (Panagos et al., 2013). In Catalonia, the "Agència de Residus de Catalunya" (ARC) has reported that 8% of contaminated sites are polluted with CHCs (ARC, 2020).

1.2. Health risks and contamination regulations

Chlorinated solvents pose significant threats to both environmental and human health. Exposure to organochlorides has been linked to various adverse health effects, including carcinogenicity, liver and kidney damage, and developmental issues in humans (Brüning et al., 2003; Christensen et al., 2013; Barul et al., 2017; Purdue et al., 2017). Furthermore, their toxicity extends to aquatic ecosystems, disrupting microbial and biological processes.

From CEs and CMs groups, TCE and VC are classified in Group 1 as carcinogenic to humans while CT, TCM, DCM, PCE and DCE classify in group 2A as probably carcinogenic to humans according to the International Agency for Research on Cancer (IARC, 2024). Consequently, the chlorinated solvents investigated in this thesis are also included in the list of priority pollutants of the U.S. Agency for Toxic Substances and Disease Registry (ATSDR). The ATSDR substance priority list is revised and published biannually by the U.S. Environmental Protection Agency (EPA) and is based on detection frequency of these substances at facilities on the National Priorities List and their potential threats to human health due to toxicity and exposure. The ranking for some of these solvents, out of 275 substances (ATSDR, 2022), is presented in Table 2, together with the maximum permitted contaminant levels proposed for drinking water by U.S. EPA (USEPA, 2024).

The European Commission set environmental quality standards in the field of water policy (Directive 2008/105/EC), and the quality parameters of water intended for human consumption (Directive 2020/2184). These regulations have been adapted by the Catalan Water Agency (ACA, 2009), the public company of the *Generalitat de Catalunya* that is responsible for water planning and management in accordance with the basic principles of the European Water Framework Directive and the Spanish government (Real Decreto 140/2003).

Table 2. Maximum permitted contaminant levels proposed for drinking water by U.S. EPA and in groundwater by ACA. MCLG: maximum contaminant level goal. MCL: maximum contaminant level allowed. VGNR: no-risk generic value. VGI: intervention generic value.

	ATSDR list ranking	U.S. EPA		ACA	
		MCLG (µg/L)	MCL (µg/L)	VGNR (µg/L)	VGI (µg/L)
PCE	33rd	0	5	10[b]	75
TCE	16th	0	5	10[b]	50
cis-1,2-DCE	231st	70	70	n.a.	n.a.
VC	4th	0	2	0.25	5
CT	50th	0	5	8	30
TCM	11th	70	80[a]	70	210
DCM	n/a	0	5	250	750

n.a. indicates that levels for that contaminant were not available.

[a] TCM is regulated as a part of total trihalomethanes group.

[b] The indicated value corresponds to the sum of PCE, TCE and 1,1-DCE.

1.3. Subsurface remediation techniques

A summary of the remediation techniques that are typically used for remediation of chlorinated solvents and DNAPL in the subsurface is presented below based on (Henry et al., 2002).

Containment Techniques

A. **Containment strategies:** Physical or hydraulic barriers are used to contain DNAPL transport in both the non-saturated zone (NSZ) and in the saturated zone (SZ), but do not eliminate the contaminant. Thus, there is always the risk of leakage. They are usually applied together with other remediation techniques.

B. **Permeable Reactive Barrier (PRB):** These barriers create an in-situ treatment zone both in the NSZ and the SZ that passively captures and removes pollutants from groundwater via chemical, biological, or physical reactions such as adsorption (Warner et al., 2002; Higgins et al., 2009).

Physical techniques

C. **Soil excavation:** Consists in the excavation and extraction of the DNAPL contaminated soil from the NSZ. Early application of this technique can stop or entirely prevent contaminants from further leaching to groundwater. However, this strategy generates large amounts of waste that require further treatment ex-situ.

D. **Pump and treat (P&T):** Consists on the construction of groundwater wells to extract contaminated groundwater, which is then treated ex-situ in a treatment facility (Rivett et al., 2006). The flow of groundwater through the source zone eases DNAPL dilution and its recovery from the aqueous phase. It is not a cost-effective strategy for DNAPL polluted sites due to the slow dilution process (Mackay et al., 1989; Ciampi et al., 2023), and the risk of DNAPL displacement and contamination of previously clean zones.

E. **Soil Vapor Extraction (SVE) and dual-phase extraction:** SVE is a widely accepted in-situ technology for removing chlorinated solvents in the unsaturated zone. It consists on the application of vacuum to induce air-vapor flow through the open interstitial pores in the soil, causing the chlorinated solvent to volatilize and partition into the vapor phase. The extracted soil vapor is treated ex-situ to remove chlorinated solvents prior to atmospheric release. Similarly, dual-phase extraction is used to pump and remove DNAPL or contaminated groundwater and vapors near the water table.

F. **Air sparging:** Consists of the injection of air beneath the water table and is used to volatilize chlorinated solvents and other VOCs from the groundwater and transfer them to the vadose zone. In some cases, aeration of groundwater also promotes in-situ aerobic oxidation (Alvarez et al., 2005). The use of air sparging at sites where DNAPLs are suspected to be present must be applied cautiously, as it may exacerbate the extent of contamination by mobilizing DNAPL.

G. **Thermal desorption:** This technique is based on the application of electrical resistive heating that can effectively degrade and/or volatilize VOCs in both soil and groundwater. VOCs are captured via SVE and condensed into liquid for off-site disposal (Heron et al., 1998) or destroyed by the effect of the temperature (Friis et al., 2007). In many cases, it is combined with bioremediation, as temperature induces aquifer changes that may be favorable to microorganisms (Badin et al., 2016).

Chemical techniques

H. **Surfactant application:** Surfactants are applied to improve DNAPL dissolution into groundwater and increase their mobility and availability in the SZ, allowing their treatment with other techniques such as biodegradation, groundwater P&T or soil washing (Wang et al., 2019). The cost-effectiveness of this strategy depends on the characteristics of the injections, heterogeneity of the media and surfactant distribution, and the risks of uncontrolled DNAPL mobility.

I. **In Situ Chemical Oxidation (ISCO):** ISCO consists in the injection of strong chemical oxidants to the subsoil to treat pollutants in the SZ (Krembs et al., 2010). Hydrogen peroxide and persulfate (PS) are commonly used oxidants in ISCO of organic contaminants (Devi et al., 2016). Chemical oxidation transforms contaminants into innocuous substances, in the case of organochlorides, CO2 and Cl^-.

J. **In Situ Chemical Reduction (ISCR):** ISCR is based on the use of chemical reductants to degrade contaminants in the SZ. This approach involves a broader and more complex spectrum of reductive pathways, is strongly surface dependent and can be enhanced through the use of chemical and/or biological reduction (Brown et al., 2009; Brown, 2010). These reductants can be injected into the subsoil (e.g. nano-zero valent iron, nZVI) or installed as a Permeable Reactive Barrier (PRB) (Audí-Miró et al., 2015).

Bioremediation techniques

K. **Monitored natural attenuation (MNA):** This remediation strategy relies on the conversion of pollutants mainly by autochthonous microorganisms metabolism (Declercq et al., 2012) but also by a variety of physical and chemical processes without human intervention (Stroo, 2010; Wilson, 2010). This remediation process needs to be measured and assessed in order to plan and verify the achievement of site-specific remediation goals within a reasonable timeframe.

L. **Biostimulation:** This in-situ and/or ex-situ strategy is based on the use of the metabolic processes of autochthonous living organisms to degrade pollutants. Ex-situ techniques include biopiles, windrow and in-vessel composting, landfarming, and bioreactors; in-situ techniques, instead, include permeable reactive barriers (PRB), bioventing, biosparging or bioslurping (Atlas et al., 2005; Majone et al., 2015). The stimulation of bacterial activity can be achieved either by the addition of substrates that can take up the role of carbon source, electron donor or acceptor or by the control of parameters such as temperature, redox potential or pH (Stroo et al., 1998; Atlas et al., 2005). This remediation technique can completely remediate sites contaminated with chlorinated solvents (Chen et al., 2020) with little impact on infrastructure and with a lower cost compared to other remediation strategies (Stroo, 2010).

M. **Bioaugmentation:** Enhances the biodegradation capacity of the aquifer for a target contaminant by introducing specific bacterial strains or consortia. This approach is used

when native degrading bacteria are either inactive or absent in the ecosystem (Schaefer et al., 2010). This process can be applied both ex-situ and in-situ.

Remediation technologies such as pump-and-treat, soil vapor extraction, and air sparging involve significant operational/maintenance costs and high energy consumption. ISCO and enhanced in situ bioremediation (EISB) are two of the most promising in situ technologies that have been applied for the remediation of contaminant source zones (Bryck, 2014). Consequently, this thesis is focused on two novel methodologies that will be researched using isotopic analyses: (i) Alkaline-activated persulfate ISCO combined with an alkaline interception trench which acts as a PRB and (ii) EISB with emulsified vegetable oil (EVO) as slow-release electron donor. These methods are extensively described in Chapter 1 and Chapter 2.

1.4. Target contaminants degradation pathways

Degradation pathway refers to the biochemical reactions through which an original contaminant is transformed to degradation byproducts, typically simpler compounds. Degradation pathways and their reaction rates depend strongly on the hydrochemical conditions in groundwater. A summary of the main degradation pathways of CMs and CEs is presented below, and a detailed description of the degradation mechanisms studied in this thesis can be found in the corresponding chapters.

CEs and CMs can be degraded through abiotic degradation pathways that involve non-biological degradation processes such as chemical oxidation, hydrolysis or reduction reactions with minerals. Biotic degradation pathways, instead, rely on the activity of microorganisms in degrading the chlorinated compounds via metabolic or co-metabolic processes.

ABIOTIC

Abiotic Oxidation: Strong oxidants such as persulfate ($S_2O_8^{2-}$) or permanganate (MnO_4^-) have been successfully applied to remediate contaminated sites, effectively degrading CEs and CMs at high concentrations or even in DNAPL (Tobiszewski et al., 2012). However, CMs are less susceptible to oxidation than CEs due to the higher state of carbon oxidation in CT and TCM (Huling et al., 2006).

Alkaline hydrolysis: Hydrolysis is typically a slow process in groundwater pH values (7-8). However, under strong acid and basic conditions, alkaline hydrolysis can occur, accelerating the degradation of certain compounds. For instance, TCM can be effectively remediated through

alkaline hydrolysis, while for other CMs and CEs the rates remain too low even in alkaline conditions (Torrentó et al., 2014; Rodríguez-Fernández et al., 2018).

Reduction by Fe(0) and Fe-bearing minerals: Zero-valent iron (Fe(0)) is a strong reducing agent that effectively degrade CEs and CMs (Audí-Miró et al., 2013a; Rodríguez-Fernández et al., 2018). Fe(0) or other Fe-bearing materials such as magnetite (Fe(II) and Fe(III)) or pyrite (Fe(II)), can be used in PRBs. Hydrogenolysis is the principal reductive degradation mechanism that drives this pathway, involving the substitution of a chlorine atom by a hydrogen atom, coupled with addition of two electrons to the molecule (Mohn et al., 1992).

BIOTIC

Anaerobic biodegradation: Under reducing conditions chlorinated solvents can be degraded by different anaerobic processes such as reductive dechlorination (RD), fermentation, anaerobic organohalide-respiring bacteria (OHRB) or co-metabolically under methanogenic environments (Wackett et al., 1992; Ferguson et al., 2000; Leeson et al., 2004). Among these processes, RD is often a growth-supporting reaction, while the other may be catalyzed by biological molecules. RD involves breaking the C-Cl bond releasing the chlorine atom. This reaction can occur via:

- Hydrogenolysis: similarly to the reduction by (Fe(0), where a single chlorine atom is replaced by an hydrogen atom.
- Dichloroelimination: A two-electron transfer to a molecule resulting in the elimination of two chlorine atoms, which typically occurs under methanogenic conditions, but it may also occur under partially anoxic conditions (Dolfing, 2016). This includes β-dichloroelimination, when chlorine atoms are removed from two different carbon atoms and α-dichloroelimination when chlorine atoms are removed from the same carbon atom.

Aerobic biodegradation: Some chlorinated solvents, for example cis-1,2-DCE, VC and DCM can undergo biotic oxidation under oxic conditions, due to the lower oxidation state of carbon compared to highly chlorinated compounds (Heraty et al., 1999; Abe et al., 2009a). This pathway is less common, but it can occur under oxic conditions and in transition zones between oxic and anoxic conditions (Mattes et al., 2010).

The occurrence and efficiency of degradation pathways depend on several environmental factors (Leeson et al., 2004; McCarty et al., 2007):

A. pH, redox potential and temperature: The optimal redox potential (Eh) range for anaerobic dechlorination of chlorinated solvents is between -250 and -50 mV (Leeson et al., 2004; Bouwer, 2017). While the typical pH range in aquifers (6-8) is generally suitable for anaerobic dechlorination, the acidity produced by contaminant dechlorination and the fermentation of the amended electron donor during biostimulation can alter pH levels and affect degradation activity (Adrian et al., 2016; Yang et al., 2017). Regarding temperature, the optimal growth of OHRB occurs between 20-30 °C. Although bacteria can survive at lower temperatures, the dechlorination process slows significantly (Adrian et al., 2016).

B. Availability of a carbon source and suitable electron donors and acceptors: Organic fermentable substrates are commonly used as amendments to condition the soil for anoxic conditions, as they serve both as carbon source (e.g., acetate) and as an electron donor (e.g., dihydrogen) for anaerobic degrading bacteria. The fermentation of the amendment by indigenous fermentative bacteria results in the release of dihydrogen, depletion of dissolved oxygen through aerobic respiration, and subsequent reduction of other terminal electron acceptors in the aquifer, thereby lowering the redox potential (Eh). Under these reductive conditions, anaerobic degraders can outcompete other microorganisms in the aquifer and effectively degrade the pollutants anaerobically (Lovley, 2001).

C. Microbial communities: The presence and activity of specialized microorganisms (e.g., *Dehalococcoides* spp.) are critical for biotic degradation pathways, particularly for RD. While RD is a common mechanism for the degradation of chlorinated solvents, it is not the only one described in the literature. Based on their metabolism, two main groups of bacteria are known to degrade organohalides into less chlorinated compounds: OHRB and organohalide fermenting bacteria. Additionally, other facultative anaerobes such as *Pseudomonas* or *Xanthobacter*, can degrade various chlorinated solvents through co-metabolic processes (Bhatt et al., 2007).

D. Hydrogeological factors: The physical properties of the aquifer, such as permeability, porosity, and mineral composition can influence the contaminant distribution, the mobility and availability of reactants and the progression of the degradation process.

1.5. Strategies for remediation assessment

To assess degradation processes affecting a target pollutant in a contaminated aquifer, especially in sites where bioremediation is applied, it is recommended to combine multiple methodologies. This approach helps overcome the limitations of individual methods while integrating complementary information, resulting in a more reliable characterization of in situ degradation processes (Bombach et al., 2010; Blázquez-Pallí et al., 2019). Commonly used techniques are briefly described below.

1.5.1. Concentration mass balance

Mass balances based on concentrations of pollutants and the molar ratios of parent to daughter products compounds have traditionally been used to estimate the efficiency of remediation treatments in the field (Andrew James et al., 2009). However, contaminants concentrations in the subsurface can fluctuate, and these variations are not necessarily indicative of their transformation. For example, concentrations of pollutants in groundwater can decrease during transport in the aquifer by processes like dilution, dispersion, or sorption. Additionally, some degradation products can be present at trace levels in DNAPL, they can originate from different parent compounds or even be both degradation products and original contaminants simultaneously (e.g., TCE). Therefore, the contaminant concentration alone is not a reliable parameter to confirm that degradation of groundwater contaminants is occurring.

1.5.2. Hydrochemistry

The degradation pathway is dependent on the environmental conditions such as pH or redox potential. When organic contaminants are introduced to an aquifer, the hydrochemistry can change rapidly due to the use of naturally occurring electron acceptors by microorganisms metabolizing the organic compounds (Leeson et al., 2004). Oxygen is preferentially used as electron acceptor, but it is rapidly depleted in contaminated aquifers, leading to the use of alternative electron acceptors such as nitrate, manganese, Fe^{3+}, sulfate and carbon dioxide. Therefore, knowledge of hydrochemical parameters such as the redox potential (Eh), the dissolved oxygen, and other terminal electron acceptor dissolved species can provide valuable information to evaluate whether the necessary conditions for the selected degradation pathway on a remediation site have been achieved (Christensen et al., 2000; McMahon et al., 2011). However, this information alone cannot directly confirm or quantify the degradation of specific target contaminants. Moreover, while redox conditions in the aquifer can be heterogeneous,

field measurements from fully screened monitoring wells provide weighted Eh value. In such cases, the use of multi-level nested piezometers and a low flow pumping system could enhance the characterization of the aquifer's redox conditions.

1.5.3. Molecular biology tools (MBTs)

The detection of specific microorganisms in the aquifer can provide a qualitative indication of the reductive dechlorination potential in a specific contaminated site, which is crucial for the remediation strategy selection. Quantitative methods based on polymerase chain reaction (PCR) allow for the detection of specific microorganisms, such as *Dehalococcoides*, and functional genes related to the metabolism of certain contaminants (van der Zaan et al., 2010). MBTs are used as indicator for the potential MNA or bioestimulation at contaminated sites. The qualitative (presence/expression) or quantitative assessment of specific genes, such 16S rRNA, can serve as biomarkers to assess the natural bioremediation potential or the activity of OHRB in a contaminated aquifer (Lebrón et al., 2011).

1.5.4. Isotope analysis

The isotopic analysis of specific chlorinated contaminants in groundwater samples, commonly referred to as "Compound-specific stable isotope analysis" (CSIA), has been used in the last decade to provide additional data to improve the understanding of contaminant transformation processes. Carbon ($^{13}C/^{12}C$) and more recently chlorine ($^{37}Cl/^{35}Cl$) isotopes are usually analysed for chlorinated hydrocarbons. Isotopes are atoms with the same number of protons and electrons but different number of neutrons, resulting in variations in their mass. In nature, two or more stable isotopes of the same element have different natural abundances. For instance, 98.93% of carbon in nature is ^{12}C, while only 1.07% is ^{13}C, where the exponent refers to the sum of protons and neutrons. For chlorine, 75.76% occurs as ^{35}Cl, while the remaining 24.24% is ^{37}Cl.

The isotope ratios of an element "E" (i.e., $^{H}E/^{L}E$) are reported in delta notation ($\delta^{h}E$, in ‰, Eq. 1), relative to the international standards VPDB (Vienna Pee Dee Belemnite) and SMOC (Viena Standard Mean Ocean Chlorine) (Kaufmann et al., 1984; Coplen, 1996), respectively. The isotopic ratio (e.g., $^{13}C/^{12}C$, $^{37}Cl/^{35}Cl$) of a sample and the standard is denoted as R_{sample} and R_{std}, respectively:

$$\delta^{h}E = \left(\frac{R_{sample}}{R_{std}} - 1\right) \quad \text{Eq. 1}$$

Isotopes of the same element exhibit nearly the same chemical behaviour, generally linked to electrons rather than neutrons. However, heavy isotopes form shorter and more stable chemical bonds due to their mass difference than light ones (Michener & Lajtha, 2008). This is reflected

in environmental processes like biochemical transformations, where different rates can be obtained for the same mechanism/reaction for molecules with varying isotopes in the reacting position, causing the so-called kinetic isotopic effect (KIE). Those molecules with light isotopes are commonly degraded faster by enzymatic reactions, leading to an enrichment of light isotopes in the daughter product. At the same time, the residual parent compound is enriched in heavy isotopes. This isotopic fractionation that occurs during biochemical transformations causes a shift in the isotopic composition of the pollutants, which can be measured by CSIA (Aelion et al., 2009).

Contrarily to changes in concentration, which can be affected by different processes, the isotopic shifts are mainly linked to compound transformation since the isotopic composition is barely affected by physical processes in groundwater such as dilution, sorption or dispersion, which are often regarded as negligible (Figure 2) (Hunkeler et al., 1999; Aelion et al., 2009). Thereby, the information obtained from isotopic measurements is more reliable and conclusive for remediation efficiency assessment. Hence, CSIA is of great interest for site characterization and evaluation of contaminant remediation, as it provides complementary lines of evidence of degradation, usually required by legislation and regulatory administration (Nijenhuis et al., 2007; Aelion et al., 2009; Elsner, 2010; Palau et al., 2014).

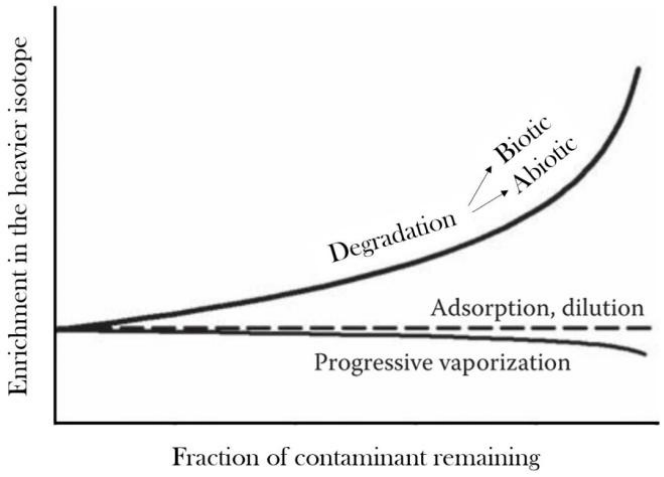

Figure 2. Illustration of the potential of CSIA to distinguish between physical (non-degradative) processes and degradation (both biotic and abiotic) in the field. Source: adapted from (Aelion et al., 2009).

The isotopic data can also be used for contaminant source elucidation and apportionment: identifying different sources of pollutants and quantifying their relative contribution. Source

identification is necessary before monitoring transformation processes in the field (Hunkeler et al., 2008; Elsner, 2010), and quantitative estimation of the biodegradation extent (Aelion et al., 2009). Isotopic study of more than one element (2D-CSIA or multi-element) has been proven valuable for source identification and elucidation of pollutant fate in the field. The relationship between isotopic shifts of different elements in the same compound can be used to identify specific ongoing reaction mechanisms (Elsner, 2010; Hermon et al., 2018). These reaction mechanisms must be studied first in laboratory experiments under controlled conditions before degradation processes in the field can be identified (Aelion et al., 2009).

1.5.5. Interpretation of changes in isotopic data

Isotopic fractionation (ε)

Changes in the isotopic composition of an element (E) in a compound can be correlated with changes in its concentration for a given reaction ($f=C_t/C_0$). These changes result in an isotopic fractionation for that element (ε), which is characteristic of a given reaction mechanism (Elsner, 2010; Coplen, 2011). The ε can be calculated using a simplified version of the Rayleigh equation:

$$\varepsilon(‰) \approx \left(\frac{ln\left(\frac{R}{R_0}\right)}{ln(f)}\right) \cdot 1000$$

Eq. 2

where R_t/R_0 can be expressed as $(\delta^hE_t + 1) / (\delta^hE_0 + 1)$ according to δ^hE definition (Eq. 2). The uncertainty of the ε^hE value can be expressed as the 95% confidence interval (CI) of the regression slope (Eq. 2) in a double logarithmic plot, also called the Rayleigh plot. For degradation to be considered significant, differences in isotope values in the field for both carbon and chlorine must be >2‰ (Elsner et al., 2008).

Before evaluating isotopic changes in field applications, laboratory-derived site-specific ε^hE values should be obtained from microcosm experiments, under controlled laboratory conditions, prepared with soil and groundwater from the contaminated site. Alternatively, these values can also be obtained from the literature when available.

Isotopic mass balance

The isotopic mass balance is used to assess the degradation of a family of contaminants or to estimate the isotopic signature of the original contaminant source when all the products are accounted for. It is calculated as the weighted average isotopic composition of all the compounds in one specific degradation pathway. In the case of reductive dechlorination (RD), PCE is the parent compound, while TCE, cis-DCE, VC, and ethene are the sequential degradation products.

For example, the carbon isotopic mass balance has been calculated in the literature for the sequential RD of the chlorinated compounds (Hunkeler et al., 2008; Aeppli, Hofstetter, et al., 2010; Blázquez-Pallí et al., 2019). Ethene is normally not considered in the balance as it can be easily further degraded to CO_2 or lost by volatilisation. Besides, ethene is a ubiquitous gas that can be produced by multiple environmental processes.

Hence, the isotopic mass balance of CEs (PCE to VC) is calculated using the following equation:

$$\delta^{13}C_{CEs} = \chi_{PCE} \cdot \delta^{13}C_{PCE} + \chi_{TCE} \cdot \delta^{13}C_{TCE} + \chi_{DCE} \cdot \delta^{13}C_{DCE} + \chi_{VC} \cdot \delta^{13}C_{VC} \qquad \text{Eq. 3}$$

where χ refers to the molar fraction of each compound for a given sample. It is calculated as the moles of a compound over the total moles of CEs.

While the isotopic difference between two sequential compounds is controlled by the specific isotopic fractionation of the primary compound, the isotopic mass balance value will remain constant. It will equal the source value until VC is degraded to non-toxic ethene, which is not considered in the balance (Eq. 3). When ethene is produced, the isotopic mass balance will become more positive $\delta^{13}C_{CEs}$ than the source or initial value. Balance values higher than the source value will thus indicate that the degradation sequence reached ethene generation, a non-chlorinated, non-toxic product.

The uncertainty associated with the isotope balance is calculated based on the error propagation using the standard deviation of the isotope measurements and considering a precision for the concentration measurements of 10% for each CE species (Eq. 4) (Stelzer et al., 2009).

$$\Delta_{tot}\delta^{13}C_{CEs} = \frac{\sqrt{\sum(C_i \cdot \Delta\delta^{13}C_i)^2 + \sum([\delta^{13}C_i - \delta^{13}C_{CEs}] \cdot \Delta C_i)^2}}{C_{CEs}} \qquad \text{Eq. 4}$$

Dual C-Cl isotope analysis

Kinetic isotope effects can be used to prove and characterize organic contaminants transformation, however a substantial variability of isotopic fractionation values (ε) has been observed in previous studies for some CEs and CMs. For example, for PCE biotransformation, ε values ranging from -0.4 to -19.0‰ for $\delta^{13}C$ have been reported (Slater et al., 2001; Nijenhuis et al., 2005; Cichocka et al., 2008; Cretnik et al., 2014a). This might be caused by masking of isotope fractionation by either limited intracellular mass transfer (Renpenning et al., 2014, 2015) or rate limitations within the enzymatic multistep reaction (Soder-Walz et al., 2022). Previous studies (Palau et al., 2017; Büsing et al., 2020) suggested that despite variable single-element isotope

fractionation, similar slopes of dual-element isotope plots ($\Lambda_{C\text{-}Cl}$) could indicate a common reaction mechanism for PCE degradation. However, some exceptions have been already found for different enzymes catalyzing the same exact reaction likely via different transition states or connected to enzyme-substrate binding (Rosell et al., 2012; Gafni, et al., 2020). Experiments for the indirect assessment of these isotope-masking effects can be performed using cell suspensions (concentrate of active cells) and/or crude protein extract, where the cell membrane is disrupted, mass transfer is absent and, therefore, the enzyme is directly available for electron transfer and reductive dehalogenation reactions, for example.

While single isotope analysis can provide information of isotopic fractionation values caused by a specific biodegradation process under controlled conditions in the laboratory, dual C-Cl isotope analysis can reveal the contaminant degradation processes that occur in the field by measuring the relative change of the two elements, which is specific to a certain reaction (Figure 3).

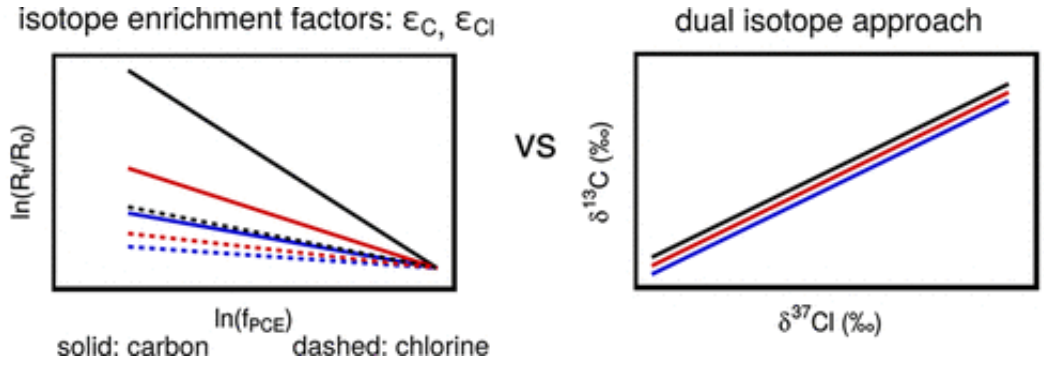

Figure 3. Carbon and chlorine isotopic fractionation (left) and C-Cl dual plot (right) for PCE biodegradation by Desulfitobacterium spp. Strains. Adapted from Büsing et al., (2020).

Besides, dual isotope analysis is also key for contaminant source identification. Due to differences in manufacturing methods and the utilized raw materials (organic compounds and brines), certain chlorinated hydrocarbons can exhibit a range of $\delta^{13}C$ and $\delta^{37}Cl$ values. The difference in the isotopic composition of original contaminants allows the identification of different sources in the field. This approach can be used to distinguish different potential sources of PCE in field sites and it is also useful to discriminate isotopic differences due to degradation processes instead of different contaminant sources (Emsbo-Mattingly et al., 2023) (Figure 4).

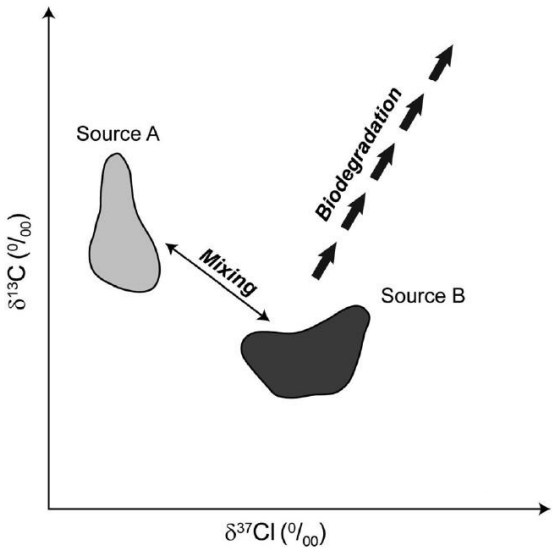

Figure 4. Chlorine and carbon isotope fractionation during source mixing and biodegradation of TCE in groundwater, adapted from Yuan et al., (2021).

Calculation of biodegradation extent

The $\varepsilon^{h}E$ value can be used to quantify the extent of biodegradation of a target contaminant when a site-specific ε value is available (Aeppli, et al., 2010; Elsner, 2010; Amaral et al., 2011). For instance, when differences in the contaminant carbon isotope values in the field ($\Delta\delta^{h}E$) are >2‰ degradative processes can be considered to be significant (Hunkeler et al., 2008). For a given contaminant (i.e. PCE), the extent of degradation (B%) in the field can be evaluated with the following equation:

$$B_{PCE}(\%) = \left[1 - \left(\frac{\delta^{13}C_{PCE} + 1000}{\delta^{13}C_{PCE}^{Source} + 1000}\right)^{1000/\varepsilon_{PCE}}\right] \cdot 100$$

Eq. 5

where ε_{PCE} refers to the enrichment factor, $\delta^{13}C_{PCE}$ is the isotope data from groundwater samples, and $\delta^{13}C^{Source}_{PCE}$ is the most depleted value found at the field site, assumed to be the closest to the source (Hunkeler et al., 2008). In the case of metabolites, this equation will also be valid for evaluating their degradation. However, the precursors must be completely degraded for its application.

In analogy to Eq. 5, the isotopic mass balance of CEs can be used to assess the biodegradation to non-chlorinated compounds:

$$B_{\sum CEs}(\%) = 1 - \left(\frac{\delta^{13}C_{\sum(CEs)} + 1000}{\delta^{13}C^{Source}_{\sum(CEs)} + 1000}\right)^{1000/\varepsilon_{\sum(CEs)}} \quad \text{Eq. 6}$$

Where $\varepsilon_{\sum CEs}$ is the isotopic fractionation value associated with the complete PCE dechlorination. Due to the masking of single-step isotopic fractionation within a multistep reaction, $\varepsilon_{\sum CEs}$-values are influenced by the kinetics of individual reaction steps (Kohen et al., 2005). The minimum and maximum limits of $\varepsilon_{\sum CEs}$ -values can still be estimated from isotopic fractionation values of individual dechlorination steps (Amaral et al., 2011; Höhener et al., 2015):

$$\varepsilon^{min}_{\Sigma CES} \approx \varepsilon_{PCE} + \varepsilon_{TCE} + \varepsilon_{cDCE} + \varepsilon_{VC} \quad \text{Eq. 7}$$

$$\varepsilon^{max}_{\Sigma CES} \approx \varepsilon_{VC} \quad \text{Eq. 8}$$

Eq. 7 represents the limit of the instantaneous transformation of PCE to VC, whereas Eq. 8 represents a significantly slower transformation of VC than the preceding reaction steps. As the value given by the first equation will be more negative (ε_{min}), it will calculate the lower limit of biodegradation percentage. In contrast, the second equation will calculate a higher limit of biodegradation (ε_{max}). The result will be a range of biodegradation extent based on the scenarios stated above.

The uncertainty of the biodegradation extent calculation (ΔB) is determined using error propagation according to (Thullner et al., 2012):

$$|\Delta B| = \frac{1}{|\varepsilon|} \cdot (100 - B[\%]) \cdot \sqrt{\left(ln(1 - B[\%]/100)\right)^2 \cdot (\Delta\varepsilon)^2 + (\Delta\delta_x)^2 + (\Delta\delta_0)^2} \quad \text{Eq. 9}$$

In this equation, the error in the measurement of the isotopic mass balance of a given point ($\Delta\delta_x$), in the source ($\Delta\delta_0$) and the isotopic fractionation ($\Delta\varepsilon$) are used, but the biodegradation extent (B[%]) is also a factor to be considered for the calculation of the uncertainty. The relative accuracy of B[%] is lowest at low amounts of degradation and steadily increases towards higher amounts of degradation.

1.6. Study sites

To increase the understanding of multi-isotopic tools in investigating the fate of chlorinated solvents, it is essential to complement laboratory experiments with field-scale investigation. This thesis investigates two distinct contaminated sites to assess different remediation strategies: **site A**, involving in-situ biostimulation by the injection of EVO, and **site B**, for which field conditions were reproduced in laboratory batch experiments.

Site A is an industrial site located near Barcelona (Spain) heavily contaminated with PCE, with groundwater concentrations reaching values of 19 mg/L due to former improper storage and handling practices. The aquifer consists of an unconfined sedimentary layer formed by Quaternary sand and sandy-silt deposits, with a thickness ranging between 4 and 8 meters. Below this unit lies a Miocene detrital deposit composed of alternating clay and silt layers, forming the aquifer bedrock. Groundwater flows toward southeast, following the dip of the Quaternary/Miocene interface (Figure 5). The water table is located between 2 and 4 meters below ground surface, with hydraulic conductivity values between 0.25 to 0.35 cm/s and transmissivity ranging from 0.8 to 1.7 m^2/day, as determined by pumping tests.

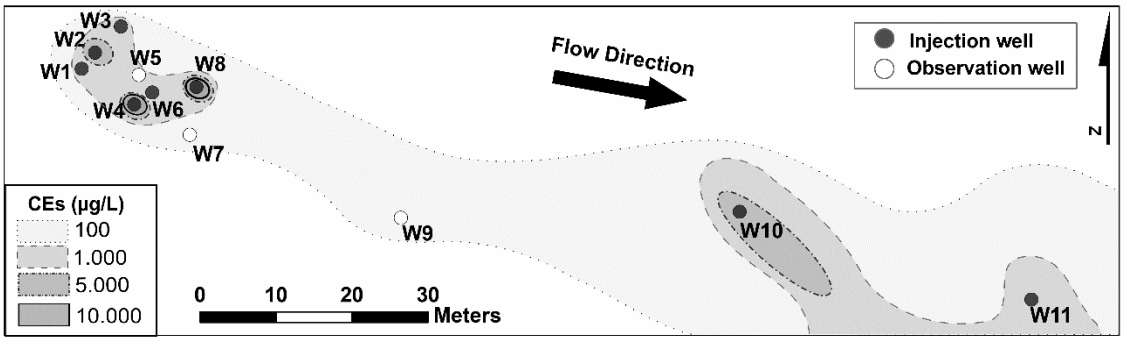

Figure 5. Site map and groundwater monitoring well network. The filled contour lines represent total CEs concentrations in groundwater (in µg/L) prior to the EVO injection (June 2020).

Site B is an experimental site located in a complex fractured aquifer in Òdena, near Barcelona (Spain). Due to improper disposal practices of a chemical plant that operated from 1978 to 1985, the site is still multi-contaminated by CEs, CMs, chlorinated ethanes, chlorobenzenes, traces of BTEX and pesticides such as methoxychlor (Palau et al., 2014; Torrentó et al., 2014; Rodríguez-Fernández et al., 2018).

The geology of the study area is represented by Eocene limestone, sandstone and marl layers, overlayed by Quaternary deposits of silt and sand (Palau et al., 2014). The aquifer is formed in a system of fractures in the low permeable Eocene blue-grey limestones.

The remediation of this site started in 1995, and in 2006, approximately 2000t of contaminated soil were removed from the source areas. The holes left by these excavations were filled with recycled concrete-based aggregates. The objective was that the contaminants in the unsaturated zone and mobilized by rainwater infiltration could be captured in this infiltration trenches. Moreover, the induction of alkaline conditions (pH ≈ 12) by the dissolution of concrete minerals (e.g. portlandite) allowed the alkaline hydrolysis of TCM as confirmed by its carbon isotopic fractionation in the trench (Torrentó et al., 2014). A detailed hydrogeological model of the alkaline trench is provided in Torrentó et al. (2014). Briefly, the connection between the aquifer and the percolation water in the unsaturated zone occurs through fractures and in the contact between the detrital unit and the underlying limestone layers (Figure 6).

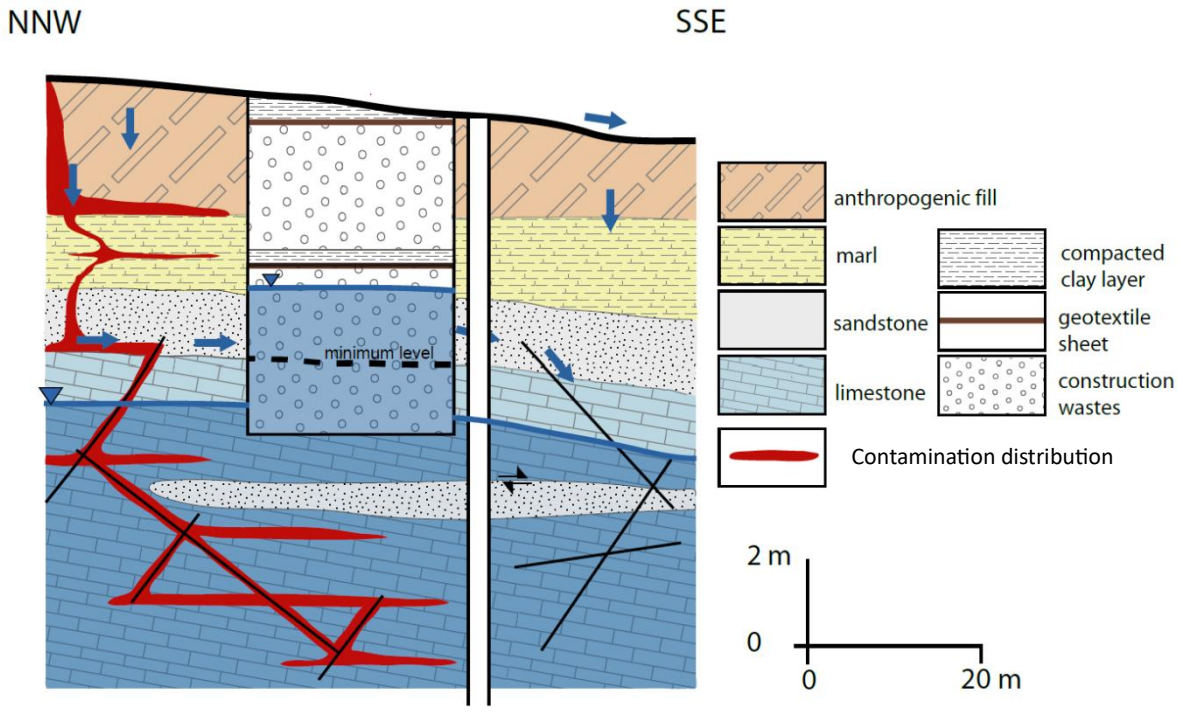

Figure 6. Schematic cross-section of the study site B with the representation of the fractured system and the alkaline interception trenches constructed in 2006 (adapted from Torrentó et al., 2014).

1.7. Goals of the thesis

Environmental contamination by chlorinated solvents represents a widespread challenge to be solved. Although various remediation techniques can be implemented at contaminated sites, a deeper understanding of the underlying pollutants transformation processes and how environmental conditions can affect them is essential. Such understanding is crucial not only for improving the selection and efficacy of existing remediation techniques but also for facilitating the assessment of innovative strategies in the future. In this context, this thesis aims to investigate the application of multi-isotopic tools for the assessment of novel remediation techniques on chlorinated solvents. The ultimate goal is to enhance our understanding of the degradation pathways and environmental fate of CEs and CMs in contaminated groundwater.

The central hypothesis of this thesis is that multi-element isotopic tools can be used to effectively assess the degradation and fate of chlorinated solvents in field-scale applications under varying environmental conditions and remediation techniques. Furthermore, it is hypothesized that 2D-CSIA can distinguish specific reaction mechanisms and provide direct assessment of remediation performance.

To address this overarching goal, the following specific objectives were defined:

Objective A: Assessment of CEs degradation by enhanced in situ bioremediation with emulsified vegetable oil (EVO).

A.1. Evaluate whether abiotic processes, specifically the partitioning of CEs between water and oil phases, can induce significant isotopic shifts.

A.2. Investigate carbon and chlorine isotopic fractionation and dual (C, Cl) isotope trends of CEs during reductive dechlorination in microcosm experiments and compare these trends with the data observed in field application.

A.3. Integrate isotopic data with complementary analytical tools, including hydrochemical analyses and molecular biology tools.

Objective B: Investigation of CEs and CMs transformation, with special focus on TCM, using a 2D-CSIA approach in alkaline-activated persulfate in ISCO treatments with alkaline-activated PS, in combination with an interception trench that induces alkaline conditions.

B.1. Assess the influence of diverse field conditions, typically encountered at contaminated sites, on the efficacy of this innovative remediation strategy.

B.2. Special focus on the carbon and chlorine isotopic fractionation and dual (C, Cl) isotope trends of TCM in laboratory batch experiments to evaluate the feasibility of identifying its potential transformation processes by alkaline-activated persulfate and distinguish them from alkaline hydrolysis.

1.8. Thesis outline

To achieve the objectives outlined in this thesis, a series of tasks were undertaken, encompassing both laboratory and field-scale studies.

For the investigation of enhanced in situ bioremediation using EVO for CEs degradation, the research included:

A. Laboratory experiments for the assessment of potential isotopic fractionation resulting from water-oil partitioning of chlorinated ethenes.

B. Laboratory microcosm experiments under controlled anoxic conditions, using the autochthonous microbial community of the study site, to simulate enhanced reductive dechlorination processes.

C. Field-scale application for the evaluation of the findings from laboratory studies in a real-site context to validate the observed degradation pathways and isotopic trends and quantify the efficiency of the treatment.

For the remediation of CEs and CMs (with special focus on TCM) using ISCO with PS activated by an alkaline interception trench, the research involved:

A. Laboratory batch experiments to reproduce variations in environmental conditions typically encountered in field applications, such as oxidant-to-contaminant molar ratio, pH, and the presence of carbonates.

B. A field-condition simulation was conducted in a final batch experiment using water and solid materials sampled from an experimental field-site alkaline interception trench to replicate actual field conditions and examine the degradation mechanisms affecting TCM.

As a result of the research carried out during this thesis, two scientific articles have been produced. Both articles have been published in international peer-reviewed journals indexed in

the Science Citation Index (SCI). A list of these articles, along with the rankings of the corresponding SCI journals according to the Web of Science (WOS, Thomson Reuters), is provided below. The complete published documents are included in Appendix 1. Figure 7 illustrates the relationship between scientific articles and the objectives of this thesis.

I. **Gil-Villalba, S.;** Palau, J; Soder-Walz, J.M; Vallecillo, M.A.; Corregidor, J.; Tirado, A.; Shouakar-Stash, O.; Guivernau, M.; Viñas, M.; Soler, A.; Rosell, M. (2024) Use of isotopic (C, Cl) and molecular biology tools to assess biodegradation in a source area of chlorinated ethenes after biostimulation with Emulsified Vegetable Oil (EVO). *Science of The Total Environment*, Volume 951, 175351. DOI: https://doi.org/10.1016/j.scitotenv.2024.175351. Q1 in Environmental Sciences, IF = 8.2 (2023).

II. **Gil-Villalba, S.;** Rosell, M.; Torrentó, C.; Vinyes-Nadal, M.; Soler, A.; Palau, J. (2025) Variable dual C-Cl isotope slopes of trichloromethane transformation by alkaline-activated persulfate under different simulated field conditions. *Journal of Hazardous Materials*, Volume 489, 137702. DOI: https://doi.org/10.1016/j.jhazmat.2025.137702. Q1 in Environmental engineering and in Environmental Sciences, IF = 12.2 (2023).

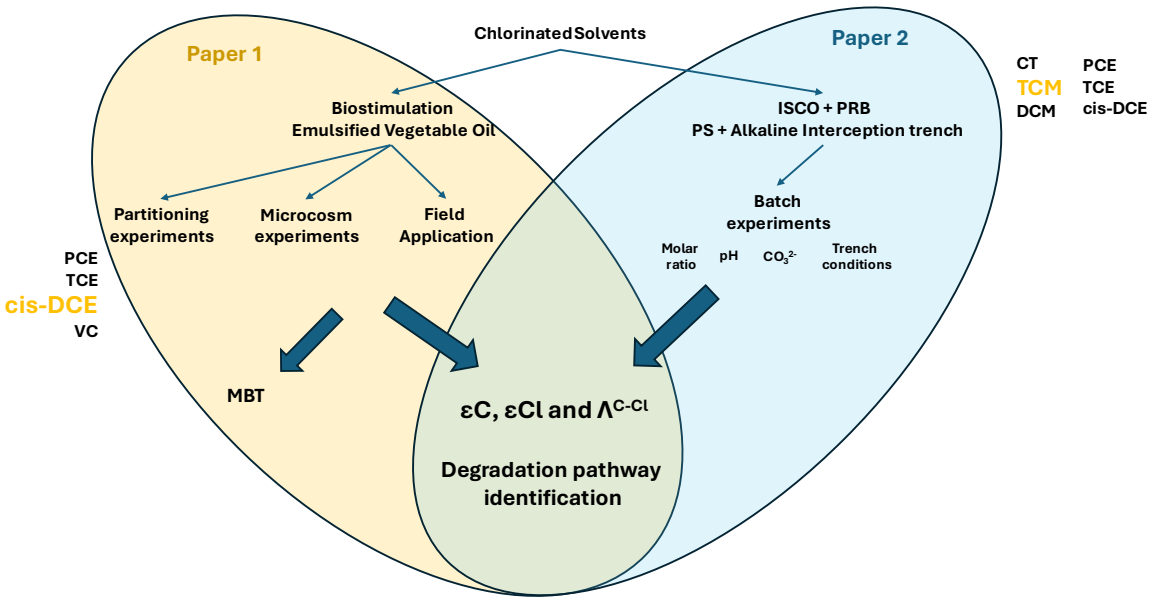

Figure 7. Schematic of thesis outline, related with the chapters and publications.

Apart from the two articles derived directly from this thesis, a third article was published as a result of research collaboration in MAiMA group:

Vinyes-Nadal, M.; **Gil-Villalba, S.**; Rosell, M.; Otero, N.; Torrentó, C. Fate and degradation of methoxychlor in a contaminated aquifer: insights from dual carbon-chlorine isotope analysis and isomeric fraction. Journal of Hazardous Materials, Volume 488, 137447. DOI: https://doi.org/10.1016/j.jhazmat.2025.137447. Q1 in Environmental engineering and in Environmental Sciences, IF = 12.2 (2023).

Other contributions related with this thesis were presented in conferences:

Gil-Villalba, S.; Vinyes-Nadal, M.; Torrentó, C.; Soler, A.; Palau, J.; Rosell, M. Multi-isotopic assessment of potential chloroform remediation by a combined treatment of alkaline-activated persulphate in alkaline recharge water interception trenches. International Association of Hydrogeologists – AIH 2021. Brussels, Belgium. Poster.

Corregidor, J.; **Gil-Villalba, S.**; Vallecillo, M.A.; Rosell, M.; Tirado, A.; Herrero, S.; Villanueva, A.; Soder-Walz, J.; Palau, J. Eficiente bioremediación de disolventes clorados en un acuífero complejo. Validación por técnicas isotópicas duales, moleculares y geoquímicas. Congreso Ibérico de las Aguas Subterráneas – CIAS 2021. Valencia, Spain.

Gil-Villalba, S.; Rosell, M.; Soder-Walz, J.; Corregidor, J.; Vallecillo, M.A.; Tirado, A.; Shouakar-Stash O.; Viñas, M.; Palau, J. Combined isotopic (C-Cl) and molecular approach for the assessment of EVO biostimulation treatment of an aquifer polluted with chlorinated ethenes. Joint European Stable Isotope User Meeting – JESIUM 2022. Kuopio, Finland. Poster.

Gil-Villalba, S.; Rosell, M.; Soder-Walz, J.; Corregidor, J.; Vallecillo, M.A.; Tirado, A.; Shouakar-Stash, O.; Guivernau, M.; Viñas, M.; Palau, J. Uso de análisis isotópicos (13C, 37Cl) en etenos clorados para la evaluación de la bioremediación mediante la inyección de aceite vegetal emulsionado en un acuífero contaminado. Congreso Ibérico de Aguas Subterráneas – CIAS 2022. Oral.

Vinyes-Nadal, M.; **Gil-Villalba, S.**; Soler, A.; Otero, N.; Torrentó, C. Assessing methoxychlor contamination and natural attenuation in a polluted aquifer using carbon compound specific isotope analyses. 12th Isotopes Conference - 2022. Dübendorf, Switzerland. Poster.

Gil-Villalba, S.; Rosell, M.; Soder-Walz, J.; Corregidor, J.; Vallecillo, M.A.; Tirado, A.; Shouakar-Stash, O.; Guivernau, M.; Viñas, M.; Soler, A.; Palau, J. Evaluación de bioremediación

de etenos clorados con EVO mediante análisis isotópicos. Water Innovation Day – WID 2023. Oral. *Award to best R+D project presented in the event.

Herrero, S.; Torrentó, C.; Rosell, M.; Palau, J.; Domènech, C.; Cappelli, C.; **Gil-Villalba, S.**; Vinyes-Nadal, M.; Fernández-Lagunas, A.; Otero, N.; Soler, A. Pilot scale validation of two combined innovative solutions for the remediation of complex sites contaminated with chlorinated organic compounds. AquanConSoil 2023. Prague, Czech Republic. Poster.

Torrentó, C.; Rosell, M.; **Gil-Villalba, S.**; Fernández-Lagunas, A.; Vinyes-Nadal, M.; Cappelli, C.; Palau, J.; Domènech, C.; Herrero, S.; Otero, N.; Soler, A. REMECLOR (Tratamiento de REMEdiación de compuestos organoclorados en la zona no saturada. IV Jornades sobre la Contaminació del sòl. Barcelona, Spain. Oral.

Gil-Villalba, S.; Rosell, M.; Soder-Walz, J.; Corregidor, J.; Vallecillo, M.A.; Tirado, A.; Shouakar-Stash, O.; Guivernau, M.; Viñas, M.; Soler, A.; Palau, J. Assessment of bioremediation of chlorinated ethenes with EVO using isotopic analysis. Siti contaminati. Esperienze negli interventi di risanamento – SiCon 2024. Oral.

Gil-Villalba, S.; Rosell, M.; Torrentó, C.; Vinyes-Nadal, M.; Soler, A.; Palau, J. Use of dual C-Cl isotope analysis of trichloromethane for the assessment of active radical species during alkaline persulfate activation. World Groundwater Congress – IAH 2024. Davos, Switzerland. Oral.

Fernández-Lagunas, A.; **Gil-Villalba, S.**; Domènech, C.; Rosell, M.; Soler, A.; Palau, J. Multi-isotopic (34S, 18O) tracing of persulfate activation: preliminary results from batch experiments. World Groundwater Congress – IAH 2024. Davos, Switzerland. Poster.

2. Background

2.1. CEs biostimulation with Emulsified Vegetable Oil (EVO)

The successful complete dechlorination of CEs through EISB is contingent upon achieving proper pH and oxidation-reduction potential (ORP) values, as well as the presence of OHRB from the *Dehalococcoides* (*Dhc*) or *Dehalogenimonas* (*Dhg*) species. *Dhc* populations have been demonstrated as the key and most common bacteria capable of transforming TCE, cis-1,2-DCE and VC into non-toxic end products such as ethene and ethane under anoxic conditions (Löffler et al., 2013; Chen et al., 2022) via RD. Failure to meet and sustain the mentioned conditions may result in an incomplete RD of CEs, causing the accumulation of toxic degradation byproducts in the subsoil, i.e., cis-DCE and VC.

During RD of CEs, these are used as electron acceptors by OHRBs, while an electron donor is required to provide energy (Harkness et al., 2013). Hydrogen (H_2) is commonly regarded as the primary electron donor for RD, which is typically generated through the anaerobic fermentation of carbon substrates by other native microbial populations. There is a wide range of commercially available electron donors, including soluble donors such as sugars, organic acids, and alcohols, as well as slow-release donors with low aqueous solubility like lactic acid polymers, emulsified vegetable oil (EVO), chitin, and wood chips (Leeson et al., 2004). These donors undergo microbial fermentation via different pathways and at different rates in groundwater under anoxic conditions, leading to varying levels of hydrogen production and, thus, enhancing the growth and competitive advantage of OHRB against other hydrogen-consuming microorganisms (e.g. sulfate reducing bacteria and methanogens).

The RD of CEs by OHRB is catalyzed by diverse reductive dehalogenases (Rdh) which contain catalytic subunits (Ni et al., 1995; Magnuson et al., 2000). Rdh is a diverse protein family from which there are still a lot of unanswered questions regarding sequence diversity, substrate specificities, global distribution, and modes of inheritance (Hug, 2016). Nevertheless, the Rdh that have been characterized and proved to be functional in microbial respiration are encoded by Rdh operons, mainly composed by the *rdhA* and *rdhB* genes. The RdhA enzymes act as catalyst for cleaving the C-Cl bond during organohalide respiration (West et al., 2013; Badin et al., 2014). The expression of rdh genes has been established as a biomarker for the physiological activity of *Dhc* (Lee et al., 2008; Löffler et al., 2013; Blázquez-Pallí et al., 2019). *PceA* gene is active for the RD of PCE and both *tceA* and *vcrA* genes are active for that of TCE and cis-DCE. In addition, both

vcrA and *bvcA* are primarily and exclusively responsible for the RD of VC to ethene under anoxic conditions (He et al., 2005; Lee et al., 2008; Franke et al., 2020).

EVO is a commercially available bioremediation substrate which consists of an emulsion of soybean oil, surfactants, soluble substrates (e.g., lactate), and nutrients (Newman et al., 2006; Harkness et al., 2013). Due to its low aqueous solubility and composition, that includes soybean oil containing long-chain fatty acid groups, EVO undergoes slow fermentation over time, producing hydrogen and volatile fatty acids. In contrast to more soluble donors, the slow fermentation of EVO prevents the need for its continuous or semi-continuous injection (Lalman et al., 2000; Harkness, 2000). The injection of vegetable oil in the subsurface of a contaminated site can lead to abiotic processes such as the sorption of CEs into oily phases. These phenomena can cause significant changes of the concentration of CEs in groundwater (Yang et al., 2000; Pfeiffer et al., 2005), hampering the evaluation of biodegradation by using contaminant concentration data alone.

The isotopic effect of physical processes on organic compounds (e.g. sorption and diffusion in the saturated zone) has often been disregarded, due to their small fractionation compared to biodegradation (Abe et al., 2009; Audí-Miró et al., 2013; Torrentó et al., 2017; Rodríguez-Fernández et al., 2018). However, other studies on physical processes highlighted their potential impact on the carbon isotope ratios of organic compounds, which might need to be considered for an accurate interpretation of reactive processes using CSIA (Höhener et al., 2012; Wanner et al., 2017; Halloran et al., 2021). To the best of our knowledge, there is only one previous study documenting the water-vegetable oil phase partitioning of CEs (Pfeiffer et al., 2005) and the potential isotopic fractionation caused by this process has not been evaluated so far. Therefore, the investigation of potential isotope effects during sorption of CEs into EVO is warranted.

Previous studies have investigated the application of EVO as an electron donor for CEs bioremediation in laboratory experiments (Long et al., 2006; Lee et al., 2007; Harkness et al., 2013; Hiortdahl et al., 2014; Yu et al., 2018; Underwood et al., 2022). However, research dealing with contaminant remediation using EVO in the field is still limited (Hirschorn et al., 2007; Révész et al., 2014; Chen et al., 2022). These previous studies provided insights into certain effects of RD after the injection of an electron donor, namely acidification of groundwater and changes in microbial community dynamics. As far as we know, only two studies have used the carbon isotopic fractionation of CEs to assess the efficiency of the biostimulation with EVO (Hirschorn et al., 2007, Révész et al., 2014). This thesis addressed the existing knowledge gap regarding the

potential of 2D-CSIA to investigate the fate of PCE, TCE, and cis-DCE following an EVO injection in the field. In particular, the dual (C, Cl) isotope analysis could be useful to identify the degradation pathway of cis-DCE, which can be transformed via both microbial anaerobic RD and aerobic oxidation (Tiehm et al., 2011). Besides, contrarily to PCE and TCE, few studies have reported the dual-element (C, Cl) isotope fractionation trend for cis-DCE during RD (Abe et al., 2009; Kuder et al., 2013; Doğan-Subaşı et al., 2017; Lihl et al., 2019).

The exploration of the potential of a multi-method approach (i.e. isotopic and biomolecular tools) to improve the assessment of CEs degradation by EISB with EVO is carried out in this thesis. To this end, research focused on the following: (i) whether water – EVO phase partitioning processes of CEs result in significant isotopic effects; (ii) the C and Cl isotopic fractionation and dual (C, Cl) isotope trends of PCE, TCE and cis-DCE during RD in microcosm experiments with a bacterial community from the contaminated site; (iii) the dual (C, Cl) isotope fractionation trend of cis-DCE during the EISB with EVO in the field; and (iv) the *Dhc* bacterial populations and functional genes responsible for RD of CEs in both microcosm experiments and field samples. Finally, the isotopic fractionation values and dual element isotope trends were also compared with the available literature data.

2.2. TCM transformation by alkaline-activated persulfate ISCO

Among different oxidants, activated persulfate ($S_2O_8^{2-}$, PS) has been increasingly applied in ISCO treatments of contaminated soil and groundwater due to its capacity to generate sulfate radicals ($SO_4^{\cdot-}$), which are as reactive as the classically used hydroxyl radicals ($OH^{\cdot}$), but more selective (Tsitonaki et al., 2010; Devi et al., 2016; Li et al., 2017). Furthermore, activated PS exhibits both oxidative and nucleophilic reactivity, leading to the generation of various reactive oxygen species (ROS) besides sulfate radicals ($SO_4^{\cdot-}$), such as $OH^{\cdot}$ and superoxide radicals ($O_2^{\cdot-}$), facilitating the degradation of multiple contaminants (Furman et al., 2010; Ike et al., 2018; Tian et al., 2022).

Base activation of PS, widely used in field application (Tian et al., 2022), involves two sequential reactions: (i) HO_2^- formation through base-catalyzed PS hydrolysis (Eq. 10) and (ii) reduction of PS by HO_2^- to form $SO_4^{\cdot-}$ (Eq. 11). Additionally, under highly alkaline conditions, sulfate radical reactions can transition from a $SO_4^{\cdot-}$ dominated oxidation process to one dominated by $OH^{\cdot}$ (Criquet et al., 2009; Furman et al., 2011; Liang et al., 2015). This transition occurs through a one-electron oxidation of OH^- by $SO_4^{\cdot-}$ (Eq. 12) (Buxton et al., 1988; Criquet et al., 2009; Liang et al., 2009).

$$S_2O_8{}^{2-} + 2H_2O \xrightarrow{OH^-} HO_2{}^- + 2SO_4{}^{2-} + 3H^+ \quad \text{Eq. 10}$$

$$HO_2{}^- + S_2O_8{}^{2-} \rightarrow SO_4{}^{\cdot-} + O_2{}^{\cdot-} + SO_4{}^{2-} + H^+ \quad \text{Eq. 11}$$

$$SO_4{}^{\cdot-} + OH^- \xrightarrow{pH>10.3} SO_4{}^{2-} + OH^{\cdot} \quad \text{Eq. 12}$$

Although the change in the primary oxidant species from $SO_4^{\cdot-}$ to $OH^{\cdot}$ can result in an equally effective removal of persistent organic compounds (Liang et al., 2009), the lower selectivity of $OH^{\cdot}$ may result in its consumption by organic matter naturally present in the water matrix with the consequent mitigation of the contaminant degradation (Furman et al., 2010; Qi et al., 2016; Lee et al., 2020). Contrastingly, the role of superoxide radical in alkaline-activated persulfate treatments is expected to be minor due to its relatively lower reactivity with organic contaminants, including TCM (Liang et al., 2015).

Anions commonly present as major species in groundwater such as hydrogen carbonate and carbonate anions (HCO_3^-/CO_3^{2-}) can scavenge $SO_4^{\cdot-}$ and $OH^{\cdot}$ (Eq. 13, 14) and consequently decrease the overall oxidation of target pollutants (Nie et al., 2014; Ma et al., 2018; Lee et al., 2020). The second-order rate constants for the reaction of HCO_3^-/CO_3^{2-} with $SO_4^{\cdot-}$ (Eq. 14) are within the same order of magnitude, but with higher values for the deprotonated species (Lee et al., 2020). However, the transition of the primary oxidant from $SO_4^{\cdot-}$ to $OH^{\cdot}$ at elevated pH (Eq. 12) leads to a greater scavenging, as the latter is more readily quenched by CO_3^{2-} (Buxton et al., 1988), leading to the formation of $CO_3^{\cdot-}$. This introduces another layer of complexity to the system, as anion-derived radicals such as $CO_3^{\cdot-}$ and $Cl^{\cdot}$ (Eq. 14, 15) are generated through the reaction between naturally occurring anions in groundwater and $SO_4^{\cdot-}$ (Ji et al., 2017; Lian et al., 2017). Besides decreasing the overall oxidation kinetics (Zuo et al., 1999), these weaker oxidants are very selective and preferentially abate specific classes of electron-rich organics and lead to products that are not typically expected with $SO_4^{\cdot-}$ (Lee et al., 2020). In natural waters and wastewater effluents, $CO_3^{\cdot-}$ often becomes the dominant oxidant species due to HCO_3^-/CO_3^{2-} oxidation, not only by $SO_4^{\cdot-}$ but also by halogen radicals (Eq. 16) (Lian et al., 2017). For example, $Cl^{\cdot}$ and $Cl_2^{\cdot-}$ formed through one-electron abstraction from Cl^- by $SO_4^{\cdot-}$ (Eq. 15) (Lian et al., 2017; Lee et al., 2020). Since the reported rate constants for $CO_3^{\cdot-}$ induced oxidation of organics can be an order of magnitude below that of $Cl^{\cdot}$ (Canonica et al., 2005; Criquet et al., 2009; Kwon et al., 2015; Yang et al., 2017; Wojnárovits et al., 2020), the treatment efficiency generally decreases.

$$OH^{\cdot} + {CO_3}^{2-} \rightarrow HO^{-} + {CO_3}^{\cdot-} \quad \text{Eq. 13}$$

$${SO_4}^{\cdot-} + {CO_3}^{2-} \rightarrow {SO_4}^{2-} + {CO_3}^{\cdot-} \quad \text{Eq. 14}$$

$$Cl^{-} + {SO_4}^{\cdot-} \rightarrow Cl^{\cdot} + {SO_4}^{2-} \quad \text{Eq. 15}$$

$$Cl^{\cdot} + {CO_3}^{2-} \rightarrow Cl^{-} + {CO_3}^{\cdot-} \quad \text{Eq. 16}$$

Previous studies have shown that multiple degradation pathways of contaminants (e.g. TCE) can co-exist in base activated systems due to the presence of various ROS (Liu et al., 2021). Moreover, alkaline hydrolysis (AH) might play a significant role in TCM degradation under the elevated pH conditions employed for PS activation (Torrentó et al., 2014) and should be carefully considered within this approach. In this context, dual-element compound specific isotope analysis (2D-CSIA) is a tool that may help to distinguish the reaction mechanisms or degradation pathways by relying on the specificity in stable isotope fractionation during degradative processes (Elsner, 2010; Wiegert et al., 2012; Palau et al., 2016; Lincker et al., 2022). Assuming that different ROS would lead to different TCM degradation mechanisms and that other degradation pathways could occur (i.e., AH), this approach might shed light on the processes responsible for TCM transformation by alkaline activation of PS in different conditions.

Several dual C-Cl slope values (i.e., $\Lambda^{C\text{-}Cl}$) for TCM transformation processes have been previously reported. Regarding reductive processes, TCM degradation with cast zero valent iron, Fe(0), yields a $\Lambda^{C\text{-}Cl}$ value of 8 ± 2 at pH 7 (Torrentó et al., 2017) that remains unchanged at pH 12 (Rodríguez-Fernández et al., 2018) and has also been reported as $\Lambda^{C\text{-}Cl}$ = 5.8 ± 0.4 (Asfaw et al., 2023). TCM bacterial RD has been studied abiotically through the use of the corrinoid cofactor vitamin B12 (present in almost all reductive dehalogenases identified to date), obtaining a $\Lambda^{C\text{-}Cl}$ = 6.5 ± 0.2 (Heckel et al., 2019). When smaller doses of vitamin B12 were used to biostimulate anoxic microbial cultures, similar values (7 ± 1) were observed (Rodríguez-Fernández et al., 2018). A recent work (Heckel et al., 2022) attributed the reactivity of vitamin B12 and *Dehalobacter* CF (strain UNSWDHB) (with a $\Lambda^{C\text{-}Cl}$ = 6.6 ± 0.1) to a second-order nucleophilic substitution (S_N2) reaction. However, experiments using *Dehalobacter strain* 8M exhibited a very different $\Lambda^{C\text{-}Cl}$ value of 2.8 ± 0.3, which were ascribed to enzyme binding masking effects created by the structure of different enzymatic pockets (Heckel et al., 2017, 2019; Soder-Walz et al., 2022). A different TCM reductive mechanism, concerted dissociative Outer-Sphere Single Electron Transfer (OS-SET), was studied by experiments with $CO_2^{\cdot-}$ radical anion (Heckel et al., 2017), which produced a SET to a σ* orbital concerted with C-Cl breakage, leading to a similar $\Lambda^{C\text{-}Cl}$ = 6.7 ± 0.4. These reported $\Lambda^{C\text{-}Cl}$ values for reductive processes are in general lower compared

to those observed for AH ($\Lambda^{C\text{-}Cl}$ = 13.0 ± 0.8) and oxidation by thermally activated PS ($\Lambda^{C\text{-}Cl}$ = 17 ± 2) (Torrentó et al., 2017). This is consistent with an oxidative C-H bond cleavage by a hydrogen atom abstraction (HAA) in the case of the heat-activated PS oxidation and a stepwise $E1_{CB}$ elimination reaction, consisting of the base-catalyzed deprotonation of the TCM followed by the loss of a chloride ion, for AH degradation mechanism (Torrentó et al., 2014).

In the light of the above information, this thesis focused on the assessment of the use of C-Cl 2D-CSIA to identify the potential TCM transformation processes occurring when applying alkaline-activated persulfate in ISCO treatments. Specifically, this thesis focused on the application of PS in combination with a novel remediation strategy consisting in interception trenches filled with concrete-based residues that induce alkaline conditions in site B (Torrentó et al., 2014). TCM transformation by alkaline activated PS was reproduced in batch experiments under controlled laboratory conditions where the influence of different TCM:PS molar ratios, pH, the presence of radical-scavenger species commonly found in groundwater such as CO_3^{2-}, the remediation conditions in an alkaline trench with multiple contaminants typically found in contaminated sites (CMs and CEs), were assessed.

Chapter II. METHODOLOGY

3. General methodology

3.1. General analytical methods

3.1.1. Concentration analysis

Concentration measurements of CEs and CMs were performed by headspace gas chromatography mass spectrometry (HS-GC-MS) as explained elsewhere (Torrentó et al., 2017). The GC/MS system, located in the Scientific and Technological Centers of the University of Barcelona (CCiT-UB), consisted of a FOCUS GC coupled with a DSQ II MS (Thermo Fisher Scientific, Waltham, MA, USA). Compounds were separated in a Zebron ZB-624plus column (60m x 0.32mm x 1.8µm, Phenomenex, Torrance, CA, USA) with helium as the carrier gas (flow of 1.8 mL min^{-1}). The column was initially held at 60 ^{o}C for 2 min, ramped at 8 ^{o}C min^{-1} to 220 ^{o}C and held for 5 min. The HS extraction was conducted for 30 min at 80 ^{o}C in 10 mL vials containing 7 mL of sample or dilution. A HS volume of 1 mL was injected in split mode (11:1 split ratio) at 220 ^{o}C through a split/splitless injector using a Triplus headspace autosampler (Thermo Fisher Scientific). The interface and the ionization source were set to 260 ^{o}C and 200 ^{o}C, respectively and MS (EI, 70eV) was performed in full scan mode between 35 and 350 amu. Concentration calculations were performed using seven-point calibration curves. The error based on replicate measurements was around 5% for all the compounds. CEs and ethene concentrations in microcosm samples were measured by a GC attached with a FID at UAB laboratories.

Redox-sensitive species such as nitrate and sulfate were measured using a discrete analyzer following the modified US EPA methods Sulfate 375.4 and NH_4^+ 350.1 by Element Materials Technology (EMT), Deeside, United Kingdom. Manganese measurements were carried out by Inductively Coupled Plasma – Optical Emission Spectrometry (WATERS^{TM} ICP-OES) following the modified US EPA method 200.7. Determination of ferrous iron was conducted by spectrophotometry after reaction with sodium carbonate and morfamquat sulfate.

3.1.2. Isotopic analysis

Stable carbon isotope analysis of CT, TCM, DCM, PCE, TCE cis-DCE and VC was performed using a GC coupled to an Isotope Ratio Mass Spectrometer (GC-IRMS) at the Technological Centers of the University of Barcelona (CCiT-UB) (Blázquez-Pallí et al., 2019). The system consisted of a

Thermo Finnigan Trace GC Ultra instrument coupled via a GC-Isolink interface to a Delta V Advantage IRMS (Thermo Fisher Scientific). This GC was equipped with a Teknokroma TRB-624 column (60 m x 0.32 mm x 1.8 µm, Barcelona, Spain). The oven temperature was kept at 60 ^{o}C for 2 min, heated to 220 ^{o}C at a rate of 8 ^{o}C min^{-1} and held at 220 ^{o}C for 5 min. The injector was set to split mode with a split ratio of 1:10 at a temperature of 250 ^{o}C. Helium was used as a carrier gas (1.8 mL min^{-1}). The VOCs were extracted from the aqueous samples by automated headspace solid phase micro-extraction (HS-SPME) using a 75 µm Carboxen-PDMS fiber (Supelco, Bellefonte, PA, USA). The 20 mL vials filled with 10 mL aqueous samples were placed in a TriPlus Autosampler equipped with a SPME holder (Thermo Fisher Scientific) (Palau et al., 2007). Samples were extracted for 20 min at 40 ^{o}C and constant agitation and the SPME fibers were desorbed for 10 min at 250 ^{o}C. To correct slight carbon isotopic fractionation induced by the SPME preconcentration technique (Palau et al., 2007), the samples delta values obtained with the GC/IRMS were corrected by daily values of calibrated in-house standards of known C isotope ratios, prepared at the same concentration range than the samples and that were previously determined using a Delta V (Thermo Fisher Scientific) elemental analyzer (EA) coupled to a Delta C IRMS (Thermo Fisher Scientific) through a Conflo IV interface (Thermo Fisher Scientific) using four internal standards with known isotopic composition relative to the Vienna Pee Dee Belemnite (VPDB) standard, according to (Coplen et al., 2006). The analytical uncertainty 2 σ of carbon isotopic measurements with the GC/IRMS was ± 0.5‰.

Stable chlorine isotope analyses of CT, TCM, DCM, PCE and TCE were performed using GC-quadrupole mass spectrometry (GC-qMS). The system consisted of an Agilent 7890A GC coupled to a 5975C qMS (Agilent, Santa Clara, CA, US). Samples were prepared in 20 mL HS vials filled with 10 mL of solution. After incubating at 60 ^{o}C for 3 min, headspace samples of 1 mL were injected in the split/splitless injector (1:10 split ratio) at 250 ^{o}C using a MPS2XL combipal autosampler (Gerstel, Mülheim a/d Ruhr, Germany). The GC was equipped with a Sapiens-X5MS column (30 m x 0.25 mm x 0.25 µm, Teknokroma, Barcelona, Spain). The He flow rate was 1mL min^{-1} and the temperature program was 40 ^{o}C (2min) followed by a ramp of 15 ^{o}C min^{-1} to 130 ^{o}C and held at 130 ^{o}C for 1 min. A dwell time of 50msec was defined for all measurements and positive electron impact ionization at 70 eV was used. Chlorine isotopic analyses of cis-DCE were carried out using an Agilent 6890 GC coupled with a MAT253 IRMS (Thermo Fisher Scientific) at Isotope Tracer Technologies Inc. (Waterloo, Canada). The GC was equipped with a VOCOL column (30 m x 0.25 mm x 1.5 µm, Supelco) with He as a carrier gas (flow 6 mL min^{-1}). The oven

temperature was held at 60 ^{o}C for 22 min, ramped at 45 ^{o}C min^{-1} to 225 ^{o}C and held for 5 min. The injector was set to splitless mode at a temperature of 260 ^{o}C. The VOCs were extracted from the aqueous samples by automated HS-SPME using a 75 µm Carboxen-PDMS fiber (Supelco, Bellefonte, PA, USA). The 20 mL vials filled with 10 mL aqueous samples were placed in an autosampler equipped with a SMPE holder. Samples were extracted for 20 min at 50 ^{o}C and constant agitation and the SPME fiber was desorbed for 3 min at 260 ^{o}C.

In the GC/qMS, average δ^{37}Cl values were determined based on ten injections of each sample while two external working standards were interspersed along the sequence. In the GC/IRMS, four measurements of an external working standard were performed at the beginning, from a pure cis-DCE stored in the bellows of the Dual Inlet (DI) system of this IRMS (Shouakar-Stash et al., 2009). Raw values were determined by referencing versus one of the external working standards according to Eq.1. Precision 2σ of chlorine isotopic measurements using this system was in all the cases below ± 0.5‰ based on replicate measurements.

Raw δ^{37}Cl values were determined by evaluation of the most abundant ion peaks: m/z 164 and 166 for PCE, m/z 130 and 132 for TCE and m/z 96 and 98 for cis-DCE, which correspond to isotopologue pairs that differ by one heavy chlorine isotope ([$^{35}Cl_2{}^{12}C_2H_2$] and [$^{37}Cl^{35}Cl^{12}C_2H_2$], in the case of cis-DCE). The isotope ratio was obtained from the ratio of these isotopologues according to the molecular ion method (Elsner et al., 2008; Aeppli, et al., 2010; Jin et al., 2011):

$$R_{PCE} = \frac{1}{4} \cdot \frac{I_{166}}{I_{164}} \quad \text{Eq. 17}$$

$$R_{TCE} = \frac{1}{3} \cdot \frac{I_{132}}{I_{130}} \quad \text{Eq. 18}$$

$$R_{cDCE} = \frac{1}{2} \cdot \frac{I_{98}}{I_{96}} \quad \text{Eq. 19}$$

Where I indicates the corresponding molecular ion peak intensities at different m/z values and R is the chlorine isotope ratio. The conversion to delta values relative to the SMOC was performed by an external two-point calibration for PCE and TCE and by an external one-point calibration for cis-DCE. Precision (1σ) of the δ^{37}Cl analysis was ≤ 0.5‰ for PCE and TCE, and ≤ 0.2‰ for δ^{37}Cl of cis-DCE.

Regarding the **dual isotope slope (Λ)** calculation and its uncertainty, recent studies by Ojeda et al. (2019, 2020) suggested to use the York regression method instead of ordinary linear regression (OLR). Indeed, the OLR approach does not consider errors in the x- variable while the York method uses error in the x and y variables. According to Ojeda et al. (2019, 2020), C-Cl dual

isotope plots would be more susceptible to slope attenuation (i.e., a slope closer to zero) introduced by OLR because the analytical uncertainty for C and Cl measurements is comparable, and ignoring the error in the x- variable would lead to a stronger slope attenuation and to an artificially smaller standard error associated to OLR. A comparison between lambda values and their uncertainties obtained with the York and the OLR regression methods will be conducted in this thesis.

3.1.3. Biomolecular analysis

Biomass was harvested, either from 30 mL of field-sampled slurry or 5 mL samples from selected microcosm experiments, in sterile falcon tubes that were centrifuged at 4000 x *g* and 4 ^{o}C for 30 minutes. The supernatants were discarded, and the resulting pellets were immediately stored at -80 ^{o}C until DNA extraction. DNA extraction was performed by Institute of Agrifood Research and Technology (IRTA, Barcelona, Spain) using the DNeasy PowerSoil Pro Kit (Qiagen, Venlo, The Netherlands), following the manufacturer's instructions.

The RD genes quantified were: i) *tceA* gene, encoding for the RD enzyme of TCE to cis-DCE; ii) *vcrA* gene, encoding for VC reductase enzyme responsible for RD of cis-DCE and VC; and iii) *bvcA* gene, encoding for VC reductase enzyme responsible for RD of VC to ethene, as described elsewhere (van der Zaan et al., 2010).

qPCR analyses were conducted in the laboratories of IRTA (Barcelona, Spain) in a Real Time PCR System MX3000P (Stratagene, La Jolla, CA, US). For the quantification of 16S rRNA gene of the total bacterial population by qPCR, a Brilliant II SYBR® Green qPCR Master Mix (Agilent, Santa Clara, CA, US) was used, and amplification specificity was verified with a melting curve analysis, on a AriaMx Real Time PCR System (Agilent Technologies). For quantification, the specific 16S rRNA gene belonging to *Dhc*, as well as their functional genes for RD, specific double quenched PrimeTime® probes (IDT) were used in combination with a Brilliant II qPCR Master Mix (Agilent). Fluorescence capture was performed at 80 ^{o}C to minimize fluorescence from dimerized primers, unrelated to gene copy detection. Ten-fold serial dilutions of synthetic genes were subjected to generate standard curves, and duplicate qPCR assays were conducted within a linear range of 10^1 to 10^8 gene copies per reaction. qPCR reactions met quality standards, with efficiencies between 90% and 110% and R^2 values above 0.985. Data analysis was performed using AriaMx qPCR software (Agilent).

Log transformed qPCR data was tested for normality and homogeneity of variance using the Shapiro-Wilk test and Levene's test ($p>0.05$). Once these parameters were validated, a parametric statistical analysis was carried out (ANOVA and post hoc Tukey's test with a significance level of 5%).

3.2. Preparation of biostimulation experiments and EVO field application for CEs degradation

3.2.1. EVO injection details

A commercial EVO (EOS PRO®, EOS Remediation, LLC, Research Triangle Park, North Carolina, USA) was selected as a long-term electron donor for the site bioremediation. It is a physical emulsion consisting of soybean oil in water, vitamin B_{12} and other minor substances as emulsifiers and nutrients.

The EVO injection was conducted in eight wells (Figure 5). The injection process involved the sequential injection of 13 m^3 of an EVO solution (8% v/v), followed by 5.6 m^3 of an aqueous lactate solution (5% v/v). Lactate is a more soluble and mobile electron donor, and this solution was used to induce anoxic conditions in a shorter term. Both solutions were prepared using tap water, previously circulated through an activated carbon filter.

3.2.2. Collection of water samples

The site was equipped with 20 long screen wells installed in 2010. Eleven monitoring wells, located on the source and downgradient areas (Figure 5) were selected for the assessment of the potential natural attenuation of CEs before the EVO injection and the evolution of the contamination after the biostimulation treatment. To do so, an initial groundwater sampling campaign was carried out in June 2020, followed by the injection of EVO (September 2020) and five monitoring campaigns (November 2020, January, March, May, and September 2021). Slurry was sampled for biomolecular analysis in four injection wells (W4, W8, W10 and W11) and one control well (W5) in June 2020 (3 months before the EVO injection), in March 2021 (6 months after the injection) and only in W4 in June 2021 (Figure 5). Hydrochemical parameters, including temperature, pH, electric conductivity, Dissolved Oxygen (DO), and ORP, were measured on-site, before each sampling, using a multiparameter probe (HANNA HI98194 and sensors HANNA HI7698194) together with a flow cell to minimize contact of the sample with the atmosphere. Data were collected after parameter stabilization and ORP values were corrected to the standard hydrogen electrode (SHE). For CEs concentration and isotopic analyses, triplicate groundwater samples were collected in amber glass bottles (125 mL) filled without headspace (HS) and closed

with screw PTFE-lined septum caps to minimize adsorption and volatilization of CEs. The samples were preserved by adding concentrated HNO_3 (to pH < 2) and stored in the dark at 4 ^{o}C until analysis. Slurry for the microcosm experiments was collected from the bottom of the well W4 in June 2021. This well was selected for microcosm preparation because it presented the highest CEs concentrations and bacterial populations in the sampling before the injection (June 2020).

3.2.3. CEs-EVO partitioning experiments

Experiments were conducted to assess whether the potential partitioning of CEs between the water and EVO phases result in significant isotopic fractionation. The experimental setup (total volume of 140 mL) consisted of two polypropylene syringes connected through a 14.000 Dalton dialysis membrane (Medicell Membranes Ltd, London, UK), permeable to CEs while impermeable to EVO (Figure 8).

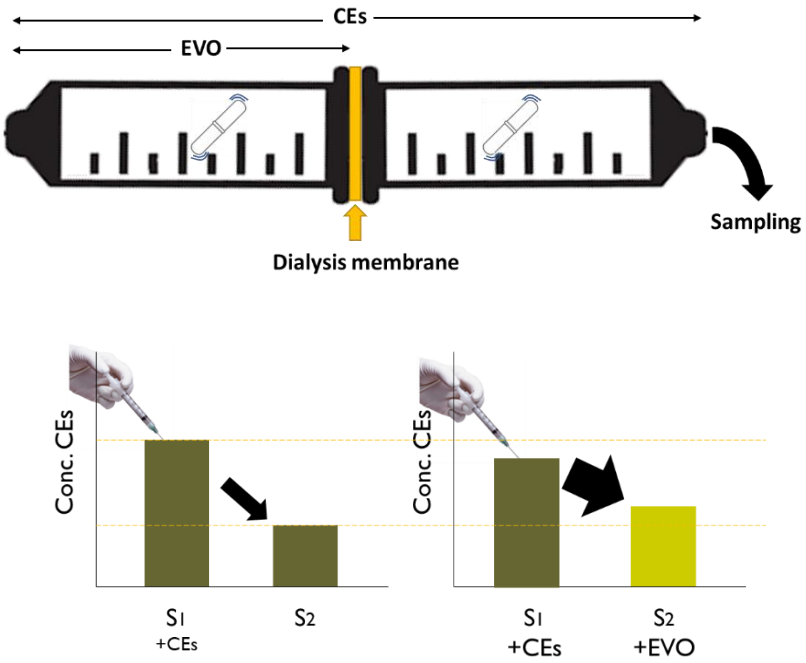

Figure 8. Above: Experiment setup consisted of two 60 mL syringes assembled with a dialysis membrane permeable to CEs but not to EVO. The controls contained water instead of the EVO solution. Below: Conceptual model of the experiments carried out to assess a possible isotopic fractionation of CEs caused by partitioning to the EVO phase. The left bar always indicates the CEs injection syringe (S1), while the second syringe (S2) does not contain CEs initially. The light green bar indicates the syringe where EVO was injected. CEs concentration bars show the expected relative differences in the CEs concentration if sorption to EVO occurs after a certain time.

One side of the system was filled with an aqueous EVO solution (8 % v/v) and the other with an aqueous CEs solution (PCE, TCE and cis-DCE) leading to initial concentrations in the system of

1.570 µg PCE/L, 2.290 µg TCE/L and 2.750 µg cis-DCE/L. All solutions were prepared using deionized water (18.2 MΩ cm at 25˚C, Direct-Q UV-3, Millipore) and their concentrations were selected to be in the range of those present in the field during the EVO injection (Table 3). Both sides of the system were stirred during the experiment using PTFE-coated magnetic stir bars to ensure the homogeneity of the solutions. The syringe tips were capped and all connections were sealed with PTFE tape and Parafilm® to minimize losses of CEs by volatilization. Two water samples (5mL) were collected after 12 and 48 hours from the side of the system filled with the CEs solution (without EVO). The water samples were stored, without headspace, in amber vials with PTFE-sealed caps, and refrigerated until concentration and isotopic analysis. The dialysis membrane prevented the presence of EVO phase in the samples as it could provoke the release of CEs from the EVO to the water during the heating of the samples in subsequent analyses. Experiments were performed in triplicates to ensure reproducibility. Control triplicates without EVO were included to account for possible losses in the system.

Table 3. CEs stock mix in methanol prepared for the partitioning experiments, the isotopic composition of each species and injected amount in the system.

CE	Stock concentration ($mg \cdot L^{-1}$)	Injected in experiment (µmol)	Isotopic composition $\delta^{13}C$ (‰)	SD
PCE	44	1.35	-30.3	0.1
TCE	64	2.47	-27.4	0.1
cis-DCE	77	3.87	-22.5	0.2

Therefore, for a given compound, sorption into the EVO phase (P_{EVO}) was evaluated as the relative difference between the average CEs concentration in the control triplicates without EVO ($CEs_{control}$) and in the experiments with EVO ($CEs_{experiment}$) (Eq. 20). We assumed that the control setup would reproduce the same behaviour as the experimental setup and, therefore, differences in the CEs concentration could be attributed to water - EVO phase partitioning.

$$P_{EVO} = \frac{CEs_{control} - CEs_{experiment}}{CEs_{control}} \quad \text{Eq. 20}$$

3.2.4. Microcosm experiments for anaerobic degradation of CEs

Laboratory microcosm experiments were conducted in order to obtain field site-specific $\varepsilon^{13}C$, $\varepsilon^{37}Cl$, and $\Lambda^{C\text{-}Cl}$ values for the RD of PCE, TCE and cis-DCE. Initially, the collected slurry from the well W4 on June 2021 (9 months after EVO injection) was purged with N_2 for 3 hours to remove

CEs. Subsequently, the microcosms were prepared inside an anoxic chamber filling 100 mL glass serum sterile bottles with 70 mL of slurry and sealed with PTFE-coated butyl rubber stoppers and aluminum crimp caps. Three sets of 13 bottles each were spiked with PCE, TCE, or cis-DCE respectively at 160 µM. Ten bottles of each set were amended with lactate (3 mM) to assess the effect of a supplementary electron donor while 3 bottles remained in field conditions (Figure 10). Three additional killed control bottles were spiked with all the contaminants together (PCE, TCE, and cis-DCE) and the biodegradation activity was immediately stopped by adding a solution of NaOH (to pH>12). The killed controls were set up to account for contaminant losses through the cap or unexpected abiotic reactions. All these bottles were incubated in the dark at 25 ^{o}C. The concentration was monitored on a daily basis by injecting 0.5 mL of microcosm HS in a GC coupled to a Flame Ionization Detector (GC-FID). Biodegradation was stopped at different degradation extents to assess the associated isotopic fractionation, by adding NaOH as described previously.

Figure 9. Microcosm bottles prepared inside an anoxic chamber at BIOREM group laboratories (UAB). Different colour labels indicated different parent compounds (PCE, TCE, cis-DCE).

In those cases where the rapid kinetics led to the complete biodegradation of the original compound before sufficient data could be obtained for the calculation of ε-values, the corresponding CE was spiked again, and subsequent sampling was performed. When multiple spikes were conducted and degradation products (particularly cis-DCE) accumulated, microcosm bottles were purged with N_2 for 20 minutes prior to the following spike. This precautionary step was taken based on previous studies that observed inhibition of RD at high CEs concentrations (Duhamel et al., 2002).

3.3. Preparation of experiments for TCM degradation

3.3.1. Batch experiments of TCM degradation by alkaline-activated PS

Batch experiments were performed to assess the TCM carbon and chlorine isotopic fractionation during its transformation by alkaline-activated PS under different conditions (see summary in Table 4). Both commercial PS with an integrated alkaline activator (PersulfOx®, from now on "PSOX") and pure sodium persulfate ("PS") were used in different experiments consisting of: (i) deionized water with PSOX (resulting in a pH of 10.2 ± 0.2) with different TCM:PS molar ratios (1:125 and 1:65), to assess the feasibility of the TCM oxidation at different PSOX dosages or in different parts of a contamination plume; (ii) deionized water basified with NaOH at different alkaline pHs (11.4 ± 0.4 and 12.83 ± 0.03), to assess if changes in pH could induce changes in the oxidation reaction, other than a greater extent of AH; (iii) basified deionized water as in experiment ii but adding Na_2CO_3 (at 200 mg/L), to resemble groundwater conditions and to evaluate the effect of CO_3^{2-} anion in the radical cascade activity; and (iv) trench-sampled water (pH 10.3 ± 0.5), co-contaminants (either CMs or CEs) and filling material, to reproduce the field conditions of an alkaline interception trench.

In the last set-up (exp. iv), solid samples from an active alkaline interception trench, composed of 40-70 mm-sized recycled concrete-based aggregates from a construction waste recycling plant (Torrentó et al., 2014) were grinded to a diameter between 2 and 8 mm and 25 g were introduced in each vial. This experiment simulated the possible interactions of the solid phases in the oxidation reaction, while maintaining the alkaline pH for PS activation via equilibrium with the portlandite ($Ca(OH)_2$) present in the concrete. In this experiment, to reproduce the oxidation reaction in the mentioned alkaline trench, and to assess the potential of 2D-CSIA to identify the underlying oxidation process and quantify the extent of the degradation, two batch experiments were conducted, one containing all CMs (CT, TCM and DCM) and another one with all the CEs (PCE, TCE, cis-DCE). For the preparation of the experiments, trench-sampled water was purged with N_2 gas for 8 hours to eliminate all volatile organic compounds present at the field site. After purging, a known concentration of the target compounds (either CMs or CEs), with a known initial isotopic composition, was added. Additionally, control vials prepared in the same conditions as the experimental ones but without PS were analyzed to account for the extent of AH in experiments i, ii and iv.

Batch experiments were prepared filling 40mL EPA VOA glass vials with a mixture of PS and TCM stock solutions to reach pre-established concentrations. In all vials, the reaction was started by adding the appropriate volume of the contaminant stock solution. The vials were filled without

headspace to avoid partitioning of the TCM between the aqueous and gas phases and were closed with PTFE-lined caps. The experiments were conducted at 23°C in the dark in a thermostatic chamber.

Table 4. Summary of alkaline-activated persulfate experiments conditions: pH, TCM:PS molar ratio, contaminants in the aqueous solution and measured initial CO_3^{2-} concentrations.

Code	Conditions	pH	Molar ratio TCM:PS	Contaminants	Initial CO_3^{2-} (mg/L)
i.a	PSOX	10.2 ± 0.2	1:65	TCM	0
i.b	PSOX	10.2 ± 0.2	1:125	TCM	0
ii.a	PS + NaOH	11.4 ± 0.4	1:65	TCM	0
ii.b	PS + NaOH	12.8 ± 0.1	1:65	TCM	0
iii.a	PS + NaOH + CO_3^{2-}	11.3 ± 0.4	1:65	TCM	110
iii.b	PS + NaOH + CO_3^{2-}	12.8 ± 0.1	1:65	TCM	110
iv.a	PS + Trench conditions	11.6 ± 0.7	1:65	TCM, CT, DCM	95
iv.b	PS + Trench conditions	11.7 ± 0.6	-	PCE, TCE, cis-DCE	95

The oxidation reaction was stopped after different reaction times by replacing 7.5 mL of the experimental solution with a 1.5M ascorbic acid (AA) solution, resulting in a molar ratio of AA:PS equal to 4:1, inducing a rapid dissociation of the PS (Huling et al., 2011). At this molar ratio, any radical reacts rapidly with the AA, inhibiting further TCM degradation (Huling et al., 2011; Cao et al., 2019). In experiment iv, the solution was previously filtered using a 0.45 µm nylon filter to separate the solid phase from the liquid samples, before the quenching procedure with AA. The 7.5 mL aliquots extracted from the experimental vials were used to measure the pH of the experiment with a pH probe (WTW pH SenTix pH 940 electrode). Duplicate samples were always collected for each reaction time and stored at 4°C in darkness until analysis.

Chapter III. RESULTS AND PARTIAL DISCUSSIONS

4. Results of the study on biostimulation of CEs using EVO

4.1. Carbon isotopic effect during water- EVO phase partitioning

The extent of CEs partitioning into the EVO phase in the laboratory tests was estimated based on the difference in the measured aqueous concentrations between the experiments with EVO and the controls without it (Eq. 20). The permeability of the dialysis membrane to CEs was confirmed in control experiments, where in general similar concentrations were observed on both sides of the system after 48 hours. The experiments with EVO showed a decrease in aqueous concentrations after 48 hours equal to 83%, 69% and 65% for PCE, TCE and cis-DCE, respectively, compared to the controls (Figure 10). These results reflected a significant partitioning of CEs into the EVO phase and were consistent with the trend to higher sorption with increasing chlorination of CEs determined in a previous study using food-grade soybean oil and synthetic groundwater (Pfeiffer et al., 2005). These authors determined soybean oil - groundwater partition coefficients (L water / L oil) of 539, 351 and 56 for PCE, TCE and cis-DCE, respectively, in a CEs solution with PCE, TCE, cis-DCE and vinyl chloride at 20 ºC.

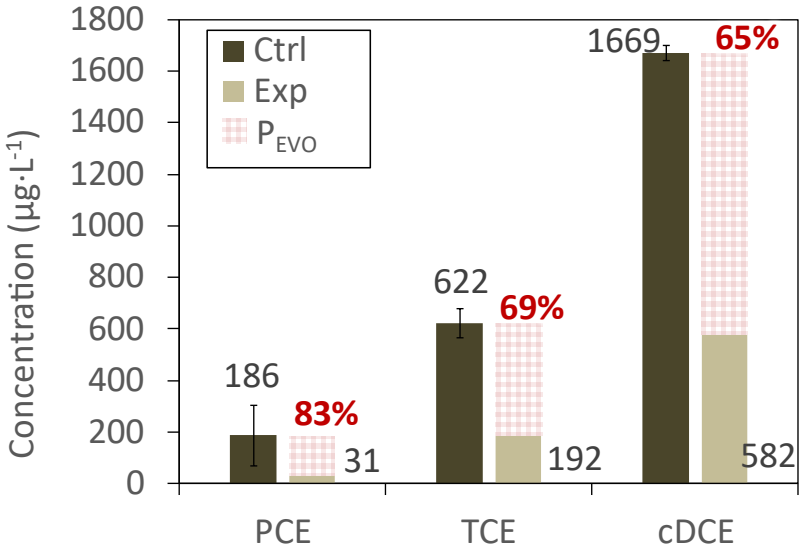

Figure 10. Aqueous concentration of CEs from the water - EVO partitioning experiments (Exp) and controls (Ctrl) after 48h. Estimated P_{EVO} in percent is depicted in the red dashed areas.

Despite the high partitioning of CEs into the EVO phase, the carbon isotopic values of the remaining CEs fraction in the aqueous phase did not exhibit significant differences (based on the

typical uncertainty of $\delta^{13}C$ analysis, ±0.5 ‰) between control and EVO experiments. Although low concentrations did not allow the measurement of $\delta^{13}C$ of PCE, nor for all the triplicates of TCE and cis-DCE, a change in the isotopic composition was not observed for TCE or cis-DCE after 48h (Figure 11). These results suggest that the carbon isotopic effect of the partitioning of these compounds into EVO during field applications will be small or insignificant compared to the biodegradation of the CEs in the groundwater.

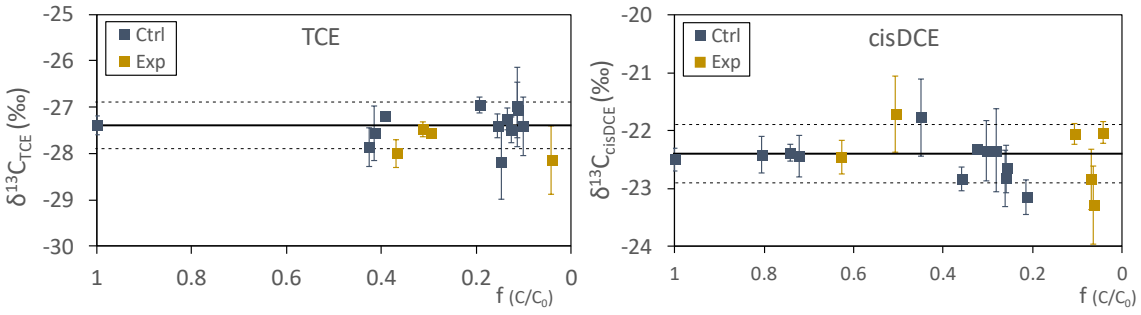

Figure 11. Carbon isotopic values of TCE and cis-DCE versus time in the experiments (yellow) and controls (dark blue) in the EVO-phase partitioning experiment. The black line indicates the carbon isotopic composition of the original compound (measured by Elemental Analyzer - IRMS) and the dashed lines show the typical analytical uncertainty of ±0,5‰.

4.2. CEs biodegradation in microcosm experiments

Complete biodegradation of PCE, TCE and cis-DCE was observed in all active microcosm experiments (see Figures A2.1, A2.2 and A2.3, in Appendix 2), while the concentrations in the killed controls remained unchanged. In microcosm bottles without lactate addition, no significant differences in biodegradation dynamics were observed (treated equally hereinafter). This can be attributed to the fact that the used slurry was already biostimulated, sampled after 9 months of EVO injection. This observation demonstrates that EVO serves as a long-term carbon source, indicating that the availability of an electron donor is not a limiting factor for RD in the microcosm experiments where lactate was not added.

Following a latency period of about 48 hours after PCE and TCE were spiked (Figures A2.1 and A2.2, in Appendix 2), rapid biodegradation was observed, as these compounds were completely depleted after 96 hours. In this case, re-spiking of the compounds was necessary to obtain samples at different degradation extents for the calculation of ε-values. When it was necessary, the microcosms were purged to prevent inhibition of OHRB due to toxicity caused by the accumulation of degradation products as this process has been previously documented

(Duhamel et al., 2002). Unlike PCE and TCE, cis-DCE microcosms did not exhibit a latency period and its degradation rate was slower, requiring around 16 days to complete the transformation of cis-DCE into VC (Figure 12). This longer biodegradation period allowed for detailed sampling, representative of different extents of cis-DCE transformation (Figure A2.3, in Appendix 2). The absence of a lag face for cis-DCE might be attributed to the fact that cis-DCE and VC were already the predominant contaminants in the sampled slurry, rendering the functional genes for PCE and TCE degradation inactive.

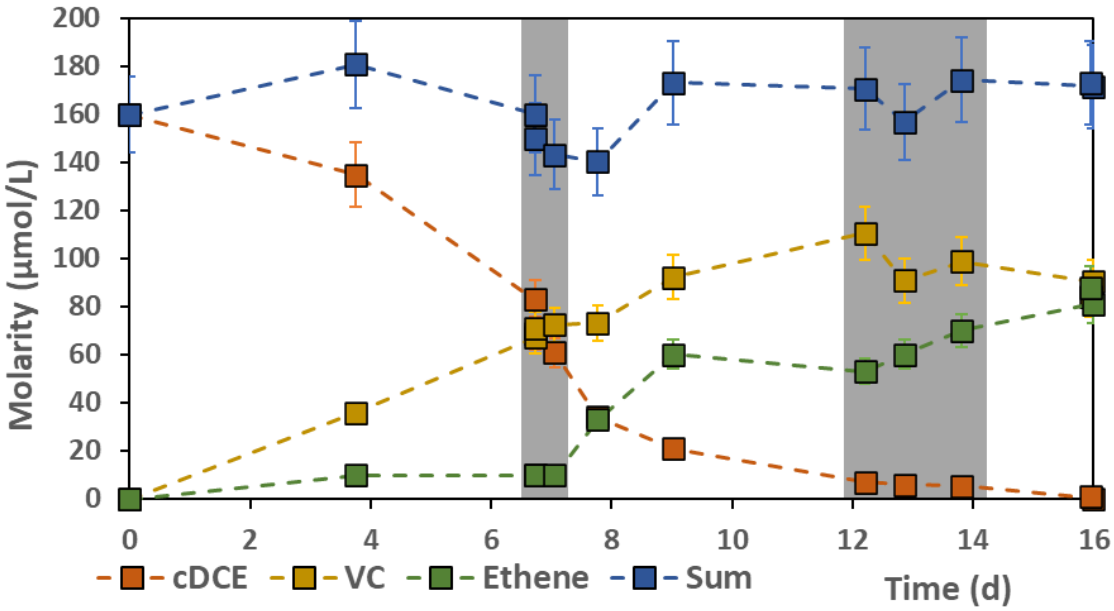

Figure 12. Molarity of original compound and degradation products in microcosms amended with cis-DCE (160µM). The shaded areas indicate the microcosms sampled for subsequent microbiological analysis.

4.3. Geochemical conditions and CEs biodegradation in the field

In general, groundwater was characterized by anoxic conditions prior to the injection, with DO values close to 0 mg/L in all measurements, except for well W6 with 0.29 mg/L. Other redox-sensitive species, such as nitrate and sulfate, with concentrations up to 33 mg/L and 125 mg/L, respectively, before the injection (June 2020) were strongly depleted by March 2021 (Figure 13). On the other hand, dissolved manganese and methane concentrations strongly increased (even in observation wells such as W9 located around 30m downstream from the source area), with some wells showing methane concentrations exceeding 20 mg/L (Figure 13). This shift to stronger reducing conditions after the EVO injection, which fall within the range of sulfate-reducing to methanogenic conditions, was favorable for RD of CEs (Leeson et al., 2004). ORP values indicated a clear transition to stronger reducing conditions after the EVO injection (Figure

13) from values higher than +100 mV to values as low as -150 mV. These values indicated favorable conditions for RD according to Leeson et al., 2004 and Henterly et al., 2015. On the other hand, pH values first slightly decreased from the initial average value of 7.1 to 6.5, probably due to both the fermentation of electron donors and the dechlorination of CEs (McCarty et al., 2007). However, the natural buffering capacity of the aquifer slowly shifted pH towards the original values over the sampling period, with an average value of 6.8 after 12 months.

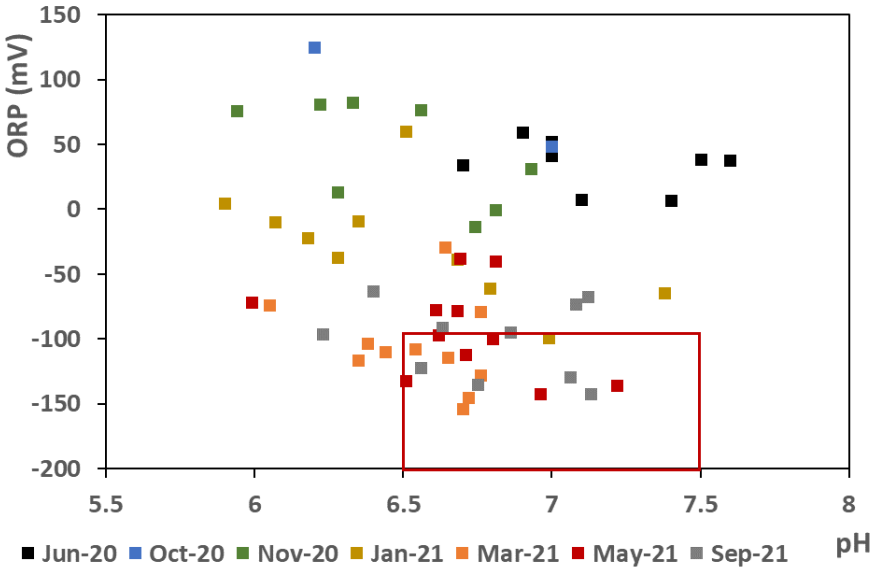

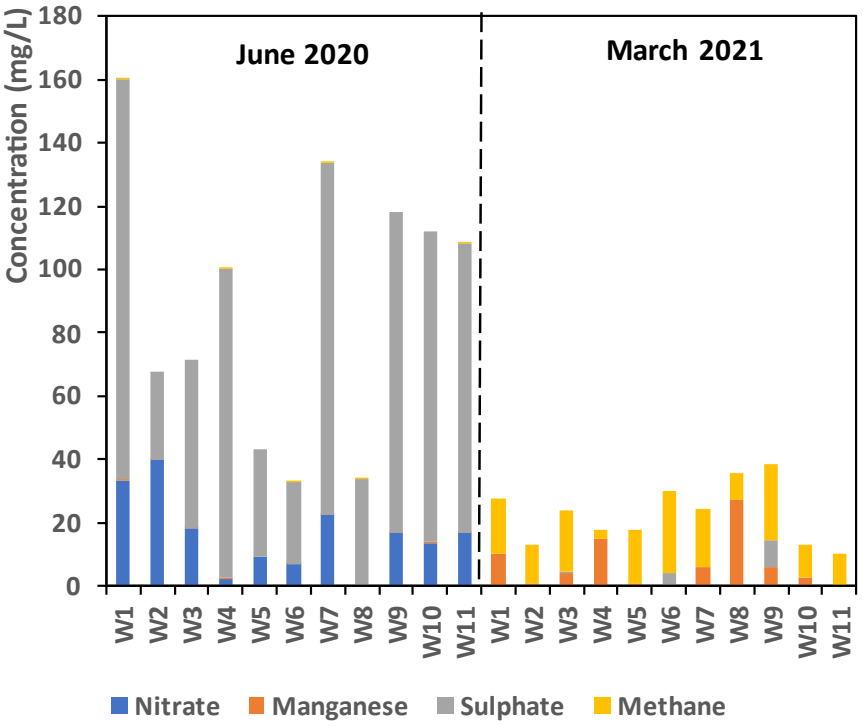

Figure 13. Above: Field values of pH vs ORP measured over 12 months after injection. The area in the red square indicates the optimal conditions for RD according to Leeson et al. (2004); Below: Concentration of nitrate, sulfate, manganese, and methane before the injection of EVO (June 2020) and six months after the injection (March 2021).

Regarding the concentration of CEs, prior to the EVO injection (June 2020) PCE and TCE were the predominant CEs in the contaminated area, accounting for 50 to 90% of the dissolved CEs molar concentration (Figure 14 and Figure 15). However, the presence of the dechlorination products cis-DCE and VC in some wells was indicative of PCE and TCE natural attenuation to some extent, in agreement with the anoxic conditions observed previous to the EVO injection (Figure 13). Two months after the injection, the degradation products cis-DCE and VC were already predominant in all the wells, accounting for nearly 100% of the dissolved CEs in many of them (Figure 14). The average measured PCE and TCE concentration dropped from 4.599 to 44 µg/L and from 3.074 to 37 µg/L, respectively. Conversely, the degradation products average concentrations increased from 3.323 to 22.082 µg/L for cis-DCE and from 1.515 to 4.035 µg/L for VC.

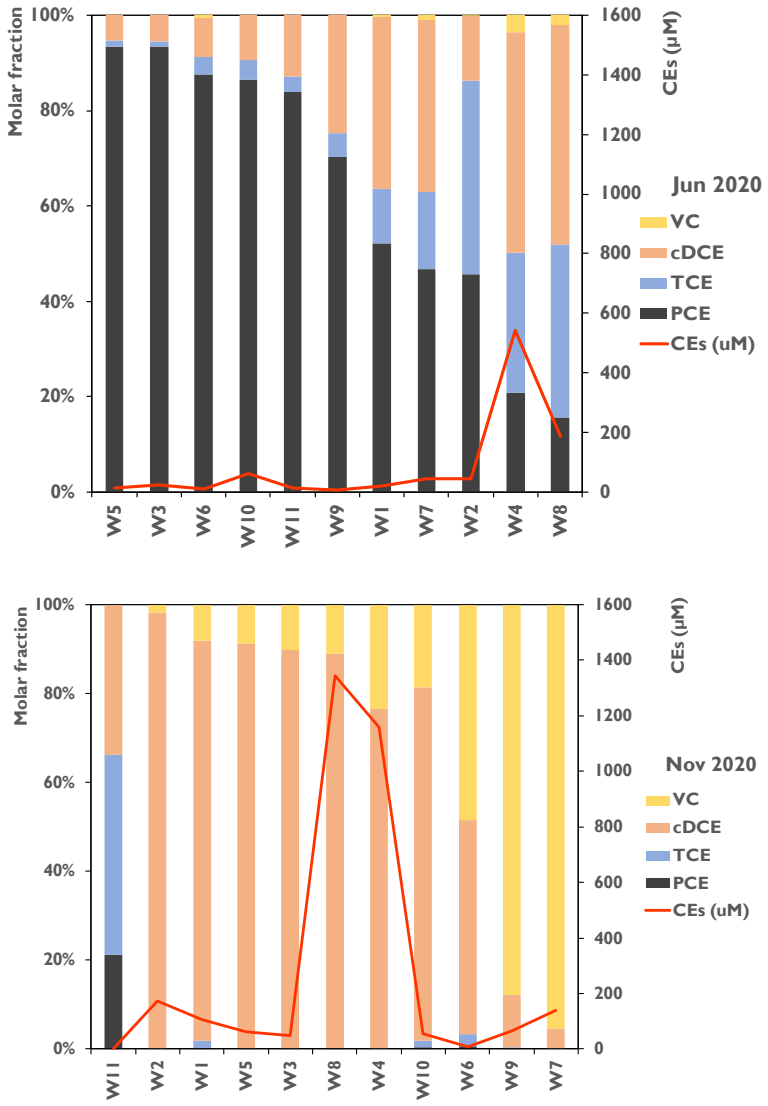

Figure 14. Molar fraction (µM/µM) of CEs in the 11 monitoring wells before the biostimulation (above) and two months after EVO and lactate injection (below). The red line represents the total concentration of CEs in µmol L^{-1}.

The analysis of the total molarity of CEs showed, in most of the wells, an increase after the injection (Figure 15). This phenomenon has been previously observed in other EVO field applications (Révész et al., 2014) and it could be caused by the mobilization of remaining DNAPL or adsorbed CEs on the aquifer solid material. In the studied site, this mobilised DNAPL could have been rapidly degraded to cis-DCE, as rapid biodegradation rates were observed in microcosm experiments, causing the high cis-DCE concentrations measured after the injection. On the other hand, wells W4 and W8, located in the source area (Figure 5), showed significantly higher concentrations than the other wells, which might indicate that DNAPL existed nearby.

Additionally, well W11 was the only one which presented high PCE and TCE molar fractions in the following campaigns, until March, while on W9 PCE and TCE were not found in the November monitoring, but a rebound was observed in March and May. Finally, the total CEs concentration had significantly decreased in all wells by September 2021, apart from the well W1, where an increase in the total molarity of CEs was observed.

The rapid transition to a system dominated by degradation products cis-DCE and VC indicates that PCE and TCE are rapidly transformed at the site, in agreement with the fast PCE and TCE biodegradation observed in the microcosm experiments. However, other processes such as partitioning of CEs to the injected EVO phase (higher for PCE and TCE compared to cis-DCE, see Figure 10) and CEs mobilization/desorption during the EVO injection can also affect the parent compounds / daughter products ratios. Therefore, the use of isotopic and biomolecular tools to document CEs transformation in complex systems, like the in-situ biodegradation using EVO, is warranted. In most wells, a slow decrease of cis-DCE molar fraction is observed over time, transitioning to a VC-dominated system. In this scenario, the assessment of cis-DCE (and VC) transformation is crucial to evaluate the effectiveness of the biostimulation treatment. Overall, concentration data indicate that the injection of EVO enhances the degradation of PCE and TCE within a relatively short timeframe, while the degradation kinetics of cis-DCE to VC is slower.

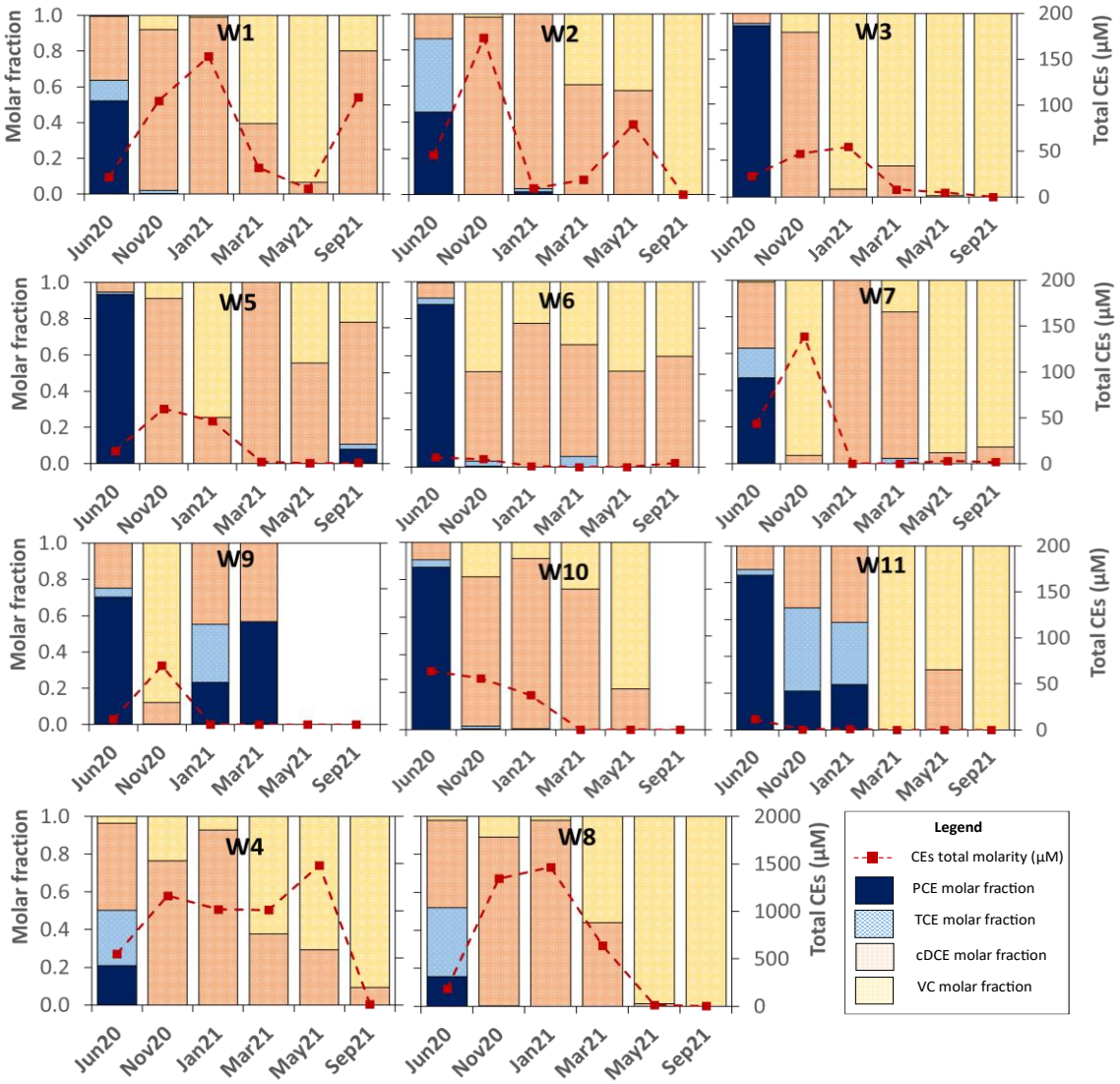

Figure 15. Sixteen-month evolution of CEs molar fractions in µM/µM (stacked charts) and total concentration of CEs (dashed lines) in the eleven monitored wells. First column shows the data of the sampling before the EVO injection. The following columns indicate molar fractions after injection.

4.4. Microbiological analyses in microcosms and field samples

For the microcosm experiments, only the data from those spiked with cis-DCE are discussed. For the experiments with PCE or TCE correlating microbiological activity with the degradation of the respective parent compound was not possible due to their rapid biodegradation, as well as the re-spikes and purges (see figure A2.1 and A2.2 in Appendix 2). Additionally, the limited number of samples hindered the analysis of triplicates with similar degradation extent. In contrast, the slower degradation of cis-DCE allowed for more extensive sampling and triplicate qPCRs were conducted for 60% degradation after 7 days (t_1), and over 97% degradation after 12 days (t_2).

Original triplicates of unpurged groundwater collected from W4 well (Figure 5) were also analyzed as the initial value (t_0).

At t_1, the population of *Dhc* and Rdhase abundance slightly decreased (10 %, $P > 0.05$) compared to the initial value (Table 5). This *Dhc* decline, along with a significant total bacterial population drop, could have been caused by purging disturbance and a period of absence of CEs until they were spiked. Similar observations of decay in *Dhc* populations and Rdhs gene population due to the absence of CEs have been previously reported (P. K. H. Lee et al., 2006). Contrastingly, at t_2 the *Dhc* population had increased significantly ($P < 0.05$), by 35-fold compared to the initial measurements, reaching values of 7.0 10^6 16S-Dhc mL^{-1}, while the functional gene populations also showed a substantial increase ($P < 0.05$): 8-fold higher for *tceA (8.7 10^6 gene copies mL^{-1})*, 1.4-fold for *bvcA (4.1 10^5 gene copies mL^{-1})* and 5-fold for *vcrA (6.1 10^6 gene copies mL^{-1})*.

Table 5. qPCR results for groundwater samples and microcosm experiments regarding total bacterial population (16S rRNA), *Dhc* and functional genes tceA, bvcA and vcrA. All analyses were performed in triplicate. n.a. and n.d. stand for not analyzed and not detected, respectively. Different subscript letters in each gene population represent significant differences (n = 3, $P < 0.05$, Post Hoc Tukey tests).

Field data							
Well	Date	Gene copies 16S rRNA mL^{-1}	Gene copies 16S rRNA *Dhc* mL^{-1}	%*Dhc*	Gene copies *tceA* mL^{-1}	Gene copies *bvcA* mL^{-1}	Gene copies *vcrA* mL^{-1}
W4	Jun-20	1.14E+05$_a$	1.10E+03$_a$	1.0	8.57E+01$_a$	9.13E+01$_a$	3.77E+03$_a$
W4	Mar-21	1.04E+05$_a$	1.40E+04$_b$	13.5	3.83E+04$_b$	2.00E+04$_b$	3.75E+04$_b$
W4	Jun-21	1.67E+06$_b$	1.97E+05$_c$	11.8	1.08E+06$_c$	3.02E+05$_c$	1.19E+06$_c$
W5	Jun-20	4.76E+04$_a$	2.88E+00$_d$	0.0	n.a.	n.a.	n.a.
W5	Mar-21	2.05E+06$_b$	2.89E+04$_b$	1.4	n.a.	n.a.	n.a.
W8	Jun-20	1.49E+04$_c$	4.17E+00$_d$	0.0	n.a.	n.a.	n.a.
W8	Mar-21	1.36E+07$_d$	4.19E+06$_e$	30.8	1.78E+07$_d$	1.55E+06$_c$	3.53E+06$_c$
W10	Jun-20	1.12E+05$_a$	4.77E+01$_d$	0.0	n.d.	n.d.	n.d.
W10	Mar-21	1.79E+07$_d$	1.02E+06$_e$	5.7	5.18E+06$_e$	1.09E+02$_d$	3.83E+06$_c$
W11	Jun-20	7.59E+02$_e$	1.50E+01$_d$	2.0	n.a.	n.a.	n.a.
W11	Mar-21	1.46E+07$_d$	8.95E+04$_{bc}$	0.6	n.a.	n.a.	n.a.
Microcosm experiments							
Microcosm	Degradation (%)	Gene copies 16S rRNA mL^{-1}	Gene copies 16S rRNA *Dhc* mL^{-1}	%*Dhc*	Gene copies *tceA* mL^{-1}	Gene copies *bvcA* mL^{-1}	Gene copies *vcrA* mL^{-1}
cDCE (t_0)	0	1.67E+06$_b$	1.97E+05$_c$	11.8	1.08E+06$_c$	3.02E+05$_c$	1.19E+06$_c$
cDCE_1 (t_1)	58	9.70E+05$_b$	7.02E+03$_{ab}$	0.7	7.61E+04$_b$	1.12E+04$_b$	2.92E+04$_b$
cDCE_2 (t_2)	98	4.81E+06$_{ab}$	7.03E+06$_e$	>70	8.66E+06$_c$	4.12E+05$_c$	6.11E+06$_c$

The expression of *tceA* and bvcA genes are associated with the transformation of cis-DCE to VC and VC to ethene, respectively, which is in agreement with the rise of the molar fraction of

ethene in the microcosms (Figure 12). The functional gene *vcrA* can be associated with both cis-DCE and VC degradation (Lee et al., 2006; Blázquez-Pallí et al., 2019; Franke et al., 2020). These results showed that Dhc populations and RD functional genes were good indicators of cis-DCE and VC biodegradation in the microcosm experiments performed.

In the field, the total bacterial population was heterogeneously distributed in the contaminated site before the injection of EVO, with values from different wells between 10^2 and 10^5 gene copies of 16S rRNA (see Table 5). The lowest population was observed in W11, while the highest ones were found in W4 and W10 (Figure 5). This distribution was apparently neither related to initial CEs concentrations nor redox conditions. However, it could have influenced the PCE and TCE slower biodegradation observed in the well with lower population (W11). *Dhc* populations were present in all the wells before the EVO injection, with a maximum value of $1 \cdot 10^3$ gene copies mL^{-1} in W4. Previous studies indicated that *Dhc* populations in groundwater must exceed 10^4 copies mL^{-1} for acceptable RD to occur (Lu et al., 2006; Ernst, 2009; Ritalahti et al., 2010). Consequently, although the quantification of *Dhc* was indicative of the potential of bioremediation in the contaminated site, the *Dhc* population was not sufficient for effective natural attenuation. A different situation was observed six months after the EVO injection. Then, *Dhc* gene copies mL^{-1} above 10^4 were measured in all wells, reaching values up to 10^6 gene copies mL^{-1} in W8 and W10 ($P < 0.05$ compared to initial values in each well, Table 5). The amount of *Dhc* relative to the total bacterial population, between 0 and 2% before the EVO injection, generally increased after the biostimulation reaching values above 10% in W4 and 30% in W8 wells. Only groundwater from the W4 well was analyzed in June 2021, but *Dhc* gene copies were still increasing, accounting for $1.95 \cdot 10^5$ *Dhc* $mL^{-1}$and suggesting that RD could be still ongoing.

Functional gene quantification was conducted in samples from W4 and W10 in June 2020 and March 2021, from W8 in March 2021 and from W4 in June 2021. Prior to the injection, (June 2020) functional genes *tceA, bvcA* and *vcrA* were detected in W4 but not in W10. This result could explain the much higher molar fraction of cis-DCE and VC in W4 compared to W10 before the treatment. Six months after the EVO injection, *Dhc* population in W10 had increased by 5 orders of magnitude, and genes *tceA* and *vcrA* reached values of 10^6 copies mL^{-1}. However, bvcA gene copies remained lower than in the other wells (10^2 genes mL^{-1}). This could indicate that, although having the capacity for RD of TCE, the *Dhc* population in W10 was different from those in W4 and W8, where the *bvcA* gene copies increased the same magnitude as *tceA* and *vcrA*. It is important to note that the number of copies of the *vcrA* gene in field samples is often higher

than the total *Dhc* population. This may indicate that vcrABC cluster, typically found in *Dhc* genomic islands, could also be present in other OHRB by horizontal transfer or that this cluster is repeatedly present in *Dhc* genome as described by McMurdie et al (2011).

Microbiological analyses of field samples were consistent with the results observed in the cis-DCE microcosm experiments. Microbiological field data also showed an increase in i) *Dhc* population relative to the total bacterial population and ii) functional genes related to RD (*tceA, bvcA* and *vcrA*). This suggests that the *Dhc* were most probably the drivers of RD in both the field and the microcosm experiments. Hence, the isotopic results obtained in the microcosm experiments might be representative for the analysis of biodegradation pathway and extent in the field.

4.5. Carbon and chlorine isotope fractionation values and dual element isotope trends from the field-derived microcosms

In microcosm experiments, selected bottles were sacrificed at different extent of CEs degradation (see Appendix 2). Water samples were collected for isotopic analysis and the isotopic fractionation ($\varepsilon^{13}C$ and $\varepsilon^{37}Cl$) for the RD of PCE, TCE and cis-DCE was determined according to Eq.2. The carbon isotopic fractionation of VC was also estimated from the cis-DCE microcosms experiment using only the $\delta^{13}C_{VC}$ values of those samples where cis-DCE was already consumed (see section 4.5.3.). Given the fast degradation of PCE and TCE in both the microcosm experiments and in the contaminated site after the EVO injection, cis-DCE was the predominant contaminant in the experiments (Figure 12) and in many wells during the investigated period (Figure 15). Furthermore, as the use of multi-element isotope data to investigate the fate of cis-DCE in the field is still very scarce in the literature (Zimmermann et al., 2020), the discussion of isotopic data from both the experiments and field samples will be focussed on cis-DCE (section 4.6), while the results for all the compounds are briefly described in the following subsections. All the εC, εCl and $\Lambda^{C\text{-}Cl}$ values calculated by OLR are summarised in Table 6.

Table 6. Calculated values of εC, εCl and ΛC-Cl for all compounds in the microcosm experiments and for cis-DCE in the field application.

	εC	95% CI	εCl	95% CI	$\Lambda^{C\text{-}Cl}$	95% CI	N
PCE microcosms	-1.1	0.7	-0.4	1.3	0.8	0.4	7
TCE microcosms	-8	5	-2	1	5	1	8
cis-DCE microcosms	-7	2	-1.5	0.4	4.9	0.8	14
VC microcosms	-31	7	n.a.	n.a.	n.a.	n.a.	4
cis-DCE (field application)	n.a.	n.a.	n.a.	n.a.	5	3	21

A comparison between lambda values and their uncertainties obtained in our experiments study with York and the OLR regression methods is shown in Table 7. For OLR, slope attenuation is observed for $\Lambda^{C/Cl}$ in all cases as predicted by Ojeda et al. (2019, 2020). It is also worth noting the contribution of York method to reduce the bias or associated error of $\Lambda^{C/Cl}$ for cis-DCE in the field samples. Nevertheless, the differences between slopes obtained with both methods are not significant for microcosm experiments or the field application data. Since no systematic bias introduced by OLR was observed for $\Lambda^{C/Cl}$ and because there has not been sufficient time for the York methods to be routinely adopted in 2D-CSIA studies, we therefore decided to use OLR, while reporting the York results for future reference.

Table 7. 2D-dual C-Cl isotope slope calculated for all compounds in the microcosm experiments, obtained by OLR or by the York regression method. Two-tailed hypothesis testing was used for comparison between OLR and York methods results. All comparisons were considered statistically significant at the α=0.05 level. N=number of points, 95% CI = 95% confidence interval.

		$\Lambda^{C/Cl}$	95% CI	N	z-score	p-value	Significant difference (α = 0.05)
PCE microcosms	Linear regression	0.8	0.4	7	-0.555	0.592	no
	York Method	1.0	0.7	7			
TCE microcosms	Linear regression	5	1	8	-0.636	0.537	no
	York Method	6	2	8			
cis-DCE microcosms	Linear regression	4.9	0.8	14	-0.819	0.421	no
	York Method	5.2	0.1	14			

4.5.1. PCE isotope data and dual-element isotope trends

The reductive dechlorination of PCE in the microcosm experiments was associated with small carbon and chlorine isotope effects (ε_C = -1.1 ± 0.7, ε_{Cl} = -0.2 ± 1, Table 6). The obtained (Λ^{C-Cl} = 0.8 ± 0.4) was similar to that reported for *Sulfurospirillum* (consortium SL2-PCEb), with $PceA_{PCE}$ enzyme (Λ^{C-Cl} = 0.7 ± 0.2) (Badin et al., 2014) and different than those reported for *Desulfitobacterium* (Λ^{C-Cl} between 2.9 ± 0.9 and 3.8 ± 0.2) (Wiegert et al., 2013; Cretnik et al., 2014a; Lihl et al., 2019) and *Sulfurospirillum* (consortium SL2-PCEc) with with $PceA_{TCE}$ enzyme

($\Lambda^{C\text{-}Cl}$ = 2.7 ± 0.3) (Badin et al., 2014) (Figure 16). To the best of our knowledge, the $\Lambda^{C\text{-}Cl}$ values for PCE degradation by *Dhc* have not been reported so far.

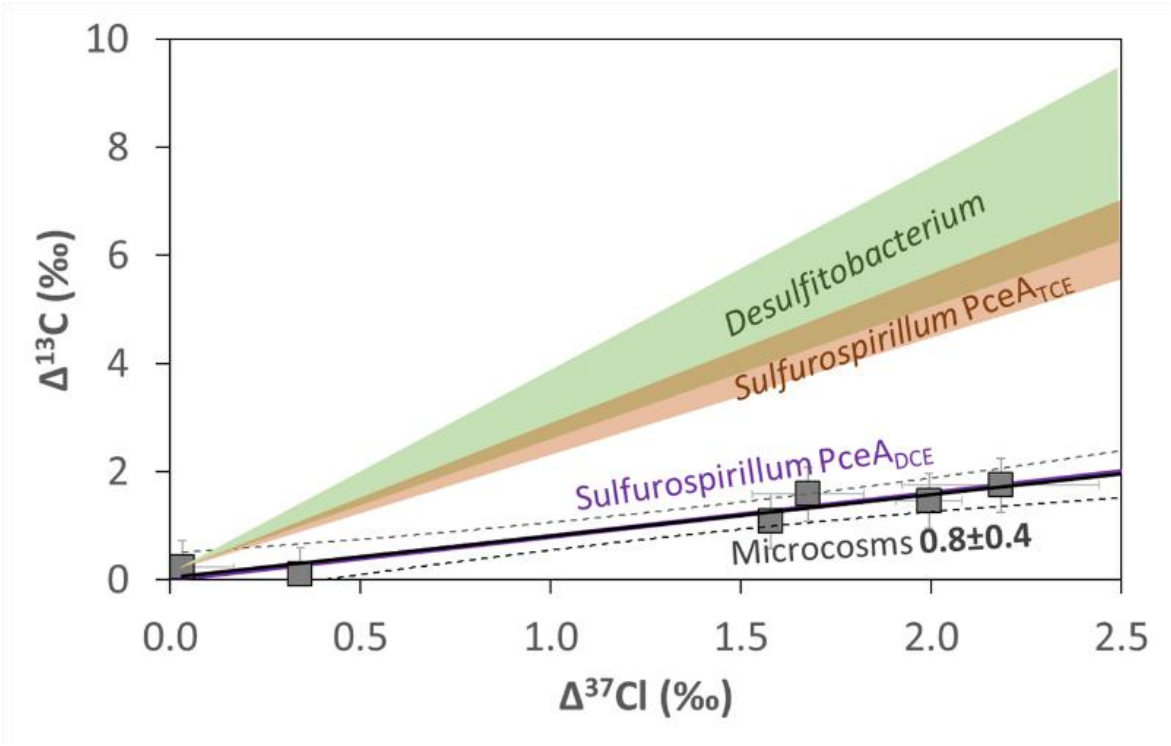

Figure 16. PCE dual element isotope plot obtained for the microcosm experiments (black line) with 95% CI (dashed lines). The previously reported slopes for *Sulfurospirillum* (with gene $PceA_{DCE}$ or $PceA_{TCE}$) and *Desulfitobacterium* are also shown in green and orange shaded areas, respectively.

4.5.2. TCE isotope data and dual-element isotope trends

The carbon and chlorine isotope effects of TCE during RD in the microcosm experiments where ε_C = -8 ± 5, and ε_{Cl} = -2 ± 1 (Table 6). The dual-element isotope trend ($\Lambda^{C\text{-}Cl}$ = 5 ± 1) is similar to previously reported values for RD by *Dhc* (4.8 ± 4.5, Kuder et al., 2013) and *Sulfurospirillum* (5.3 ± 0.3, Renpenning et al., 2014) (Figure 17). In contrast, the slopes reported for *Desulfitobacterium* and *Geobacter* are significantly different, ranging from 2.7 ± 0.8 to 3.4 ± 0.2 (Wiegert et al., 2013; Cretnik et al., 2013, 2014a; Lihl et al., 2019). Recent studies on TCE aerobic biodegradation by methane oxidizers showed low carbon isotope fractionation, leading to dual slope values ranging from 1.1 to 1.8 (Gafni et al., 2020). The $\Lambda^{C\text{-}Cl}$ values determined in previous studies for abiotic RD of TCE (e.g., by Fe (0) or FeS) are also indicated in Figure 17 (Audí-Miró et al., 2013b; Liu et al., 2014; Zimmermann et al., 2020).

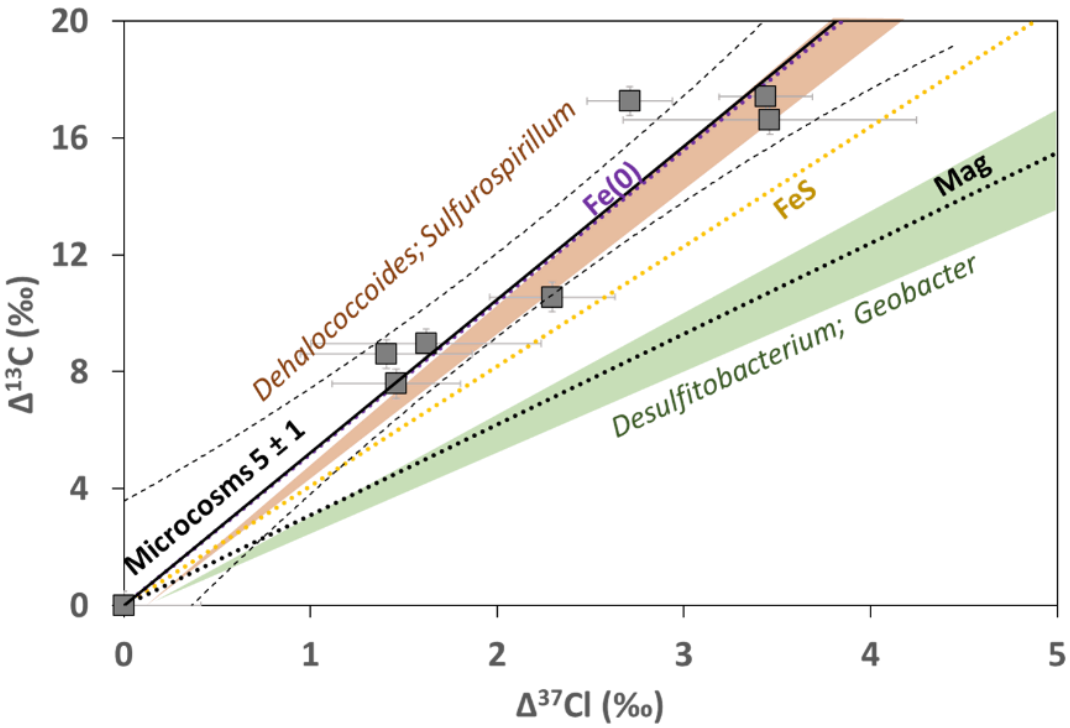

Figure 17. TCE dual-element isotope plot obtained from the microcosm experiments (black line) with 95% CI (dashed lines). Previously reported slopes for microbial RD by *Dhc*, *Sulfurospirillum*, *Geobacter*, as well as abiotic RD by Fe(0), FeS and magnetite are illustrated.

4.5.3. VC isotope data

The carbon isotopic fractionation of VC was estimated from the microcosm experiment of cis-DCE. To minimise the effect of ongoing VC formation from RD of cis-DCE, only isotopic data from microcosms with cis-DCE molar fraction < 5% and $\delta^{13}C$ values of VC more enriched in ^{13}C than the original cis-DCE were used for the calculation. Only four measurements met both criteria, which resulted in a relatively high uncertainty of the estimated εVC (i.e., -31 ± 7 ‰, Table 6). Nevertheless, this value is consistent with those reported in previous studies for RD of VC: -25.0 ± 0.7‰ and -28 ± 2‰ (Abe et al., 2009b; Kuder et al., 2013).

4.5.4. cis-1,2-DCE isotope data

For cis-DCE, determined isotope fractionation values, i.e., $\varepsilon^{13}C$ = -7 ± 2‰ and $\varepsilon^{37}Cl$ = -1.5 ± 0.4‰ (Table 6), were lower than those reported in previous isotopic laboratory studies of anaerobic biodegradation of cis-DCE using pure and mixed cultures (Bloom et al., 2000; Abe et al., 2009b; Fletcher et al., 2011; Kuder et al., 2013; Doğan-Subaşı et al., 2017; Lihl et al., 2019): from -31 to -14.9‰ (n=7) and from -3.3 to -1.6‰ (n=5) for $\varepsilon^{13}C$ and $\varepsilon^{37}Cl$,

respectively. This suggests that despite following the same degradation pathway, isotope masking could significantly influence isotopic fractionation. Masking processes can be associated with the effect of rate-limiting (non or slightly isotope fractionating) steps preceding the bond cleavage such as contaminant mass transfer (Aeppli et al., 2009; Renpenning et al., 2015). Although considerable partitioning of the contaminant between the EVO and water phases, described in subsection 3.1, might cause a mass transfer-related masking effect as reported by Aeppli et al., 2009, this is an unlikely explanation, as the microcosms did not contain an observable EVO phase and the injected amendment was lactate.

In contrast to single-element isotope fractionation analysis, combined shifts in isotope ratios of two elements in a dual-element isotope plot ($\Lambda^{C\text{-}Cl}$) should avoid the effect of isotope masking since the proportion of changes in isotope ratios of both elements relative to each other ($\Delta\delta^{13}C$ / $\Delta\delta^{37}Cl$) is largely unaffected by nondegradative processes (Elsner, 2010; Thullner et al., 2013).

The dual-element isotope trend determined from microcosm experiments, i.e., $\Lambda^{C\text{-}Cl}$ = 4.9 ± 0.8 (Figure 19) was lower than the range observed from previous laboratory studies with pure and mixed cultures, i.e., between 17.8 and 8.3, n = 4 (Ojeda et al., 2020). However, the value obtained in this study agrees well with the one reported in a previous study using field-derived microcosms, i.e. $\Lambda^{C\text{-}Cl}$ = 4.5 ± 3.4 (Doğan-Subaşı et al., 2017) (see discussion in subsection 4.6).

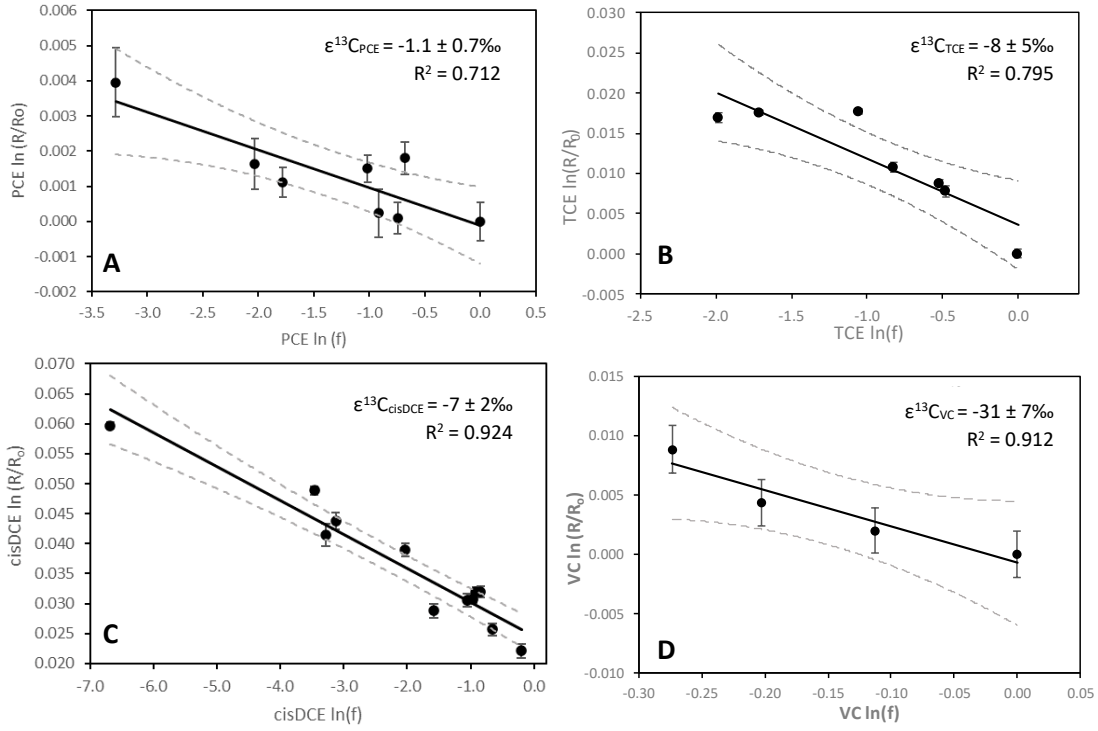

Figure 18. Rayleigh plots for carbon isotope ratios of PCE (A), TCE (B), cis-DCE (C), and VC (D) from the laboratory microcosm experiments. Isotopic fractionation values were estimated using Eq. 2 (95% confidence interval).

4.6. ^{13}C- and ^{37}Cl-CSIA of cis-DCE in field samples and dual-element isotope trend

In contrast to PCE and TCE, which were rapidly consumed in most of the wells, high fractions of cis-DCE were in general measured during the investigated period (Figure 15), allowing the analysis of both carbon and chlorine isotopes in groundwater samples from all wells at multiple times.

The samples collected before the EVO injection (June 2020) showed cis-DCE $\delta^{13}C$ values ranging from -34.1 to -14.9‰ and most $\delta^{37}Cl$ values ranging between +2.7 and +5.1‰. This isotopic pattern would reflect the formation of cis-DCE from TCE, which is consistent with values reported by (Cretnik et al., 2014c) and coherent with the high molar fractions of TCE and PCE in June 2020 (Figure 15).

Conversely, the samples collected after the EVO injection showed in general a trend towards more positive $\delta^{13}C$ and $\delta^{37}Cl$ values (Figure 19). Such enrichment in both ^{13}C and ^{37}Cl indicate the transformation of cis-DCE following the biostimulation treatment. In order to determine the dual-element isotope trend during cis-DCE transformation in the field after the EVO injection, $\delta^{13}C$ and $\delta^{37}Cl$ values were combined in Figure 19. To avoid the effect of ongoing cis-DCE formation from RD of TCE, only isotopic data from those samples where PCE and TCE were not detected were considered (n = 21). As a result, a $\Lambda^{C\text{-}Cl}$ value of 5 ± 3 was determined (Figure 19), which is similar to the value obtained from the laboratory experiments performed in this study ($\Lambda^{C\text{-}Cl}$ = 4.9 ± 0.8). This result indicates that microbial RD of cis-DCE via hydrogenolysis to VC was controlling the fate of cis-DCE at the site after the EVO injection. These results agree with the detection of VC (molar fraction > 5%) in all selected samples.

For field samples, the difference in slopes obtained using the ORL and York method highlights the York method contribution to reduce the bias or associated error in $\Lambda^{C/Cl}$ for cis-DCE (Table 8). Nevertheless, the differences between obtained slopes with both methods are not significant. Therefore, the ORL results will be used hereafter.

Table 8. 2D-dual C-Cl isotope slope calculated for cis-DCE in the field application, obtained by linear regression (OLR) or by the York regression method. Two-tailed hypothesis testing was used for comparison between OLR and York methods results. All comparisons were considered statistically significant at the α=0.05 level. n=number of points, 95% CI = 95% confidence interval.

		$\Lambda^{C/Cl}$	N	95% CI	z-score	p-value	Significant different (α = 0.05)
Field application cis-DCE	Linear regression	5	21	3	-2.344	0.025	no
	York Method	7.7	21	0.2			

It is interesting to note that despite microbiological data pointed to *Dhc* bacteria as the most likely responsible for RD of cis-DCE in both the field site and microcosm experiments (see section 4.4), reported Λ^{C-Cl} values for microbial RD of cis-DCE by *Dhc* strains (i.e., *D. mccartyi* strain BTF08, 18 ± 1, and strain 195, 10.0 ± 0.4 (Lihl et al., 2019)) and mixed cultures containing *Dhc* spp. (8.3 (Kuder et al., 2013) and 11.4 ± 0.6 (Abe et al., 2009a)) were higher than those determined in this study (Figure 19). This difference might be related with distinct reaction mechanisms during RD of cis-DCE by *Dhc* bacteria. Furthermore, discrepancies on Λ^{C-Cl} values, especially when small isotopic fractionation is observed for both carbon and chlorine, might not reflect the chemical reaction mechanism, but preceding rate-limiting steps during enzyme – substrate association or enzymatic structure, as previously reported for other compounds such as PCE (Renpenning et al., 2014), TCE (Gafni et al., 2020) and TCM (Heckel et al., 2019). Further research will be necessary to unravel the mechanics behind these observed differences for RD of cis-DCE. On the other hand, the slope determined in this study from field samples is strongly different compared to that determined for aerobic oxidation (32 ± 6, Abe et al., (2009a)), indicating a non-significant biodegradation of cis-DCE under oxic conditions during the EISB treatment (Figure 19).

Finally, for abiotic degradation processes, the starkly contrasting slope determined for oxidation by permanganate, -125 ± 47 (Doğan-Subaşı et al., 2017), will allow to differentiate between abiotic oxidation and microbial RD of cis-DCE in applications of in situ chemical oxidation by permanganate. However, for cis-DCE dichloroelimination by Fe(0) (via single electron transfer), a value relatively close to the slope of 5 ± 3 obtained in this study (Figure 19) was reported (i.e. 3.1 ± 0.2 (Audí-Miró et al., 2013b)), which could make it difficult to differentiate between cis-DCE transformation by microbial and abiotic RD in engineered remediation treatments such as Fe(0) permeable reactive barriers. In summary, the results of this thesis show the potential of a dual-

element isotope approach to investigate transformation processes of cis-DCE in remediation of contaminated sites by EISB with EVO.

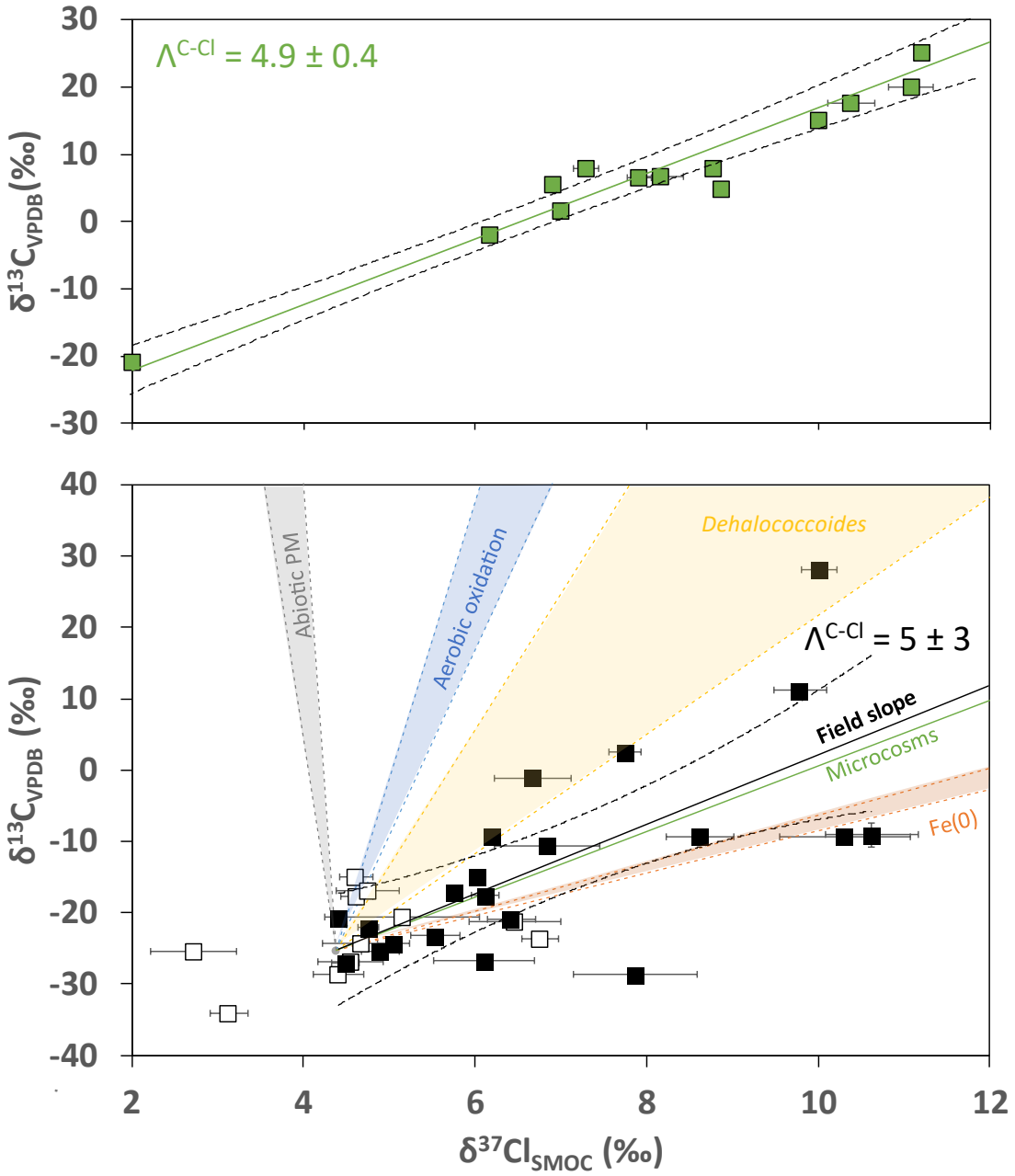

Figure 19. Dual element C-Cl isotope plot of cis-DCE from samples of the microcosm experiments (upper panel) and the field (lower panel). Λ values (±95% C.I.) are given by the slope of the ORL and the black dashed lines correspond to the 95% C.I. Error bars for $\delta^{13}C$ values are generally smaller than the symbols. In the lower panel, the empty markers represent data from samples collected prior to the injection, while filled black markers correspond to those measured after the EVO injection. The green line represents the slope obtained from the microcosm experiments and the colored areas correspond to ranges of previously reported slopes for different degradation processes: grey for abiotic oxidation by permanganate (Doğan-Subaşı et al., 2017), blue for aerobic oxidation (Abe et al., 2009a), yellow for reductive

dechlorination in Dhc cultures (Bloom et al., 2000; Abe et al., 2009b; Fletcher et al., 2011; Kuder et al., 2013; Lihl et al., 2019), and orange for abiotic degradation with Fe(0) (Audí-Miró et al., 2013).

4.7. Evaluation of biodegradation extent

Since 2D-CSIA confirmed RD as the primary degradation pathway in the field, and given that other degradative processes, such as aerobic oxidation, have negligible effects on the degradation of CEs, microcosm-derived εC values can be reliably used to estimate the extent of contaminant degradation. Furthermore, isotopic mass balance can be applied to assess the degree of complete dechlorination of PCE to ethene.

However, determining the extent of biodegradation requires knowledge of the initial $\delta^{13}C$ signature of the source PCE. Fortunately, DNAPL (PCE) was identified in a monitoring well and sampled in a nearby area of the same contaminated site, approximately 50 meters north of the study area, in September 2020. The isotopic composition of the PCE_{DNAPL} was measured and values of -25.9 ± 0.1‰ for $\delta^{13}C$ and -0.08 ± 0.2‰ for $\delta^{37}Cl$ were obtained. In cases where DNAPL is not found, the isotopic balance of CEs prior to the injection can be used to evaluate the presence of one or more potential sources of contaminant. In our case, the $\delta^{13}C_{CEs}$ (Eq. 3) from the eleven sampled wells ranged from -27.9‰ to -23.6‰, values typical of commercial solvents and closely matching the isotopic signature of the above mentioned DNAPL, so this was considered as a unique source for calculations. In fact, all the PCE $\delta^{13}C$ values measured on the baseline water samples (prior to injection) were already enriched versus the PCE_{DNAPL} giving more consistency to this hypothesis and proving the existence of a certain degree of isotopic enrichment due to natural attenuation processes prior to the injection of EVO (Figure 20).

Indeed, when the C-Cl isotope slope observed in the microcosm experiments for PCE is plotted on the dual isotope plot, considering the measured DNAPL as the source of the contamination, the distribution of data points suggests RD as the predominant degradation mechanism of PCE before the EVO injection (Figure 20). This interpretation is further corroborated by the presence of degradation metabolites such as TCE, cis-DCE and VC in the baseline samples.

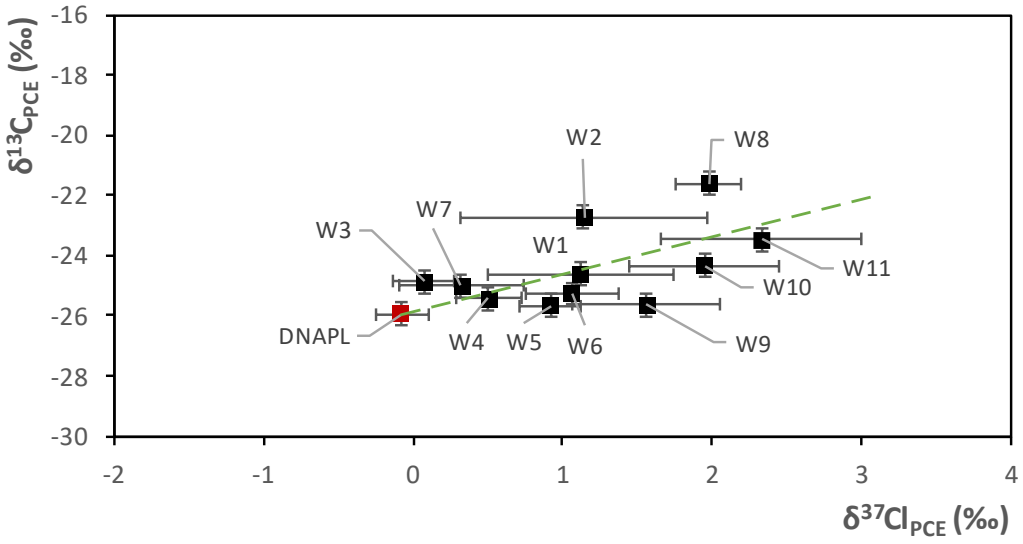

Figure 20. Dual isotope plot ($\delta^{13}C$ vs $\delta^{37}Cl$) of PCE in the eleven wells before the injection (June 2020) and DNAPL found in a nearby piezometer monitoring well (red). The dashed green line represents the dual isotope slope observed for PCE RD in microcosm experiments ($\Lambda^{C\text{-}Cl}$= 0.8 ± 0.4).

4.7.1. Extent of PCE biodegradation

Using microcosm-derived ε values and assuming that the $\delta^{13}C$ value of the DNAPL PCE is representative of the contamination source, the extent of PCE transformation to TCE (B_{PCE}) was calculated (Eq. 5) for all samples in which PCE was detected. This analysis included eleven wells before the EVO injection (June 2020), five wells after the injection (November 2020) and two wells in January 2021.

The B_{PCE} calculations confirmed that PCE transformation to TCE was already occurring before the EVO injection. However, B_{PCE} values varied across the studied site. Prior to the injection, three wells exhibited B_{PCE} values exceeding 90%, while other three showed values above 60%. In contrast, three piezometers showed B_{PCE} values below 40%. Wells W10 and W11, located downstream of the source area, showed biodegradation extents of 78% and 90%, respectively, which is consistent with greater degradation occurring further downstream in the contamination plume (Figure 21).

In the source area, degradation was more heterogeneous. For example, among the two wells with the highest CEs concentrations, W8 exhibited a B_{PCE} of 98%, whereas the nearby W4 had a B_{PCE} of only 39% (Figure 5 and Figure 21). This difference could be attributed to the potential presence of DNAPL near W4, which had the highest CEs concentrations. Additionally, the

dissolution of free-phase PCE could explain the lower $\delta^{13}C_{PCE}$ values and the lower B_{PCE} in W4 compared to neighbouring wells, despite a molar fraction of PCE degradation products exceeding 75% (Figure 21).

Following the EVO injection, PCE concentrations declined rapidly, and $\delta^{13}C$ could only be measured in five wells. In four of these, where biodegradation was already advanced prior to the injection, B_{PCE} values exceeded 90%. In W9, an observation well located downstream of the source area, B_{PCE} increased from 25% before the injection to 62% two months after. PCE was either undetectable or present at concentration too low for isotopic measurements in the other wells. In W4, where DNAPL presence was suspected, PCE was no longer detected after the injection, suggesting that the DNAPL pool may have been mobilized or removed.

During the second post-injection sampling (January 2021), B_{PCE} could only be estimated in W11 and W2 with values of 79% and 97%, respectively. In all other wells and subsequent samplings, PCE was either undetectable or present at concentration too low for isotopic analysis (Table 9).

Table 9. PCE biodegradation extent (B_{PCE}) in percentage. Grey cells indicate PCE concentration below detection limit for $\delta^{13}C$ analysis while green cells indicate that PCE was not detected (<1µg/L).

MW	B_{PCE} Jun20	B_{PCE} Nov20	B_{PCE} Jan21	B_{PCE} Mar21	B_{PCE} May21	B_{PCE} Sep21
W8	98	98				
W2	95		97			
W11	90	99	79			
W10	78	94				
W1	71	97				
W3	63					
W7	58					
W6	47					
W4	39					
W9	25	62				
W5	24					

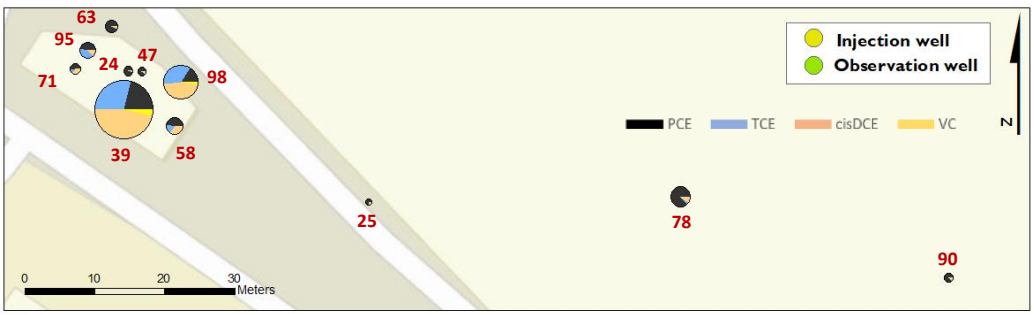

Figure 21. Estimated biodegradation extent of PCE (B_{PCE}) in the baseline sampling (red labels). The labels indicate the B_{PCE} (%) while the pie chart depicts the molar fraction of PCE and its metabolites (see legend), while its size is proportional to the total concentration of CEs.

4.7.2. Extent of cis-DCE biodegradation

Additional considerations must be taken into account when estimating the extent of cis-DCE biodegradation. In contrast to PCE, the original contaminant, cis-DCE is a degradation product and the changes in its isotopic composition due to its formation via TCE RD may lead to misleading results in B_{cDCE} calculations. Consequently, B_{cDCE} could only be determined in samples where neither PCE nor TCE was detected.

However, due to the rapid decline in PCE and TCE concentrations, B_{cDCE} could be calculated for several piezometers across multiple sampling campaigns. In eight wells, B_{cDCE} reached high values ranging from 91 to 99%. Conversely, in wells W9, W10 and W11 located downstream of the source (Figure 4), B_{cDCE} could not be quantified, as PCE or TCE were still present in all samples were cis-DCE was detected until November 2020 or January 2021. Furthermore, in the final four sampling campaigns, cis-DCE concentrations decreased to <1µg/L, suggesting either almost complete degradation or contaminant mobilization towards the eastern part of the study area.

Nonetheless, the calculated B_{cDCE} values indicate that cis-DCE accumulation did not impede the RD stepwise process, as this compound was effectively degraded to VC (Table 10).

Certain monitoring wells exhibited distinct behaviors that require further analysis:

- W1: By March 2021, B_{cDCE} had reached 98%. However, in subsequent sampling events, it declined to 93 and later to 77%. This trend may indicate the mobilization of less degraded cis-DCE from adjacent areas into the study site.
- W3: This well was the only location where cis-DCE $\delta^{13}C$ values more depleted in ^{13}C were observed over time. However, the $\delta^{13}C$ depletion was accompanied by a $\delta^{37}Cl$ values enriched in ^{37}Cl. This observation suggests the occurrence of a mixture of cis-DCE from distinct sources with different isotopic composition and/or different extent of degradation, precluding the calculation of B_{cDCE}.

Table 10. cis-DCE biodegradation extent (BcDCE) in percentage. Orange cells indicate the presence of a cis-DCE precursor in the sample (PCE or TCE) while green cells indicate cis-DCE concentration <1µg/L. n.m. stands for not measurable.

MW	B_{cDCE} Jun20	B_{cDCE} Nov20	B_{cDCE} Jan21	B_{cDCE} Mar21	B_{cDCE} May21	B_{cDCE} Sep21
W8			24	92	98	
W2		40		72	91	
W11						
W10						
W1			7	98	93	77
W3		n.m.	n.m.	n.m.		
W7		99	99			
W6			99			99
W4			45	75	92	92
W9						
W5			77	95		

4.7.3. Extent of dechlorination to non-toxic ethene

The isotopic mass balance equation (Eq. 3) accounts for the concentration-weighted isotopic composition of PCE, TCE, cis-DCE and VC. While the isotopic fractionation between sequential compounds is governed by the specific ε of the primary compound, the overall isotopic mass balance remains unchanged until VC is degraded to ethene, which is not included in the balance. The carbon isotopic balance, and thereby the total dechlorination extent, was only determined when concentrations were sufficient to measure the isotopic compositions of all CEs with a molar fraction exceeding 10 %.

As already mentioned, prior to the injection, the isotopic balance of CEs in the eleven sampled wells ranged from -27.9 ‰ to -23.6 ‰ closely matching the isotopic signature of the DNAPL, indicating minimal degradation to ethene. Post-injection, wells W7, W9 and W10 exhibited carbon isotope mass balances enriched in ^{13}C (more positive $\delta^{13}C_{CEs}$ values), surpassing the initial range and indicating active degradation to ethene. Notably, W7 demonstrated an isotopic shift of +52 ‰. In contrast, the other piezometers showed no significant evidence of degradation to ethene until the March 2021 sampling event. By the final sampling in September 2021, all wells with calculable isotopic balances displayed significant enrichment in ^{13}C compared to pre-injection values (Figure 22).

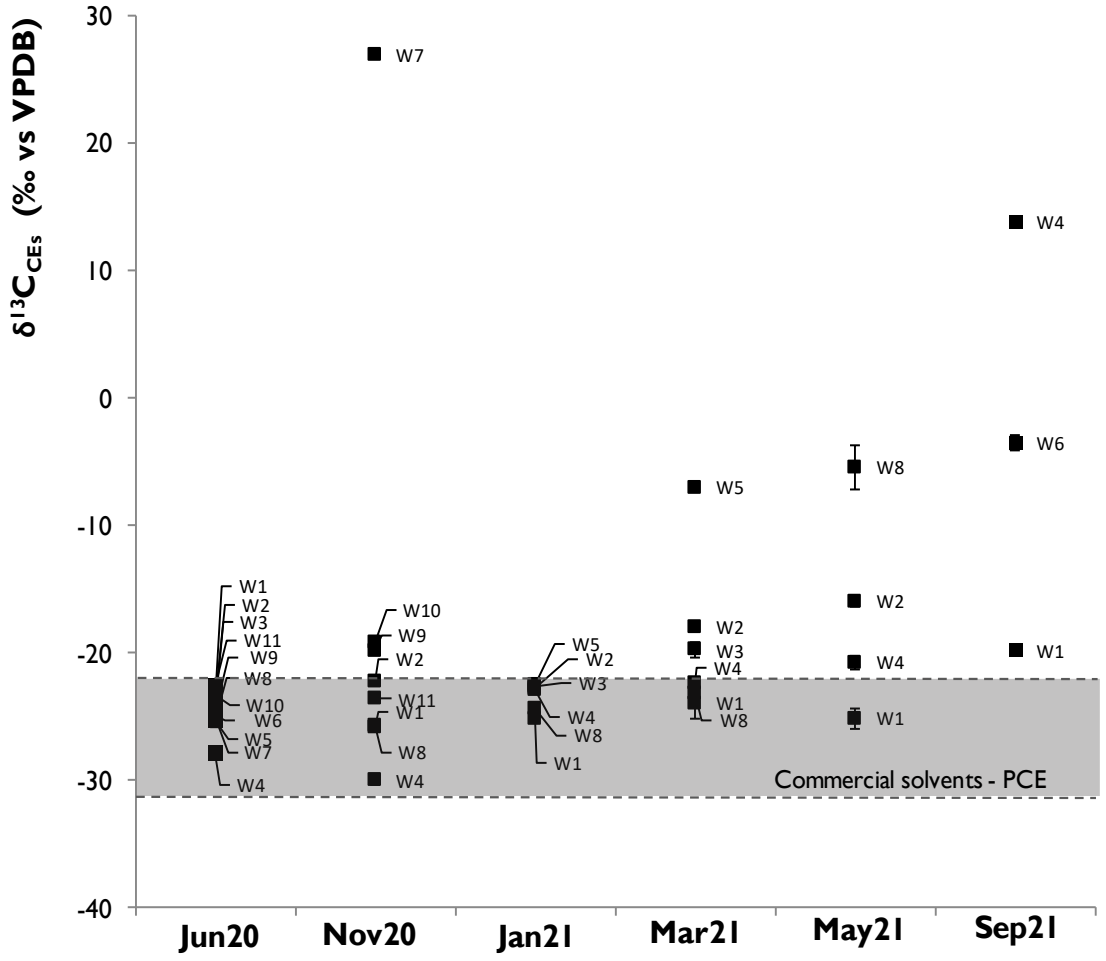

Figure 22. Isotopic mass balance calculated for all wells across different sampling campaigns. In the initial sampling, isotopic balances were within the range typical of PCE commercial solvents. Gradual isotopic enrichment in ^{13}C was observed, indicating progressive CEs degradation to ethene.

To quantify the transformation of PCE beyond VC into non-chlorinated ethene, Eq. 6, 7 and 8 were employed using microcosm-derived ε values. Equations 7 and 8 enabled the calculation of maximum and minimum expected biodegradation extents to ethene. In wells W2, W3, W4, W5, W7 and W8, where isotopic mass balance data were available for most samplings (Figure 23), biodegradation to ethene ranged from 30 to 80 %. Generally, a significant increase in biodegradation to ethene was observed after a notable decrease in cis-DCE concentrations. Specifically, in W7, which had the lowest contaminant concentration among these wells (Figure 23), the extent of complete dechlorination reached the highest observed values (79-88%) during November 2020 sampling event. Subsequent samplings showed significantly reduced concentrations, precluding isotopic composition measurement of CEs.

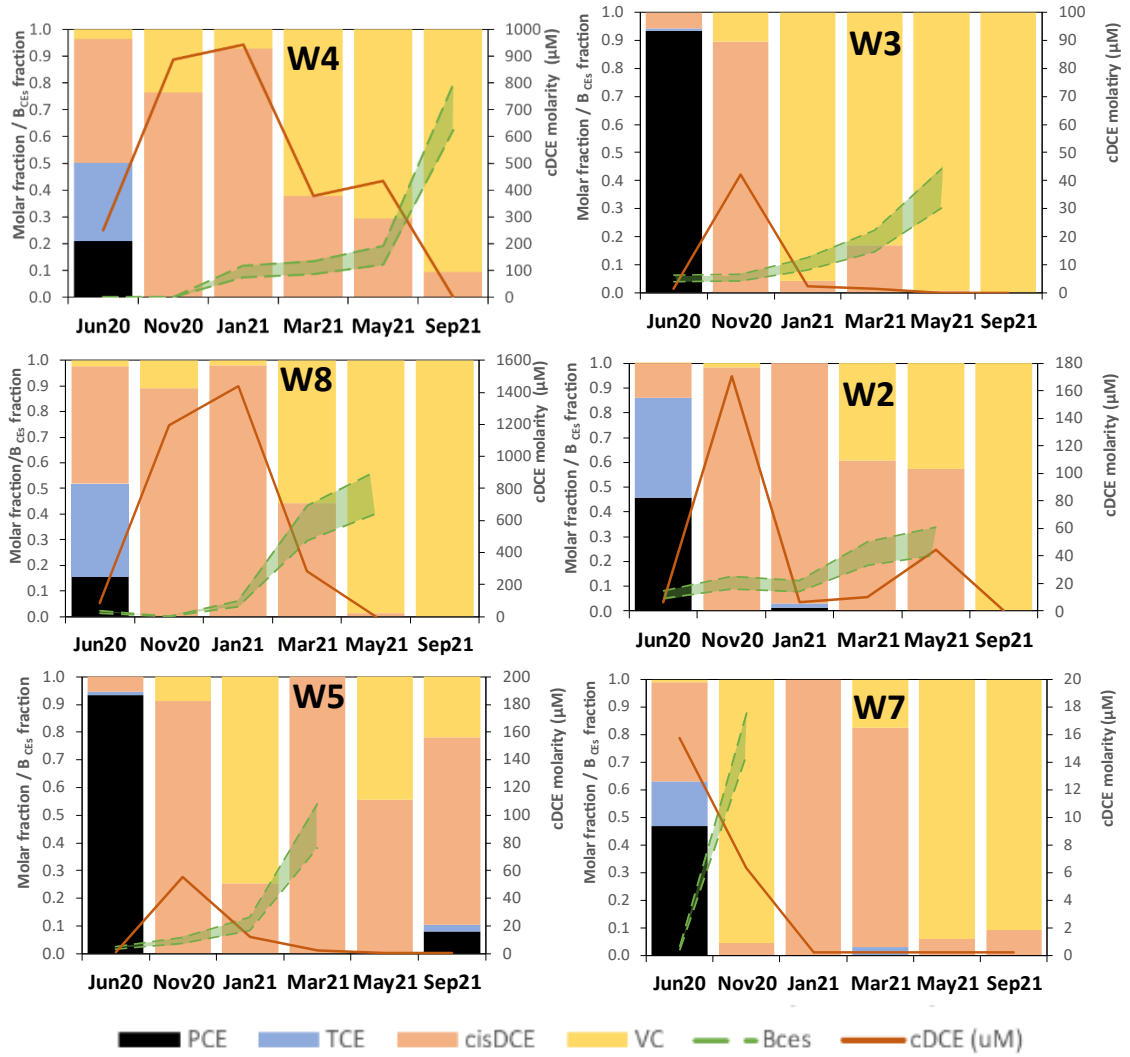

Figure 23. Estimated range of CEs biodegradation extent to ethene across different wells (green area). Cis-DCE molarity (dark orange line) and CEs molar fractions (stacked bars) are also plotted for reference. Note that the right vertical axis varies for each well.

Well W1 exhibited a different pattern. Despite abrupt changes in concentration, isotopic data indicated that biodegradation to ethene did not exceed 15 – 22 %, representing the lowest dechlorination rates among the wells with available isotopic mass balance data (Figure 24). This suggests that between March and May 2021, VC accumulated, but degradation to ethene remained limited.

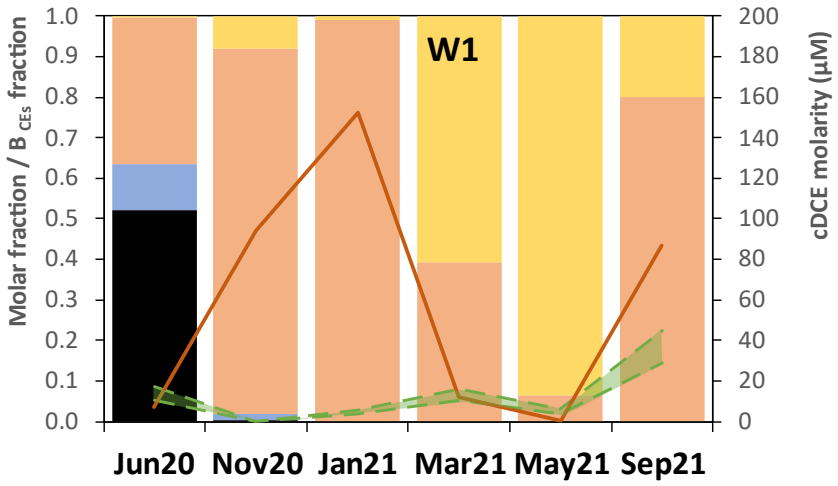

Figure 24. Estimated range of CEs biodegradation extent to ethene in W1 (green area). Cis-DCE molarity (dark orange line) and CEs molar fractions (stacked bars) are also plotted for reference.

Other wells exhibited CEs concentrations too low to reliably calculate biodegradation extents to ethene (Figure 25).

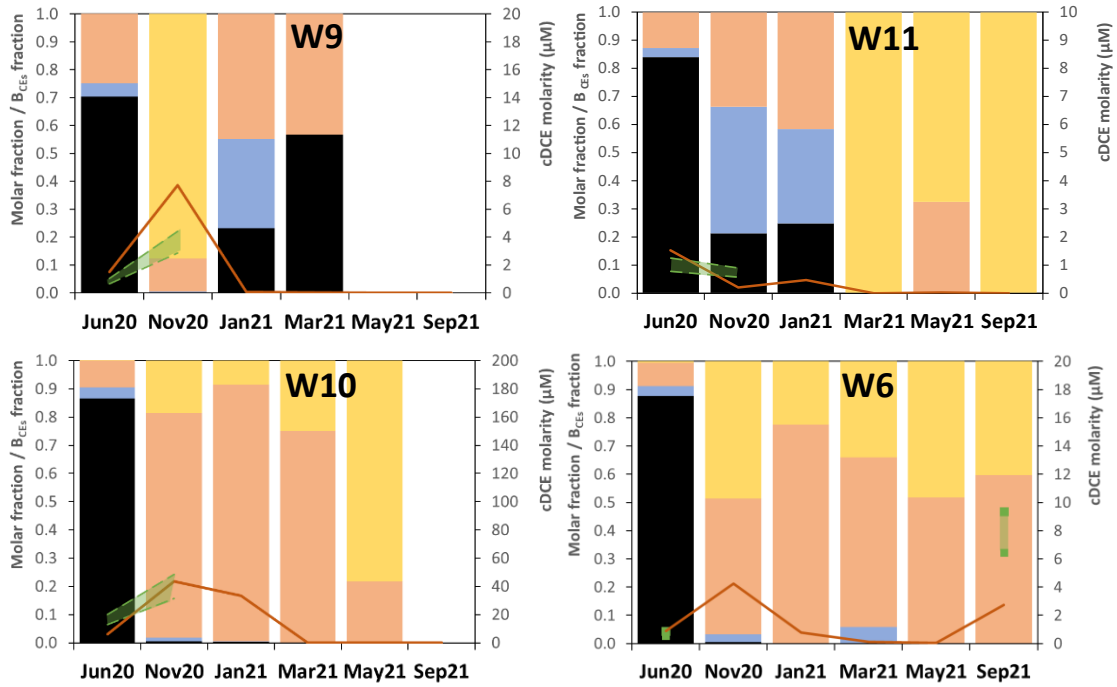

Figure 25. Estimated range of CEs biodegradation extent to ethene in wells where isotopic balance could only be calculated during two sampling events (green area). Cis-DCE molarity (dark orange line) and CEs molar fractions (stacked bars) are also plotted for reference. Note that the right vertical axis varies for each well.

Finally, eq. 6 served to calculate absolute dechlorination extents to ethene. These results correlate directly with the carbon isotopic balance across samples, assuming common PCE source and degradation pathways. A comprehensive graph was generated to depict degradation percentages across all wells over the six sampling campaigns (Figure 26).

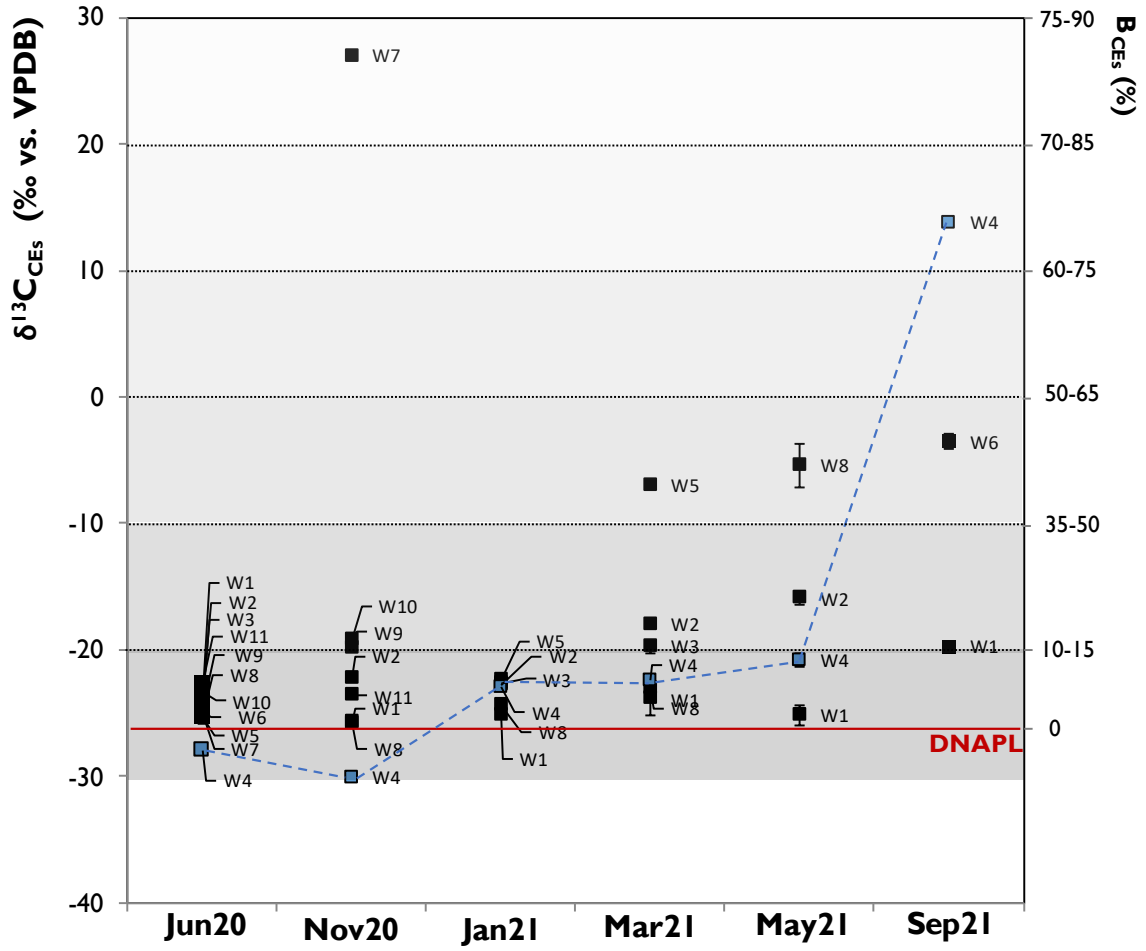

Figure 26. Carbon isotopic balance across all measured samples and sampling campaigns. The DNAPL source is indicated by the red line, with complete dechlorination extent ranges (in %) shown on the right vertical axis.

These findings demonstrate successful bioremediation, as all monitored wells showed increasing dechlorination rates. The enrichment of $\delta^{13}C_{CEs}$ confirms that biodegradation to ethene occurred. While complete dechlorination could not be measured in four wells due to low concentrations, five out of the remaining seven wells exhibited complete dechlorination extents exceeding 50%.

5. Results of the study on TCM transformation via alkaline activated PS

5.1. Experiment i: Effect of TCM:PS molar ratio

The commercial product PSOX used in experiment i kept the pH at 10.2 ± 0.2, independently of the TCM:PS molar ratio. At this pH, the primary radicals driving td $OH^{\cdot}$ (Furman et al., 2011; Liang et al., 2015). Degradation of TCM was observed over time, reaching 98% after 30 days at the molar ratio of 1:65 (experiment i.a) and after 13 days at the molar ratio of 1:125 (i.b). In the control vials, the concentration of TCM remained unchanged for up to 35 days (Figure 27), discarding TCM degradation by AH and ruling out potential TCM losses due to other processes such as volatilization through the caps. Therefore, TCM degradation was attributed solely to chemical oxidation, which followed pseudo-first-order kinetics, as evidenced by the good linear correlation between $\ln(C/C_0)$ and time (Figure 27). The results show that the rate of TCM degradation increases with higher PS concentrations, with pseudo-first-order rate constant (k'obs) values of 0.151 and 0.232 d^{-1}, corresponding to half-lives of 4.6 and 3.0 days for molar ratios of 1:65 and 1:125, respectively.

Despite these differences in degradation rates, experiments i.a and i.b exhibited comparable enrichment in ^{13}C and ^{37}Cl at different molar ratios, while isotopic changes in the controls were not statistically significant ($p>0.05$) (Figure 28 and Figure 29). The calculated εC values were -12 ± 1 and -11 ± 1‰, while for chlorine the obtained εCl values were much lower, -0.30 ± 0.05 and -0.4 ± 0.2‰, for experiments i.a and i.b, respectively (see Table 11 for all calculated εC, εCl and $\Lambda^{C\text{-}Cl}$ values). The determined $\Lambda^{C\text{-}Cl}$ values did not show a significant difference, being 33 ± 6 and 23 ± 10 for experiments i.a and i.b, respectively. Due to the notably higher carbon isotope fractionation compared to chlorine, both $\Lambda^{C\text{-}Cl}$ values exceeded any previously reported in the literature, confirming that TCM oxidation by alkaline-activated PS at this pH (10.2) is distinguishable from other degradation processes using 2D isotopic tools.

5.2. Experiment ii: Effect of pH increase

Experiments ii.a and ii.b were conducted at pH > 10.3, where both $SO_4^{\cdot-}$ and $OH^{\cdot}$ radicals were supposed to be present (Liang et al., 2009). An important reduction in TCM concentration was observed over time, reaching degradation percentages of 92% after 20 days at pH 11.4 and 98% after 67 days at pH 12.8. Interestingly, control experiments without PS also exhibited noticeable

TCM degradation within the same time period, attributed to AH. In control ii.a (pH=11.4), a 10% reduction in TCM was observed over 20 days, while in control ii.b (pH=12.8), TCM concentration decreased by 50% after 30 days, reaching 87% degradation after 78 days (Figure 27). TCM degradation, under stronger alkaline conditions than experiment i, followed pseudo-first order kinetics in both the experimental and control vials (and Figure 27). The observed k'obs values were 0.12 ± 0.02 and 0.053 ± 0.009 d^{-1} for experiments ii.a and ii.b, and 0.006 ± 0.003 and 0.026 ± 0.001 d^{-1} for the corresponding controls (Table 11). These results indicated that the rate of TCM degradation decreases with an increasing pH. This is likely due to the predominance of AH, which has significantly slower kinetics compared to oxidation. This hypothesis is further discussed below using the isotope data.

Isotopic analysis of experiments ii.a and ii.b revealed different εC values of -10.1 ± 0.7 and -25 ± 12‰, and also distinct εCl values of -0.40 ± 0.1 and -2.7 ± 0.3‰, respectively (Table 11), leading to $\Lambda^{C\text{-}Cl}$ values of 23 ± 7 and 9 ± 2, respectively. In contrast, control ii.b showed much higher carbon and chlorine isotopic fractionation values of εC = -59 ± 16‰ and εCl = -5 ± 2‰, with a $\Lambda^{C\text{-}Cl}$ value of 11 ± 1. These values are consistent with those reported for TCM degradation via AH (Torrentó et al., 2014, 2017). Carbon and chlorine isotopic fractionation values could not be estimated for control ii.a because the limited data points (n=3) and extent of degradation (10%) resulted in a statistically not significant regression (p>0.05) (Figure 28 and Figure 29). The isotopic findings align with the observed trends in reaction kinetics. The isotopic results for experiment ii.a (pH 11.4) are consistent with those observed at pH 10.2 (experiments i.a and i.b) (Table 11), pointing to oxidation as the predominant degradation mechanism. Conversely, the isotopic data from experiment ii.b (pH 12.8) confirmed a substantial contribution of AH in TCM degradation, as evidenced by εC and εCl values that fall within the range typically associated with AH. This result could thus explain the lower degradation rates observed in the vials at higher pH.

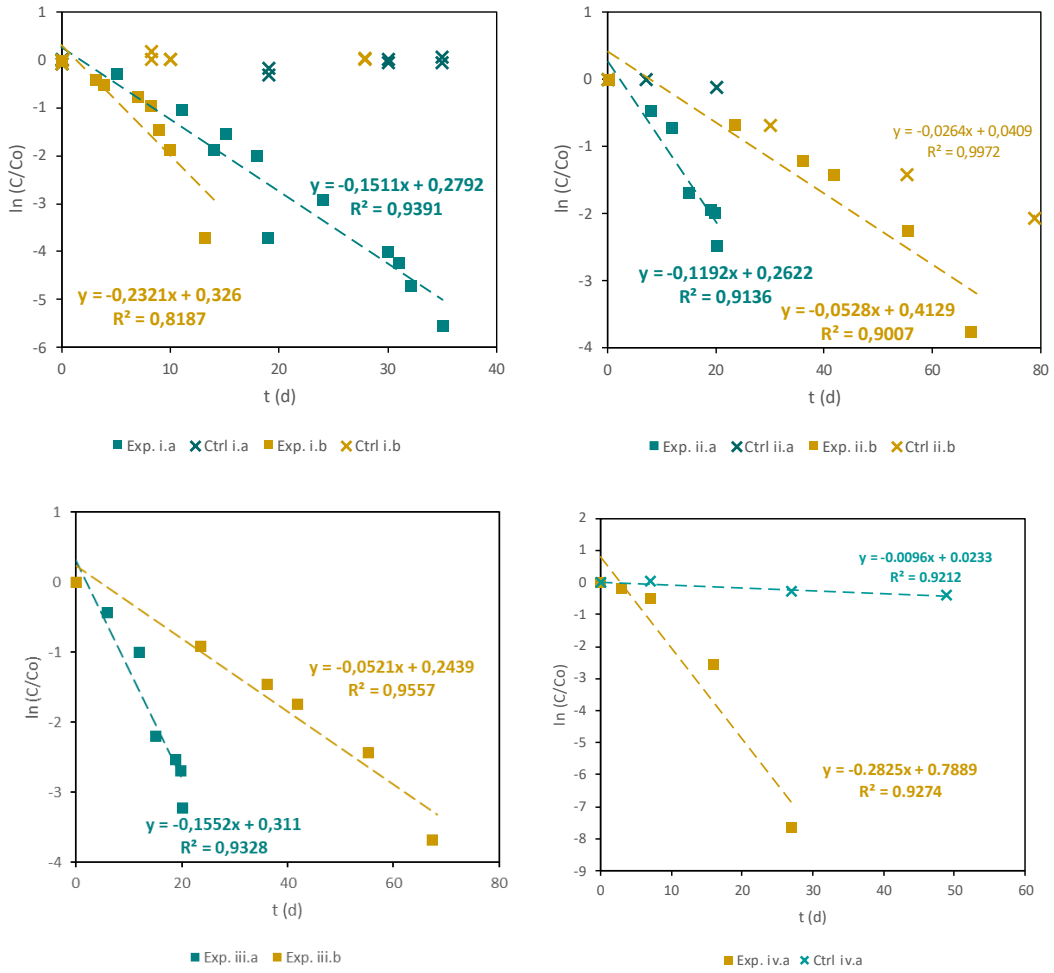

Figure 27. TCM degradation kinetics [ln(C/C_0) vs time], in the different experiments. Linear regression (dashed lines) and high correlation values (R^2) evidence pseudo-first order kinetics.

5.3. Experiment iii: Impact of CO_3^{2-} on the radical cascade

In experiment iii, where CO_3^{2-} anion was introduced to the alkaline-activated PS system, the scavenging of $SO_4^{\cdot-}$ and $OH^{\cdot}$ radicals and the resulting generation of $CO_3^{\cdot-}$ was hypothesized based on previous studies (Li et al., 2017; Lee et al., 2020). TCM degradation reached 96% after 20 days at pH 11.3 (iii.a) and 97% after 67 days at pH 12.8 (iii.b). Estimated k'obs values were 0.16 ± 0.02 d^{-1} for experiment iii.a and 0.05 ± 0.01 d^{-1} for experiment iii.b (Figure 27 and Table 11). At pH 11.3, the presence of CO_3^{2-} anion slightly enhanced TCM degradation kinetics ($t_{1/2}$ = 4.5 days) compared to experiment ii.a ($t_{1/2}$ = 5.8 days). However, the kinetics of experiments ii.b and iii.b

were almost identical ($t_{1/2}$ = 13.1 and 13.3 days, respectively), indicating that at pH 12.8, the degradation was mainly driven by AH, regardless of the presence of CO_3^{2-} anion.

Experiments iii.a and iii.b showed significant differences in isotopic fractionation (Figure 28 and Figure 29), with εC values of -7.0 ± 0.6‰ and -26 ± 11‰, and εCl values of -0.5 ± 0.2‰ and -3.7 ± 0.3‰, respectively (Table 11). While the obtained $\Lambda^{C\text{-}Cl}$ values of 11 ± 5 and 10 ± 4 for these experiments could initially indicate an AH mechanism, the differences observed in kinetics and isotopic fractionation values of C and Cl suggest that the presence of CO_3^{2-} anion might alter the TCM degradation pathway at moderate alkaline pH (iii.a). The low εCl is similar to that observed in previous oxidative degradations (exp. i.a, i.b, iia) but the εC value is a bit lower. This difference may be related to the presence of different oxidative radicals, possibly $CO_3^{\cdot-}$. The contribution of superoxide anion radical ($O_2^{\cdot-}$) to TCM degradation cannot be discarded (Teel et al., 2002; Smith et al., 2006). Considering this, the $\Lambda^{C\text{-}Cl}$ value observed in experiment iii.a may reflect a mixed pathway of oxidative degradation (as seen in experiment i.a, i.b and ii.a) and a reductive mechanism. This hypothesis is further discussed in section 5.6.

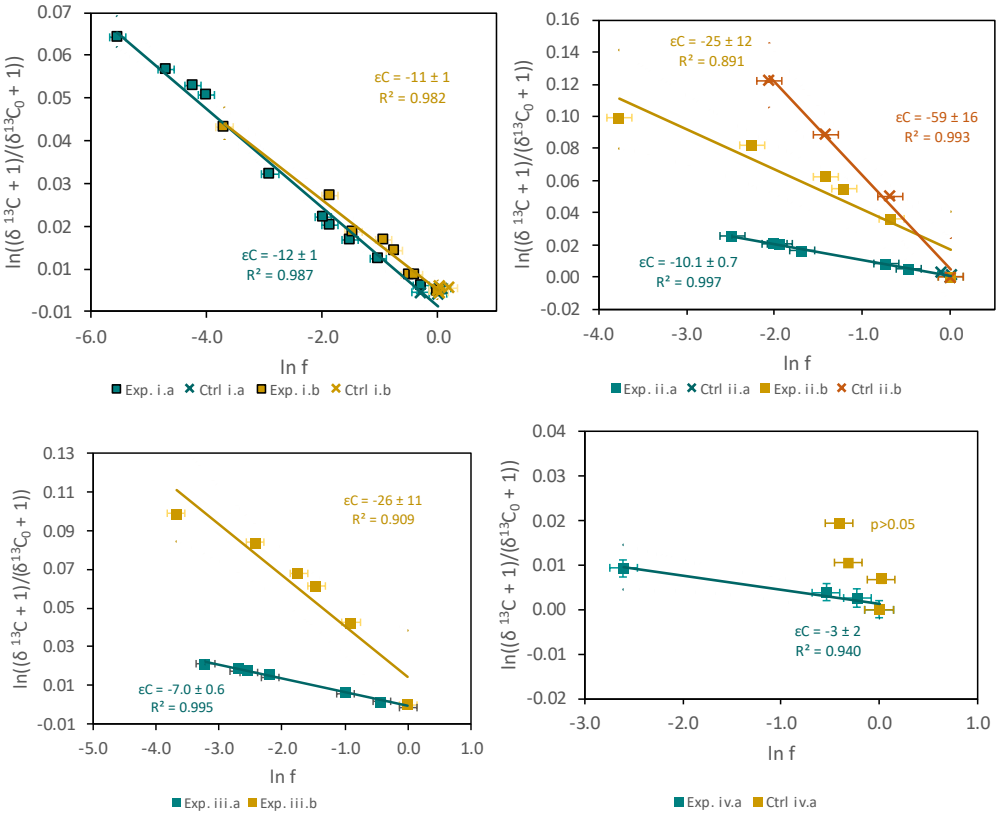

Figure 28. Carbon isotopic fractionation of TCM during degradation experiments and controls. Following Eq. 2, the slope of the OLR (solid lines) corresponds to the εC values. The dashed lines represent 95% confidence intervals. Error bars display the error calculated by propagation of the known total errors for concentration and $\delta^{13}C$ measurements.

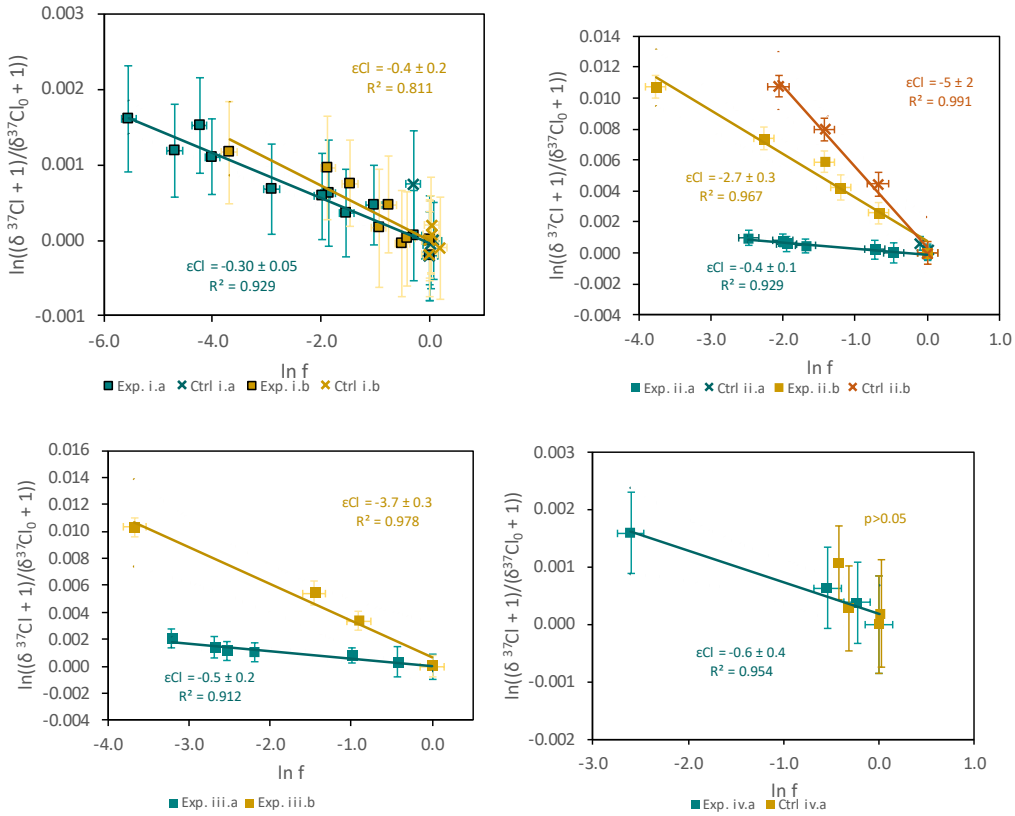

Figure 29. Chlorine isotopic fractionation of TCM during degradation experiments. Following Eq. 2 in the main text, the slope of the OLR (solid lines) gives the εCl values. The dashed lines represent the corresponding 95% confidence intervals. Error bars display the error calculated by propagation of the known total errors for concentration and $\delta^{37}Cl$ measurements.

5.4. Experiment iv: Mimicking alkaline trench conditions

5.4.1. Results of TCM

In the PS experiments conducted under alkaline trench conditions, containing trench-sampled solids and alkaline water, TCM degradation reached 99.9% after 27 days (Figure 27). In contrast, control vials without PS exhibited slower degradation kinetics, consuming only 27% of TCM within the same time period. The estimated k'obs for the vials with PS was 0.28 ± 0.05 d^{-1}, with a half-life of 2.5 days, while the control vials showed values of 0.010 ± 0.002 d^{-1} and a half-life of 72.4 days (Table 11 and Figure 27). Notably, TCM degradation in the presence of PS under alkaline trench conditions exhibited the fastest kinetics among all the experiments performed.

Experimental vials exhibited significant shifts in both $\delta^{13}C$ and $\delta^{37}Cl$ of TCM, resulting in isotopic fractionation values of εC = -3 ± 2‰ (Figure 28) and εCl = -0.6 ± 0.4‰ (Figure 29), and a dual-element slope of 5.5 ± 0.6. In contrast, the control experiments yielded very different isotopic

values, although εC and εCl could not be estimated because the linear regressions were not statistically significant ($p>0.05$), a reliable $\Lambda^{C\text{-}Cl}$ value of 16 ± 6 was obtained.

These results indicate that in such a complex system, other processes may be influencing the removal of TCM in the control vials. One potential process is adsorption of organic compounds onto the solid phase, which may result in a reduction of the concentration of TCM without significantly changing its isotopic composition. In our study, the $\Lambda^{C\text{-}Cl}$ value obtained in the control experiments and an observed pH of 11.6± 0.7 are consistent with AH being the dominant process as already observed in similar conditions (Torrentó et al., 2017). In addition, the AH process could be enhanced due to the equilibrium between the solid phase (portlandite) and the solution.

The experimental vials exhibited the lowest $\Lambda^{C\text{-}Cl}$ value (5.5 ± 0.6) among all the experiments, suggesting a minimal contribution of the AH mechanism, in agreement with the relatively moderate alkaline pH of 10.6. Similar $\Lambda^{C\text{-}Cl}$ values of 5.8 ± 0.4, 8 ± 2 and 6.7 ± 0.4 have been reported for abiotic reductive degradation of TCM by Fe(0) at neutral and alkaline pH (Torrentó et al., 2017; Asfaw et al., 2023) and by $CO_2^{\cdot-}$ radicals (via OS-SET), generated by thermal activation of PS and reaction with formate (Heckel et al., 2017). Although the initial CO_3^{2-} concentration in this experiment (95 mg/L) was similar to that in experiment iii.a (110 mg/L), the equilibrium with the solid phase in experiment iv.a resulted in a higher final CO_3^{2-} concentration of 300 mg/L. This suggests that there was sufficient CO_3^{2-} to scavenge hydroxide and sulfate radicals. Consequently, superoxide radicals ($O_2^{\cdot-}$, Eq. 11) might have contributed to TCM degradation, as ionic strength has been shown to enhance $O_2^{\cdot-}$ reactivity (Furman et al., 2010). $O_2^{\cdot-}$ is known to act as both reducing and oxidizing agent (Watts et al., 1999). In this case, given the low $\Lambda^{C\text{-}Cl}$ value determined for TCM in this experiment, $O_2^{\cdot-}$ radicals could drive TCM degradation primarily through reductive pathways. These findings suggest that the presence of PS and CO_3^{2-} could transform TCM degradation into an In Situ Chemical Reduction (ISCR) process rather than an ISCO.

A comparison between $\Lambda^{C\text{-}Cl}$ values and their uncertainties obtained in this study with York and OLR regression methods is shown in Table 12. For OLR, slope attenuation compared to York method is observed for $\Lambda^{C\text{-}Cl}$ in all cases as predicted by Ojeda et al. (2019, 2020). Nevertheless, the differences between slopes obtained with both methods are not significant. Since no systematic bias introduced by OLR was observed for $\Lambda^{C\text{-}Cl}$ and because there has not been sufficient time for the York methods to be routinely adopted in 2D-CSIA studies, we therefore decided to use OLR method while reporting the York results for future reference.

Table 11. Results of TCM degradation kinetics (k'obs and t1/2), isotopic fractionation (εC and εCl) and dual C-Cl slope (ΛC-Cl) for each experiment (Exp) and their corresponding controls without PS (below). Isotopic fractionation and dual slope values are stated together with their ±95% confidence intervals. N = number of points; n.s. = not statistically significant ($p > 0.05$).

	Exp	pH	k'obs (d^{-1})	R^2	$t_{1/2}$ (d)	εC (‰)	εCl (‰)	Λ^{C-Cl}	N
Experimental	i.a	10.2 ± 0.2	0.15	0.939	4.6	-12 ± 1	-0.30 ± 0.05	33 ± 6	11
	i.b	10.2 ± 0.2	0.23	0.819	3.0	-11 ± 1	-0.4 ± 0.2	23 ± 10	10
	ii.a	11.4 ± 0.4	0.12	0.914	5.8	-10.1 ± 0.7	-0.4 ± 0.1	23 ± 7	7
	ii.b	12.8 ± 0.1	0.05	0.901	13.1	-25 ± 12	-2.7 ± 0.3	9 ± 2	6
	iii.a	11.3 ± 0.4	0.16	0.933	4.5	-7.0 ± 0.6	-0.5 ± 0.2	11 ± 5	7
	iii.b	12.8 ± 0.1	0.052	0.956	13.3	-26 ± 11	-3.7 ± 0.3	10 ± 4	5
	iv.a	10.6 ± 0.6	0.28	0.927	2.5	-3 ± 2	-0.6 ± 0.4	5.5 ± 0.6	4
Control	i.a	10.2 ± 0.2	0.001	0.008	802	n.s.	n.s.	n.s.	10
	i.b	10.2 ± 0.3	0.001	0.004	481	n.s.	n.s.	n.s.	10
	ii.a	11.4 ± 0.1	0.006	0.828	120	n.s.	n.s.	5 ± 3	3
	ii.b	12.8 ± 0.1	0.026	0.997	26.2	-59 ± 16	-5 ± 2	11 ± 1	4
	iv.a	11.6 ± 0.7	0.010	0.921	72.4	n.s.	n.s.	16 ± 15	4

Table 12. Dual C-Cl isotope slopes for TCM calculated for all experiments obtained by OLR and the York regression method. Two-tailed hypothesis testing was used for comparison between OLR and York methods results. All comparisons were considered statistically significant at the α=0.05 level. 95% CI = 95% confidence interval, N=number of points.

		Λ^{C-Cl}	95% CI	N	z-score	p-value	Significant difference (α = 0.05)
Exp. i.a	Linear regression	33	6	11	-0.842	0.411	no
	York Method	41	7	11			
Exp. i.b	Linear regression	23	10	9	-0.288	0.777	no
	York Method	27	9	9			
Exp. ii.a	Linear regression	23	7	7	-0.195	0.849	no
	York Method	25	7	7			
Exp. ii.b	Linear regression	9	2	6	-0.196	0.849	no
	York Method	9.4	0.4	6			
Exp. iii.a	Linear regression	11	5	7	-0.514	0.618	no
	York Method	14	3	7			
Exp. iii.b	Linear regression	10	4	4	0.149	0.889	no
	York Method	9.4	0.4	4			
Exp. iv	Linear regression	5.5	0.6	4	-0.239	0.823	no
	York Method	6	2	4			

5.4.2. Results of other CMs and CEs

Further insights into the potential reductive degradation of TCM were explored by comparing the results obtained for TCM with those for other CMs and CEs in experiments iv.a and iv.b.

For CEs, PCE displayed low chlorine fractionation (εCl = -0.4 ± 0.2) and a $\Lambda^{C\text{-}Cl}$ value of 5 ± 3 (Table 13). This value is similar to the $\Lambda^{C\text{-}Cl}$ range of 4.6 - 7 reported for abiotically mediated RD by corrinoids (Renpenning et al., 2014) but diverge from those obtained for reduction of PCE, TCE and cis-DCE via OS-SET in experiments with $CO_2^{\cdot-}$ radical anion, which are reported to approach infinity because of the negligible chlorine isotopic fractionation (Heckel et al., 2017). In line with these discrepancies, TCE and cis-DCE in our experiments showed $\Lambda^{C\text{-}Cl}$ values of 6 ± 4 and 4 ± 2, respectively, contrasting with the OS-SET behavior.

The $\Lambda^{C\text{-}Cl}$ values for TCE (6 ± 4) and cis-DCE (2 ± 1) are somewhat consistent with the values reported for Fe(0)-induced (5.2 ± 0.3 for TCE and 3.1 ± 0.2 for cis-DCE, (Audí-Miró et al., 2013a) and corrinoids-induced reductive degradation (3.7 to 4.5 for TCE, Renpenning et al., 2014). On the other hand, the isotopic results were also consistent with those for CEs degradation with oxidation reactants. First, obtained εC values align with those reported for TCE degradation with Fe(0)-activated PS at acid pH, both with (-3.4 to -4.3‰, Liu et al., 2016) and without (-3.9 to -4.7‰, Liu et al., 2018) carbonates, where both $SO_4^{\cdot-}$ and $OH^{\cdot}$ radicals are expected to contribute in the degradation mechanism. Unfortunately, chlorine isotope data are not available for such reactions for comparison. Second, obtained εC value for TCE is similar to that reported for Fenton-like degradation of TCE (-2.9 ± 0.3‰), where it was assumed that $OH^{\cdot}$ radicals predominated and secondary chlorine isotopic fractionation resulted in a $\Lambda^{C\text{-}Cl}$ value of 3.1 ± 0.2 (Liu et al., 2014).

Overall, these results suggest that reductive processes could play a role in CEs degradation in the alkaline-activated PS system in presence of carbonates, and the observable chlorine isotopic fractionation dismisses a stepwise OS-SET mechanism for CEs, in contrast to the observations with $CO_2^{\cdot-}$ radicals (Heckel et al., 2017).

For the other CMs, for which limited isotopic data is available in the literature compared to TCM, CT exhibited a $\Lambda^{C\text{-}Cl}$ value of 2.2 ± 0.4 (Table 13), closer to the values reported for magnetite ($Fe^{2+}Fe^{3+}{}_2O_4$)-mediated reductive reactions than to Fe(0) (2 ± 1 and 5.8 ± 0.4, respectively) at pH 12 (Rodríguez-Fernández et al., 2018). A potential reductive degradation of CT via reaction with $O_2^{\cdot-}$ could also be possible in our experiments. The reductive degradation of CT by $O_2^{\cdot-}$ radical

anion has been reported in previous studies (Teel et al., 2002; Smith et al., 2006), however, isotope data is still not available for this reaction.

DCM, on the other hand, showed no statistically significant chlorine fractionation (with or without PS) and no $\Lambda^{C\text{-}Cl}$ values could be obtained (Figure 30).

Table 13. Summary of removal kinetics (K'obs and $t_{1/2}$) and percentage (R %) and calculated isotopic values of εC, εCl and $\Lambda^{C\text{-}Cl}$ (confidence interval = 95%) for different compounds (Cpd): CMs: CT, TCM and DCM in experiment iv.a and CEs: PCE, TCE, cis-DCE in experiment iv.b; N = number of points; n.s. = not statistically significant (p>0.05). Conditions (Cond.) letters stand for: A – PS in deionized water; B – PS in trench conditions (experiments iv.a for CMs and iv.b for CEs); C- Control without PS in trench conditions.

Cpd	Cond.	pH	R (%)	K'obs (d^{-1})	$t_{1/2}$ (d)	εC (‰)	εCl (‰)	$\Lambda^{C\text{-}Cl}$	N
PCE	A	13.4 ± 0.4	93	0.471	1.5	-11 ± 8	n.s.	∞ (-1 ± 63)	5
	B	11.7 ± 0.7	95	0.351	2.0	-3 ± 1	-0.4 ± 0.2	5 ± 3	10
	C	11.8 ± 0.3	81	0.262	2.7	n.s.	n.s.	n.s.	3
TCE	A	13.4 ± 0.4	98	0.969	0.8	-9 ± 3	-1.0 ± 0.3	8 ± 4	5
	B	11.7 ± 0.7	98	0.428	1.6	-3.3 ± 0.4	-0.3 ± 0.2	6 ± 4	10
	C	11.8 ± 0.3	60	0.148	4.7	n.s.	n.s.	n.s.	3
cis-DCE	A	13.4 ± 0.4	95	0.758	0.9	-7 ± 4	n.s.	7 ± 7	5
	B	11.7 ± 0.7	99	0.418	1.7	-3.3 ± 0.3	-1.1 ± 0.4	2 ± 1	10
	C	11.8 ± 0.3	41	0.083	8.3	n.s.	n.s.	n.s.	3
CT	B	10.6 ± 0.6	98	0.150	4.6	-7 ± 3	-3 ± 2	2.2 ± 0.4	5
	C	11.6 ± 0.7	44	0.012	59	-1.4 ± 0.5	n.s.	n.s.	4
TCM	B	10.6 ± 0.6	93	0.283	2.5	-3 ± 2	-0.6 ± 0.4	5.5 ± 0.6	4
	C	11.6 ± 0.7	34	0.010	72	n.s.	n.s.	16 ± 15	4
DCM	B	10.6 ± 0.6	91	0.268	2.6	-4 ± 2	n.s.	n.s.	4
	C	11.6 ± 0.7	16	0.006	114	n.s.	n.s.	n.s.	4

Statistically significant isotopic effects (ORL, 95% CI) were observed for both carbon and chlorine in all CMs and CEs (except DCM) when using persulfate (PS) under trench conditions (Figure 30). For CEs, the observed fractionation was mainly attributed to the action of PS, as neither C nor Cl were significantly fractionated in control C (trench conditions without PS). However, a remarkable decrease of CEs concentrations in the control vials (81%, 60% and 41% for PCE, TCE and cis-DCE respectively) was detected probably due to other physical processes such as adsorption onto the solid particles, which was already proved for CT (Torrentó et al., 2014). AH of the tested CEs and CT is extremely slow and therefore not viable at the studied time range (half-life of 40 years for CT and over thousands of years for CEs, according to Jeffers et al. (1989)).

However, significant CT carbon fractionation (εC = -1.4 ± 0.5‰) was observed in the control C, so other process/es maybe linked to the gravel mineral phases should be playing a role, as it was also observed in the field interception trenches (Torrentó et al., 2014). The isotopic pattern for the experiments with Fe-bearing minerals (Rodríguez-Fernández, Heckel, et al., 2018) supported the occurrence of parallel CT thiolytic reduction (evidenced also by CS_2 formation) alongside hydrogenolysis (leading to TCM formation). However, in controls under trench conditions, CT behaved differently, exhibiting a much lower εC with no significant chlorine fractionation (Table 13), ruling out Fe-minerals as the sole driver of the reactions. This carbon isotopic behavior for CT was previously observed at the alkaline trench from which the solid phases added to our experiments were obtained (Torrentó et al., 2014).

Contrarily to TCM experiments, the vials for CEs with only deionized water and PS (cond. A in Table 13) revealed faster kinetics than in trench conditions. However, this is most probably related to higher pH values in these CEs experiments (13.4 vs. 11.4 and 12.8 of TCM experiments ii.a and ii.b in the main text, respectively), and the absence of other competing processes (discarded also in the control C), resulting overall in faster kinetics for alkaline-activated PS degradation. Additionally, TCE displayed isotopic fractionation on C and Cl when PS was used in deionized water getting a similar dual slope than for trench conditions. While for PCE and cis-DCE only C fractionation was obtained.

Heckel 2017 proposed that OS-SET in water leads to chlorine isotope effects in TCM, but not in CEs. However, our results showed significant chlorine fractionation for the three CEs with PS under trench conditions, indicating that Heckel's model does not fully explain the fractionation observed in our experiments. This suggests that degradation pathways other than OS-SET, are occurring under trench conditions. Since exploring these alternative mechanisms falls outside the scope of this thesis, further investigation will be required to clarify the processes driving the degradation of CEs and CMs during PS treatments in alkaline trench field conditions.

5.5. Precipitate formation and chlorinated byproducts in experiments ii and iii

During experiments ii.a and iii.a (at pH 11.4 and 11.3, respectively), precipitate aggregates were observed in the vials containing PS (Figure 31), but not in the controls (Table 14). HS-GC-qMS analysis identified and quantified higher chlorinated hydrocarbons alongside the degradation of TCM in the ii.a and iii.a experimental vials, while such byproducts were not detected in the controls. This suggests that their formation is linked to the radical cascade in the oxidation process. Unexpectedly, the degradation of TCM in these conditions led thus to the formation of more chlorinated compounds than the original contaminant, with hexachloroethane (HCA)

emerging as the primary byproduct, and CT also detected. These compounds have been previously reported in photocatalytic degradation reactors of TCM and TCE (Hung et al., 1997; Cohen et al., 2009) but, to the best of our knowledge, have never been associated with PS degradation. The accumulation of HCA suggests that $OH^{\cdot}$ radicals, rather than $SO_4^{\cdot-}$ radicals, likely

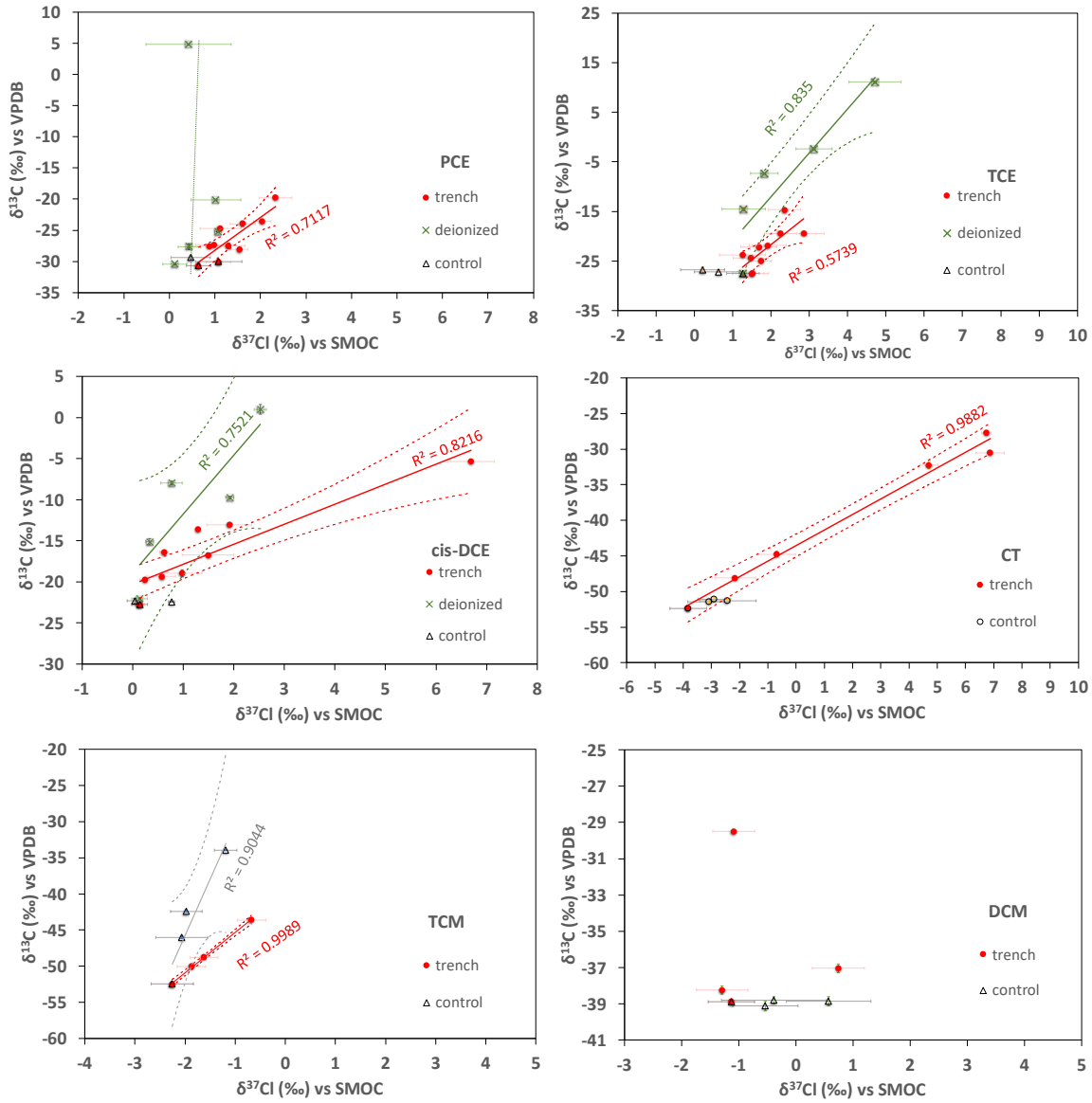

Figure 30. Dual C-Cl isotope plot for each studied compound under different conditions (alkaline trench conditions, deionized water and controls without PS). Please note that the regression line with 95% CI is only represented for significative results ($p<0.05$).

drove TCM degradation in experiments ii.a and iii.a, as prior findings have shown that $SO_4^{\cdot-}$ initiates HCA degradation (Zhu et al., 2018a) while HCA has low reactivity with $OH^{\cdot}$ (Teel et al.,

2002). In experiment iv.a, although precipitates could not be observed because of the presence of solid materials, HCA was also detected.

Figure 31. Picture of the precipitate observed in experiment iii.a vials.

Table 14. Precipitate formation and byproducts analysis in TCM experiments. n.a. = not analyzed, bdl = below detection limit.

	Exp.	Precipitate observed	Byproducts analysis (GC-qMS)	Estimated total chlorine converted into HCA
Experimental	i.a	No*	n.a.	-
	i.b	No*	n.a.	-
	ii.a	Yes	HCA and CT detected and quantified	53%
	ii.b	No	n.a.	-
	iii.a	Yes	HCA and CT detected and quantified	65%
	iii.b	No	n.a.	-
	iv.a	No*	HCA and CT detected but n.q.	-
Control	i.a	No	n.a.	-
	i.b	No	n.a.	-
	ii.a	No	<bdl	0%
	ii.b	No	n.a.	-
	iv.a	No	n.a.	-

* In experiment iv, precipitates could not be observed because of the presence of solid materials and small particles in the vials representing field conditions. An HCA peak was observed in later analysis by GC-qMS analysis, but

concentrations were not quantified. In experiment i.a and i.b lower initial concentrations of TCM probably led to lower generation of HCA and the formation of precipitates was never observed in the vials.

Due to the low solubility of HCA (50 mg/L) (Horvath et al., 1999), it is likely that the observed precipitates corresponded to HCA. Direct quantification of precipitated HCA was challenging due to its volatility, which made filtration, drying, and weighing unreliable. Therefore, an indirect calculation of the solid HCA formed during the experiments was performed using a chlorine mass balance equation (Eq. 21).

$$Cl_{TOT} = Cl^{-}_{aq} + Cl_{TCM} + Cl_{CT} + Cl_{HCA(aq)} + Cl_{HCA(s)} \quad \text{Eq. 21}$$

The total chlorine content in each experimental vial comprises the chloride anion present in the aqueous phase (measured by HPLC), chlorine atoms in the dissolved organic chlorinated compounds (TCM, CT and HCA), and chlorine precipitated as solid HCA. Since the experiments were conducted in deionized water, the only initial source of chlorine was TCM (690 mg/L). The amount of solid HCA was thus calculated by closing the chlorine mass balance. Results are detailed in Table F.2. After near-complete transformation of TCM, approximately 55-65% of the initial chlorine from TCM was converted into HCA, predominantly as precipitate (Figure 32).

Table 15. Measured concentrations of chloride, TCM, HCA and CT in experiments ii.a, iii.a and control ii.a followed by calculation of chlorine concentrations in each compound and estimation of $Cl_{HCA(s)}$ using Eq. 21. The calculated percentage of initial chlorine in TCM to HCA is indicated in the last column. Please note that chloride concentrations marked as n.a. could not be analyzed as interference with ascorbic acid, used to quench the PS reaction, did not permit the measurement of low concentrations of chloride in non-diluted samples.

	t (d)	Measured concentrations (mg/L)				Chlorine concentrations (mg/L)					HCA(s)	HCA(s)	$Cl_{HCA(s)}$
		Cl^-	TCM	HCA	CT	Cl_{TCM}	$Cl_{HCA(aq)}$	Cl_{CT}	$Cl_{TOTAL(aq)}$	$Cl_{HCA(s)}$*	mg/L	mg	%
Exp. ii.a	0	n.a.	691	0	0	616	0.0	0.0	616	-	-	-	-
	8	50	431	8	2	384	6.9	1.6	443	175	195	8.2	28%
	12	119	335	8	2	298	7.6	1.7	427	191	213	8.9	31%
	15	200	128	10	1	114	8.6	1.2	323	295	328	13.8	48%
	18	229	99	17	3	88	15.2	2.7	335	283	315	13.2	46%
	19	188	94	11	2	84	9.8	2.1	284	334	372	15.6	54%
	20	233	58	7	1	51	6.4	1.1	292	326	362	15.2	53%
Exp. iii.a	0	n.a.	696	0	0	621	0.0	0.0	621	-	-	-	-
	8	27	457	6	3	407	5.8	3.1	442	176	195	8.2	28%
	12	119	259	9	5	231	7.7	4.7	362	256	284	11.9	41%
	15	159	78	7	9	69	6.7	7.9	243	375	417	17.5	60%
	18	175	55	10	7	49	8.6	6.7	240	378	420	17.6	61%
	19	164	48	18	6	42	16.4	5.7	229	389	433	18.2	63%

	20	176	28	9	6	25	8.1	5.5	214	404	449	18.8	65%
Ctrl ii.a	0	n.a.	742	0	0	661	0.0	0.0	661	-	-	-	-
	6	n.a.	749	0	0	668	0.0	0.0	-	-	-	-	-
	24	n.a.	667	0	0	595	0.0	0.0	-	-	-	-	-

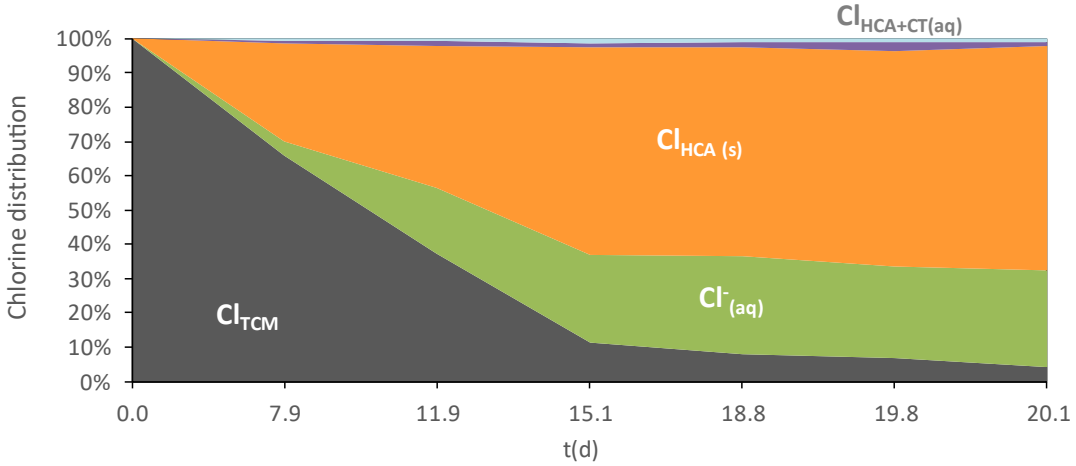

Figure 32. Chlorine mass balance of experiment iii.a, showing quantified aqueous chloride and chlorine in dissolved TCM, CT and HCA, alongside the calculated chlorine precipitated as solid HCA in the experimental vials of experiment iii.a (representative of TCM oxidation scenario with PS in deionized water).

5.6. Insights into TCM degradation from 2D-CSIA

After analyzing these experimental findings, isotope data from experiments for which differences between their dual element isotope trends were not significant ($p > 0.05$) were merged to derive combined $\Lambda^{C\text{-}Cl}$ values (i.e., experiments i.a + i.b + ii.a, and experiments ii.b + iii.b). Obtained results are summarized in Figure 33, where three distinct isotopic trends can be observed: (i) $\Lambda^{C\text{-}Cl}$ of 29 ± 4 during TCM oxidation by alkaline-activated PS (experiments ii.a + i.a + i.b). Compared to the slope from thermally activated PS (17 ± 2) (Torrentó et al., 2017), where $SO_4^{\cdot-}$ radicals are formed, the different slope obtained in this study suggest the involvement of $OH^{\cdot}$ radicals; (ii) $\Lambda^{C\text{-}Cl}$ between 11 ± 1 and 9 ± 1, accompanied by significantly higher carbon and chlorine isotopic fractionation values for AH (Ctrl ii.b, and experiments ii.b and iii.b), where degradation predominantly follows the $E1_{CB}$ mechanism; and (iii) $\Lambda^{C\text{-}Cl}$ of 5.5 ± 0.6 during TCM degradation by alkaline-activated PS in the presence of excess of CO_3^{2-} (iv.a). The CO_3^{2-} anion can scavenge $SO_4^{\cdot-}$ and $OH^{\cdot}$ radical species (Eq. 13, 14) and it could give rise to the contribution of other radical species, such as $O_2^{\cdot-}$ (Eq. 11) on TCM transformation. The reaction of TCM with $O_2^{\cdot-}$ could proceed via a reductive mechanism (Teel et al., 2002; Smith et al., 2006), however, the obtained slope differs from that reported for an OS-SET (Heckel et al., 2017).

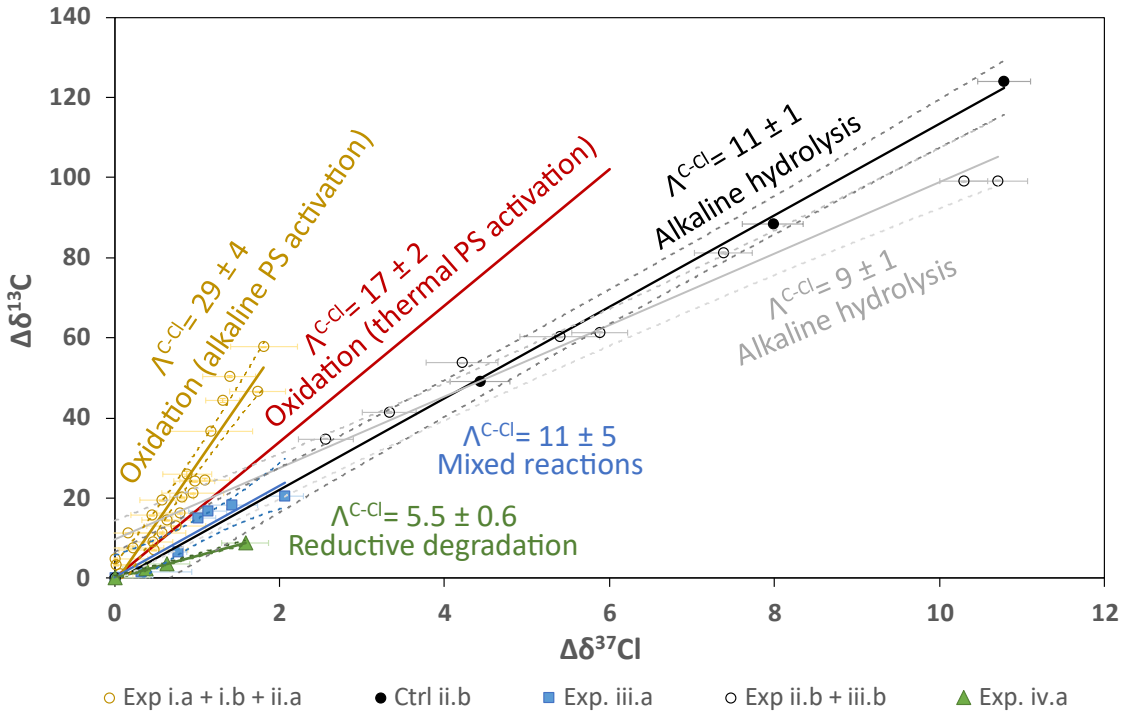

Figure 33. Dual C-Cl isotope plot displaying results from different experiments with alkaline-activated PS (Exp) and control experiments without it (Ctrl), as well as the proposed TCM degradation mechanisms. Trends for thermally activated PS (in red) and alkaline hydrolysis (ΛC-Cl of 13.0 ± 0.8 at pH ~ 12, not shown) from Torrentó et al., 2017 are shown for comparison. Dashed lines indicate the 95% CI of the linear regression.

Since the obtained isotopic results in experiment iii.a (εC = -7 ± 0.6, εCl = -0.5 ± 0.2, and $\Lambda^{C\text{-}Cl}$ = 11 ± 5) suggest the coexistence of competing oxidative and reductive mechanisms for TCM degradation, extended Rayleigh-type equations (Eq. 22) were used to estimate the contribution of each of them, F, expressed as a percentage (Van Breukelen, 2007).

$$F(\%) = \frac{\Lambda\varepsilon_{Cl_2} - \varepsilon_{C_2}}{(\varepsilon_{C_1} - \varepsilon_{C_2}) - \Lambda(\varepsilon_{Cl_1} - \varepsilon_{Cl_2})} \times 100 \qquad \text{Eq. 22}$$

In Eq. 22, the ε_A the observed Λ for the mixture is used in the 2D-CSIA approach and the respective ε_C, ε_{Cl} for each selected potential mechanism (1 and 2) expected to co-occur.

Considering the data from experiments i.a, i.b and ii.a representative for the oxidative mechanism driven by $OH^{\cdot}$ (εC = -11 ± 0.2, εCl = -0.4 ± 0.2) and data from experiment iv.a, representative from the reductive mechanism (εC = -3 ± 2, εCl = -0.6 ± 0.4), the estimated degradation by the oxidative mechanism ($OH^{\cdot}$) was 37% while 63% of the degradation was due to the reductive process ($O_2^{\cdot-}$).

Chapter IV. GENERAL DISCUSSION

The overall discussion of the results in this section synthesizes the findings obtained from the different laboratory experiments and the field application that explored the use of isotopic tools for the assessment of novel remediation strategies for sites contaminated with chlorinated solvents.

The structure of this discussion follows that of the thesis. First, it addresses the remediation of CEs contamination using EVO through laboratory experiments designed to evaluate potential isotopic fractionation caused by water-EVO partitioning and microcosm experiments to characterize the isotopic changes in CEs associated with RD using the site-specific microbial community. Subsequently, the field application of this approach was examined to assess the CEs degradation processes and quantify the individual biodegradation and complete dechlorination extent.

Second, the remediation of CMs and CEs, with a particular focus on TCM, through ISCO using alkaline-activated PS was studied in laboratory experiments reproducing diverse conditions simulating naturally occurring field environments, and an alkaline interception trench. The primary objective was to determine whether different degradation mechanisms could emerge from this treatment and whether isotopic analysis could effectively distinguish these transformations.

6.1. Laboratory experiments of CEs treatment with EVO

This section discusses the results obtained from the experiments conducted to evaluate both biotic and abiotic processes associated with EVO injection for the remediation of a site contaminated with CEs. Detailed results of abiotic experiments to assess potential isotopic fractionation caused by the partitioning of CEs between the water and EVO phases are presented in section 4.1, while results of biotic microcosm experiments for the assessment of RD are provided in sections 4.2, 4.4 and 4.5.

Partitioning experiments revealed a significant decrease in CEs concentrations after 48 hours in the presence of EVO compared to the control experiments. The obtained trend (PCE > TCE > cis-DCE) was consistent with a higher partitioning for CEs with increasing chlorination, as previously observed by Pfeiffer et al. (2005). However, despite the high partitioning of CEs into the EVO phase, the carbon isotopic values of the remaining CEs fraction in the aqueous phase did not exhibit significant differences between control and EVO experiments. These results suggest that,

during field applications, the isotopic effect of the partitioning into EVO will be minimal or insignificant compared to the isotopic shifts linked to the biodegradation of CEs in groundwater. Consequently, although water – EVO partitioning is expected to be a relevant process in the field, it does not need to be considered when interpreting isotopic shifts of the studied contaminants, as isotopic fractionation is primarily attributed to degradation processes.

Microcosm experiments demonstrated the complete degradation of PCE, TCE and cis-DCE under anoxic conditions by the native microbial community. However, differences in the degradation kinetics were observed. In microcosm bottles containing PCE and TCE, degradation commenced after a 48-hour lag phase, while microcosms containing cis-DCE exhibited no lag phase, requiring approximately 16 days for complete transformation into VC. The absence of a lag phase for cis-DCE may be attributed to its prevalence – along with VC – as the dominant contaminant in the sampled slurry, which likely rendered the functional genes for these compounds active while those for PCE and TCE degradation inactive. Under experimental conditions, the degradation rates of PCE and TCE were significantly higher than that of cis-DCE.

Due to the rapid degradation of PCE and TCE, correlating microbiological activity with degradation was only feasible for the cis-DCE microcosms. Although an initial decrease in *Dhc* and Rdhase abundance was hypothesized to result from disturbances caused by purging during preparation and, temporary depletion of CEs until the microcosms were spiked, the expression of *tceA* and *bvcA* was successfully associated with the transformation of cis-DCE to VC and VC to ethene, respectively, aligning with the observed increase in the molar fraction of ethene in microcosms. These findings indicate that *Dhc* populations and RD functional genes served as reliable indicators of cis-DCE and VC biodegradation in microcosm experiments.

Contaminated site-specific isotopic fractionation values ($\varepsilon^{13}C$ and $\varepsilon^{37}Cl$) for the RD of PCE, TCE and cis-DCE, as well as $\varepsilon^{13}C$ for VC, were determined in the microcosm experiments and $\Lambda^{C\text{-}Cl}$ values could be compared with those available in the literature. Similarities to PCE isotopic patterns observed in *Sulfurospirillum*-containing cultures indicate that the microbial community in the field most probably degraded the PCE using $PceA_{PCE}$ enzyme. The calculated values for TCE were also similar to previously reported values for RD by *Dhc* and *Sufurospirillum* (Kuder et al., 2013; Renpenning et al., 2014), so other microbial communities or abiotic degradation processes like iron-mediated reduction, could be dismissed. While the calculated $\Lambda^{C\text{-}Cl}$ for cis-DCE agreed well with the value reported in a previous study using field-derived microcosms (Doğan-Subaşı et al., 2017), those were significantly lower than the range observed in previous laboratory

studies with pure, enrichment and mixed cultures (Ojeda et al., 2020). These differences are further discussed in section 6.2.

The determination of field-specific $\Lambda^{C\text{-}Cl}$ values in laboratory experiments facilitated the precise identification of degradation processes in field applications, helping to bridge the gap between laboratory and field studies. Additionally, the determined $\Lambda^{C\text{-}Cl}$ values contribute to the general database of dual isotope slopes for biotic RD.

6.2. Field scale application of EVO for CEs remediation

This section discusses the results obtained from the field application of EVO at a site contaminated with CEs. Isotopic and molecular analysis of samples collected over 16 months were studied to identify the process controlling biodegradation and estimate its extent. Detailed results of the field-scale biostimulation application and degradation mechanism identification are provided in sections 4.3, 4.4 and 4.6, while the results of the biodegradation extent calculation are detailed in section 4.7.

In general, groundwater exhibited anoxic conditions prior to injection, with DO values close to zero in all measurements. Following the EVO injection, a shift towards stronger reducing conditions was observed, falling within the range of sulfate-reducing to methanogenic conditions, as nitrate and sulfate redox-sensitive species were completely depleted and ORP values dropped as low as -150 mV. These observations confirm that the EVO injection effectively enhanced reducing conditions within the aquifer, creating an adequate environment for RD according to Leeson et al. (2004) and Henterly et al. (2015).

Prior to EVO injection, PCE and, to a lesser extent, TCE were the principal contaminants in terms of molar concentration. The presence of degradation products cis-DCE and VC in some wells indicated a certain extent of natural attenuation, suggesting that biostimulation could be an effective approach. After the EVO injection, a significant shift of CEs relative distribution in groundwater was observed, with the system becoming dominated by cis-DCE and VC, while PCE and TCE were only detected in four wells. This rapid transition suggests that PCE and TCE were rapidly transformed in situ, in agreement with the rapid biodegradation observed in microcosm experiments. However, other processes such as partitioning of CEs into the EVO phase and CEs mobilization/desorption during the EVO injection may also influence parent compound / daughter product ratios. Therefore, isotopic and biomolecular analyses were key data to document CEs transformation in this complex system.

The total concentration of CEs in groundwater increased in most wells (especially high at W4 and W8) immediately following the injection. Similar trends in other EVO field applications (Révész et al., 2014) were often attributed to the mobilization of DNAPL or adsorbed CEs from aquifer materials. At the studied site, dissolved DNAPL may have been rapidly degraded to cis-DCE, as rapid biodegradation rates were observed in microcosm experiments, leading to the high post-injection cis-DCE concentrations. By September 2021, total CEs concentrations had significantly decreased across all wells except for well W1, where an increase was observed.

The total bacterial population showed a heterogeneous distribution across the site before the EVO injection, with no apparent correlation to initial CEs concentrations or redox conditions. *Dhc* populations were detected in all the wells before the EVO injection but were considered insufficient for effective natural attenuation according to literature (Lu et al., 2006; Ernst, 2009; Ritalahti et al., 2010). However, significant changes were observed six months after the EVO injection: (i) *Dhc* gene copies increased by 1 to 3 orders of magnitude; (ii) *Dhc* relative abundance rose from 0-2% to 10-30% of the total bacterial population and (iii) RD functional genes abundance increased. These findings indicate that the EVO biostimulation successfully enhanced the anaerobic OHRB community, particularly *Dhc*, consistent with the results observed in cis-DCE microcosm experiments.

Following the rapid degradation of PCE and TCE, cis-DCE became the predominant contaminant in most post-injection samples (Figure 15). Furthermore, as the use of multi-element isotope data to investigate the fate of cis-DCE in the field is still very scarce in the literature (Zimmermann et al., 2020), the discussion of isotopic data in field samples is focused on cis-DCE transformation. Pre-injection samples cis-DCE isotopic pattern (June 2020) suggested cis-DCE formation from TCE, consistent with values reported by Cretnik et al. (2014c) and with high molar fractions of TCE and PCE (Figure 15). While post-injection trend towards more positive $\delta^{13}C_{DCE}$ and $\delta^{37}Cl_{DCE}$ values (Figure 19) was indicative of cis-DCE transformation following the biostimulation treatment. The field derived $\Lambda^{C\text{-}Cl}$ value of 5 ± 3 (Figure 19), aligned with the laboratory-determined $\Lambda^{C\text{-}Cl}$ = 4.9 ± 0.8. This suggests that microbial RD via hydrogenolysis to VC controlled cis-DCE transformation at the site, together with the detection of VC (molar fraction > 5%) in all selected samples.

Dhc bacteria were identified as the primary responsible for RD of cis-DCE in both field site and microcosm experiments. However, previously reported $\Lambda^{C\text{-}Cl}$ values for microbial RD of cis-DCE by *Dhc* strains and mixed cultures containing *Dhc* spp. were significantly higher than those

determined in this study (Figure 19). These differences might be related with distinct reaction mechanisms during RD within *Dhc* strains. Furthermore, discrepancies on $\Lambda^{C\text{-}Cl}$ values, especially when small isotopic fractionation is observed for both carbon and chlorine, might not reflect the chemical reaction mechanism, but preceding rate-limiting steps during enzyme – substrate association or enzymatic structure, as previously reported for other compounds such as PCE (Renpenning et al., 2014), TCE (Gafni et al., 2020) and TCM (Heckel et al., 2019). Further research is necessary to unravel the mechanics behind these observed differences for RD of cis-DCE. Notably, the observed $\Lambda^{C\text{-}Cl}$ slope was distinct from those associated with aerobic oxidation or abiotic degradation processes (e.g., oxidation by permanganate), indicating that RD was the primary degradation pathway during enhanced in situ bioremediation (Figure 19).

By confirming RD as the major degradation mechanism and ruling out a significant contribution of other processes such as aerobic oxidation, the extent of contaminant degradation could be estimated using microcosm-derived εC values. Additionally, isotopic mass balance calculations were applied to assess the complete dechlorination extent of PCE to ethene. To this end, the initial isotopic composition of the original contaminant (i.e. PCE) needs to be known or estimated. The isotopic value of DNAPL (PCE) found approximately 50 meters north of the study area was evaluated and considered as a probable isotopic composition of the original contamination. This was supported by the fact that the $\delta^{13}C$ and $\delta^{37}Cl$ of the PCE-DNAPL fitted well with the distribution of isotopic values for PCE in groundwater before the EVO injection in the dual C-Cl isotope plot (Figure 20).

Before injection, B_{PCE} calculations indicated that PCE transformation to TCE exceeded 90% in three piezometers, while for others it ranged from 24% to 78%. However, no clear spatial trends were observed (Table 9, Figure 21). During the post-injection monitoring period, B_{cDCE} reached values ranging from 91 to 99% in eight wells confirming effective cis-DCE transformation, while in the remaining three wells isotopic data was not available due to low cis-DCE concentrations. These isotopic results indicate that cis-DCE accumulation was transient and, and that EVO was an effective long-term electron donor throughout the sampling period.

Finally, isotopic mass balance calculations (Eq. 3) demonstrated that, while some extent of natural attenuation occurred pre-injection, the $\delta^{13}C_{CEs}$ was for all wells in the range of commercial PCE, closely matching the isotopic signature of the DNAPL, and indicating minimal degradation to ethene at that stage. Post-injection, wells W7, W9 and W10 exhibited enriched $\delta^{13}C_{CEs}$ values enriched in ^{13}C, suggesting active degradation to ethene. The extent of biodegradation to ethene in wells W2, W3, W4, W5, W7 and W8, where isotopic mass balance

data were available for most samplings (Figure 23), ranged from 30 to 80%, confirming the successful stimulation of RD processes at the contaminated site.

6.3. Laboratory experiments for the evaluation of TCM degradation mechanisms with alkaline-activated persulfate

This section discusses the results obtained from laboratory batch experiments conducted to evaluate TCM degradation by alkaline-activated PS. Carbon and chlorine isotopic fractionation for TCM transformation under different simulated field conditions was investigated to evaluate whether it might result in diverse degradation mechanisms. Detailed experimental results are provided in Section 5.

The experiments evaluating the effect of the TCM:PS molar ratio demonstrated that increasing the PS molar ratio enhanced TCM degradation rates. Despite the observed differences in kinetics, experiments with different TCM:PS molar ratios (1:65 and 1:125) exhibited comparable enrichment of TCM in both ^{13}C and ^{37}Cl, while isotopic changes in the controls were not statistically significant ($p>0.05$) (Figure 28 and Figure 29). The determined Λ^{C-Cl} values did not show a significant difference, being 33 ± 6 and 23 ± 10 for experiments i.a and i.b (**Errore. L'origine riferimento non è stata trovata.**), respectively. The notably higher carbon isotope fractionation compared to chlorine suggests an oxidation mechanism by alkaline-activated PS at pH 10.2.

Experiments conducted at different pH values (11.4 and 12.8) revealed a shift in the degradation mechanism at higher pH. At pH 11.4 the kinetics and isotopic fractionation were similar to those observed at pH 10.2, indicating that oxidation remained the dominant mechanism. However, at pH 12.8, the degradation rate decreased significantly, and control vials without PS also exhibited noticeable degradation, attributed to AH. Isotopic results corroborated this observation, with Λ^{C-Cl} values aligning with previously reported values for TCM AH-driven degradation. These results highlight the increasing contribution of AH at higher pH levels, leading to a reduction in the overall degradation rate of TCM in the experimental vials. These results also highlight the utility of isotopic analysis in distinguishing TCM degradation mechanisms.

The introduction of carbonate anions influenced TCM degradation, causing variations in kinetic and isotopic fractionation. At pH 11.3, carbonate appeared to slightly enhance degradation

kinetics, potentially by altering radical chemistry and promoting carbonate radicals as additional oxidants. However, at higher pH (12.8), degradation kinetics closely resembled those observed in the absence of PS, reinforcing the dominance of AH. Isotope fractionation trends suggest that the presence of carbonate anions may introduce alternative degradation mechanisms, potentially involving a combination of oxidative and reductive processes.

Under conditions mimicking an alkaline trench, TCM degradation occurred notably faster than in other experiments. The presence of PS significantly enhanced degradation, while control vials exhibited much slower kinetics. Isotopic fractionation results suggest that alternative degradation mechanisms might be involved, with a lower $\Lambda^{C\text{-}Cl}$ value suggesting a shift toward reductive processes. The excess carbonate anion in this solution, resulting from equilibrium with the solid phase, may have played a crucial role, as this anion can act as a scavenger of sulfate and hydroxyl radicals. The reduced availability of these radicals may have enhanced the contribution of superoxide radicals in TCM degradation. This hypothesis is supported by the observed $\Lambda^{C\text{-}Cl}$ trend, which suggests that ISCR might be occurring alongside oxidation. These findings raise important considerations regarding TCM degradation mechanisms in complex environmental matrices containing carbonate and show the potential of dual isotopic analysis to detect variations in the reaction mechanisms responsible of degradation.

Overall, these findings emphasize the complexity of TCM degradation in alkaline-activated PS systems. The interplay between oxidation, AH and potentially a reductive mechanism, influenced by the pH and carbonate presence, affects the degradation kinetics and isotopic fractionation. The ability to distinguish degradation mechanisms using isotopic analysis provides a valuable tool for assessing remediation strategies. Further research is needed to clarify the mechanisms and role of mixed oxidative-reductive pathways and their implications for ISCO treatments at contaminated sites.

Unexpectedly, higher chlorinated compounds than the original contaminant accumulated, with HCA emerging as the primary byproduct in experiments that contained PS at pH 11.4 with and without carbonate (iii.a and ii.a, respectively, Table 4). Besides the potential environmental implications of HCA formation during alkaline-activated PS treatment of TCM, its accumulation may indicate that hydroxyl radicals, rather than sulfate radical, were the predominant oxidant. Sulfate radicals are known to initiate the degradation of HCA, whereas hydroxyl radicals exhibit low reactivity toward it (Teel et al., 2002; Zhu et al., 2018). The conversion extent of the initial TCM to HCA was estimated at approximately 55-65%. However, the relatively high concentration of TCM in a closed system might have enhanced the formation and accumulation of HCA in

experimental vials. Further investigation in field applications will be required to assess the generation and fate of HCA in an alkaline trench or in an aquifer.

Chapter V. CONCLUSIONS

The primary objective of this thesis was to deepen the understanding of the application of multi-isotopic tools for the assessment of novel remediation techniques in sites contaminated with chlorinated solvents under varying environmental conditions. An integrative approach combining hydrogeochemical data, biomolecular analysis and 2D-CSIA techniques was employed both at laboratory and field scales to evaluate biostimulation using EVO at Site A, contaminated with CEs, and to assess degradation mechanisms following ISCO with alkaline-activated PS at site B, simulating different field conditions in laboratory batch experiments.

The main achievements and general conclusions derived from this thesis are:

- The use of EVO, which involves a high partitioning of the organic contaminants into the oil phase, did not show significant isotopic effects associated with partitioning processes and, therefore, it did not interfere with the application of isotopic analysis for the identification of degradation mechanisms in field applications. Consequently, microcosm experiments provided valuable insights that could allow the identification of the degradation process in the field despite partitioning processes, while improving general knowledge for future applications.

- Isotopic analysis of field samples during bioremediation with EVO yielded a cis-DCE $\Lambda^{C\text{-}Cl}$ value of 5 ± 3, which align with the value of 4.9 ± 0.8 obtained from the laboratory experiments. This indicates that microbial RD via hydrogenolysis to VC controlled the fate of cis-DCE at the site following the EVO injection. Interestingly, field-derived microcosm experiments produced $\Lambda^{C\text{-}Cl}$ values different than those reported in previous literature. This discrepancy may be attributed to variations in the reaction mechanism during RD of cis-DCE by *Dhc* bacteria or to rate-limiting preceding steps during enzyme-substrate association. This underscores the importance of conducting microcosm experiments closer to field conditions for advancing a more accurate assessment of predominant degraders in the microbial community under in situ conditions.

- Microbiological analyses, in conjunction with hydrogeochemical data of the aquifer, provide complementary lines of evidence essential for understanding the various processes occurring in the field that may influence RD following an EVO injection. The presence of specific bacterial communities before the injection and the subsequent changes in population dynamics and functional gene expression during bioremediation can serve as indicators of particular degradation pathways. This is especially relevant in

cases where isotopic values have not been previously reported or where different treatments could result in similar $\Lambda^{C\text{-}Cl}$ values.

- Isotopic mass balance is a valuable tool for estimating the extent of biodegradation of the primary contaminant (PCE) into non-chlorinated and non-toxic ethene. Before the EVO injection, although the detection of degradation products (TCE, cis-DCE, VC) and a certain degree of PCE isotopic enrichment in ^{13}C indicated that natural attenuation processes were already occurring at the site, isotopic balance analysis indicated that significant degradation to ethene had not yet been achieved. However, following the EVO injection the isotopic mass balance indicated that degradation to ethene ranged from 30 to 80%.

- Overall, the study of bioestimulation using EVO at a site contaminated with CEs highlights the importance of determining site-specific Λ and ε values derived from microcosm experiments to enhance the identification and quantification of transformation processes in contaminated sites using isotopic data. Our findings provide valuable insight into the practical application of dual (C, Cl) isotopic analysis and biomolecular tools to i) assess degradation mechanism of CEs, particularly cis-DCE, in contaminated sites undergoing EISB with EVO, and ii) improve the understanding of the complex interactions among EVO, contaminant concentrations, and microbial communities in future field studies.

- Dual (C, Cl) isotope analysis revealed that the degradation mechanisms of TCM by alkaline-activated PS can vary under different field conditions. First, alkaline-activated PS in DI water under moderate alkaline pH (10.2-11.4) yielded a $\Lambda^{C\text{-}Cl}$ value of 29 ± 4, indicating an oxidative process that can be differentiated from that of thermal-activated PS, possibly due to the generation of hydroxyl radicals under alkaline pH. Second, at higher pH (12.8), AH became the predominant reaction mechanism even in the presence of PS, with $\Lambda^{C\text{-}Cl}$ values of 11 ± 1 and 9 ± 1, lowering overall degradation rates. Finally, under trench conditions, and hypothetically due to an excess in dissolved carbonate concentrations, a reductive degradation mechanism might be predominant. As the carbonate anion is known to act as sulfate radical and hydroxyl radical scavenger, the reduced availability of these radicals may have enhanced the contribution of superoxide radicals in TCM degradation. This hypothesis is supported by the observed $\Lambda^{C\text{-}Cl}$ trend,

which suggests that ISCR may be occurring alongside oxidation. These findings raise important considerations regarding TCM degradation mechanisms during alkaline-activated PS treatments in complex environmental matrices containing carbonate. These results also show the potential of dual isotopic analysis to identify the reaction mechanisms controlling TCM degradation.

- The different carbon isotope fractionation values obtained in the experiments performed in this thesis underscores the need for caution when applying CSIA for the quantification of TCM degradation in PS-based ISCO treatments. Relying on εC values obtained from simplified, deionized water experiments, common in literature, could lead to a significant underestimation of degradation extent when assessing TCM transformation with PS.

- Overall, the distinct $\Lambda^{C\text{-}Cl}$ values obtained in this thesis provide compelling evidence to differentiate between the AH pathway and various degradation reactions involving ROS that may co-occur when using alkaline-activated PS in TCM-contaminated sites. The range of $\Lambda^{C\text{-}Cl}$ values observed in our experiments also suggests that distinguishing between the action of alkaline-activated PS and TCM reductive biodegradation in the field may not always be possible based solely on isotopic C-Cl data. The range of $\Lambda^{C\text{-}Cl}$ values for TCM RD overlaps with the slopes obtained in the presence of carbonates, probably associated with a reductive degradation mechanism. In such cases, a more comprehensive analysis, including detailed hydrogeochemical and biological molecular tools, may be required to fully characterize the degradation mechanisms.

- To the best of the authors' knowledge, this is the first study to document the formation of highly chlorinated byproducts such as HCA and CT during the chemical oxidation of TCM by PS. The formation of these byproducts raises important environmental concerns as both HCA and CT are toxic and persistent in the environment. Several factors need to be considered when translating these findings to field applications: (i) our experiments were conducted in a closed system, leading to elevated byproducts concentrations that may be mitigated by dilution in natural settings; (ii) the initial TCM concentration was 690 mg/L, which represents conditions near free-phase (DNAPL) zones or source areas of pollution, where PS treatments are often applied. Along the contamination plume, where the concentration of the contaminant is lower, expected generation of HCA would be reduced; (iii) processes such as volatilization and adsorption could reduce HCA concentrations in the field. Despite these considerations, the detection of HCA and CT in

this study highlights the need for further investigation into the potential unintended consequences of PS-based ISCO techniques in TCM-contaminated sites. The results of this study might have thus important implications for the selection and evaluation of remediation strategies by environmental consultants and site managers.

Overall, the conclusions derived from this thesis validate the use of multi-isotopic tools, complemented with other techniques such as biomolecular tools, to evaluate and monitor remediation strategies in the field, elucidate degradation mechanisms, and assess the degradation extent, providing relevant information for future environmental studies.

Future research

The results obtained in this thesis lead to the following considerations to further advance in the application of multi-isotopic techniques at sites contaminated with chlorinated solvents.

Carbon and chlorine CSIA of cis-DCE has proven useful for identifying degradation process in the field (i.e. RD), as the measured $\Lambda^{C\text{-}Cl}$ slope in the field was statistically similar to that obtained in field-specific microcosm experiments. This result highlights the potential of multi-element CSIA to fill the gap between laboratory and field studies. Additionally, microbiological data indicated that *Dhc* bacteria were most likely responsible for RD of cis-DCE in both the field site and the microcosm experiments. However, the observed dual-element isotope slope was lower than expected based on the range reported in previous laboratory studies using pure, enrichment cultures and mixed cultures (Abe et al., 2009b; Kuder et al., 2013; Lihl et al., 2019). On the other hand, the value obtained in this thesis aligns well with findings from a previous study using field-derived microcosms (Doğan-Subaşı et al., 2017). Therefore, further research could try to enrich the microbial community or even isolate the cis-DCE degrader in order to explore if this isotopic pattern repeats and to discover the enzymes and/or mechanisms behind these observed differences in RD of cis-DCE.

For TCM, distinct $\Lambda^{C\text{-}Cl}$ values obtained from experiments simulating different field conditions provided strong evidence for the potential of 2D-CSIA to differentiate between AH and other TCM degradation mechanisms during an ISCO treatment with base-activated PS, likely involving different reactive oxygen species (i.e., $OH^{\cdot}$, $SO_4^{\cdot-}$, $O_2^{\cdot-}$ and $CO_3^{\cdot-}$). While these findings revealed that multiple processes may co-occur during ISCO with alkaline-activated PS in TCM-contaminated sites, further research should be made to identify the predominant reactive radical(s) in each case. For instance, experiments using scavengers such as methanol/ethanol (which can effectively quench both $SO_4^{\cdot-}$ and $OH^{\cdot}$) versus tert-butyl alcohol (more selective for $OH^{\cdot}$) or employing advanced techniques such as electron paramagnetic resonance (EPR) spectroscopy to fully elucidate the specific radical species responsible for TCM degradation under the different conditions investigated. Furthermore, there is still space to better understand the role of mixed oxidative-reductive mechanisms and their implications for ISCO applications at contaminated sites. Validating the TCM C-Cl slope in the presence of carbonates at field scale remains a key challenge, as does identifying alternative tools to distinguish it from biotic RD in the aquifer of the same site.

Finally, the formation of highly chlorinated byproducts such as HCA and CT during chemical oxidation of TCM by alkaline-activated PS raises important environmental concerns, given the toxicity and persistence of both HCA and CT in the environment. Therefore, the assessment of the potential accumulation of these byproducts at field scale is also necessary. This should consider more realistic open system conditions, with lower or varying TCM concentrations at the injection point and along the contamination plume, to better understand whether this potential accumulation could really occur.

BIBLIOGRAPHIC REFERENCES

Abe, Y., Aravena, R., Zopfi, J., Shouakar-Stash, O., Cox, E., Roberts, J. D., & Hunkeler, D. (2009a). Carbon and chlorine isotope fractionation during aerobic oxidation and reductive dechlorination of vinyl chloride and cis-1, 2-dichloroethene. *Environmental Science and Technology*, *43*(1), 101–107. https://doi.org/10.1021/es801759k

Abe, Y., Aravena, R., Zopfi, J., Shouakar-Stash, O., Cox, E., Roberts, J. D., & Hunkeler, D. (2009b). Carbon and chlorine isotope fractionation during aerobic oxidation and reductive dechlorination of vinyl chloride and cis-1, 2-dichloroethene. *Environmental Science and Technology*, *43*(1), 101–107. https://doi.org/10.1021/es801759k

ACA. (2009). *Criteris d'aplicació dels valors genèrics per a la restauració d'aigües subterrànies en emplaçaments contaminants per fonts d'origen puntual*. https://aca.gencat.cat/web/.content/10_ACA/J_Publicacions/04-protocols/09-criteris_aplicaciovalors_generics_rest.pdf

Adrian, L., & Löffler, F. E. (2016). *Organohalide-Respiring Bacteria* (L. Adrian & F. E. Löffler, Eds.). Springer Berlin Heidelberg. https://doi.org/10.1007/978-3-662-49875-0

Aelion, C. M., Höhener, P., Hunkeler, D., & Aravena, R. (2009). Environmental isotopes in biodegradation and bioremediation. In *Environmental Isotopes in Biodegradation and Bioremediation*. https://doi.org/10.1201/9781420012613

Aeppli, C., Berg, M., Cirpka, O. A., Holliger, C., Schwarzenbach, R. P., & Hofstetter, T. B. (2009). Influence of mass-transfer limitations on carbon isotope fractionation during microbial dechlorination of trichloroethene. *Environmental Science and Technology*, *43*(23), 8813–8820. https://doi.org/10.1021/es901481b

Aeppli, C., Hofstetter, T. B., Amaral, H. I. F., Kipfer, R., Schwarzenbach, R. P., & Berg, M. (2010). Quantifying in situ transformation rates of chlorinated ethenes by combining compound-specific stable isotope analysis, groundwater dating, and carbon isotope mass balances. *Environmental Science and Technology*, *44*(10), 3705–3711. https://doi.org/10.1021/es903895b

Aeppli, C., Holmstrand, H., Andersson, P., & Gustafsson, Ö. (2010). Direct compound-specific stable chlorine isotope analysis of organic compounds with quadrupole GC/MS using standard isotope bracketing. *Analytical Chemistry*, *82*(1), 420–426. https://doi.org/10.1021/ac902445f

Alvarez, P. J. J., & Illman, W. A. (2005). Introduction to Bioremediation. In *Bioremediation and Natural Attenuation*. https://doi.org/10.1002/047173862x.ch1

Amaral, H. I. F., Aeppli, C., Kipfer, R., & Berg, M. (2011). Assessing the transformation of chlorinated ethenes in aquifers with limited potential for natural attenuation: Added values of compound-specific carbon isotope analysis and groundwater dating. *Chemosphere*, *85*(5), 774–781. https://doi.org/10.1016/j.chemosphere.2011.06.063

Andrew James, C., Xin, G., Doty, S. L., Muiznieks, I., Newman, L., & Strand, S. E. (2009). A mass balance study of the phytoremediation of perchloroethylene-contaminated groundwater. *Environmental Pollution*, *157*(8–9). https://doi.org/10.1016/j.envpol.2009.02.033

ARC. (2020). *Memòria de l'Agència de Residus de Catalunya*.

Asfaw, B. A., Sakaguchi-Söder, K., Schiedek, T., Michelsen, N., Bernstein, A., Siebner, H., & Schüth, C. (2023). Isotopic evidence (δ13C, δ37Cl, δ2H) for distinct transformation mechanisms of chloroform: Catalyzed H2-water system vs. zero-valent iron (ZVI). *Journal of Environmental Chemical Engineering*, *11*(3). https://doi.org/10.1016/j.jece.2023.110005

Atlas, R. M., Philp, J., & Washington, A. P. (2005). Bioremediation Applied Microbial Solutions for Real-World Environmental Cleanup Library of Congress Cataloging-in-Publication Data. In *Bioremediation. I. Atlas, Ronald M* (Vol. 5).

ATSDR. (2022). *ATSDR's Substance Priority List.* Https://Www.Atsdr.Cdc.Gov/Programs/Substance-Priority-List.Html.

Audí-Miró, C., Cretnik, S., Otero, N., Palau, J., Shouakar-Stash, O., Soler, A., & Elsner, M. (2013a). Cl and C isotope analysis to assess the effectiveness of chlorinated ethene degradation by zero-valent iron: Evidence from dual element and product isotope values. *Applied Geochemistry*, *32*, 175–183. https://doi.org/10.1016/j.apgeochem.2012.08.025

Audí-Miró, C., Cretnik, S., Otero, N., Palau, J., Shouakar-Stash, O., Soler, A., & Elsner, M. (2013b). Cl and C isotope analysis to assess the effectiveness of chlorinated ethene degradation by zero-valent iron: Evidence from dual element and product isotope values. *Applied Geochemistry*, *32*, 175–183. https://doi.org/10.1016/j.apgeochem.2012.08.025

Audí-Miró, C., Cretnik, S., Torrentó, C., Rosell, M., Shouakar-Stash, O., Otero, N., Palau, J., Elsner, M., & Soler, A. (2015). C, Cl and H compound-specific isotope analysis to assess natural versus Fe(0) barrier-induced degradation of chlorinated ethenes at a contaminated site. *Journal of Hazardous Materials*, *299*. https://doi.org/10.1016/j.jhazmat.2015.06.052

Azadpour-Keeley, A., Sewell, G. W., & Russell, H. H. (2005). Microbial Processes Affecting Monitored Natural Attenuation of Contaminants in the Subsurface. In *Water Encyclopedia* (pp. 578–594). https://doi.org/https://doi.org/10.1002/047147844X.gw1555

Badin, A., Broholm, M. M., Jacobsen, C. S., Palau, J., Dennis, P., & Hunkeler, D. (2016). Identification of abiotic and biotic reductive dechlorination in a chlorinated ethene plume after thermal source remediation by means of isotopic and molecular biology tools. *Journal of Contaminant Hydrology*, *192*, 1–19. https://doi.org/10.1016/j.jconhyd.2016.05.003

Badin, A., Buttet, G., Maillard, J., Holliger, C., & Hunkeler, D. (2014). Multiple dual C-Cl isotope patterns associated with reductive dechlorination of tetrachloroethene. *Environmental Science and Technology*, *48*(16), 9179–9186. https://doi.org/10.1021/es500822d

Barul, C., Fayossé, A., Carton, M., Pilorget, C., Woronoff, A. S., Stücker, I., & Luce, D. (2017). Occupational exposure to chlorinated solvents and risk of head and neck cancer in men: A population-based case-control study in France. *Environmental Health: A Global Access Science Source*, *16*(1). https://doi.org/10.1186/s12940-017-0286-5

Bhatt, P., Kumar, M. S., Mudliar, S., & Chakrabarti, T. (2007). Biodegradation of chlorinated compounds - A review. In *Critical Reviews in Environmental Science and Technology* (Vol. 37, Issue 2). https://doi.org/10.1080/10643380600776130

Blázquez-Pallí, N., Rosell, M., Varias, J., Bosch, M., Soler, A., Vicent, T., & Marco-Urrea, E. (2019). Multi-method assessment of the intrinsic biodegradation potential of an aquifer contaminated with chlorinated ethenes at an industrial area in Barcelona (Spain). *Environmental Pollution*, *244*, 165–173. https://doi.org/10.1016/j.envpol.2018.10.013

Bloom, Y., Aravena, R., Hunkeler, D., Edwards, E., & Frape, S. K. (2000). Carbon isotope fractionation during microbial dechlorination of trichloroethene, cis-l,2-dichloroethene, and vinyl chloride: Implications for assessment of natural attenuation. *Environmental Science and Technology*, *34*(13), 2768–2772. https://doi.org/10.1021/es991179k

Bombach, P., Richnow, H. H., Kästner, M., & Fischer, A. (2010). Current approaches for the assessment of in situ biodegradation. In *Applied Microbiology and Biotechnology* (Vol. 86, Issue 3). https://doi.org/10.1007/s00253-010-2461-2

Bouwer, E. J. (2017). Bioremediation of chlorinated solvents using alternate electron acceptors. In *Handbook of Bioremediation*. https://doi.org/10.1201/9780203712764

Brown, R. A. (2010). *Chemical Oxidation and Reduction for chlorinated Solvent Remediation*. https://doi.org/10.1007/978-1-4419-1401-9_15

Brown, R. A., Mueller, J. G., Seech, A. G., Henderson, J. K., & Wilson, J. T. (2009). Interactions between biological and abiotic pathways in the reduction of chlorinated solvents. *Remediation*, *20*(1). https://doi.org/10.1002/rem.20226

Brüning, T., Pesch, B., Wiesenhütter, B., Rabstein, S., Lammert, M., Baumüller, A., & Bolt, H. M. (2003). Renal cell cancer risk and occupational exposure to trichloroethylene: Results of a consecutive case-control study in Arnsberg, Germany. *American Journal of Industrial Medicine*, *43*(3), 274–285. https://doi.org/10.1002/ajim.10185

Brusseau, M. L., Sabatini, D. A., Gierke, J. S., & Annable, M. D. (1999). Innovative subsurface remediation: field testing of physical, chemical and characterization technologies. ACS. In *Innovative subsurface remediation : field testing of physical, chemical and characterization technologies. ACS symposium series 725.*

Bryck, S. (2014). *Numerical Modeling of Thermal Enhancement of In Situ Chemical Oxidation (ISCO) and Enhanced In Situ Bioremediation (EISB)*. Queen's University (Canada).

Büsing, J., Buchner, D., Behrens, S., & Haderlein, S. B. (2020). Deciphering the Variability of Stable Isotope (C, Cl) Fractionation of Tetrachloroethene Biotransformation by Desulfitobacterium strains Carrying Different Reductive Dehalogenases Enzymes. *Environmental Science and Technology*, *54*(3), 1593–1602. https://doi.org/10.1021/acs.est.9b05606

Buxton, G. V, Greenstock, C. L., Helman, W. P., & Ross, A. B. (1988). Critical Review of rate constants for reactions of hydrated electrons, hydrogen atoms and hydroxyl radicals (·OH/·O− in Aqueous Solution. *Journal of Physical and Chemical Reference Data*, *17*(2), 513–886. https://doi.org/10.1063/1.555805

Canonica, S., Kohn, T., Mac, M., Real, F. J., Wirz, J., & Von Gunten, U. (2005). Photosensitizer method to determine rate constants for the reaction of carbonate radical with organic compounds. *Environmental Science and Technology*, *39*(23), 9182–9188. https://doi.org/10.1021/es051236b

Cao, M., Hou, Y., Zhang, E., Tu, S., & Xiong, S. (2019). Ascorbic acid induced activation of persulfate for pentachlorophenol degradation. *Chemosphere*, *229*, 200–205. https://doi.org/10.1016/j.chemosphere.2019.04.135

Chen, G., Kara Murdoch, F., Xie, Y., Murdoch, R. W., Cui, Y., Yang, Y., Yan, J., Key, T. A., & Löffler, F. E. (2022). Dehalogenation of Chlorinated Ethenes to Ethene by a Novel Isolate, "Candidatus Dehalogenimonas etheniformans." *Applied and Environmental Microbiology*, *88*(12). https://doi.org/10.1128/aem.00443-22

Chen, S. K., Yang, H. Y., Huang, S. R., Hung, J. M., Lu, C. J., & Liu, M. H. (2020). Complete degradation of chlorinated ethenes and its intermediates through sequential anaerobic/aerobic biodegradation in simulated groundwater columns (complete degradation of chlorinated ethenes). *International Journal of Environmental Science and Technology*, *17*(11). https://doi.org/10.1007/s13762-020-02792-z

Chen, W., Chen, K., Surmpalli, R. Y., Zhang, T. C., Ou, J., & Kao, C. (2022). Bioremediation of trichloroethylene-polluted groundwater using emulsified castor oil for slow carbon release and acidification control. *Water Environment Research*, *94*(1). https://doi.org/10.1002/wer.1673

Christensen, K. Y., Vizcaya, D., Richardson, H., Lavoué, J., Aronson, K., & Siemiatycki, J. (2013). Risk of selected cancers due to occupational exposure to chlorinated solvents in a case-control study in montreal. *Journal of Occupational and Environmental Medicine*, *55*(2). https://doi.org/10.1097/JOM.0b013e3182728eab

Christensen, T. H., Bjerg, P. L., Banwart, S. A., Jakobsen, R., Heron, G., & Albrechtsen, H. J. (2000). Characterization of redox conditions in groundwater contaminant plumes. *Journal of Contaminant Hydrology*, *45*(3–4), 165–241. https://doi.org/10.1016/S0169-7722(00)00109-1

Ciampi, P., Esposito, C., Bartsch, E., Alesi, E. J., & Petrangeli Papini, M. (2023). Pump-and-treat (P&T) vs groundwater circulation wells (GCW): Which approach delivers more sustainable and effective groundwater remediation? *Environmental Research*, *234*. https://doi.org/10.1016/j.envres.2023.116538

Cichocka, D., Imfeld, G., Richnow, H. H., & Nijenhuis, I. (2008). Variability in microbial carbon isotope fractionation of tetra- and trichloroethene upon reductive dechlorination. *Chemosphere*, *71*(4), 639–648. https://doi.org/10.1016/j.chemosphere.2007.11.013

Cohen, L. R., Peña, L. A., Seidl, A. J., Chau, K. N., Keck, B. C., Feng, P. L., & Hoggard, P. E. (2009). Photocatalytic degradation of chloroform by bis (bipyridine)dichlororuthenium(III/II). *Journal of Coordination Chemistry*, *62*(11), 1743–1753. https://doi.org/10.1080/00958970802702254

Coplen, T. B. (1996). New guidelines for reporting stable hydrogen, carbon, and oxygen isotope-ratio data. *Geochimica et Cosmochimica Acta*, *60*(17), 3359–3360. https://doi.org/10.1016/0016-7037(96)00263-3

Coplen, T. B., Brand, W. A., Gehre, M., Grhning, M., Meljer, L. H. A. J., Toman, B., & Verkouteren, R. M. (2006). New Guidelines for b 13 C Measurements. *Analytical Chemistry*, *78*(7), 2439–2441.

Cretnik, S., Bernstein, A., Shouakar-Stash, O., Löffler, F., & Elsner, M. (2014a). Chlorine isotope effects from isotope ratio mass spectrometry suggest intramolecular C-Cl bond competition in trichloroethene (TCE) reductive dehalogenation. *Molecules*, *19*(5), 6450–6473. https://doi.org/10.3390/molecules19056450

Cretnik, S., Bernstein, A., Shouakar-Stash, O., Löffler, F., & Elsner, M. (2014b). Chlorine isotope effects from isotope ratio mass spectrometry suggest intramolecular C-Cl bond competition in trichloroethene (TCE) reductive dehalogenation. *Molecules*, *19*(5), 6450–6473. https://doi.org/10.3390/molecules19056450

Cretnik, S., Bernstein, A., Shouakar-Stash, O., Löffler, F., & Elsner, M. (2014c). Chlorine isotope effects from isotope ratio mass spectrometry suggest intramolecular C-Cl bond competition in trichloroethene (TCE) reductive dehalogenation. *Molecules*, *19*(5), 6450–6473. https://doi.org/10.3390/molecules19056450

Cretnik, S., Thoreson, K. A., Bernstein, A., Ebert, K., Buchner, D., Laskov, C., Haderlein, S., Shouakar-Stash, O., Kliegman, S., McNeill, K., & Elsner, M. (2013). Reductive Dechlorination of TCE by Chemical Model Systems in Comparison to Dehalogenating Bacteria: Insights from Dual Element Isotope Analysis (13C/12C, 37Cl/35Cl). *Environmental Science & Technology*, *47*(13), 6855–6863. https://doi.org/10.1021/es400107n

Criquet, J., & Leitner, N. K. V. (2009). Degradation of acetic acid with sulfate radical generated by persulfate ions photolysis. *Chemosphere*, *77*(2), 194–200. https://doi.org/10.1016/j.chemosphere.2009.07.040

Declercq, I., Cappuyns, V., & Duclos, Y. (2012). Monitored natural attenuation (MNA) of contaminated soils: State of the art in Europe-A critical evaluation. *Science of the Total Environment*, *426*. https://doi.org/10.1016/j.scitotenv.2012.03.040

Devi, P., Das, U., & Dalai, A. K. (2016). In-situ chemical oxidation: Principle and applications of peroxide and persulfate treatments in wastewater systems. *Science of the Total Environment*, *571*, 643–657. https://doi.org/10.1016/j.scitotenv.2016.07.032

Doğan-Subaşı, E., Elsner, M., Qiu, S., Cretnik, S., Atashgahi, S., Shouakar-Stash, O., Boon, N., Dejonghe, W., & Bastiaens, L. (2017). Contrasting dual (C, Cl) isotope fractionation offers potential to distinguish reductive chloroethene transformation from breakdown by permanganate. *Science of the Total Environment*, *596–597*, 169–177. https://doi.org/10.1016/j.scitotenv.2017.03.292

Dolfing, J. (2016). Energetic considerations in organohalide respiration. In *Organohalide-Respiring Bacteria*. https://doi.org/10.1007/978-3-662-49875-0_3

Duhamel, M., Wehr, S. D., Yu, L., Rizvi, H., Seepersad, D., Dworatzek, S., Cox, E. E., & Edwards, E. A. (2002). *Comparison of anaerobic dechlorinating enrichment cultures maintained on*

tetrachloroethene , trichloroethene , cis -dichloroethene and vinyl chloride. *36*, 4193–4202.

Elsner, M. (2010). Stable isotope fractionation to investigate natural transformation mechanisms of organic contaminants: Principles, prospects and limitations. *Journal of Environmental Monitoring*, *12*(11), 2005–2031. https://doi.org/10.1039/c0em00277a

Elsner, M., & Hunkeler, D. (2008). Evaluating chlorine isotope effects from isotope ratios and mass spectra of polychlorinated molecules. *Analytical Chemistry*, *80*(12), 4731–4740. https://doi.org/10.1021/ac702543y

Emsbo-Mattingly, S. D., Flanders, K. L., & Litman, E. R. (2023). Integrated differentiation of multiple trichloroethylene and tetrachloroethylene groundwater impacts using spatial concentration, biodegradation indices, chemical fingerprinting and carbon/chlorine isotope patterns. *Environmental Forensics*, *24*(5–6). https://doi.org/10.1080/15275922.2022.2047832

Ernst, T. J. (2009). Use of "Dehalococcoides" to bioremediate groundwater contaminated with chlorinated solvents. *Basic Biotechnology EJournal*, *5*(1), 72–77.

Favre, H. A., & Powell, W. H. (2013). *Nomenclature of Organic Chemistry*. The Royal Society of Chemistry. https://doi.org/10.1039/9781849733069

Ferguson, J. F., & Pietari, J. M. H. (2000). Anaerobic transformations and bioremediation of chlorinated solvents. *Environmental Pollution*, *107*(2). https://doi.org/10.1016/S0269-7491(99)00139-6

Fletcher, K. E., Nijenhuis, I., Richnow, H. H., & Löffler, F. E. (2011). Stable carbon isotope enrichment factors for cis -1,2-dichloroethene and vinyl chloride reductive dechlorination by dehalococcoides. *Environmental Science and Technology*, *45*(7), 2951–2957. https://doi.org/10.1021/es103728q

Franke, S., Seidel, K., Adrian, L., & Nijenhuis, I. (2020). Dual Element (C/Cl) Isotope Analysis Indicates Distinct Mechanisms of Reductive Dehalogenation of Chlorinated Ethenes and Dichloroethane in Dehalococcoides mccartyi Strain BTF08 With Defined Reductive Dehalogenase Inventories. *Frontiers in Microbiology*, *11*(July). https://doi.org/10.3389/fmicb.2020.01507

Friis, A. K., Kofoed, J. L. L., Heron, G., Albrechtsen, H. J., & Bjerg, P. L. (2007). Microcosm evaluation of bioaugmentation after field-scale thermal treatment of a TCE-contaminated aquifer. *Biodegradation*, *18*(6). https://doi.org/10.1007/s10532-006-9098-y

Furman, O. S., Teel, A. L., Ahmad, M., Merker, M. C., & Watts, R. J. (2011). Effect of Basicity on Persulfate Reactivity. *Journal of Environmental Engineering*, *137*(4), 241–247. https://doi.org/10.1061/(asce)ee.1943-7870.0000323

Furman, O. S., Teel, A. L., & Watts, R. J. (2010). Mechanism of base activation of persulfate. *Environmental Science and Technology*, *44*(16), 6423–6428. https://doi.org/10.1021/es1013714

Gafni, A., Gelman, F., Ronen, Z., & Bernstein, A. (2020). Variable carbon and chlorine isotope fractionation in TCE co-metabolic oxidation. *Chemosphere*, *242*. https://doi.org/10.1016/j.chemosphere.2019.125130

Gafni, A., Siebner, H., & Bernstein, A. (2020). Potential for co-metabolic oxidation of TCE and evidence for its occurrence in a large-scale aquifer survey. *Water Research*, *171*, 115431. https://doi.org/https://doi.org/10.1016/j.watres.2019.115431

Halloran, L. J. S., Vakili, F., Wanner, P., Shouakar-Stash, O., & Hunkeler, D. (2021). Sorption- and diffusion-induced isotopic fractionation in chloroethenes. *Science of the Total Environment*, *788*, 147826. https://doi.org/10.1016/j.scitotenv.2021.147826

Harkness, M. (2000). Economic considerations in enhanced anaerobic biodegradation. *Bioremediation and Phytoremediation of Chlorinated and Recalcitrant Compounds*, 9–14.

Harkness, M., & Fisher, A. (2013). Use of emulsified vegetable oil to support bioremediation of TCE DNAPL in soil columns. *Journal of Contaminant Hydrology*, *151*, 16–33. https://doi.org/10.1016/j.jconhyd.2013.04.002

He, J., Sung, Y., Krajmalnik-Brown, R., Ritalahti, K. M., & Löffler, F. E. (2005). Isolation and characterization of Dehalococcoides sp. strain FL2, a trichloroethene (TCE)- and 1,2-dichloroethene-respiring anaerobe. *Environmental Microbiology*, *7*(9), 1442–1450. https://doi.org/10.1111/j.1462-2920.2005.00830.x

Heckel, B., Cretnik, S., Kliegman, S., Shouakar-Stash, O., McNeill, K., & Elsner, M. (2017). Reductive Outer-Sphere Single Electron Transfer Is an Exception Rather than the Rule in Natural and Engineered Chlorinated Ethene Dehalogenation. *Environmental Science and Technology*, *51*(17), 9663–9673. https://doi.org/10.1021/acs.est.7b01447

Heckel, B., & Elsner, M. (2022). Exploring Mechanisms of Biotic Chlorinated Alkane Reduction: Evidence of Nucleophilic Substitution (SN2) with Vitamin B12. *Environmental Science and Technology*, *56*(10), 6325–6336. https://doi.org/10.1021/acs.est.1c06066

Heckel, B., Phillips, E., Edwards, E., Sherwood Lollar, B., Elsner, M., Manefield, M. J., & Lee, M. (2019). Reductive Dehalogenation of Trichloromethane by Two Different Dehalobacter restrictus Strains Reveal Opposing Dual Element Isotope Effects. *Environmental Science and Technology*, *53*(5), 2332–2343. https://doi.org/10.1021/acs.est.8b03717

Henry, S. M., Hardcastle, C. H., & Warner, S. D. (2002). *Chlorinated Solvent and DNAPL Remediation: An Overview of Physical, Chemical, and Biological Processes*. https://doi.org/10.1021/bk-2002-0837.ch001

Henterly, R. W., & Harms, W. D. (2015). Optimal Treatment Zone Moves During Enhanced Reductive Dechlorination in Fractured Bedrock. *Remediation Journal*, *25*(4), 81–88. https://doi.org/https://doi.org/10.1002/rem.21441

Heraty, L. J., Fuller, M. E., Huang, L., Abrajano, T., & Sturchio, N. C. (1999). Isotopic fractionation of carbon and chlorine by microbial degradation of dichloromethane. *Organic Geochemistry*, *30*(8 A). https://doi.org/10.1016/S0146-6380(99)00062-5

Higgins, M. R., & Olson, T. M. (2009). Life-cycle case study comparison of permeable reactive barrier versus pump-and-treat remediation. *Environmental Science and Technology*, *43*(24). https://doi.org/10.1021/es9015537

Hiortdahl, K. M., & Borden, R. C. (2014). Enhanced reductive dechlorination of tetrachloroethene dense nonaqueous phase liquid with EVO and Mg(OH)2. *Environmental Science and Technology*, *48*(1), 624–631. https://doi.org/10.1021/es4042379

Hirschorn, S. K., Grostern, A., Lacrampe-Couloume, G., Edwards, E. A., MacKinnon, L., Repta, C., Major, D. W., & Sherwood Lollar, B. (2007). Quantification of biotransformation of chlorinated hydrocarbons in a biostimulation study: Added value via stable carbon isotope analysis. *Journal of Contaminant Hydrology*, *94*(3–4), 249–260. https://doi.org/10.1016/j.jconhyd.2007.07.001

Höhener, P., Elsner, M., Eisenmann, H., & Atteia, O. (2015). Improved constraints on in situ rates and on quantification of complete chloroethene degradation from stable carbon isotope mass balances in groundwater plumes. *Journal of Contaminant Hydrology*, *182*, 173–182. https://doi.org/10.1016/j.jconhyd.2015.09.006

Höhener, P., & Yu, X. (2012). Stable carbon and hydrogen isotope fractionation of dissolved organic groundwater pollutants by equilibrium sorption. *Journal of Contaminant Hydrology*, *129–130*, 54–61. https://doi.org/10.1016/j.jconhyd.2011.09.006

Horvath, A. L., Getzen, F. W., & Maczynska, Z. (1999). IUPAC-NIST Solubility Data Series 67. Halogenated Ethanes and Ethenes with Water. *Journal of Physical and Chemical Reference Data*, *28*(2), 395–627. https://doi.org/10.1063/1.556039

Hug, L. A. (2016). *Diversity, Evolution, and Environmental Distribution of Reductive Dehalogenase Genes BT - Organohalide-Respiring Bacteria* (L. Adrian & F. E. Löffler, Eds.; pp. 377–393). Springer Berlin Heidelberg. https://doi.org/10.1007/978-3-662-49875-0_16

Huling, S. G., Ko, S., & Pivetz, B. (2011). Groundwater Sampling at ISCO Sites: Binary Mixtures of Volatile Organic Compounds and Persulfate. *Ground Water Monitoring and Remediation*, *31*(2), 72–79. https://doi.org/10.1111/j.1745-6592.2011.01332.x

Huling, S., & Pivetz, B. (2006). Engineering Issue Paper: In-Situ Chemical Oxidation. *Engineering*.

Hung, C.-H., & MariÑas, B. J. (1997). Role of Chlorine and Oxygen in the Photocatalytic Degradation of Trichloroethylene Vapor on TiO2 Films. *Environmental Science & Technology*, *31*(2), 562–568. https://doi.org/10.1021/es960465i

Hunkeler, D., Aravena, R., & Butler, B. J. (1999). Monitoring microbial dechlorination of tetrachloroethene (PCE) in groundwater using compound-specific stable carbon isotope ratios: Microcosm and field studies. *Environmental Science and Technology*, *33*(16), 2733–2738. https://doi.org/10.1021/es981282u

Hunkeler, D., Meckenstock, R. U., Lollar, B. S., Schmidt, T. C., & Wilson, J. T. (2008). A Guide for Assessing Biodegradation and Source Identification of Organic Ground Water Contaminants using Compound Specific Isotope Analysis (CSIA). *USEPA Publication*, *EPA 600/R*-(December), 1–82. https://doi.org/EPA/600/R-08/148

IARC. (2024). *Agents classified by the IARC monographs, volumes 1-137*. Https://Monographs.Iarc.Who.Int/List-of-Classifications.

Ike, I. A., Linden, K. G., Orbell, J. D., & Duke, M. (2018). Critical review of the science and sustainability of persulphate advanced oxidation processes. *Chemical Engineering Journal*, *338*(January), 651–669. https://doi.org/10.1016/j.cej.2018.01.034

Jeffers, P. M., Ward, L. M., Woytowitch, L. M., & Wolfe, N. L. (1989). Homogeneous hydrolysis rate constants for selected chlorinated methanes, ethanes, ethenes, and propanes. *Environmental Science & Technology*, *23*(8), 965–969. https://doi.org/10.1021/es00066a006

Ji, Y., Wang, L., Jiang, M., Lu, J., Ferronato, C., & Chovelon, J. M. (2017). The role of nitrite in sulfate radical-based degradation of phenolic compounds: An unexpected nitration process relevant to groundwater remediation by in-situ chemical oxidation (ISCO). *Water Research*, *123*, 249–257. https://doi.org/10.1016/j.watres.2017.06.081

Jin, B., Laskov, C., Rolle, M., & Haderlein, S. B. (2011). Chlorine isotope analysis of organic contaminants using GC-qMS: Method optimization and comparison of different evaluation schemes. *Environmental Science and Technology*, *45*(12), 5279–5286. https://doi.org/10.1021/es200749d

Kaufmann, R., Long, A., Bentley, H., & Davis, S. (1984). Natural chlorine isotope variations. *Nature*, *309*(5966), 338–340. https://doi.org/10.1038/309338a0

Kohen, Amnon; Limbach, H.-H. (2005). *Isotope Effects In Chemistry and Biology* (A. Kohen & H.-H. Limbach, Eds.). CRC Press. https://doi.org/10.1201/9781420028027

Krembs, F. J., Siegrist, R. L., Crimi, M. L., Furrer, R. F., & Petri, B. G. (2010). ISCO for groundwater remediation: Analysis of field applications and performance. *Ground Water Monitoring and Remediation*, *30*(4). https://doi.org/10.1111/j.1745-6592.2010.01312.x

Kuder, T., & Philp, P. (2013). Demonstration of compound-specific isotope analysis of hydrogen isotope ratios in chlorinated ethenes. *Environmental Science and Technology*, *47*(3), 1461–1467. https://doi.org/10.1021/es303476v

Kuder, T., Van Breukelen, B. M., Vanderford, M., & Philp, P. (2013). 3D-CSIA: Carbon, chlorine, and hydrogen isotope fractionation in transformation of TCE to ethene by a dehalococcoides culture. *Environmental Science and Technology*, *47*(17), 9668–9677. https://doi.org/10.1021/es400463p

Kwon, M., Kim, S., Yoon, Y., Jung, Y., Hwang, T. M., Lee, J., & Kang, J. W. (2015). Comparative evaluation of ibuprofen removal by UV/H2O2 and UV/S2O82- processes for wastewater treatment. *Chemical Engineering Journal*, *269*, 379–390. https://doi.org/10.1016/j.cej.2015.01.125

Lalman, J. A., & Bagley, D. M. (2000). Anaerobic degradation and inhibitory effects of linoleic acid. *Water Research*, *34*(17), 4220–4228. https://doi.org/10.1016/S0043-1354(00)00180-9

Lebrón, C. A., Petrovskis, E., Loffler, F., & Henn, K. (2011). Application of Nucleic Acid-Based Tools for Monitoring Monitored Natural Attenuation (MNA), Biostimulation and Bioaugmentation at Chlorinated Solvent Sites - ESTCP ER-0518 Guidance Protocol. *ResearchGate*, *January*.

Lee, J., Von Gunten, U., & Kim, J. H. (2020). Persulfate-Based Advanced Oxidation: Critical Assessment of Opportunities and Roadblocks. *Environmental Science and Technology*, *54*(6), 3064–3081. https://doi.org/10.1021/acs.est.9b07082

Lee, P. K. H., Johnson, D. R., Holmes, V. F., He, J., & Alvarez-Cohen, L. (2006). Reductive dehalogenase gene expression as a biomarker for physiological activity of Dehalococcoides spp. *Applied and Environmental Microbiology*, *72*(9), 6161–6168. https://doi.org/10.1128/AEM.01070-06

Lee, P. K. H., Macbeth, T. W., Sorenson, K. S., Deeb, R. A., & Alvarez-Cohen, L. (2008). Quantifying genes and transcripts to assess the in situ physiology of "Dehalococcoides" spp. in a trichloroethene-contaminated groundwater site. *Applied and Environmental Microbiology*, *74*(9), 2728–2739. https://doi.org/10.1128/AEM.02199-07

Lee, Y.-C., Kwon, T.-S., Yang, J.-S., & Yang, J.-W. (2007). Remediation of groundwater contaminated with DNAPLs by biodegradable oil emulsion. *Journal of Hazardous Materials*, *140*(1), 340–345. https://doi.org/https://doi.org/10.1016/j.jhazmat.2006.09.036

Leeson, A., Beevar, E., Henry, B., Fortenberry, J., & Coyle, C. (2004). Microbiological and geochemical considerations. *Principles and Practices of Enhanced Anaerobic Bioremdiation of Chlorinated Solvents*, *Section 2*, 2-1_2-11.

Li, W., Orozco, R., Camargos, N., & Liu, H. (2017). Mechanisms on the Impacts of Alkalinity, pH, and Chloride on Persulfate-Based Groundwater Remediation. *Environmental Science and Technology*, *51*(7), 3948–3959. https://doi.org/10.1021/acs.est.6b04849

Lian, L., Yao, B., Hou, S., Fang, J., Yan, S., & Song, W. (2017). Kinetic Study of Hydroxyl and Sulfate Radical-Mediated Oxidation of Pharmaceuticals in Wastewater Effluents. *Environmental Science and Technology*, *51*(5), 2954–2962. https://doi.org/10.1021/acs.est.6b05536

Liang, C., & Lei, J. (2015). Identification of Active Radical Species in Alkaline Persulfate Oxidation. *Water Environment Research*, *87*(7), 656–659. https://doi.org/10.2175/106143015x14338845154986

Liang, C., & Su, H. W. (2009). Identification of sulfate and hydroxyl radicals in thermally activated persulfate. *Industrial and Engineering Chemistry Research*, *48*(11), 5558–5562. https://doi.org/10.1021/ie9002848

Lihl, C., Douglas, L. M., Franke, S., Pérez-De-Mora, A., Meyer, A. H., Daubmeier, M., Edwards, E. A., Nijenhuis, I., Sherwood Lollar, B., & Elsner, M. (2019). Mechanistic Dichotomy in Bacterial Trichloroethene Dechlorination Revealed by Carbon and Chlorine Isotope Effects. *Environmental Science and Technology*, *53*(8), 4245–4254. https://doi.org/10.1021/acs.est.8b06643

Lincker, M., Lagneau, V., Guillon, S., & Wanner, P. (2022). Identification of chlorohydrocarbon degradation pathways in aquitards using dual element compound-specific isotope measurements in aquifers. *Chemosphere*, *303*(P2), 135131. https://doi.org/10.1016/j.chemosphere.2022.135131

Liu, Y., Gan, Y., Zhou, A., Liu, C., Li, X., & Yu, T. (2014). Carbon and chlorine isotope fractionation during Fenton-like degradation of trichloroethene. *Chemosphere*, *107*, 94–100. https://doi.org/10.1016/j.chemosphere.2014.03.011

Liu, Y., Zhang, Y., Zhou, A., & Li, M. (2021). Insights into carbon isotope fractionation on trichloroethene degradation in base activated persulfate process: The role of multiple reactive oxygen species. *Science of the Total Environment*, *800*, 149371. https://doi.org/10.1016/j.scitotenv.2021.149371

Liu, Y., Zhou, A., Gan, Y., & Li, X. (2016). Variability in carbon isotope fractionation of trichloroethene during degradation by persulfate activated with zero-valent iron: Effects of inorganic anions. *Science of the Total Environment*, *548–549*. https://doi.org/10.1016/j.scitotenv.2016.01.011

Liu, Y., Zhou, A., Gan, Y., & Li, X. (2018). Roles of hydroxyl and sulfate radicals in degradation of trichloroethene by persulfate activated with Fe2+ and zero-valent iron: Insights from carbon isotope fractionation. *Journal of Hazardous Materials*, *344*, 98–103. https://doi.org/10.1016/j.jhazmat.2017.09.048

Löffler, F. E., Ritalahti, K. M., & Zinder, S. H. (2013). *Dehalococcoides and Reductive Dechlorination of Chlorinated Solvents BT - Bioaugmentation for Groundwater Remediation* (H. F. Stroo, A. Leeson, & C. H. Ward, Eds.; pp. 39–88). Springer New York. https://doi.org/10.1007/978-1-4614-4115-1_2

Long, C. M., & Borden, R. C. (2006). Enhanced reductive dechlorination in columns treated with edible oil emulsion. *Journal of Contaminant Hydrology*, *87*(1), 54–72. https://doi.org/https://doi.org/10.1016/j.jconhyd.2006.04.010

Lovley, D. R. (2001). Bioremediation: Anaerobes to the rescue. In *Science* (Vol. 293, Issue 5534). https://doi.org/10.1126/science.1063294

Lu, X., Wilson, J. T., & Kampbell, D. H. (2006). Relationship between Dehalococcoides DNA in ground water and rates of reductive dechlorination at field scale. *Water Research*, *40*(16), 3131–3140. https://doi.org/https://doi.org/10.1016/j.watres.2006.05.030

Ma, J., Yang, Y., Jiang, X., Xie, Z., Li, X., Chen, C., & Chen, H. (2018). Impacts of inorganic anions and natural organic matter on thermally activated persulfate oxidation of BTEX in water. *Chemosphere*, *190*, 296–306. https://doi.org/10.1016/j.chemosphere.2017.09.148

Mackay, D. M., & Cherry, J. A. (1989). Groundwater contamination: Pump-and-treat remediation. *Environmental Science and Technology*, *23*(6). https://doi.org/10.1021/es00064a001

Magnuson, J. K., Romine, M. F., Burris, D. R., & Kingsley, M. T. (2000). Trichloroethene reductive dehalogenase from Dehalococcoides ethenogenes: Sequence of tceA and substrate range characterization. *Applied and Environmental Microbiology*, *66*(12), 5141–5147. https://doi.org/10.1128/AEM.66.12.5141-5147.2000

Majone, M., Verdini, R., Aulenta, F., Rossetti, S., Tandoi, V., Kalogerakis, N., Agathos, S., Puig, S., Zanaroli, G., & Fava, F. (2015). In situ groundwater and sediment bioremediation: Barriers and perspectives at European contaminated sites. *New Biotechnology*, *32*(1). https://doi.org/10.1016/j.nbt.2014.02.011

Mattes, T. E., Alexander, A. K., & Coleman, N. V. (2010). Aerobic biodegradation of the chloroethenes: Pathways, enzymes, ecology, and evolution. In *FEMS Microbiology Reviews* (Vol. 34, Issue 4). https://doi.org/10.1111/j.1574-6976.2010.00210.x

McCarty, P. L., Chu, M. Y., & Kitanidis, P. K. (2007). Electron donor and pH relationships for biologically enhanced dissolution of chlorinated solvent DNAPL in groundwater. *European Journal of Soil Biology*, *43*(5–6), 276–282. https://doi.org/10.1016/j.ejsobi.2007.03.004

McMahon, P. B., Chapelle, F. H., & Bradley, P. M. (2011). Evolution of redox processes in groundwater. *ACS Symposium Series*, *1071*(December 2015), 581–597. https://doi.org/10.1021/bk-2011-1071.ch026

McMurdie, P. J., Hug, L. A., Edwards, E. A., Holmes, S., & Spormann, A. M. (2011). Site-Specific Mobilization of Vinyl Chloride Respiration Islands by a Mechanism Common in Dehalococcoides. *BMC Genomics*, *12*(1), 287. https://doi.org/10.1186/1471-2164-12-287

Michener, R., & Lajtha, K. (2008). Stable Isotopes in Ecology and Environmental Science: Second Edition. In *Stable Isotopes in Ecology and Environmental Science: Second Edition*. https://doi.org/10.1002/9780470691854

Mohn, W. W., & Tiedje, J. M. (1992). Microbial reductive dehalogenation. *Microbiological Reviews*, *56*(3), 482–507. https://doi.org/10.1128/mr.56.3.482-507.1992

Newman, W. A., & Pelle, R. C. (2006). Enhanced anaerobic bioremediation of chlorinated solvents utilizing vegetable oil emulsions. *Remediation*, *16*(3), 109–122. https://doi.org/10.1002/rem.20095

Ni, S., Fredrickson, J. K., & Xun, L. (1995). Purification and characterization of a novel 3-chlorobenzoate-reductive dehalogenase from the cytoplasmic membrane of Desulfomonile tiedjei DCB-1. *Journal of Bacteriology*, *177*(17), 5135–5139. https://doi.org/10.1128/jb.177.17.5135-5139.1995

Nie, M., Yang, Y., Zhang, Z., Yan, C., Wang, X., Li, H., & Dong, W. (2014). Degradation of chloramphenicol by thermally activated persulfate in aqueous solution. *Chemical Engineering Journal*, *246*, 373–382. https://doi.org/10.1016/j.cej.2014.02.047

Nijenhuis, I., Andert, J., Beck, K., Kästner, M., Diekert, G., & Richnow, H. H. (2005). Stable isotope fractionation of tetrachloroethene during reductive dechlorination by Sulfurospirillum multivorans and Desulfitobacterium sp. strain PCE-S and abiotic reactions with cyanocobalamin. *Applied and Environmental Microbiology*, *71*(7), 3413–3419. https://doi.org/10.1128/AEM.71.7.3413-3419.2005

Nijenhuis, I., Nikolausz, M., Köth, A., Felföldi, T., Weiss, H., Drangmeister, J., Großmann, J., Kästner, M., & Richnow, H. H. (2007). Assessment of the natural attenuation of chlorinated ethenes in an anaerobic contaminated aquifer in the Bitterfeld/Wolfen area using stable isotope techniques, microcosm studies and molecular biomarkers. *Chemosphere*, *67*(2), 300–311. https://doi.org/10.1016/j.chemosphere.2006.09.084

Ojeda, A. S., Phillips, E., Mancini, S. A., & Lollar, B. S. (2019). Sources of Uncertainty in Biotransformation Mechanistic Interpretations and Remediation Studies using CSIA. *Analytical Chemistry*, *91*(14), 9147–9153. https://doi.org/10.1021/acs.analchem.9b01756

Ojeda, A. S., Phillips, E., & Sherwood Lollar, B. (2020). Multi-element (C, H, Cl, Br) stable isotope fractionation as a tool to investigate transformation processes for halogenated hydrocarbons. *Environmental Science: Processes & Impacts*, *22*(3), 567–582. https://doi.org/10.1039/C9EM00498J

Palau, J., Jamin, P., Badin, A., Vanhecke, N., Haerens, B., Brouyère, S., & Hunkeler, D. (2016). Use of dual carbon-chlorine isotope analysis to assess the degradation pathways of 1,1,1-trichloroethane in groundwater. *Water Research*, *92*, 235–243. https://doi.org/10.1016/j.watres.2016.01.057

Palau, J., Marchesi, M., Chambon, J. C. C., Aravena, R., Canals, À., Binning, P. J., Bjerg, P. L., Otero, N., & Soler, A. (2014). Multi-isotope (carbon and chlorine) analysis for fingerprinting and site characterization at a fractured bedrock aquifer contaminated by chlorinated ethenes. *Science of the Total Environment*, *475*, 61–70. https://doi.org/10.1016/j.scitotenv.2013.12.059

Palau, J., Soler, A., Teixidor, P., & Aravena, R. (2007). Compound-specific carbon isotope analysis of volatile organic compounds in water using solid-phase microextraction. *Journal of Chromatography A*, *1163*(1), 260–268. https://doi.org/https://doi.org/10.1016/j.chroma.2007.06.050

Palau, J., Yu, R., Hatijah Mortan, S., Shouakar-Stash, O., Rosell, M., Freedman, D. L., Sbarbati, C., Fiorenza, S., Aravena, R., Marco-Urrea, E., Elsner, M., Soler, A., & Hunkeler, D. (2017). Distinct Dual C-Cl Isotope Fractionation Patterns during Anaerobic Biodegradation of 1,2-Dichloroethane: Potential to Characterize Microbial Degradation in the Field. *Environmental Science and Technology*, *51*(5), 2685–2694. https://doi.org/10.1021/acs.est.6b04998

Panagos, P., Van Liedekerke, M., Yigini, Y., & Montanarella, L. (2013). Contaminated sites in Europe: Review of the current situation based on data collected through a European network. In *Journal of Environmental and Public Health* (Vol. 2013). https://doi.org/10.1155/2013/158764

Pankow, J. F., & Cherry, J. A. (1996). DENSE CHLORINATED SOLVENTS and other DNAPLs in Groundwater: History, Behavior, and Remediation. *DENSE CHLORINATED SOLVENTS and Other DNAPLs in Groundwater: History, Behavior, and Remediation*, 538.

Pfeiffer, P., Bielefeldt, A. R., Illangasekare, T., & Henry, B. (2005). Partitioning of dissolved chlorinated ethenes into vegetable oil. In *Water Research* (Vol. 39, Issue 18, pp. 4521–4527). Water Research. https://doi.org/10.1016/j.watres.2005.09.016

Purdue, M. P., Stewart, P. A., Friesen, M. C., Colt, J. S., Locke, S. J., Hein, M. J., Waters, M. A., Graubard, B. I., Davis, F., Ruterbusch, J., Schwartz, K., Chow, W. H., Rothman, N., & Hofmann, J. N. (2017). Occupational exposure to chlorinated solvents and kidney cancer: A case-control study. *Occupational and Environmental Medicine*, *74*(4). https://doi.org/10.1136/oemed-2016-103849

Qi, C., Liu, X., Ma, J., Lin, C., Li, X., & Zhang, H. (2016). Activation of peroxymonosulfate by base: Implications for the degradation of organic pollutants. *Chemosphere*, *151*, 280–288. https://doi.org/10.1016/j.chemosphere.2016.02.089

Renpenning, J., Keller, S., Cretnik, S., Shouakar-Stash, O., Elsner, M., Schubert, T., & Nijenhuis, I. (2014). Combined C and Cl isotope effects indicate differences between corrinoids and enzyme (Sulfurospirillum multivorans PceA) in reductive dehalogenation of tetrachloroethene, but not trichloroethene. *Environmental Science and Technology*, *48*(20), 11837–11845. https://doi.org/10.1021/es503306g

Renpenning, J., Rapp, I., & Nijenhuis, I. (2015). Substrate Hydrophobicity and Cell Composition Influence the Extent of Rate Limitation and Masking of Isotope Fractionation during Microbial Reductive Dehalogenation of Chlorinated Ethenes. *Environmental Science & Technology*, *49*(7), 4293–4301. https://doi.org/10.1021/es506108j

Révész, K. M., Lollar, B. S., Kirshtein, J. D., Tiedeman, C. R., Imbrigiotta, T. E., Goode, D. J., Shapiro, A. M., Voytek, M. A., Lacombe, P. J., & Busenberg, E. (2014). Integration of stable carbon isotope, microbial community, dissolved hydrogen gas, and 2HH2O tracer data to assess bioaugmentation for chlorinated ethene degradation in fractured rocks. *Journal of Contaminant Hydrology*, *156*, 62–77. https://doi.org/https://doi.org/10.1016/j.jconhyd.2013.10.004

Ritalahti, K. M., Hatt, J. K., Lugmayr, V., Henn, K., Petrovskis, E. A., Ogles, D. M., Davis, G. A., Yeager, C. M., Lebrón, C. A., & Löffler, F. E. (2010). Comparing On-Site to Off-Site Biomass Collection for Dehalococcoides Biomarker Gene Quantification To Predict in Situ Chlorinated Ethene Detoxification Potential. *Environmental Science & Technology*, *44*(13), 5127–5133. https://doi.org/10.1021/es100408r

Rivett, M. O., Chapman, S. W., Allen-King, R. M., Feenstra, S., & Cherry, J. A. (2006). Pump-and-treat remediation of chlorinated solvent contamination at a controlled field-experiment site. *Environmental Science and Technology*, *40*(21). https://doi.org/10.1021/es0602748

Rodríguez-Fernández, D., Heckel, B., Torrentó, C., Meyer, A., Elsner, M., Hunkeler, D., Soler, A., Rosell, M., & Domènech, C. (2018). Dual element (C-Cl) isotope approach to distinguish abiotic reactions of chlorinated methanes by Fe(0) and by Fe(II) on iron minerals at neutral and alkaline pH. *Chemosphere*, *206*, 447–456. https://doi.org/10.1016/j.chemosphere.2018.05.036

Rodríguez-Fernández, D., Torrentó, C., Guivernau, M., Viñas, M., Hunkeler, D., Soler, A., Domènech, C., & Rosell, M. (2018). Vitamin B12 effects on chlorinated methanes-degrading microcosms: Dual isotope and metabolically active microbial populations assessment. *Science of the Total Environment*, *621*, 1615–1625. https://doi.org/10.1016/j.scitotenv.2017.10.067

Rodríguez-Fernández, D., Torrentó, C., Palau, J., Marchesi, M., Soler, A., Hunkeler, D., Domènech, C., & Rosell, M. (2018). Unravelling long-term source removal effects and chlorinated methanes natural attenuation processes by C and Cl stable isotopic patterns at a complex field site. *Science of the Total Environment*, *645*, 286–296. https://doi.org/10.1016/j.scitotenv.2018.07.130

Rosell, M., Gonzalez-Olmos, R., Rohwerder, T., Rusevova, K., Georgi, A., Kopinke, F. D., & Richnow, H. H. (2012). Critical evaluation of the 2D-CSIA scheme for distinguishing fuel

oxygenate degradation reaction mechanisms. *Environmental Science and Technology*, *46*(9). https://doi.org/10.1021/es2036543

Schaefer, C. E., Lippincott, D. R., & Steffan, R. J. (2010). Field-scale evaluation of bioaugmentation dosage for treating chlorinated ethenes. *Ground Water Monitoring and Remediation*, *30*(3). https://doi.org/10.1111/j.1745-6592.2010.01297.x

Shouakar-Stash, O., Frape, S. K., Aravena, R., Gargini, A., Pasini, M., & Drimmie, R. J. (2009). Analysis of compound-specific chlorine stable isotopes of vinyl chloride by continuous flow-isotope ratio mass spectrometry (FC-IRMS). *Environmental Forensics*, *10*(4), 299–306. https://doi.org/10.1080/15275920903347628

Slater, G. F., Lollar, B. S., Sleep, B. E., & Edwards, E. A. (2001). Variability in carbon isotopic fractionation during biodegradation of chlorinated ethenes: Implications for field applications. *Environmental Science and Technology*, *35*(5), 901–907. https://doi.org/10.1021/es001583f

Smith, B. A., Teel, A. L., & Watts, R. J. (2006). Mechanism for the destruction of carbon tetrachloride and chloroform DNAPLs by modified Fenton's reagent. *Journal of Contaminant Hydrology*, *85*(3–4). https://doi.org/10.1016/j.jconhyd.2006.02.002

Soder-Walz, J. M., Torrentó, C., Algora, C., Wasmund, K., Cortés, P., Soler, A., Vicent, T., Rosell, M., & Marco-Urrea, E. (2022). Trichloromethane dechlorination by a novel Dehalobacter sp. strain 8M reveals a third contrasting C and Cl isotope fractionation pattern within this genus. *Science of the Total Environment*, *813*. https://doi.org/10.1016/j.scitotenv.2021.152659

Stelzer, N., Imfeld, G., Thullner, M., Lehmann, J., Poser, A., Richnow, H. H., & Nijenhuis, I. (2009). Integrative approach to delineate natural attenuation of chlorinated benzenes in anoxic aquifers. *Environmental Pollution*, *157*(6), 1800–1806. https://doi.org/10.1016/j.envpol.2009.01.029

Stroo, H. F. (2010). *Bioremediation of Chlorinated Solvent Plumes*. https://doi.org/10.1007/978-1-4419-1401-9_10

Stroo, H. F., & Ward, C. H. (1998). In Situ Remediation of Chlorinated Solvent Plumes. In *Few-Body Systems* (Vol. 25, Issues 1–3).

Teel, A. L., & Watts, R. J. (2002). Degradation of carbon tetrachloride by modified Fenton's reagent. *Journal of Hazardous Materials*, *94*(2), 179–189. https://doi.org/10.1016/S0304-3894(02)00068-7

Thullner, M., Centler, F., Richnow, H.-H., & Fischer, A. (2012). Quantification of organic pollutant degradation in contaminated aquifers using compound specific stable isotope analysis – Review of recent developments. *Organic Geochemistry*, *42*(12), 1440–1460. https://doi.org/10.1016/j.orggeochem.2011.10.011

Thullner, M., Fischer, A., Richnow, H.-H., & Wick, L. Y. (2013). Influence of mass transfer on stable isotope fractionation. *Applied Microbiology and Biotechnology*, *97*(2), 441–452. https://doi.org/10.1007/s00253-012-4537-7

Tian, K., Hu, L., Li, L., Zheng, Q., Xin, Y., & Zhang, G. (2022). Recent advances in persulfate-based advanced oxidation processes for organic wastewater treatment. *Chinese Chemical Letters*, *33*(10), 4461–4477. https://doi.org/10.1016/j.cclet.2021.12.042

Tiehm, A., & Schmidt, K. R. (2011). Sequential anaerobic/aerobic biodegradation of chloroethenes-aspects of field application. *Current Opinion in Biotechnology*, *22*(3), 415–421. https://doi.org/10.1016/j.copbio.2011.02.003

Tobiszewski, M., & Namieśnik, J. (2012). Abiotic degradation of chlorinated ethanes and ethenes in water. *Environmental Science and Pollution Research*, *19*(6). https://doi.org/10.1007/s11356-012-0764-9

Torrentó, C., Audí-Miró, C., Bordeleau, G., Marchesi, M., Rosell, M., Otero, N., & Soler, A. (2014). The use of alkaline hydrolysis as a novel strategy for chloroform remediation: The feasibility of using construction wastes and evaluation of carbon isotopic fractionation. *Environmental Science and Technology*, *48*(3), 1869–1877. https://doi.org/10.1021/es403838t

Torrentó, C., Palau, J., Rodríguez-Fernández, D., Heckel, B., Meyer, A., Domènech, C., Rosell, M., Soler, A., Elsner, M., & Hunkeler, D. (2017). Carbon and Chlorine Isotope Fractionation Patterns Associated with Different Engineered Chloroform Transformation Reactions. *Environmental Science and Technology*, *51*(11), 6174–6184. https://doi.org/10.1021/acs.est.7b00679

Tsitonaki, A., Petri, B., Crimi, M., Mosbk, H., Siegrist, R. L., & Bjerg, P. L. (2010). In situ chemical oxidation of contaminated soil and groundwater using persulfate: A review. *Critical Reviews in Environmental Science and Technology*, *40*(1), 55–91. https://doi.org/10.1080/10643380802039303

Underwood, J. C., Akob, D. M., Lorah, M. M., Imbrigiotta, T. E., Harvey, R. W., & Tiedeman, C. R. (2022). Microbial community response to a bioaugmentation test to degrade trichloroethylene in a fractured rock aquifer, Trenton, N.J. *FEMS Microbiology Ecology*, *98*(7), fiac077. https://doi.org/10.1093/femsec/fiac077

USEPA. (2024). *National Primary Drinking Water Regulations*. https://www.epa.gov/ground-water-and-drinking-water/national-primary-drinking-water-regulations#one

Van Breukelen, B. M. (2007). Extending the Rayleigh equation to allow competing isotope fractionating pathways to improve quantification of biodegradation. *Environmental Science and Technology*, *41*(11), 4004–4010. https://doi.org/10.1021/es0628452

van der Zaan, B., Hannes, F., Hoekstra, N., Rijnaarts, H., de Vos, W. M., Smidt, H., & Gerritse, J. (2010). Correlation of Dehalococcoides> 16S rRNA and Chloroethene-Reductive Dehalogenase Genes with Geochemical Conditions in Chloroethene-Contaminated Groundwater. *Applied and Environmental Microbiology*, *76*(3), 843–850. https://doi.org/10.1128/AEM.01482-09

Wackett, L. P., Logan, M. S. P., Blocki, F. A., & Bao-li, C. (1992). A mechanistic perspective on bacterial metabolism of chlorinated methanes. *Biodegradation*, *3*(1), 19–36. https://doi.org/10.1007/BF00189633

Wang, M., Zhang, B., Li, G., Wu, T., & Sun, D. (2019). Efficient remediation of crude oil-contaminated soil using a solvent/surfactant system. *RSC Advances*, *9*(5). https://doi.org/10.1039/c8ra09964b

Wanner, P., Parker, B. L., Chapman, S. W., Aravena, R., & Hunkeler, D. (2017). Does sorption influence isotope ratios of chlorinated hydrocarbons under field conditions? *Applied Geochemistry*, *84*, 348–359. https://doi.org/10.1016/j.apgeochem.2017.07.016

Warner, S. D., & Sorel, D. (2002). *Ten Years of Permeable Reactive Barriers: Lessons Learned and Future Expectations*. https://doi.org/10.1021/bk-2002-0837.ch003

Watts, R. J., Bottenberg, B. C., Hess, T. F., Jensen, M. D., & Teel, A. L. (1999). Role of reductants in the enhanced desorption and transformation of chloroaliphatic compounds by modified Fenton's reactions. *Environmental Science and Technology*, *33*(19). https://doi.org/10.1021/es990054c

West, K. A., Lee, P. K. H., Johnson, D. R., Zinder, S. H., & Alvarez-Cohen, L. (2013). Global gene expression of Dehalococcoides within a robust dynamic TCE-dechlorinating community under conditions of periodic substrate supply. *Biotechnology and Bioengineering*, *110*(5), 1333–1341. https://doi.org/10.1002/bit.24819

Wiegert, C., Aeppli, C., Knowles, T., Holmstrand, H., Evershed, R., Pancost, R. D., Macháčková, J., & Gustafsson, Ö. (2012). Dual Carbon-chlorine stable isotope investigation of sources and fate of chlorinated ethenes in contaminated groundwater. *Environmental Science and Technology*, *46*(20), 10918–10925. https://doi.org/10.1021/es3016843

Wiegert, C., Mandalakis, M., Knowles, T., Polymenakou, P. N., Aeppli, C., Macháčková, J., Holmstrand, H., Evershed, R. P., Pancost, R. D., & Gustafsson, Ö. (2013). Carbon and chlorine isotope fractionation during microbial degradation of tetra-and trichloroethene. *Environmental Science and Technology*, *47*(12), 6449–6456. https://doi.org/10.1021/es305236y

Wilson, J. T. (2010). *Monitored Natural Attenuation of Chlorinated Solvent Plumes* (pp. 325–355). https://doi.org/10.1007/978-1-4419-1401-9_11

Wojnárovits, L., Tóth, T., & Takács, E. (2020). Rate constants of carbonate radical anion reactions with molecules of environmental interest in aqueous solution: A review. *Science of the Total Environment*, *717*. https://doi.org/10.1016/j.scitotenv.2020.137219

Yang, Y., & Ca, N. L. (2017). *Organohalide Respiration with Chlorinated Ethenes under Low pH Conditions*. https://doi.org/10.1021/acs.est.7b01510

Yang, Y., Lu, X., Jiang, J., Ma, J., Liu, G., Cao, Y., Liu, W., Li, J., Pang, S., Kong, X., & Luo, C. (2017). Degradation of sulfamethoxazole by UV, UV/H2O2 and UV/persulfate (PDS): Formation of oxidation products and effect of bicarbonate. *Water Research*, *118*, 196–207. https://doi.org/10.1016/j.watres.2017.03.054

Yang, Y., & Mccarty, P. L. (2000). Biologically enhanced dissolution of tetrachloroethene DNAPL. *Environmental Science and Technology*, *34*(14), 2979–2984. https://doi.org/10.1021/es991410u

Yu, R., Andrachek, R. G., Lehmicke, L. G., & Freedman, D. L. (2018). Remediation of chlorinated ethenes in fractured sandstone by natural and enhanced biotic and abiotic processes: A

crushed rock microcosm study. *Science of The Total Environment*, *626*, 497–506. https://doi.org/https://doi.org/10.1016/j.scitotenv.2018.01.064

Yuan, J., Li, S., Cheng, J., Guo, C., Shen, C., He, J., Yang, Y., Hu, P., Xu, J., & He, Y. (2021). Potential Role of Methanogens in Microbial Reductive Dechlorination of Organic Chlorinated Pollutants in Situ. *Environmental Science and Technology*, *55*(9), 5917–5928. https://doi.org/10.1021/acs.est.0c08631

Zanaroli, G., Negroni, A., Häggblom, M. M., & Fava, F. (2015). Microbial dehalogenation of organohalides in marine and estuarine environments. In *Current Opinion in Biotechnology* (Vol. 33). https://doi.org/10.1016/j.copbio.2015.03.013

Zhu, C., Zhu, F., Liu, C., Chen, N., Zhou, D., Fang, G., & Gao, J. (2018). Reductive Hexachloroethane Degradation by S2O8•- with Thermal Activation of Persulfate under Anaerobic Conditions. *Environmental Science and Technology*, *52*(15), 8548–8557. https://doi.org/10.1021/acs.est.7b06279

Zimmermann, J., Halloran, L. J. S., & Hunkeler, D. (2020). Tracking chlorinated contaminants in the subsurface using compound-specific chlorine isotope analysis: A review of principles, current challenges and applications. *Chemosphere*, *244*, 125476. https://doi.org/10.1016/j.chemosphere.2019.125476

Zuo, Z., Cai, Z., Katsumura, Y., Chitose, N., & Muroya, Y. (1999). Reinvestigation of the acid-base equilibrium of the (bi)carbonate radical and ph dependence of its reactivity with inorganic reactants. *Radiation Physics and Chemistry*, *55*(1), 15–23. https://doi.org/10.1016/S0969-806X(98)00308-9

Appendix 1. Scientific publications derived from this thesis

Science of the Total Environment 951 (2024) 175351

Contents lists available at ScienceDirect

Science of the Total Environment

journal homepage: www.elsevier.com/locate/scitotenv

Use of isotopic (C, Cl) and molecular biology tools to assess biodegradation in a source area of chlorinated ethenes after biostimulation with Emulsified Vegetable Oil (EVO)

Sergio Gil-Villalba [a,*], Jordi Palau [a], Jesica M. Soder-Walz [b], Miguel A. Vallecillo [c], Jordi Corregidor [c], Andrea Tirado [c], Orfan Shouakar-Stash [d], Miriam Guivernau [e], Marc Viñas [e], Albert Soler [a], Monica Rosell [a]

[a] Grup MAiMA, SGR Mineralogia Aplicada, Geoquímica i Hidrogeologia (MAGH), Departament de Mineralogia, Petrologia i Geologia Aplicada, Facultat de Ciències de la Terra, Institut de Recerca de l'Aigua (IdRA), Universitat de Barcelona (UB), Martí Franquès s/n, 08028 Barcelona, Spain
[b] Departament d'Enginyeria Química, Biològica i Ambiental, Universitat Autònoma de Barcelona (UAB), Carrer de les Sitges s/n, Bellaterra, Spain
[c] Environmental Resources Management Iberia SAU, Rambla de Catalunya 33, 08007 Barcelona, Spain
[d] Isotope Tracer Technologies Inc., Waterloo, ON, Canada
[e] Sustainability in Biosystems Programme, Institute of Agrifood Research and Technology (IRTA), Torre Marimon, Caldes de Montbui, Barcelona, Spain

HIGHLIGHTS

- Carbon isotopic effects by partitioning of CEs into EVO were not significant.
- Biostimulation using EVO was studied in laboratory experiments and the field.
- *Dhc* populations and reductive dechlorination functional genes were analyzed.
- 2D C-Cl CSIA was used for degradation pathways investigation in the field.

GRAPHICAL ABSTRACT

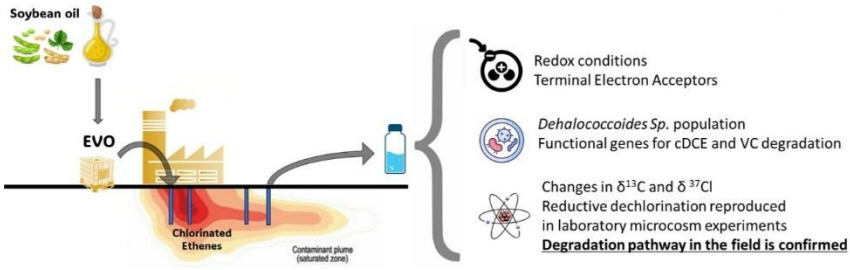

ARTICLE INFO

Editor: Elodie Passeport

Keywords:
2D-CSIA
Dichloroethene
EVO
Bioremediation
Microcosm study
Field application

ABSTRACT

Enhanced In Situ Bioremediation (EISB) using Emulsified Vegetable Oil (EVO) as a long-term electron donor has gained prominence for the treatment of groundwater contaminated with chlorinated ethenes (CEs). This study explores the potential of isotopic and molecular biology tools (MBT) to investigate the CEs (PCE, TCE and cis-DCE) bioremediation using EVO in a contaminated site. A multiple approach using C and Cl-CSIA, quantification of Dehalococcoides (Dhc) and specific reductive dechlorination (RD) gene population, and hydrochemical data in microcosm experiments and field samples was applied. Despite the high partitioning of CEs into the EVO phase, the carbon isotopic values of the remaining CEs fraction in the aqueous phase did not exhibit significant changes caused by phase partitioning in laboratory experiments. Both microcosm experiments and field data revealed a rapid RD of PCE and TCE, resulting in the transient accumulation of cis-DCE, which was slowly degraded to vinyl chloride (VC). These results agreed with the presence of Dhc populations and a shift to stronger reducing conditions in the field: i) RD functional genes (tceA, vcrA and bvcA) exhibited a trend to higher values and ii) a substantial increase in Dhc populations (up to 30% of the total bacterial populations) was observed over

* Corresponding author.
E-mail address: sergiogilv@ub.edu (S. Gil-Villalba).

https://doi.org/10.1016/j.scitotenv.2024.175351
Received 21 April 2024; Received in revised form 4 August 2024; Accepted 5 August 2024
Available online 14 August 2024

time. The dual-element isotope slope ΛC-Cl for RD of cis-DCE obtained from field data (ΛC – Cl = 5 ± 3) was similar to the one determined from the microcosm experiments under controlled anoxic conditions (ΛC – Cl = 4.9 ± 0.8). However, ΛC-Cl values differ from those reported so far for laboratory studies with Dhc strains and mixed cultures containing Dhc, i.e., between 8.3 and 17.8. This observation underscores the potential variety of reductive dehalogenases involved during cis-DCE RD and the importance of determining site-specific Λ and ε values in order to improve the identification and quantification of transformation processes in the field.

1. Introduction

Contamination of groundwater by chlorinated ethenes (CEs) has become a persistent environmental issue due to accidental releases and inappropriate historical disposal practices. In recent years, enhanced in situ bioremediation (EISB) techniques have emerged as reliable and cost-effective methods for treating these contaminants i) *Dhc* population relative to the total bacterial population and ii) functional genes related to RD (*tceA, bvcA* and *vcrA*). This suggests that the *Dhc* were most probably the drivers of RD in both the field and the microcosm experiments. Hence, the isotopic results obtained in the microcosm experiments might be representative for the analysis of biodegradation pathway and extent in the field.

However, the successful complete dechlorination of CEs through EISB is contingent upon achieving proper pH and oxidation-reduction potential (ORP) values, as well as the presence of organo-halide-respiring bacteria (OHRB) from the *Dehalococcoides* group (*Dhc*) and *Dehalogenimonas*. *Dhc* populations have been demonstrated as the key anaerobic and most common bacteria capable of transforming trichloroethylene (TCE), cis-dichloroethylene (cis-DCE) and vinyl chloride (VC) into non-toxic end products such as ethene and ethane under anaerobic conditions (Löffler et al., 2013; Chen et al., 2022b) via reductive dechlorination (RD). Failure to meet and sustain the mentioned conditions may result in an incomplete RD of CEs, causing the accumulation of degradation byproducts in the subsoil, i.e., cis-DCE and VC, which are more toxic than the original compounds. In this respect, VC ranks 4th on the 2022 Agency for Toxic Substances and Disease Registry Priority List of Hazardous Substances based on a combination of its frequency, toxicity, and potential for human exposure (ATSDR, 2023).

During RD of CEs, these are used as electron acceptors by OHRBs, while an electron donor is required to provide energy (Harkness and Fisher, 2013). Hydrogen (H_2) is commonly regarded as the primary electron donor for RD, which is typically generated through the anaerobic fermentation of carbon substrates by other native microbial populations. There is a wide range of commercially available electron donors, including soluble donors such as sugars, organic acids, and alcohols, as well as slow-release donors with low aqueous solubility like lactic acid polymers, emulsified vegetable oil (EVO), chitin, and wood chips (Leeson et al., 2004). These donors undergo microbial fermentation via different pathways and at different rates in groundwater under anaerobic conditions, leading to varying levels of hydrogen production and, thus, enhancing the growth and competitive advantage of OHRB against other hydrogen-consuming microorganisms (e.g. sulphate reducing bacteria and methanogens).

The RD of CEs by OHRB is catalyzed by diverse reductive dehalogenases (Rdh) which contain catalytic subunits (Ni et al., 1995; Magnuson et al., 2000). Rdh is a diverse protein family from which there are still a lot of unanswered questions regarding sequence diversity, substrate specificities, global distribution, and modes of inheritance (Hug, 2016). Nevertheless, the Rdh that have been characterized and proved to be functional in microbial respiration are encoded by Rdh operons, mainly composed by the *rdhA* and *rdhB* genes. The RdhA enzymes act as catalyst for cleaving the C-Cl bond during organohalide respiration (West et al., 2013; Badin et al., 2014). The expression of rdh genes has been established as a biomarker for the physiological activity of *Dhc* (Lee et al., 2008; Löffler et al., 2013; Blázquez-Pallí et al., 2019a). *PceA* gene is active for the RD of tetrachloroethylene (PCE) and both *tceA* and *vcrA* genes are active for that of TCE and cis-DCE. In addition, both *vcrA* and *bvcA* are primarily and exclusively responsible for the RD of VC to ethene under anaerobic conditions (He et al., 2005; Lee et al., 2008; Franke et al., 2020).

Compound-Specific Isotope Analysis (CSIA) is based on isotopic fractionation principles, where light isotopes (e.g., ^{12}C, ^{35}Cl) form and break bonds more readily than heavy isotopes (e.g., ^{13}C, ^{37}Cl) during (bio)chemical reactions. This results in a transient accumulation of heavy isotopes in the remaining pool of the parental organic compound due to slower reaction kinetics. CSIA leverages these variations to trace sources and transformation pathways of halogenated compounds in groundwater (Nijenhuis et al., 2016). This approach has gained significant interest in site investigation and remediation practices as it provides complementary lines of evidence for contaminant biodegradation, which are sometimes required by legislation and regulatory administrations (Nijenhuis et al., 2007; Aelion et al., 2009; Elsner, 2010; Palau et al., 2014). In contrast to the single element isotope approach, the application of dual-element isotope analysis (2D-CSIA) has demonstrated high potential for identifying the contaminant degradation pathways in the field (Wiegert et al., 2012; Blázquez-Pallí et al., 2019b; Rosell et al., 2019). By measuring the isotopic shifts of different elements in the same compound (e.g., C and Cl), specific ongoing degradation mechanisms can be identified (Elsner, 2010; Hermon et al., 2018). However, before the degradation mechanisms can be confidently identified in the field, it is crucial to characterize their specific isotopic fractionation values (εC and εCl) and dual-element isotope trends ($\Lambda^{C\text{-}Cl}$) in laboratory experiments under controlled conditions (Aelion et al., 2009).

Emulsified Vegetable Oil (EVO) is a commercially available bioremediation substrate which consists of an emulsion of soybean oil, surfactants, soluble substrates (e.g., lactate), and nutrients (Newman and Pelle, 2006; Harkness and Fisher, 2013). Due to its low aqueous solubility and composition, that includes soybean oil containing long-chain fatty acid groups, EVO undergoes slow fermentation over time, producing hydrogen and volatile fatty acids. In contrast to more soluble donors, the slow fermentation of EVO prevents the need for its continuous or semi-continuous injection (Lalman and Bagley, 2000; Harkness, 2000). The injection of vegetable oil in the subsurface of a contaminated site can lead to abiotic processes such as the partitioning of CEs into oily phases. These phenomena can cause significant changes of the concentration of CEs in groundwater (Yang and Mccarty, 2000; Pfeiffer et al., 2005), hampering the evaluation of biodegradation by using contaminant concentration data alone.

The isotopic effect of physical processes on organic compounds (e.g. sorption and diffusion) has often been disregarded in the saturated zone, due to their expected small effects compared to biodegradation (Abe et al., 2009; Audí-Miró et al., 2013; Torrentó et al., 2017; Rodríguez-Fernández et al., 2018). Specific studies on sorption and diffusion demonstrated that they could compensate each other to some degree as these processes fractionate isotopes in opposite directions. However, when strong sorption dominates in the field, carbon isotope fractionation of volatile chlorinated compounds can become significant ≥2 ‰, which might need to be considered for an accurate interpretation of reactive processes using CSIA (Höhener and Yu, 2012; Wanner et al., 2017; Halloran et al., 2021). To the best of our knowledge, there is only one study documenting the water-vegetable oil phase partitioning of CEs (Pfeiffer et al., 2005) and the potential isotopic fractionation caused by

this process has not been evaluated so far. Therefore, the investigation of potential isotope effects during partitioning of CEs into EVO is warranted.

Previous studies have investigated the application of EVO as an electron donor for CEs bioremediation in laboratory experiments (Long and Borden, 2006; Lee et al., 2007; Harkness and Fisher, 2013; Hiortdahl and Borden, 2014; Yu et al., 2018; Underwood et al., 2022). However, research dealing with contaminant remediation using EVO in the field is still limited (Hirschorn et al., 2007; Révész et al., 2014; Chen et al., 2022a). These previous studies provide insights into certain effects of RD after the injection of an electron donor, namely acidification of groundwater and changes in microbial community dynamics. As far as we know, only two studies have used the carbon isotopic fractionation of CEs to assess the efficiency of the biostimulation with EVO (Hirschorn et al., 2007; Révész et al., 2014). Currently, there is still a knowledge gap regarding the potential of 2D-CSIA to investigate the fate of PCE, TCE, and cis-DCE following an EVO injection in the field. In particular, the dual (C, Cl) isotope analysis could be useful to identify the degradation pathway of cis-DCE, which can be transformed via both microbial anaerobic RD and aerobic oxidation (Tiehm and Schmidt, 2011). Besides, contrarily to PCE and TCE, few studies have reported the dual-element (C, Cl) isotope fractionation trend for cis-DCE during RD (Abe et al., 2009; Kuder and Philp, 2013; Doğan-Subaşı et al., 2017; Lihl et al., 2019).

The main goal of this study was to explore the potential of a multi-method approach (i.e. isotopic and biomolecular tools) to improve the assessment of CEs degradation by EISB with EVO. To this end, we investigated (i) whether water – EVO phase partitioning processes of CEs result in significant isotopic effects; (ii) the C and Cl isotopic fractionation and dual (C, Cl) isotope trends of PCE, TCE and cis-DCE during RD in microcosm experiments with a bacterial community from the contaminated site; (iii) the dual (C, Cl) isotope fractionation trend of cis-DCE during the EISB with EVO in the field; and (iv) the *Dhc* bacterial populations and functional genes responsible for RD of CEs in both microcosm experiments and field samples. Finally, the isotopic fractionation values and dual element isotope trends were compared with the available literature data.

2. Material and methods

2.1. Study site

The study site, located near Barcelona (Spain), was strongly contaminated with PCE (reaching a value of 19 mg/L in groundwater), due to former improper storage and handling practices. The unconfined aquifer layer consists of a Quaternary sand and sandy-silt bed with a thickness ranging between 4 and 8 m. Below this unit, Miocene detrital deposits of alternating clay and silt layers represent the bottom of the aquifer (bedrock). The groundwater flows toward the southeast, following the dip of the Quaternary/Miocene contact. The water table depth ranges between 2 and 4 m below ground surface. Hydraulic conductivity values between 0.25 and 0.35 cm/s and transmissivity ranging from 0.8 to 1.7 m^2/day were determined through pumping tests.

2.2. EVO injection details

A commercial EVO (EOS PRO®, EOS Remediation, LLC, Research Triangle Park, North Carolina, USA) was selected as a long-term electron donor for the site bioremediation. It is a physical emulsion consisting of soybean oil in water, vitamin B_{12} and other minor substances as emulsifiers and nutrients.

The EVO injection was conducted in eight wells (Fig. 1). The injection process involved the sequential injection of 13 m^3 of an EVO solution (8 % *v*/v), followed by 5.6 m^3 of an aqueous lactate solution (5 % v/v). Lactate is a more soluble and mobile electron donor, and this solution was used to induce anoxic conditions in a shorter term. Both solutions were prepared using tap water, previously circulated through an activated carbon filter to remove any potential volatile halogenated compound that can result from the chlorination process and free chlorine (Cl_2) which could kill a wide range of bacteria.

2.3. Collection of water samples

The site was equipped with 20 long screen wells installed in 2010. Eleven monitoring wells, located on the source and downgradient areas (Fig. 1) were selected for the assessment of the potential natural attenuation of CEs before the EVO injection and the evolution of the contamination after the biostimulation treatment. To do so, an initial groundwater sampling campaign was carried out in June 2020, followed by the injection of EVO (September 2020) and five monitoring campaigns (November 2020, January, March, May, and September 2021). Slurry was sampled for biomolecular analysis in four injection wells (W4, W8, W10 and W11) and one control well (W5) in June 2020 (3 months before the EVO injection), in March 2021 (6 months after the injection) and only in W4 in June 2021 (Table 1). Hydrochemical parameters, including temperature, pH, electric conductivity, Dissolved Oxygen (DO), and ORP, were measured on-site, before each sampling, using a multiparameter probe (HANNA HI98194 and sensors HANNA HI7698194) together with a flow-through cell to minimize contact of the sample with the atmosphere. Data were collected after stabilization and ORP values were corrected to the standard hydrogen electrode (SHE). For CEs concentration and isotopic analyses, triplicate groundwater samples were collected in amber glass bottles (125 mL) filled without headspace (HS) and closed with screw PTFE-lined septum caps to minimize adsorption and volatilization of CEs. The samples were preserved by adding concentrated HNO_3 (to pH < 2) and stored in the dark

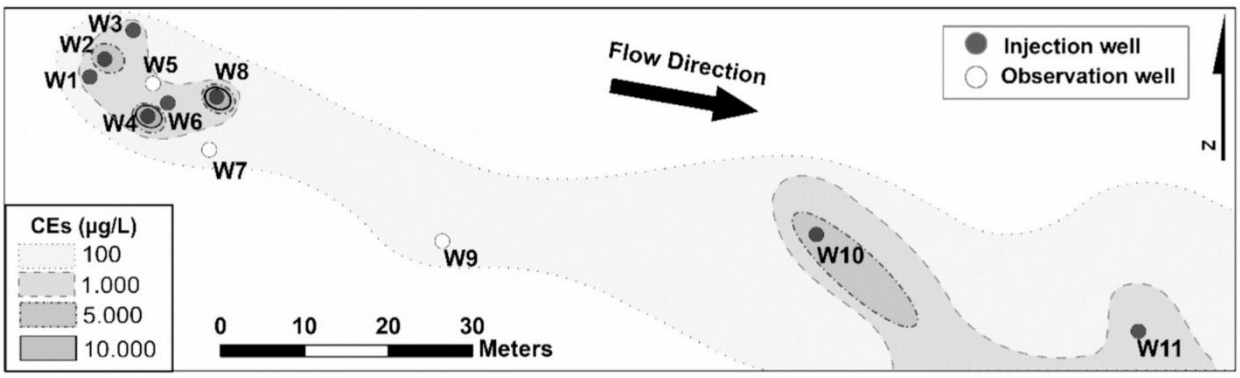

Fig. 1. Site map and groundwater monitoring wells network. The filled contour lines represent the total CEs concentrations in groundwater (in µg/L) prior to the injection (June 2020).

Table 1
qPCR results for groundwater samples and microcosm regarding total bacterial population (16S rRNA), *Dehalococcoides* ssp. and functional genes *tceA, bvcA* and *vcrA*. All analyses were performed in triplicate. n.a. and n.d. stand for not analyzed and not detected, respectively. Different subscript letters in each gene population represents significant differences ($n = 3$, $P < 0.05$, Post Hoc Tukey tests).

Field data							
Well	Date	Gene copies 16S rRNA mL^{-1}	Gene copies 16S rRNA *Dhc* mL^{-1}	% *Dhc*	Gene copies *tceA* mL^{-1}	Gene copies *bvcA* mL $^{-1}$	Gene copies *vcrA* mL $^{-1}$
W4	Jun-20	$1.14E+05_a$	$1.10E+03_a$	1.0	$8.57E+01_a$	$9.13E+01_a$	$3.77E+03_a$
W4	Mar-21	$1.04E+05_a$	$1.40E+04_b$	13.5	$3.83E+04_b$	$2.00E+04_b$	$3.75E+04_b$
W4	Jun-21	$1.67E+06_b$	$1.97E+05_c$	11.8	$1.08E+06_c$	$3.02E+05_c$	$1.19E+06_c$
W5	Jun-20	$4.76E+04_a$	$2.88E+00_d$	0.0	n.a.	n.a.	n.a.
W5	Mar-21	$2.05E+06_b$	$2.89E+04_b$	1.4	n.a.	n.a.	n.a.
W8	Jun-20	$1.49E+04_c$	$4.17E+00_d$	0.0	n.a.	n.a.	n.a.
W8	Mar-21	$1.36E+07_d$	$4.19E+06_e$	30.8	$1.78E+07_d$	$1.55E+06_c$	$3.53E+06_c$
W10	Jun-20	$1.12E+05_a$	$4.77E+01_d$	0.0	n.d.	n.d.	n.d.
W10	Mar-21	$1.79E+07_d$	$1.02E+06_e$	5.7	$5.18E+06_e$	$1.09E+02_d$	$3.83E+06_c$
W11	Jun-20	$7.59E+02_e$	$1.50E+01_d$	2.0	n.a.	n.a.	n.a.
W11	Mar-21	$1.46E+07_d$	$8.95E+04_{bc}$	0.6	n.a.	n.a.	n.a.
Microcosm experiments							
Microcosm	**Degradation (%)**	**Gene copies 16S rRNA mL^{-1}**	**Gene copies 16S rRNA *Dhc* mL^{-1}**	**% *Dhc***	**Gene copies *tceA* mL^{-1}**	**Gene copies *bvcA* mL $^{-1}$**	**Gene copies *vcrA* mL $^{-1}$**
cDCE (t_0)	0	$1.67E+06_b$	$1.97E+05_c$	11.8	$1.08E+06_c$	$3.02E+05_c$	$1.19E+06_c$
cDCE_1 (t_1)	58	$9.70E+05_b$	$7.02E+03_{ab}$	0.7	$7.61E+04_b$	$1.12E+04_b$	$2.92E+04_b$
cDCE_2 (t_2)	98	$4.81E+06_{ab}$	$7.03E+06_e$	>70	$8.66E+06_c$	$4.12E+05_c$	$6.11E+06_c$

at 4 °C until analysis. Slurry for the microcosm experiments was collected from the bottom of the well W4 in June 2021. This well was selected for microcosm preparation because it presented the highest CEs concentrations and bacterial populations in the sampling before the injection (June 2020).

2.4. Partitioning experiments

Experiments were conducted to assess whether the potential partitioning of CEs between the water and EVO phases result in significant isotopic fractionation. The experimental setup (total volume of 140 mL) consisted of two polypropylene syringes connected through a 14,000 Da dialysis membrane (Medicell Membranes Ltd., London, UK), permeable to CEs while impermeable to EVO (see Fig. S1, in SI). One side of the system was filled with an aqueous EVO solution (8 % *v*/v) and the other with an aqueous solution (PCE, TCE and cis-DCE) leading to initial concentrations in the system of 1570 μg PCE/L, 2290 μg TCE/L and 2750 μg cis-DCE/L. All solutions were prepared using deionized water (18.2 MΩ cm at 25 °C, Direct-Q UV-3, Millipore) and their concentrations were selected to be in the range of those present in the field during the EVO injection. Both sides of the system were stirred during the experiment using PTFE-coated magnetic stir bars to ensure the homogeneity of the solutions. The syringe tips were capped and all connections were sealed with PTFE tape and Parafilm® to minimize losses of CEs by volatilization. Two water samples (5 mL) were collected after 12 and 48 h from the side of the system filled with the CEs solution (without EVO). The water samples were stored, without headspace, in amber vials with PTFE-sealed caps, and refrigerated until concentration and isotopic analysis. The dialysis membrane prevented the presence of EVO phase in the samples as it could provoke the release of CEs from the EVO to the water during the heating of the samples in subsequent analyses. Experiments were performed in triplicates to ensure reproducibility. Control triplicates without EVO were included to account for possible losses in the system. The calculation of the partition to EVO is detailed in Appendix B of SI.

2.5. Microcosm experiments

Laboratory microcosm experiments were conducted in order to obtain field site-specific $\varepsilon^{13}C$, $\varepsilon^{37}Cl$, and $\Lambda^{C\text{-}Cl}$ values for the RD of PCE, TCE and cis-DCE. Initially, the collected slurry from the well W4 on June 2021 (9 months after EVO injection) was purged with N_2 for 3 h to remove CEs. Subsequently, the microcosms were prepared inside an anoxic chamber filling 100 mL glass serum sterile bottles with 70 mL of slurry and sealed with PTFE-coated butyl rubber stoppers and aluminum crimp caps. Three sets of 13 bottles each were spiked with PCE, TCE, or cis-DCE respectively at 160 μM. Ten bottles of each set were amended with lactate (3 mM) to assess the effect of a supplementary electron donor while 3 bottles remained in field conditions. Three additional killed control bottles were spiked with all the contaminants together (PCE, TCE, and cis-DCE) and the biodegradation activity was immediately stopped by adding a solution of NaOH (to pH > 12). The killed controls were set up to account for contaminant losses through the cap or unexpected abiotic reactions. All these bottles were incubated in the dark at 25 °C. The concentration was monitored on a daily basis by injecting 0.5 mL of microcosm HS in a Gas Chromatograph coupled to a Flame Ionization Detector (GC-FID). Biodegradation was stopped at different degradation extents to assess the associated isotopic fractionation by adding NaOH, as described previously.

In those cases where the rapid kinetics led to the complete biodegradation of the original compound before sufficient data could be obtained for the calculation of ε-values, the corresponding CE was spiked again, and subsequent sampling was performed. When multiple spikes were conducted and degradation products (particularly cis-DCE) accumulated, microcosm bottles were purged with N_2 for 20 min prior to the following spike. This precautionary step was taken based on previous studies that observed inhibition of RD at high CEs concentrations (Duhamel et al., 2002).

2.6. Analytical methods

2.6.1. Concentration

A detailed description of the analytical methods and equipment used for concentration and isotope measurements is available in the SI. Briefly, CEs concentrations in field samples were measured by headspace gas chromatography–mass spectrometry (HS-GC–MS) as explained elsewhere (Torrentó et al., 2017) while CEs and ethene concentrations in microcosm samples were measured by a GC attached with a FID at UAB laboratories. Terminal Electron Acceptors (TEAs) concentrations such as nitrate, sulphate, manganese, and iron in field samples were analyzed by Element Materials Technology (EMT), Deeside, United Kingdom (see SI).

2.6.2. Isotopic analysis

Carbon isotope analysis of PCE, TCE cis-DCE and VC was performed using a GC coupled to an Isotope Ratio Mass Spectrometer (GC-IRMS) at

the Technological Centers of the University of Barcelona (CCiT-UB) (Blázquez-Pallí et al., 2019a). Aqueous isotopic working standards of CEs with known isotopic composition were analyzed on a daily basis to ensure stability of the measurements during the course of samples analysis and, if necessary, to correct for slight deviations induced by the extraction and preconcentration technique (solid-phase micro extraction -SPME (Palau et al., 2007)). Chlorine isotope analysis of PCE and TCE was performed in a GC-qMS system in the CCiT-UB using the methodology described by (Jin et al., 2011), while chlorine isotope ratios of cis-DCE were analyzed using a GC-IRMS at Isotope Tracer Technologies Inc. (Waterloo, Canada) as described in (Shouakar-Stash et al., 2006). Raw δ^{37}Cl values were calibrated (two-point linear calibration) to the standard mean ocean chloride (SMOC) scale (Bernstein et al., 2011). For both C and Cl isotope analysis, samples and standards were analyzed by a duplicate set of injections as quality control (2 injections in the GC-IRMS and 2 sets of 5 injections in the GC-qMS). The aqueous isotopic standards were prepared similarly to the samples and measured in the same sequence. Precision (1σ) of the analysis was ≤0.5 ‰ for δ^{13}C of all compounds and for δ^{37}Cl of PCE and TCE, and ≤0.2 ‰ for δ^{37}Cl of cis-DCE.

Recent studies by (Ojeda et al., 2019, 2020) suggested to use the York regression method instead of ORL to determine Λ and its uncertainty. A comparison between $\Lambda^{C\text{-}Cl}$ values and their uncertainties obtained in this study with the York and the OLR regression methods will be conducted.

2.6.3. Biomolecular analysis

Biomass was harvested, either from 30 mL of field-sampled slurry or 5 mL samples from selected microcosm experiments, in sterile falcon tubes that were centrifuged at 4000 ×*g* and 4 °C for 30 min. The supernatants were discarded, and the resulting pellets were immediately stored at −80 °C until DNA extraction. DNA extraction was performed using the DNeasy PowerSoil Pro Kit (Qiagen, Venlo, The Netherlands), following the manufacturer's instructions.

The RD genes quantified were: i) *tceA* gene, encoding for the RD enzyme of TCE to cis-DCE; ii) *vcrA* gene, encoding for VC reductase enzyme responsible for RD of cis-DCE and VC; and iii) *bvcA* gene, encoding for VC reductase enzyme responsible for RD of VC to ethene, as described elsewhere (van der Zaan et al., 2010).

2.7. Isotope data evaluation

The carbon and chlorine isotopes ratio were reported in delta notation (δ^{h}E, in ‰, Eq. (1)), relative to the international standards VPDB (Vienna Pee Dee Belemnite) and SMOC (Standard Mean Ocean Chlorine) (Kaufmann et al., 1984; Coplen, 1996), respectively. The isotopic ratio of a sample and the standard of an element (E) (e.g., $^{13}C/^{12}C$, $^{37}Cl/^{35}Cl$) is denoted as R_{sample} and R_{std}, respectively:

$$\delta^{h}E = \left(\frac{R_{sample}}{R_{std}} - 1\right) \quad (1)$$

A simplified version of the Rayleigh equation in logarithmic form (Eq. (2)) can be used to correlate changes in the isotopic composition of an element in a compound (R_t/R_0) with changes in its concentration ($f = C_t/C_0$) for a given reaction, by using the corresponding isotopic fractionation (ε) (Elsner, 2010; Coplen, 2011):

$$ln\left(\frac{R_t}{R_0}\right) = \varepsilon \cdot ln(f) \quad (2)$$

where R_t/R_0 can be expressed as $(\delta^{h}E_t + 1)/(\delta^{h}E_0 + 1)$ according to the δ^{h}E definition. The laboratory-derived ε values according to Eq. (2) were compared to reported values in the literature. The dual isotope analysis was used to investigate the reaction pathways of CEs by comparing the slopes obtained in the laboratory with those observed in the field. The $\Lambda^{C/Cl}$ values for PCE, TCE and cis-DCE in the field and laboratory experiments were obtained from the slope of the linear regression in the dual C-Cl isotope plot (Elsner, 2010). The results were also compared with $\Lambda^{C/Cl}$ values from the literature. The uncertainty of ε and $\Lambda^{C/Cl}$ values is reported as the 95 % confidence interval (CI), derived from the standard deviation of the regression slope.

3. Results and discussion

3.1. Carbon isotopic effect during water - EVO phase partitioning

The extent of CEs partitioning into the EVO phase in the laboratory tests was estimated based on the difference in the measured aqueous concentrations between the experiments with EVO and the controls without it (see details in SI). After 48 h the experiments with EVO showed a decrease in aqueous concentrations around 83 %, 69 % and 65 % for PCE, TCE and cis-DCE, respectively, compared to the controls. These results reflected a significant partitioning of CEs into the EVO phase and were consistent with the trend to higher transfer with increasing chlorination of CEs determined in a previous study using food-grade soybean oil and synthetic groundwater (Pfeiffer et al., 2005). These authors determined soybean oil - groundwater partition coefficients (L water/L oil) of 539, 351 and 56 for PCE, TCE and cis-DCE, respectively, in a CEs solution with PCE, TCE, cis-DCE and vinyl chloride at 20 °C.

Despite the high partitioning of CEs into the EVO phase, the carbon isotopic values of the remaining CEs fraction in the aqueous phase did not exhibit significant differences between control and EVO experiments. Although low concentrations did not allow the measurement of δ^{13}C of PCE, nor for all the triplicates of TCE and cis-DCE, a change in the isotopic composition was not observed for TCE or cis-DCE after 48 h (Fig. 2). These results suggest that the carbon isotopic effect of the partitioning of these compounds into EVO during field applications will be small or insignificant compared to the biodegradation of the CEs in the groundwater.

3.2. CEs biodegradation in the microcosm experiments

Complete biodegradation of PCE, TCE and cis-DCE was observed in all active microcosm experiments (see Figs. S3, S4 and S5, in SI), while the concentrations in the killed controls remained unchanged. In microcosm bottles without lactate addition, no significant differences in biodegradation dynamics were observed (treated equally hereinafter and in the graphs). This can be attributed to the fact that the used slurry was already biostimulated, sampled after 9 months of EVO injection. This observation demonstrates that EVO serves as a long-term carbon source, indicating that the availability of an electron donor is not a limiting factor for RD in the microcosm experiments where lactate was not added.

Following a latency period of about 48 h after PCE and TCE were spiked (Figs. S3 and S4, in SI), rapid biodegradation was observed, as these compounds were completely depleted after 96 h. In this case, respiking of the compounds was necessary to obtain samples at different degradation extents for the calculation of ε-values. When it was necessary, the microcosms were purged to prevent inhibition of OHRB due to toxicity caused by the accumulation of degradation products as this process has been previously documented by (Duhamel et al., 2002). Unlike PCE and TCE, cis-DCE microcosms did not exhibit a latency period and its degradation rate was slower, requiring around 16 days to complete the transformation of cis-DCE into VC (Fig. 3). This longer biodegradation period allowed for detailed sampling, representative of different extents of cis-DCE transformation (Fig. S5, in SI). The absence of a lag phase for cis-DCE might be attributed to the fact that cis-DCE and VC were already the predominant contaminants in the sampled slurry, rendering the functional genes for PCE and TCE degradation inactive.

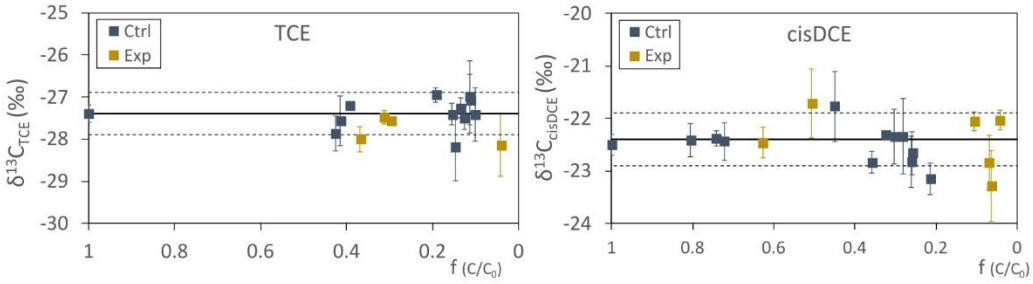

Fig. 2. Carbon isotopic values of CEs in the aqueous phase versus time in the EVO-phase partitioning experiments (yellow) and controls without EVO (dark blue). The black line indicates the carbon isotopic composition of the original compound (measured by Elemental Analyzer - IRMS) and the dashed lines show the typical analytical uncertainty of ±0.5 ‰.

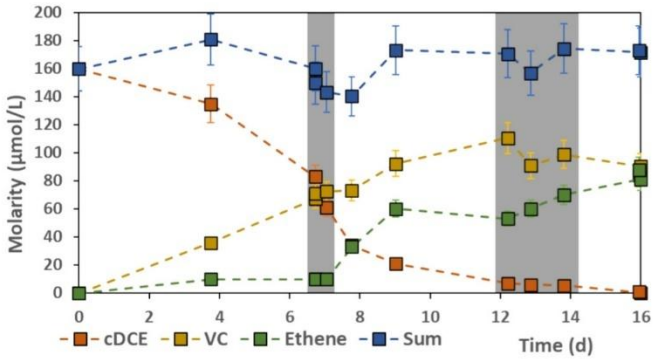

Fig. 3. Molarity of original compound and degradation products in microcosms amended with cis-DCE (160 µM). The shaded areas indicate the microcosms sampled for subsequent microbiological analysis.

3.3. Geochemical conditions and CEs biodegradation in the field

In general, groundwater was characterized by anoxic conditions prior to the injection, with DO values close to 0 mg/L in all measurements, except for well W6 with 0.29 mg/L. Other redox-sensitive species, such as nitrate and sulphate, with concentrations up to 33 mg/L and 125 mg/L, respectively, before the injection (June 2020) were strongly depleted by March 2021 (Fig. S6, in SI). On the other hand, dissolved manganese and methane concentrations strongly increased (even in observation wells such as W9 located downstream from the source area), with some wells showing methane concentrations exceeding 20 mg/L (Fig. S6, in SI). This shift to stronger reducing conditions after the EVO injection, which fall within the range of sulphate-reducing to methanogenic conditions, was favourable for RD of CEs (Leeson et al., 2004). Also, pH and ORP values presented optimal conditions for RD (see further discussion in SI).

Regarding the concentration of CEs, prior to the EVO injection (June 2020) PCE and TCE were the predominant CEs in the contaminated area, accounting for 50 to 90 % of the dissolved CEs molar concentration (Fig. 4). However, the presence of the dechlorination products cis-DCE and VC (in some wells) was indicative of PCE and TCE natural attenuation to some extent, in agreement with the anoxic conditions observed previous to the EVO injection (Fig. S6, in SI). Two months after the injection, the degradation products cis-DCE and VC were already predominant in all the wells, accounting for nearly 100 % of the dissolved CEs. The average measured PCE and TCE concentration dropped from 4599 to 44 µg/L and from 3074 to 37 µg/L, respectively. Conversely, the degradation products average concentrations increased from 3323 to 22,082 µg/L for cis-DCE and from 1515 to 4035 µg/L for VC.

The analysis of the total molarity of CEs showed, in most of the wells, an increase after the injection (Fig. 4). This phenomenon has been previously observed in other EVO field applications (Révész et al., 2014) and it could be caused by the mobilization of remaining DNAPL or adsorbed CEs on the aquifer material. In the studied site, this mobilised DNAPL could have been rapidly degraded to cis-DCE once dissolved in the aqueous phase, as rapid biodegradation rates were observed in microcosm experiments, causing the high cis-DCE concentrations measured after the injection. On the other hand, wells W4 and W8 showed significantly higher concentrations than the other wells, which might indicate that DNAPL existed nearby. Additionally, well W11 was the only one which presented high PCE and TCE molar fractions in the following campaigns, until March, while on W9 PCE and TCE where not found in the November monitoring, but a rebound was observed in March and May. Finally, the total CEs concentration decreased significantly in all wells in September 2021, apart from the well W1, where an increase in the total molarity of CEs was observed.

The rapid transition to a system dominated by degradation products cis-DCE and VC indicate that PCE and TCE are rapidly transformed at the site, in agreement with the fast PCE and TCE biodegradation observed in the microcosm experiments (see above). However, other processes such as partitioning of CEs to the injected EVO phase (higher for PCE and TCE compared to cis-DCE, see Fig. 3) and CEs mobilization/desorption during the EVO injection can also affect the parent compounds/daughter products ratios. Therefore, the use of isotopic and biomolecular tools to document CEs transformation in complex systems, like the in-situ biodegradation using EVO, is warranted. In most wells, a slow decrease of cis-DCE molar fraction is observed over time, transitioning to a VC-dominated system. In this scenario, the assessment of cis-DCE (and VC) transformation is crucial to evaluate the effectiveness of the biostimulation treatment. Overall, concentration data indicate that the injection of EVO enhances the degradation of PCE and TCE within a relatively short timeframe, while the degradation kinetics of cis-DCE to VC is slower.

3.4. Microbiological analyses in microcosms and the field samples

For the microcosm experiments, only the data from those spiked with cis-DCE are discussed. For the experiments with PCE or TCE correlating microbiological activity with the degradation of the respective parent compound was not possible due to their rapid biodegradation, as well as the re-spikes and purges (see above). Additionally, the limited number of samples hindered the analysis of triplicates with similar extent of degradation. In contrast, the slower degradation of cis-DCE allowed for more extensive sampling and triplicate qPCRs were conducted for 60 % degradation after 7 days (t_1), and over 97 % degradation after 12 days (t_2). Original triplicates of unpurged groundwater collected from W4 well (Fig. 1) were also analyzed as the initial value (t_0).

At t_1, the population of *Dhc* and Rdhase abundance slightly decreased (10 %, $P > 0.05$) compared to the initial value (Table 1). This *Dhc* decline, along with a significant total bacterial population drop, could have been caused by purging disturbance and a period of absence of CEs until they were spiked. Similar observations of decay in *Dhc* populations and Rdhs gene population due to the absence of CEs have been previously reported by (Lee et al., 2006). Contrastingly, at t_2 the *Dhc*

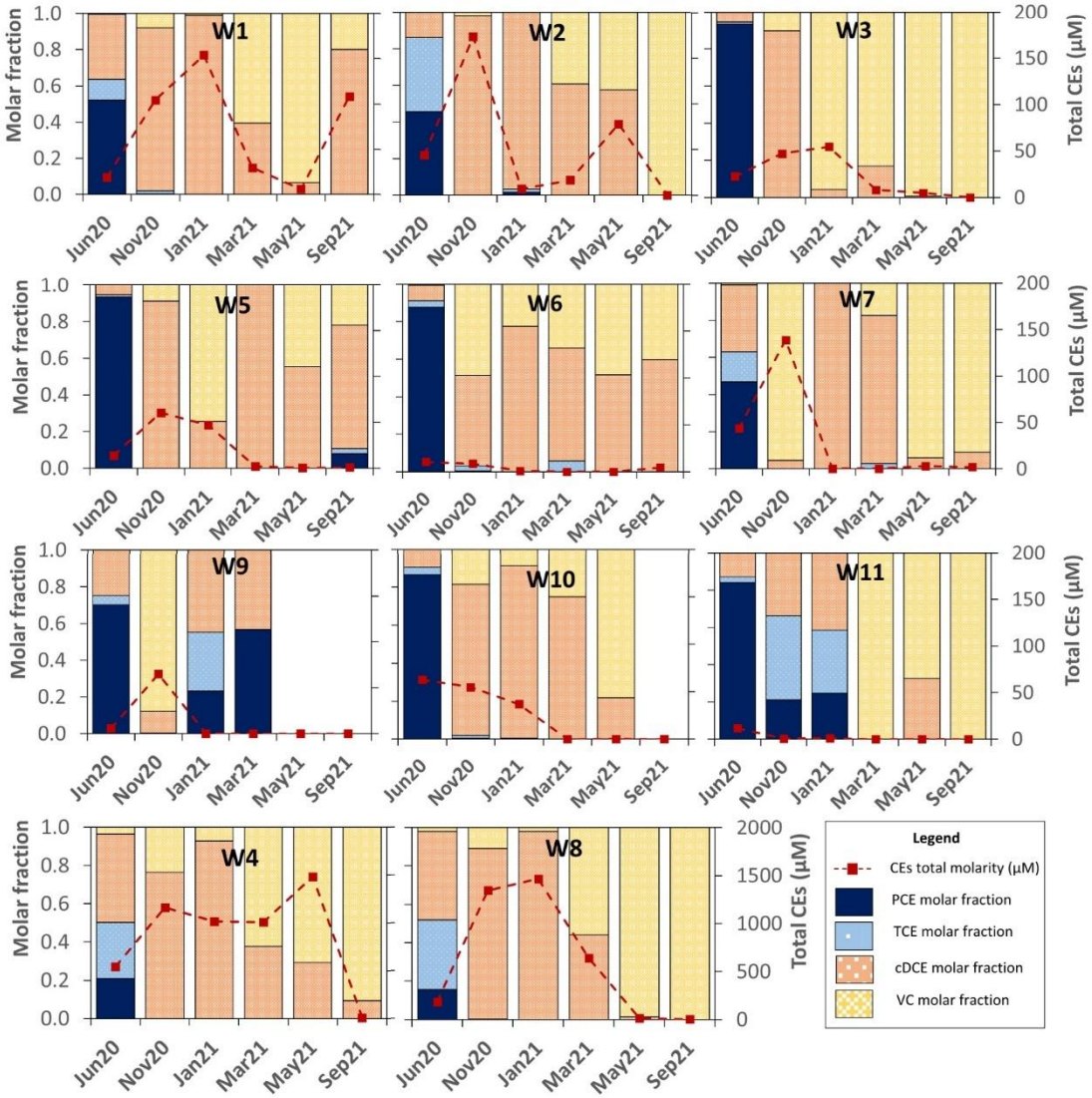

Fig. 4. 16-month evolution of CEs molar fractions in µM/µM (stacked charts) and total concentration of CEs (dashed lines) in the eleven monitored wells. First column shows the data of the sampling before the EVO injection. The following columns indicate molar fractions after injection.

population had increased significantly ($P < 0.05$), by 35-fold compared to the initial measurements, reaching values of 7.0 10^6 16S-Dhc mL^{-1}, while the functional gene populations also showed a substantial increase ($P < 0.05$): 8-fold higher for *tceA* (8.7 10^6 gene copies mL^{-1}), 1.4-fold for *bvcA* (4.1 10^5 gene copies mL^{-1}) and 5-fold for *vcrA* (6.1 10^6 gene copies mL^{-1}).

The expression of *tceA* and bvcA genes are associated with the transformation of cis-DCE to VC and VC to ethene, respectively, which is in agreement with the rise of the molar fraction of ethene in the microcosms (Fig. 3, Table 1). The functional gene *vcrA* can be associated with both cis-DCE and VC degradation (Lee et al., 2006; Blázquez-Pallí et al., 2019a; Franke et al., 2020). These results showed that Dhc populations and RD functional genes were good indicators of cis-DCE and VC biodegradation in the microcosm experiments performed.

In the field, the total bacterial population was heterogeneously distributed in the contaminated site before the injection of EVO, with values from different wells between 10^2 and 10^5 gene copies of 16S rRNA (see Table 1). The lowest bacterial population was observed in W11 well, while the highest ones were found in W4 and W10 wells (Fig. 1). This distribution was apparently neither related to initial CEs concentrations nor redox conditions. However, the lower 16S rRNA gene copies in W11 could have influenced the PCE and TCE slower biodegradation observed in this well. *Dhc* populations were present in all the wells before the EVO injection, with a maximum value of $1{\cdot}10^3$ gene copies mL^{-1} in W4. Previous studies indicated that *Dhc* populations in groundwater must exceed 10^4 copies mL^{-1} for acceptable RD to occur (Lu et al., 2006; Ernst, 2009; Ritalahti et al., 2010). Consequently, although the quantification of *Dhc* was indicative of the potential of bioremediation in the contaminated site, the *Dhc* population was not sufficient for effective natural attenuation. A different situation was observed six months after the EVO injection. Then, *Dhc* gene copies mL^{-1} above 10^4 were measured in all wells, reaching values up to 10^6 gene copies mL^{-1} in W8 and W10 ($P < 0.05$ compared to initial values in each well, Table 1). The amount of *Dhc* relative to the total bacterial population, between 0 and 2 % before the EVO injection, generally increased after the biostimulation reaching values above 10 % in W4 and 30 % in W8 wells. Only groundwater from the W4 well was analyzed in June 2021, but *Dhc* gene copies were still increasing, accounting for $1.95{\cdot}10^5$ *Dhc* $mL^{-1}$and suggesting that RD could be still ongoing.

Functional gene quantification was conducted in samples from W4 and W10 wells in June 2020 and March 2021, from W8 in March 2021 and from W4 in June 2021. Prior to the injection, (June 2020) functional

genes *tceA, bvcA* and *vcrA* were detected in W4 but not in W10. This result could explain the much higher molar fraction of cis-DCE and VC in W4 compared to W10 before the treatment. Six months after the EVO injection, *Dhc* population in W10 had increased by 5 orders of magnitude, and genes *tceA* and *vcrA* reached values of 10^6 copies mL^{-1}. However, *bvcA* gene copies remained lower than in the other wells (10^2 genes mL^{-1}). This could indicate that, although having the capacity for RD of TCE, the *Dhc* population in W10 well was different from those in W4 and W8, where the *bvcA* gene copies increased the same magnitude as *tceA* and *vcrA*. It is important to note that the number of copies of the *vcrA* gene in field samples is often higher than the total *Dhc* population. This may indicate that vcrABC cluster, typically found in *Dhc* genomic islands, could also be present in other OHRB by horizontal transfer or that this cluster is repeatedly present in *Dhc* genome as described by McMurdie et al. (2011).

Microbiological analyses of field samples were consistent with the results observed in the cis-DCE microcosm experiments. Microbiological field data also showed an increase in i) *Dhc* population relative to the total bacterial population and ii) functional genes related to RD (*tceA, bvcA* and *vcrA*). This suggests that the *Dhc* were most probably the drivers of RD in both the field and the microcosm experiments. Hence, the isotopic results obtained in the microcosm experiments might be representative for the analysis of biodegradation pathway and extent in the field.

3.5. Carbon and chlorine isotopic fractionation values and dual element isotope trends from the field-derived microcosms

In microcosm experiments, selected bottles were sacrificed at different extent of CEs degradation (Figs. S3, S4 and S5, in SI), water samples were collected for isotopic analysis and the isotopic fractionation ($\varepsilon^{13}C$ and $\varepsilon^{37}Cl$) for the RD of PCE, TCE and cis-DCE was determined according to Eq. (2) (Section 2.7). The carbon isotopic fractionation of VC was also estimated from the cis-DCE microcosms experiment using only the $\delta^{13}C_{VC}$ values of those samples where cis-DCE was already consumed (see SI). Given the fast degradation of PCE and TCE in both the microcosm experiments and in the contaminated site after the EVO injection (see above), cis-DCE was the predominant contaminant in the experiments (Fig. S2, in the SI) and in many wells during the investigated period (Fig. 4). Hereafter, the discussion of isotopic data from both the experiments and field samples is thus focussed on cis-DCE. The use of multi-element isotope data to investigate the fate of cis-DCE in the field is still very scarce in the literature (Zimmermann et al., 2020). The isotopic fractionation results for PCE, TCE ($\varepsilon^{13}C$ and $\varepsilon^{37}Cl$) and VC ($\varepsilon^{13}C$) and dual-element isotope slopes ($\Lambda^{C\text{-}Cl}$) for PCE and TCE in microcosm experiments are shown in the SI. All the εC, εCl and $\Lambda^{C/Cl}$ values calculated by OLR are summarised in Table 2. A comparison between Λ values and their uncertainties obtained in this study with the OLR and the York (Ojeda et al., 2019, 2020) regression methods is shown in the SI. Since no systematic bias introduced by ORL was observed and because there has not been sufficient time for the York method to be routinely adopted in 2D-CSIA studies, we used OLR values, but present York results in the SI.

Table 2
Calculated values of εC, εCl and $\Lambda^{C\text{-}Cl}$ for all compounds in the microcosm experiments and for cis-DCE in the field application. 95 % CI = 95 % confidence interval; N = number of points; n.a. = not analyzed.

	εC (‰)	95 % CI	εCl (‰)	95 % CI	$\Lambda^{C\text{-}Cl}$	95 % CI	N
Microcosms PCE	−1.1	0.7	−0.4	1.3	0.8	0.4	7
Microcosms TCE	−8	5	−2	1	5	1	8
Microcosms cis-DCE	−7	2	−1.5	0.4	4.9	0.8	14
Microcosms VC	−31	7	n.a.	n.a.	n.a.	n.a.	4
Field application cis-DCE	n.a.	n.a.	n.a.	n.a.	5	3	21

For cis-DCE, determined isotope fractionation values, i.e., $\varepsilon^{13}C = -7 \pm 2$ ‰ and $\varepsilon^{37}Cl = -1.5 \pm 0.4$ ‰, were lower than those reported in previous isotopic laboratory studies of anaerobic biodegradation of cis-DCE using pure and mixed cultures (Bloom et al., 2000; Abe et al., 2009; Fletcher et al., 2011; Kuder et al., 2013; Doğan-Subaşı et al., 2017; Lihl et al., 2019): from −31 to −14.9 ‰ ($n = 7$) and from −3.3 to −1.6 ‰ ($n = 5$) for $\varepsilon^{13}C$ and $\varepsilon^{37}Cl$, respectively. This suggests that despite following the same degradation pathway, isotope masking could significantly influence isotopic fractionation. Masking processes can be associated with the effect of rate-limiting (non or slightly isotope fractionating) steps preceding the bond cleavage such as contaminant mass transfer (Aeppli et al., 2009; Renpenning et al., 2015). Although considerable partitioning of the contaminant between the EVO and water phases, described in Section 3.1, might cause a mass transfer-related masking effect as reported by Aeppli et al., 2009, this effect can be discarded, as the microcosms did not contain an observable EVO phase and the injected amendment was lactate.

In contrast to single-element isotope fractionation analysis, combined shifts in isotope ratios of two elements in a dual-element isotope plot ($\Lambda^{C\text{-}Cl}$) should avoid the effect of isotope masking since the proportion of changes in isotope ratios of both elements relative to each other ($\Delta\delta^{13}C/\Delta\delta^{37}Cl$) is largely unaffected by nondegradative processes (Elsner, 2010; Thullner et al., 2013).

The dual-element isotope trend determined from microcosm experiments, i.e., $\Lambda^{C\text{-}Cl} = 4.9 \pm 0.8$ (Fig. 5) was lower than the range observed from previous laboratory studies with pure, enrichment and mixed cultures, i.e., between 8.3 and 17.8, $n = 4$ (Ojeda et al., 2020). However, the value obtained in this study agree well with the one reported in a previous study using field-derived microcosms, i.e. $\Lambda^{C\text{-}Cl} = 4.5 \pm 3.4$ (Doğan-Subaşı et al., 2017) (see further discussion below).

3.6. ^{13}C- and ^{37}Cl-CSIA of cis-DCE in field samples and dual-element isotope trend

In contrast to PCE and TCE, which were rapidly consumed in most of the wells, high fractions of cis-DCE were in general measured during the investigated period (Fig. 4), allowing the analysis of both carbon and chlorine isotopes in groundwater samples from all wells at multiple times.

The samples collected before the EVO injection (June 2020) showed cis-DCE $\delta^{13}C$ values ranging from −34.1 to −14.9 ‰ and most $\delta^{37}Cl$ values ranging between +2.7 and + 5.1 ‰. This isotopic pattern would reflect the formation of cis-DCE from the TCE, which is consistent with values reported by (Cretnik et al., 2014) and coherent with the high molar fractions of TCE and PCE in June 2020 (Fig. 4).

Conversely, the samples collected after the EVO injection showed in general a trend toward more positive $\delta^{13}C$ and $\delta^{37}Cl$ values (Fig. 5). Such enrichment in both ^{13}C and ^{37}Cl indicate the transformation of cis-DCE following the biostimulation treatment. In order to determine the dual-element isotope trend during cis-DCE transformation in the field after the EVO injection, $\delta^{13}C$ and $\delta^{37}Cl$ values were combined in Fig. 5. To avoid the effect of ongoing cis-DCE formation from RD of TCE, only isotopic data from those samples where PCE and TCE were not detected were considered ($n = 21$). As a result, a $\Lambda^{C\text{-}Cl}$ value of 5 ± 3 was determined for the field (Fig. 5), which is very similar to the value obtained from the laboratory experiments performed in this study ($\Lambda^{C\text{-}Cl} = 4.9 \pm 0.8$). This result indicates that microbial RD of cis-DCE via hydrogenolysis to VC was the main reaction mechanism controlling the fate of cis-DCE at the site after the EVO injection. These results agree with the detection of VC (molar fraction >5 %) in all selected samples.

It is interesting to note that despite microbiological data pointed to *Dhc* bacteria as the most likely responsible for RD of cis-DCE in both the field site and microcosm experiments (see above), reported $\Lambda^{C\text{-}Cl}$ values for microbial RD of cis-DCE by *Dhc* strains (i.e., *D. mccartyi* strain BTF08, 18 ± 1, strain 195, 10.0 ± 0.4 (Lihl et al., 2019)) and mixed cultures

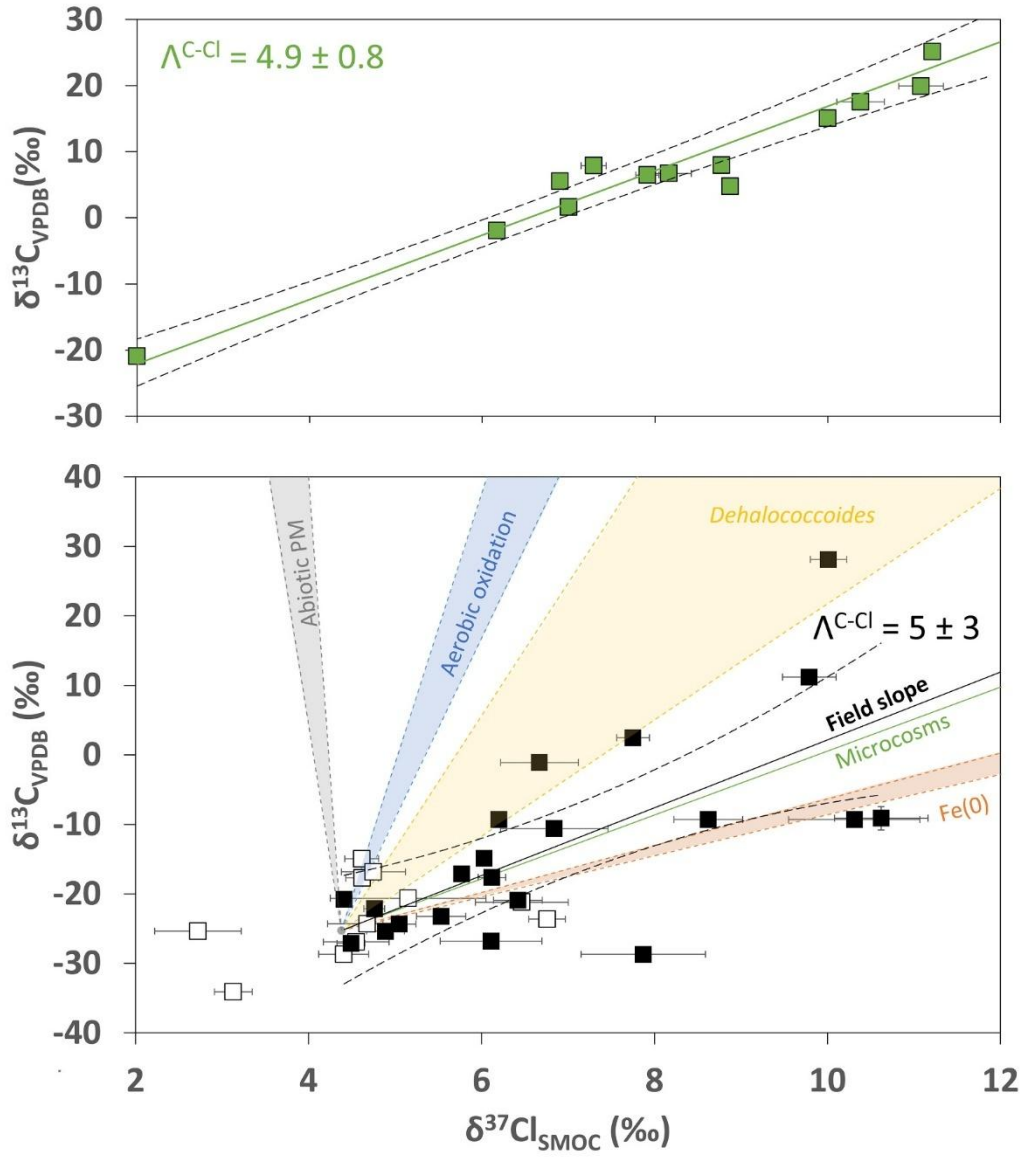

Fig. 5. Dual element C-Cl isotope plot of cis-DCE from samples of the microcosm experiments (upper panel) and the field (lower panel). Λ values (±95 % C.I.) are given by the slope of the linear regressions and the black dashed lines correspond to the 95 % C.I. Error bars for $\delta^{13}C$ values are generally smaller than the symbols. In the lower panel, the empty markers represent data from samples collected prior to the injection, while filled black markers correspond to those measured after the EVO injection. The green line represents the slope obtained from the microcosm experiments in this study and the colored areas correspond to ranges of previously reported slopes for different degradation processes: grey for abiotic oxidation by permanganate (Doğan-Subaşı et al., 2017), blue for aerobic oxidation (Abe et al., 2009), yellow for reductive dechlorination in *Dhc* cultures (Bloom et al., 2000; Abe et al., 2009; Fletcher et al., 2011; Kuder et al., 2013; Lihl et al., 2019), and orange for abiotic degradation with Fe(0) (Audí-Miró et al., 2013).

containing *Dhc* spp. (8.3 (Kuder et al., 2013) and 11.4 ± 0.6 (Abe et al., 2009)) were higher than those determined in this study (Fig. 5). This difference might be related with distinct reaction mechanisms and/or the use of different Rdhs during RD of cis-DCE by *Dhc* bacteria. Discrepancies on $\Lambda^{C\text{-}Cl}$ values, especially when small isotopic fractionation is observed for both carbon and chlorine, might not always reflect the chemical reaction mechanism, but preceding rate-limiting steps during enzyme – substrate association or enzymatic structure, as previously reported for other compounds such as PCE (Renpenning et al., 2014), TCE (Gafni et al., 2020) and trichloromethane (Heckel et al., 2019). Further research will be necessary to unravel the mechanisms behind these observed differences for RD of cis-DCE. Nevertheless, the slope determined in this study from field samples is strongly different compared to that determined for aerobic oxidation (32 ± 6, Abe et al. (2009)), indicating a non-significant biodegradation of cis-DCE under oxic conditions during the EISB treatment (Fig. 5).

Finally, for abiotic degradation processes, the starkly contrasting slope determined for oxidation by permanganate, −125 ± 47 (Doğan-Subaşı et al., 2017), will allow to differentiate between abiotic oxidation and microbial RD of cis-DCE in applications of in situ chemical oxidation by permanganate. However, for cis-DCE dichloroelimination by Fe(0) (via single electron transfer), a value relatively close to the slope of 5 ± 3 obtained in this study (Fig. 5) was reported (i.e. 3.1 ± 0.2 (Audí-Miró et al., 2013)), which could make it difficult to differentiate between cis-DCE transformation by microbial and abiotic RD in engineered remediation treatments such as Fe(0) permeable reactive barriers. In summary, the results of this study show the potential of a dual-element isotope approach to investigate transformation processes of cis-DCE in remediation of contaminated sites by EISB with EVO.

4. Conclusions

This study shows the potential of a multi-method approach for evaluating EISB of CEs with EVO in a contaminated site. Microbiological analyses indicated a significant increase in *Dhc* populations and RD functional genes in cis-DCE microcosms and the field, pointing to *Dhc* bacteria as the most likely responsible for RD of cis-DCE. The dual-element (C, Cl) isotope analysis showed similar $\Lambda^{C\text{-}Cl}$ values for i) the laboratory experiment of RD of cis-DCE and ii) the field samples collected after the EVO injection, i.e., 4.9 ± 0.8 and 5 ± 3, respectively, indicating that the fate of cis-DCE in the field was controlled by its transformation (hydrogenolysis) to VC. This result highlights the potential of the dual-element isotope approach to link the transformation processes determined in the laboratory experiments with those occurring in the field.

However, the $\Lambda^{C\text{-}Cl}$ values for RD of cis-DCE determined in this study from field-derived microcosm experiments and field samples (around 5.0) differ from those reported so far for laboratory studies with *Dhc* strains and mixed cultures containing *Dhc*., i.e., between 17.8 and 8.3 (Ojeda et al., 2020). This observation underscores the importance of determining site-specific Λ and ε values from derived microcosm experiments in order to improve the identification and quantification of transformation processes in contaminated sites using isotope data. In addition, the experiments of water – EVO phase partitioning of CEs showed, for the first time, that despite their high partitioning into the EVO, the effect on the carbon isotope ratios of CEs would be small or insignificant compared to that caused by biodegradation of the CEs in the groundwater in a field application scale.

The results of this study provide valuable insight for the practical application of dual isotopic (C, Cl) and biomolecular tools to i) assess degradation pathways of CEs, especially cis-DCE, in contaminated sites by EISB with EVO and ii) improve the understanding of the complex interactions among EVO, contaminant concentrations, and microbial communities in future field studies.

Funding

This study was financed through the following projects: INNOTECRD19-1-0006 funded by ACCIÓ, PACE-ISOTEC (CGL2017-87216-C4-1-R) financed by the Spanish Government and AEI/FEDER from the UE and the Consolidated Research Group MAGH project (2021-SGR-00308), financed by the AGAUR (Catalan Government). The experiments and work performed by S. Gil-Villalba were supported by the FPI2018/084979 contract, and the IAGC Student Research Grant (2022).

CRediT authorship contribution statement

Sergio Gil-Villalba: Writing – original draft, Methodology, Investigation, Formal analysis, Data curation. **Jordi Palau:** Writing – review & editing, Visualization, Validation, Supervision, Project administration, Methodology, Investigation, Conceptualization. **Jesica M. Soder-Walz:** Writing – review & editing, Supervision, Methodology, Investigation. **Miguel A. Vallecillo:** Validation, Supervision, Project administration, Methodology. **Jordi Corregidor:** Validation, Project administration, Methodology. **Andrea Tirado:** Methodology, Data curation. **Orfan Shouakar-Stash:** Validation, Supervision, Methodology, Investigation, Formal analysis. **Miriam Guivernau:** Writing – review & editing, Visualization, Methodology, Investigation, Data curation. **Marc Viñas:** Writing – review & editing, Validation, Supervision, Methodology. **Albert Soler:** Validation, Supervision, Resources, Funding acquisition, Conceptualization. **Monica Rosell:** Writing – review & editing, Visualization, Validation, Supervision, Project administration, Methodology, Investigation, Conceptualization.

Declaration of competing interest

The authors declare that they have no known competing financial interests or personal relationships that could have appeared to influence the work reported in this paper.

Data availability

Data will be made available on request.

Acknowledgements

We thank Anna Rigol from Department of Chemical Engineering and Analytical Chemistry, Faculty of Chemistry, in UB for providing us with the idea and the dialysis membrane for separating EVO from the water solution. We thank all technicians in MAiMA and CCiT-UB for their support. We truly appreciate all the constructive comments and suggestions from the three reviewers that have considerably improved our manuscript.

Appendix A. Supplementary data

Supplementary data to this article can be found online at https://doi.org/10.1016/j.scitotenv.2024.175351.

References

Abe, Y., Aravena, R., Zopfi, J., Shouakar-Stash, O., Cox, E., Roberts, J.D., Hunkeler, D., 2009. Carbon and chlorine isotope fractionation during aerobic oxidation and reductive dechlorination of vinyl chloride and cis-1, 2-dichloroethene. Environ. Sci. Technol. 43 (1), 101–107. https://doi.org/10.1021/es801759k.

Aelion, C.M., Höhener, P., Hunkeler, D., Aravena, R., 2009. Environmental isotopes in biodegradation and bioremediation. In: Environmental Isotopes in Biodegradation and Bioremediation. https://doi.org/10.1201/9781420012613.

Aeppli, C., Berg, M., Cirpka, O.A., Holliger, C., Schwarzenbach, R.P., Hofstetter, T.B., 2009. Influence of mass-transfer limitations on carbon isotope fractionation during microbial dechlorination of trichloroethene. Environ. Sci. Technol. 43 (23), 8813–8820. https://doi.org/10.1021/es901481b.

ATSDR, 2023. Substance Priority List [WWW Document]. Subst. Prior, List. https://www.atsdr.cdc.gov/spl/index.html#2022spl.

Audí-Miró, C., Cretnik, S., Otero, N., Palau, J., Shouakar-Stash, O., Soler, A., Elsner, M., 2013. Cl and C isotope analysis to assess the effectiveness of chlorinated ethene degradation by zero-valent iron: evidence from dual element and product isotope values. Appl. Geochem. 32, 175–183. https://doi.org/10.1016/j.apgeochem.2012.08.025.

Badin, A., Buttet, G., Maillard, J., Holliger, C., Hunkeler, D., 2014. Multiple dual C-Cl isotope patterns associated with reductive dechlorination of tetrachloroethene. Environ. Sci. Technol. 48 (16), 9179–9186. https://doi.org/10.1021/es500822d.

Bernstein, A., Shouakar-Stash, O., Ebert, K., Laskov, C., Hunkeler, D., Jeannottat, S., Sakaguchi-Söder, K., Laaks, J., Jochmann, M.A., Cretnik, S., Jager, J., Haderlein, S. B., Schmidt, T.C., Aravena, R., Elsner, M., 2011. Compound-specific chlorine isotope analysis: a comparison of gas chromatography/isotope ratio mass spectrometry and gas chromatography/quadrupole mass spectrometry methods in an Interlaboratory study. Anal. Chem. 83 (20), 7624–7634. https://doi.org/10.1021/ac200516c.

Blázquez-Pallí, N., Rosell, M., Varias, J., Bosch, M., Soler, A., Vicent, T., Marco-Urrea, E., 2019a. Multi-method assessment of the intrinsic biodegradation potential of an aquifer contaminated with chlorinated ethenes at an industrial area in Barcelona (Spain). Environ. Pollut. 244, 165–173. https://doi.org/10.1016/j.envpol.2018.10.013.

Blázquez-Pallí, N., Shouakar-Stash, O., Palau, J., Trueba-Santiso, A., Varias, J., Bosch, M., Soler, A., Vicent, T., Marco-Urrea, E., Rosell, M., 2019b. Use of dual element isotope analysis and microcosm studies to determine the origin and potential anaerobic biodegradation of dichloromethane in two multi-contaminated aquifers. Sci. Total Environ. 696, 134066 https://doi.org/10.1016/j.scitotenv.2019.134066.

Bloom, Y., Aravena, R., Hunkeler, D., Edwards, E., Frape, S.K., 2000. Carbon isotope fractionation during microbial dechlorination of trichloroethene, cis-l,2-dichloroethene, and vinyl chloride: implications for assessment of natural attenuation. Environ. Sci. Technol. 34 (13), 2768–2772. https://doi.org/10.1021/es991179k.

Chen, G., Kara Murdoch, F., Xie, Y., Murdoch, R.W., Cui, Y., Yang, Y., Yan, J., Key, T.A., Löffler, F.E., 2022b. Dehalogenation of Chlorinated Ethenes to Ethene by a Novel Isolate, "Candidatus Dehalogenimonas etheniformans". Appl. Environ. Microbiol. 88 (12) https://doi.org/10.1128/aem.00443-22.

Chen, W., Chen, K., Surmpalli, R.Y., Zhang, T.C., Ou, J., Kao, C., 2022a. Bioremediation of trichloroethylene-polluted groundwater using emulsified castor oil for slow carbon release and acidification control. Water Environ. Res. 94 (1) https://doi.org/10.1002/wer.1673.

Coplen, T.B., 1996. New guidelines for reporting stable hydrogen, carbon, and oxygen isotope-ratio data. Geochim. Cosmochim. Acta 60 (17), 3359–3360. https://doi.org/10.1016/0016-7037(96)00263-3.

Coplen, T.B., 2011. Guidelines and recommended terms for expression of stable-isotope-ratio and gas-ratio measurement results. Rapid Commun. Mass Spectrom. 25 (17), 2538–2560. https://doi.org/10.1002/rcm.5129.

Cretnik, S., Bernstein, A., Shouakar-Stash, O., Löffler, F., Elsner, M., 2014. Chlorine isotope effects from isotope ratio mass spectrometry suggest intramolecular C-Cl bond competition in trichloroethene (TCE) reductive dehalogenation. Molecules 19 (5), 6450–6473. https://doi.org/10.3390/molecules19056450.

Doğan-Subaşı, E., Elsner, M., Qiu, S., Cretnik, S., Atashgahi, S., Shouakar-Stash, O., Boon, N., Dejonghe, W., Bastiaens, L., 2017. Contrasting dual (C, Cl) isotope fractionation offers potential to distinguish reductive chloroethene transformation from breakdown by permanganate. Sci. Total Environ. 596–597, 169–177. https://doi.org/10.1016/j.scitotenv.2017.03.292.

Duhamel, M., Wehr, S.D., Yu, L., Rizvi, H., Seepersad, D., Dworatzek, S., Cox, E.E., Edwards, E.A., 2002. Comparison of anaerobic dechlorinating enrichment cultures maintained on tetrachloroethene, trichloroethene, cis -dichloroethene and vinyl chloride. Water Res. 36, 4193–4202.

Elsner, M., 2010. Stable isotope fractionation to investigate natural transformation mechanisms of organic contaminants: principles, prospects and limitations. J. Environ. Monit. 12 (11), 2005–2031. https://doi.org/10.1039/c0em00277a.

Ernst, T.J., 2009. Use of "Dehalococcoides" to bioremediate groundwater contaminated with chlorinated solvents. Basic Biotechnol. eJournal 5 (1), 72–77.

Fletcher, K.E., Nijenhuis, I., Richnow, H.H., Löffler, F.E., 2011. Stable carbon isotope enrichment factors for cis -1,2-dichloroethene and vinyl chloride reductive dechlorination by dehalococcoides. Environ. Sci. Technol. 45 (7), 2951–2957. https://doi.org/10.1021/es103728q.

Franke, S., Seidel, K., Adrian, L., Nijenhuis, I., 2020. Dual element (C/Cl) isotope analysis indicates distinct mechanisms of reductive dehalogenation of chlorinated ethenes and dichloroethane in dehalococcoides mccartyi strain BTF08 with defined reductive dehalogenase inventories. Front. Microbiol. 11 (July) https://doi.org/10.3389/fmicb.2020.01507.

Gafni, A., Gelman, F., Ronen, Z., Bernstein, A., 2020. Variable carbon and chlorine isotope fractionation in TCE co-metabolic oxidation. Chemosphere 242. https://doi.org/10.1016/j.chemosphere.2019.125130.

Halloran, L.J.S., Vakili, F., Wanner, P., Shouakar-Stash, O., Hunkeler, D., 2021. Sorption- and diffusion-induced isotopic fractionation in chloroethenes. Sci. Total Environ. 788, 147826 https://doi.org/10.1016/j.scitotenv.2021.147826.

Harkness, M., 2000. Economic considerations in enhanced anaerobic biodegradation. In: Bioremediation and Phytoremediation of Chlorinated and Recalcitrant Compounds, pp. 9–14.

Harkness, M., Fisher, A., 2013. Use of emulsified vegetable oil to support bioremediation of TCE DNAPL in soil columns. J. Contam. Hydrol. 151, 16–33. https://doi.org/10.1016/j.jconhyd.2013.04.002.

He, J., Sung, Y., Krajmalnik-Brown, R., Ritalahti, K.M., Löffler, F.E., 2005. Isolation and characterization of Dehalococcoides sp. strain FL2, a trichloroethene (TCE)- and 1,2-dichloroethene-respiring anaerobe. Environ. Microbiol. 7 (9), 1442–1450. https://doi.org/10.1111/j.1462-2920.2005.00830.x.

Heckel, B., Phillips, E., Edwards, E., Sherwood Lollar, B., Elsner, M., Manefield, M.J., Lee, M., 2019. Reductive dehalogenation of Trichloromethane by two different *Dehalobacter restrictus* strains reveal opposing dual element isotope effects. Environ. Sci. Technol. 53 (5), 2332–2343. https://doi.org/10.1021/acs.est.8b03717.

Hermon, L., Denonfoux, J., Hellal, J., Joulian, C., Ferreira, S., Vuilleumier, S., Imfeld, G., 2018. Dichloromethane biodegradation in multi-contaminated groundwater: insights from biomolecular and compound-specific isotope analyses. Water Res. 142, 217–226. https://doi.org/10.1016/j.watres.2018.05.057.

Hiortdahl, K.M., Borden, R.C., 2014. Enhanced reductive dechlorination of tetrachloroethene dense nonaqueous phase liquid with EVO and $Mg(OH)_2$. Environ. Sci. Technol. 48 (1), 624–631. https://doi.org/10.1021/es4042379.

Hirschorn, S.K., Grostern, A., Lacrampe-Couloume, G., Edwards, E.A., MacKinnon, L., Repta, C., Major, D.W., Sherwood Lollar, B., 2007. Quantification of biotransformation of chlorinated hydrocarbons in a biostimulation study: added value via stable carbon isotope analysis. J. Contam. Hydrol. 94 (3–4), 249–260. https://doi.org/10.1016/j.jconhyd.2007.07.001.

Höhener, P., Yu, X., 2012. Stable carbon and hydrogen isotope fractionation of dissolved organic groundwater pollutants by equilibrium sorption. J. Contam. Hydrol. 129–130, 54–61. https://doi.org/10.1016/j.jconhyd.2011.09.006.

Hug, L.A., 2016. In: Adrian, L., Löffler, F.E. (Eds.), Diversity, Evolution, and Environmental Distribution of Reductive Dehalogenase Genes BT - Organohalide-Respiring Bacteria. Springer, Berlin Heidelberg, pp. 377–393. https://doi.org/10.1007/978-3-662-49875-0_16.

Jin, B., Laskov, C., Rolle, M., Haderlein, S.B., 2011. Chlorine isotope analysis of organic contaminants using GC-qMS: method optimization and comparison of different evaluation schemes. Environ. Sci. Technol. 45 (12), 5279–5286. https://doi.org/10.1021/es200749d.

Kaufmann, R., Long, A., Bentley, H., Davis, S., 1984. Natural chlorine isotope variations. Nature 309 (5966), 338–340. https://doi.org/10.1038/309338a0.

Kuder, T., Philp, P., 2013. Demonstration of compound-specific isotope analysis of hydrogen isotope ratios in chlorinated ethenes. Environ. Sci. Technol. 47 (3), 1461–1467. https://doi.org/10.1021/es303476v.

Kuder, T., Van Breukelen, B.M., Vanderford, M., Philp, P., 2013. 3D-CSIA: carbon, chlorine, and hydrogen isotope fractionation in transformation of TCE to ethene by a dehalococcoides culture. Environ. Sci. Technol. 47 (17), 9668–9677. https://doi.org/10.1021/es400463p.

Lalman, J.A., Bagley, D.M., 2000. Anaerobic degradation and inhibitory effects of linoleic acid. Water Res. 34 (17), 4220–4228. https://doi.org/10.1016/S0043-1354(00)00180-9.

Lee, P.K.H., Johnson, D.R., Holmes, V.F., He, J., Alvarez-Cohen, L., 2006. Reductive dehalogenase gene expression as a biomarker for physiological activity of *Dehalococcoides* spp. Appl. Environ. Microbiol. 72 (9), 6161–6168. https://doi.org/10.1128/AEM.01070-06.

Lee, P.K.H., Macbeth, T.W., Sorenson, K.S., Deeb, R.A., Alvarez-Cohen, L., 2008. Quantifying genes and transcripts to assess the in situ physiology of "*Dehalococcoides*" spp. in a trichloroethene-contaminated groundwater site. Appl. Environ. Microbiol. 74 (9), 2728–2739. https://doi.org/10.1128/AEM.02199-07.

Lee, Y.-C., Kwon, T.-S., Yang, J.-S., Yang, J.-W., 2007. Remediation of groundwater contaminated with DNAPLs by biodegradable oil emulsion. J. Hazard. Mater. 140 (1), 340–345. https://doi.org/10.1016/j.jhazmat.2006.09.036.

Leeson, A., Beevar, E., Henry, B., Fortenberry, J., Coyle, C., 2004. Microbiological and geochemical considerations. In: Principles and Practices of Enhanced Anaerobic Bioremdiation of Chlorinated Solvents, Section 2, pp. 2-1–2-11.

Lihl, C., Douglas, L.M., Franke, S., Pérez-De-Mora, A., Meyer, A.H., Daubmeier, M., Edwards, E.A., Nijenhuis, I., Sherwood Lollar, B., Elsner, M., 2019. Mechanistic dichotomy in bacterial trichloroethene dechlorination revealed by carbon and chlorine isotope effects. Environ. Sci. Technol. 53 (8), 4245–4254. https://doi.org/10.1021/acs.est.8b06643.

Löffler, F.E., Ritalahti, K.M., Zinder, S.H., 2013. In: Stroo, H.F., Leeson, A., Ward, C.H. (Eds.), Dehalococcoides and reductive Dechlorination of chlorinated solvents BT - bioaugmentation for groundwater remediation. Springer, New York, pp. 39–88. https://doi.org/10.1007/978-1-4614-4115-1_2.

Long, C.M., Borden, R.C., 2006. Enhanced reductive dechlorination in columns treated with edible oil emulsion. J. Contam. Hydrol. 87 (1), 54–72. https://doi.org/10.1016/j.jconhyd.2006.04.010.

Lu, X., Wilson, J.T., Kampbell, D.H., 2006. Relationship between Dehalococcoides DNA in ground water and rates of reductive dechlorination at field scale. Water Res. 40 (16), 3131–3140. https://doi.org/10.1016/j.watres.2006.05.030.

Magnuson, J.K., Romine, M.F., Burris, D.R., Kingsley, M.T., 2000. Trichloroethene reductive dehalogenase from *Dehalococcoides ethenogenes*: sequence of tceA and substrate range characterization. Appl. Environ. Microbiol. 66 (12), 5141–5147. https://doi.org/10.1128/AEM.66.12.5141-5147.2000.

McMurdie, P.J., Hug, L.A., Edwards, E.A., Holmes, S., Spormann, A.M., 2011. Site-specific mobilization of vinyl chloride Respiration Islands by a mechanism common in Dehalococcoides. BMC Genom. 12 (1), 287. https://doi.org/10.1186/1471-2164-12-287.

Newman, W.A., Pelle, R.C., 2006. Enhanced anaerobic bioremediation of chlorinated solvents utilizing vegetable oil emulsions. Remediation 16 (3), 109–122. https://doi.org/10.1002/rem.20095.

Ni, S., Fredrickson, J.K., Xun, L., 1995. Purification and characterization of a novel 3-chlorobenzoate-reductive dehalogenase from the cytoplasmic membrane of *Desulfomonile tiedjei* DCB-1. J. Bacteriol. 177 (17), 5135–5139. https://doi.org/10.1128/jb.177.17.5135-5139.1995.

Nijenhuis, I., Nikolausz, M., Köth, A., Felföldi, T., Weiss, H., Drangmeister, J., Großmann, J., Kästner, M., Richnow, H.H., 2007. Assessment of the natural attenuation of chlorinated ethenes in an anaerobic contaminated aquifer in the Bitterfeld/Wolfen area using stable isotope techniques, microcosm studies and molecular biomarkers. Chemosphere 67 (2), 300–311. https://doi.org/10.1016/j.chemosphere.2006.09.084.

Nijenhuis, I., Renpenning, J., Kümmel, S., Richnow, H.H., Gehre, M., 2016. Recent advances in multi-element compound-specific stable isotope analysis of organohalides: achievements, challenges and prospects for assessing environmental sources and transformation. Trends Environ. Anal. Chem. 11, 1–8. https://doi.org/10.1016/j.teac.2016.04.001.

Ojeda, A.S., Phillips, E., Mancini, S.A., Lollar, B.S., 2019. Sources of uncertainty in biotransformation mechanistic interpretations and remediation studies using CSIA. Anal. Chem. 91 (14), 9147–9153. https://doi.org/10.1021/acs.analchem.9b01756.

Ojeda, A.S., Phillips, E., Sherwood Lollar, B., 2020. Multi-element (C, H, Cl, Br) stable isotope fractionation as a tool to investigate transformation processes for halogenated hydrocarbons. Environ. Sci.: Processes Impacts 22 (3), 567–582. https://doi.org/10.1039/C9EM00498J.

Palau, J., Soler, A., Teixidor, P., Aravena, R., 2007. Compound-specific carbon isotope analysis of volatile organic compounds in water using solid-phase microextraction. J. Chromatogr. A 1163 (1), 260–268. https://doi.org/10.1016/j.chroma.2007.06.050.

Palau, J., Marchesi, M., Chambon, J.C.C., Aravena, R., Canals, À., Binning, P.J., Bjerg, P. L., Otero, N., Soler, A., 2014. Multi-isotope (carbon and chlorine) analysis for fingerprinting and site characterization at a fractured bedrock aquifer contaminated by chlorinated ethenes. Sci. Total Environ. 475, 61–70. https://doi.org/10.1016/j.scitotenv.2013.12.059.

Pfeiffer, P., Bielefeldt, A.R., Illangasekare, T., Henry, B., 2005. Partitioning of dissolved chlorinated ethenes into vegetable oil. Water Res. 39 (18), 4521–4527. https://doi.org/10.1016/j.watres.2005.09.016.

Renpenning, J., Keller, S., Cretnik, S., Shouakar-Stash, O., Elsner, M., Schubert, T., Nijenhuis, I., 2014. Combined C and Cl isotope effects indicate differences between corrinoids and enzyme (*Sulfurospirillum multivorans* PceA) in reductive dehalogenation of tetrachloroethene, but not trichloroethene. Environ. Sci. Technol. 48 (20), 11837–11845. https://doi.org/10.1021/es503306g.

Renpenning, J., Rapp, I., Nijenhuis, I., 2015. Substrate hydrophobicity and cell composition influence the extent of rate limitation and masking of isotope fractionation during microbial reductive dehalogenation of chlorinated Ethenes. Environ. Sci. Technol. 49 (7), 4293–4301. https://doi.org/10.1021/es506108j.

Révész, K.M., Lollar, B.S., Kirshtein, J.D., Tiedeman, C.R., Imbrigiotta, T.E., Goode, D.J., Shapiro, A.M., Voytek, M.A., Lacombe, P.J., Busenberg, E., 2014. Integration of stable carbon isotope, microbial community, dissolved hydrogen gas, and $^{2}HH_{2}O$ tracer data to assess bioaugmentation for chlorinated ethene degradation in fractured rocks. J. Contam. Hydrol. 156, 62–77. https://doi.org/10.1016/j.jconhyd.2013.10.004.

Ritalahti, K.M., Hatt, J.K., Lugmayr, V., Henn, K., Petrovskis, E.A., Ogles, D.M., Davis, G. A., Yeager, C.M., Lebrón, C.A., Löffler, F.E., 2010. Comparing on-site to off-site biomass collection for Dehalococcoides biomarker gene quantification to predict in situ chlorinated Ethene detoxification potential. Environ. Sci. Technol. 44 (13), 5127–5133. https://doi.org/10.1021/es100408r.

Rodríguez-Fernández, D., Heckel, B., Torrentó, C., Meyer, A., Elsner, M., Hunkeler, D., Soler, A., Rosell, M., Domènech, C., 2018. Dual element (C-Cl) isotope approach to distinguish abiotic reactions of chlorinated methanes by Fe(0) and by Fe(II) on iron minerals at neutral and alkaline pH. Chemosphere 206, 447–456. https://doi.org/10.1016/j.chemosphere.2018.05.036.

Rosell, M., Palau, J., Mortan, S.H., Caminal, G., Soler, A., Shouakar-Stash, O., Marco-Urrea, E., 2019. Dual carbon - chlorine isotope fractionation during dichloroelimination of 1,1,2-trichloroethane by an enrichment culture containing *Dehalogenimonas* sp. Sci. Total Environ. 648, 422–429. https://doi.org/10.1016/j.scitotenv.2018.08.071.

Shouakar-Stash, O., Drimmie, R.J., Zhang, M., Frape, S.K., 2006. Compound-specific chlorine isotope ratios of TCE, PCE and DCE isomers by direct injection using CF-IRMS. Appl. Geochem. 21 (5), 766–781. https://doi.org/10.1016/j.apgeochem.2006.02.006.

Thullner, M., Fischer, A., Richnow, H.-H., Wick, L.Y., 2013. Influence of mass transfer on stable isotope fractionation. Appl. Microbiol. Biotechnol. 97 (2), 441–452. https://doi.org/10.1007/s00253-012-4537-7.

Tiehm, A., Schmidt, K.R., 2011. Sequential anaerobic/aerobic biodegradation of chloroethenes-aspects of field application. Curr. Opin. Biotechnol. 22 (3), 415–421. https://doi.org/10.1016/j.copbio.2011.02.003.

Torrentó, C., Palau, J., Rodríguez-Fernández, D., Heckel, B., Meyer, A., Domènech, C., Rosell, M., Soler, A., Elsner, M., Hunkeler, D., 2017. Carbon and chlorine isotope fractionation patterns associated with different engineered chloroform transformation reactions. Environ. Sci. Technol. 51 (11), 6174–6184. https://doi.org/10.1021/acs.est.7b00679.

Underwood, J.C., Akob, D.M., Lorah, M.M., Imbrigiotta, T.E., Harvey, R.W., Tiedeman, C.R., 2022. Microbial community response to a bioaugmentation test to degrade trichloroethylene in a fractured rock aquifer, Trenton, N.J. FEMS Microbiol. Ecol. 98 (7), fiac077 https://doi.org/10.1093/femsec/fiac077.

Wanner, P., Parker, B.L., Chapman, S.W., Aravena, R., Hunkeler, D., 2017. Does sorption influence isotope ratios of chlorinated hydrocarbons under field conditions? Appl. Geochem. 84, 348–359. https://doi.org/10.1016/j.apgeochem.2017.07.016.

West, K.A., Lee, P.K.H., Johnson, D.R., Zinder, S.H., Alvarez-Cohen, L., 2013. Global gene expression of Dehalococcoides within a robust dynamic TCE-dechlorinating community under conditions of periodic substrate supply. Biotechnol. Bioeng. 110 (5), 1333–1341. https://doi.org/10.1002/bit.24819.

Wiegert, C., Aeppli, C., Knowles, T., Holmstrand, H., Evershed, R., Pancost, R.D., Macháčková, J., Gustafsson, Ö., 2012. Dual carbon-chlorine stable isotope investigation of sources and fate of chlorinated ethenes in contaminated groundwater. Environ. Sci. Technol. 46 (20), 10918–10925. https://doi.org/10.1021/es3016843.

Yang, Y., Mccarty, P.L., 2000. Biologically enhanced dissolution of tetrachloroethene DNAPL. Environ. Sci. Technol. 34 (14), 2979–2984. https://doi.org/10.1021/es991410u.

Yu, R., Andrachek, R.G., Lehmicke, L.G., Freedman, D.L., 2018. Remediation of chlorinated ethenes in fractured sandstone by natural and enhanced biotic and abiotic processes: a crushed rock microcosm study. Sci. Total Environ. 626, 497–506. https://doi.org/10.1016/j.scitotenv.2018.01.064.

van der Zaan, B., Hannes, F., Hoekstra, N., Rijnaarts, H., de Vos, W.M., Smidt, H., Gerritse, J., 2010. Correlation of *Dehalococcoides* 16S rRNA and chloroethene-reductive dehalogenase genes with geochemical conditions in chloroethene-contaminated groundwater. Appl. Environ. Microbiol. 76 (3), 843–850. https://doi.org/10.1128/AEM.01482-09.

Zimmermann, J., Halloran, L.J.S., Hunkeler, D., 2020. Tracking chlorinated contaminants in the subsurface using compound-specific chlorine isotope analysis: a review of principles, current challenges and applications. Chemosphere 244, 125476. https://doi.org/10.1016/j.chemosphere.2019.125476.

Journal of Hazardous Materials 489 (2025) 137702

Contents lists available at ScienceDirect

Journal of Hazardous Materials

journal homepage: www.elsevier.com/locate/jhazmat

Variable dual C-Cl isotope slopes of trichloromethane transformation by alkaline-activated persulfate under different simulated field conditions

Sergio Gil-Villalba [a,*], Mònica Rosell [a], Clara Torrentó [a,b], Martí Vinyes-Nadal [a], Albert Soler [a], Jordi Palau [a]

[a] Grup MAiMA, SGR Mineralogia Aplicada, Geoquímica i Hidrogeologia (MAGH), Departament de Mineralogia, Petrologia i Geologia Aplicada, Facultat de Ciències de la Terra, Institut de Recerca de l'Aigua (IdRA), Universitat de Barcelona (UB), Martí Franquès s/n, Barcelona 08028, Spain
[b] Serra Húnter Fellowship, Generalitat de Catalunya, Spain

HIGHLIGHTS

- TCM:PS molar ratio influences oxidation kinetics, but not isotopic fractionation.
- Alkaline hydrolysis becomes predominant at pHs higher than 12.
- The presence of carbonates points to a reductive degradation reaction.
- Dual C-Cl isotope analysis allowed the identification of the different reactions.
- Hexachloroethane was observed as degradation byproduct.

GRAPHICAL ABSTRACT

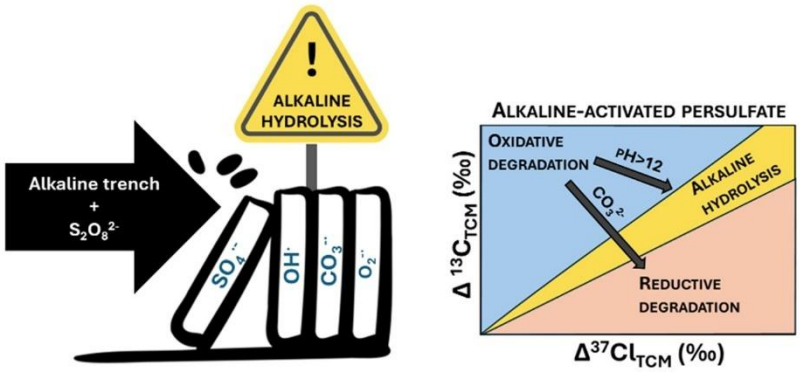

ARTICLE INFO

Keywords:
2D-CSIA
Chloroform
Advanced oxidation treatments
In situ chemical oxidation
Groundwater remediation
Chlorinated contaminants

ABSTRACT

Laboratory experiments were conducted to evaluate the potential of $\delta^{13}C$ and $\delta^{37}Cl$ isotopic values of trichloromethane (TCM) to monitor and quantify its transformation during alkaline persulfate (PS) activation. Batch experiments were designed to replicate different TCM:PS molar ratios, pH values, the presence of CO_3^{2-} ion and the simulation of an alkaline interception trench. Results revealed three distinct C-Cl isotopic trends; First, despite differences in degradation kinetics, isotopic trends were consistent across TCM:PS molar ratios ($\Lambda^{C\text{-}Cl}$ between 23 ± 10 and 33 ± 6), suggesting that radical activation remained unaffected. Conversely, at pH 12.8, alkaline hydrolysis (AH) became the predominant degradation process ($\Lambda^{C\text{-}Cl}$ of 9 ± 1 and 11 ± 1) over reaction with PS derived radical species. Finally, in the presence of excess CO_3^{2-} ion, which acts as radical scavenger probably affecting the radical species involved in TCM degradation, a $\Lambda^{C\text{-}Cl}$ value of 5.5 ± 0.6 was observed, suggesting a reductive degradation reaction. Therefore, our results reveal, for the first time, that the dual C-Cl isotope slope during TCM degradation by PS varies significantly depending on field conditions. The unexpected accumulation of higher chlorinated byproducts, such as hexachloroethane, during TCM degradation by alkaline-

* Corresponding author.
E-mail address: sergiogilv@ub.edu (S. Gil-Villalba).

https://doi.org/10.1016/j.jhazmat.2025.137702
Received 3 December 2024; Received in revised form 10 February 2025; Accepted 19 February 2025
Available online 22 February 2025

activated PS was observed for the first time and further research is needed in real open-systems to assess its potential environmental implications.

1. Introduction

Trichloromethane (TCM), commonly known as chloroform ($CHCl_3$), has had multiple industrial applications, and is today one of the most prevalent groundwater contaminants. TCM is a deemed toxic pollutant and, thus, it is ranked 11th in the Priority List of Hazardous Substances in 2022 by the Agency for Toxic Substances and Disease Registry based on a combination of its frequency, toxicity, and potential for human exposure [1].

In situ Chemical Oxidation (ISCO) is considered as an effective treatment method for the remediation of organic contaminants, including TCM [2-5]. Among different oxidants, activated persulfate ($S_2O_8^{2-}$, PS) has been increasingly applied in ISCO treatments of contaminated soil and groundwater due to its capacity to generate sulfate radicals ($SO_4^{\cdot-}$), which are as reactive as the classically used hydroxyl radicals ($OH^{\cdot}$), but more selective [6,7,4]. Furthermore, activated PS exhibits both oxidative and nucleophilic reactivity, leading to the generation of various reactive oxygen species (ROS) besides sulfate radicals ($SO_4^{\cdot-}$), such as $OH^{\cdot}$ and superoxide radicals ($O_2^{\cdot-}$), facilitating the degradation of multiple contaminants [8-10].

Base activation of PS, widely applied in field treatments [10], generates sulfate radicals ($SO_4^{\cdot-}$) that lead to hydroxyl radical formation ($OH^{\cdot}$) under highly alkaline conditions [11-13]. While both ROS can effectively degrade persistent organic compounds, the lower selectivity of $OH^{\cdot}$ may increase its consumption by natural organic matter, reducing treatment efficiency [8,14,15]. Furthermore, common groundwater anions like HCO_3^-, CO_3^{2-} and Cl^- can act as $SO_4^{\cdot-}$ and $OH^{\cdot}$ scavengers [14, 16,17], forming weaker oxidant radicals such as $CO_3^{\cdot-}$ and $Cl^{\cdot}$ [18-20]. These secondary radicals, while very selective, typically reduce overall oxidation kinetics and alter degradation pathways [14,21].

Therefore, in alkaline-activated PS systems, multiple degradation pathways of contaminants can coexist due to the presence of various ROS and/or the occurrence of alkaline hydrolysis [22,23]. Assessing degradation reaction mechanisms of TCM following an alkaline-activated PS application is crucial for evaluating contaminated site remediation; however, this area remains largely unexplored. Dual-element compound specific isotope analysis (2D-CSIA) offers a promising approach for distinguishing reaction mechanisms by leveraging the characteristic stable isotope fractionation patterns associated with specific degradation processes [24-27]. Given that different ROS might induce distinct TCM degradation mechanisms and that multiple degradation pathways may occur simultaneously, 2D-CSIA could provide valuable insights into the processes driving TCM transformation by alkaline-activated PS under varying environmental conditions.

Several dual C-Cl slope values (i.e., $\Lambda^{C\text{-}Cl}$) for TCM transformation processes have been previously reported. Regarding reductive processes, TCM degradation with cast zero valent iron, Fe(0), yields a $\Lambda^{C\text{-}Cl}$ value of 8 ± 2 at pH 7 [28] that remains unchanged at pH 12 [29], although it has also been reported as $\Lambda^{C\text{-}Cl} = 5.8 \pm 0.4$ [30]. TCM bacterial reductive dechlorination (RD) has been studied abiotically through the use of the corrinoid cofactor vitamin B12 (present in almost all reductive dehalogenases identified to date), obtaining a $\Lambda^{C\text{-}Cl} = 6.5 \pm 0.2$ [31]. When smaller doses of vitamin B12 were used to biostimulate anoxic microbial cultures, similar values (7 ± 1) were observed [32]. A recent work [33] attributed the reactivity of TCM with vitamin B12 by *Dehalobacter* CF (strain UNSWDHB) (with a $\Lambda^{C\text{-}Cl} = 6.6 \pm 0.1$) to a second-order nucleophilic substitution (S_N2) reaction. However, experiments using *Dehalobacter strain* 8 M exhibited a very different $\Lambda^{C\text{-}Cl}$ value of 2.8 ± 0.3, which was ascribed to enzyme binding masking effects created by the structure of different enzymatic pockets [34]. A different TCM reductive mechanism, concerted dissociative Outer-Sphere Single Electron Transfer (OS-SET), was studied by experiments with $CO_2^{\cdot-}$ radical [35], which produced a SET to a σ* orbital concerted with C-Cl breakage, leading to a similar $\Lambda^{C\text{-}Cl} = 6.7 \pm 0.4$. These reported $\Lambda^{C\text{-}Cl}$ values for reductive processes are in general lower compared to those observed for TCM alkaline hydrolysis (AH) ($\Lambda^{C\text{-}Cl} = 13.0 \pm 0.8$) and oxidation by thermally activated PS ($\Lambda^{C\text{-}Cl} = 17 \pm 2$) [28]. This is consistent with an oxidative C-H bond cleavage by a hydrogen atom abstraction (HAA) in the case of the heat-activated PS oxidation and a stepwise $E1_{CB}$ elimination reaction, consisting of the base-catalyzed deprotonation of the TCM followed by the loss of a chloride ion, for AH degradation mechanism [23].

In the light of the above information, the alkaline activation of PS in ISCO treatments could be influenced by varying field conditions, potentially resulting in the formation of different ROS or triggering processes such as alkaline hydrolysis. In turn, these variations can significantly affect the degradation pathways and overall efficiency of TCM remediation. To the best of the authors knowledge, the TCM degradation reaction mechanisms following ISCO with alkaline-activated PS have not been previously investigated. Since prior research has demonstrated that C-Cl 2D-CSIA is a valuable tool for distinguishing among different TCM degradation processes (e.g., reductive degradation, alkaline hydrolysis, and thermal-activated PS oxidation), this study aims to evaluate the potential of 2D-CSIA for assessing TCM degradation processes under variable field conditions during alkaline-activated persulfate ISCO treatments.

To this end, ISCO by alkaline-activated PS was replicated in batch experiments under controlled laboratory conditions where the influence of different factors was assessed: TCM:PS molar ratios, pH, and the presence of radical-scavenger species commonly found in groundwater (e.g., CO_3^{2-}). In addition, the novel remediation conditions provided by an interception alkaline trench filled with concrete-based residues (such the one previously studied in Òdena, Spain [23]) and multiple contaminants (i.e., chlorinated methanes - CMs and chlorinated ethenes - CEs) typically found in contaminated sites were considered. Most of the factors evaluated in this study are common in field applications of alkaline activated PS, including the use of a commercial mixed reagent.

2. Methodology

A list of all chemicals used in the laboratory experiments is provided in Appendix A in the Supplementary Information (SI).

2.1. Experimental design

Batch experiments were performed to assess the TCM carbon and chlorine isotopic fractionation during its transformation by alkaline-activated PS under different conditions (see summary in Table 1). Both commercial persulfate with an integrated alkaline activator (PersulfOx®, from now on "PSOX") and pure sodium persulfate ("PS") were used in different experiments consisting of: (i) deionized water with PSOX (resulting in a pH of 10.2 ± 0.2) with two different TCM:PS molar ratios (1:125 and 1:65), to assess the feasibility of TCM oxidation at different PSOX dosages or in different parts of a contamination plume; (ii) deionized water with PS basified with NaOH at two different alkaline pHs (11.4 ± 0.4 and 12.83 ± 0.03), to assess if changes in pH could induce changes in the oxidation reaction, other than a greater extent of AH; (iii) deionized water with PS basified as in experiment ii but adding Na_2CO_3 (at 200 mg/L), to resemble groundwater conditions and to evaluate the effect of CO_3^{2-} anion in the radical cascade activity; and (iv) trench-sampled water (pH 10.3 ± 0.5), co-contaminants (either CMs or

Table 1
Summary of experiments conditions: pH, TCM:PS molar ratio, contaminants in the aqueous solution and measured initial CO_3^{2-} concentrations.

Code	Conditions	pH	Molar ratio TCM:PS	Contaminants	Initial CO_3^{2-} (mg/L)
i.a	PSOX	10.2 ± 0.2	1:65	TCM	0
i.b	PSOX	10.2 ± 0.2	1:125	TCM	0
ii.a	PS + NaOH	11.4 ± 0.4	1:65	TCM	0
ii.b	PS + NaOH	12.8 ± 0.1	1:65	TCM	0
iii.a	PS + NaOH + CO_3^{2-}	11.3 ± 0.4	1:65	TCM	110
iii.b	PS + NaOH + CO_3^{2-}	12.8 ± 0.1	1:65	TCM	110
iv.a	PS + Trench conditions	11.6 ± 0.7	1:65	TCM, CT, DCM	95
iv.b	PS + Trench conditions	11.7 ± 0.6	-	PCE, TCE, cis-DCE	95

CEs) and filling material, plus PS to reproduce the field conditions of an alkaline interception trench.

In the last set-up (exp. iv), solid samples from an active alkaline interception trench, composed of 40–70 mm-sized recycled concrete-based aggregates from a construction waste recycling plant [23] were grinded to a diameter between 2 and 8 mm and 25 g were introduced in each vial. This experiment simulated the possible interactions of the solid phases in the oxidation reaction, while maintaining the alkaline pH for PS activation via equilibrium with the portlandite ($Ca(OH)_2$) present in the concrete. With this set-up, to reproduce the oxidation reaction in the mentioned alkaline trench, and to assess the potential of 2D-CSIA to identify the underlying oxidation process and quantify the extent of the degradation, two batch experiments were conducted, one containing CMs (tetrachloromethane - CT, TCM and dichloromethane - DCM) and another one with CEs (tetrachloroethene - PCE, trichloroethene - TCE, cis-dichloroethene - cis-DCE). For the preparation of the experiments, trench-sampled water was purged with N_2 gas for 8 hours to eliminate all volatile organic compounds present at the field site. After purging, a known concentration of the target compounds (either CMs or CEs), with a known initial isotopic composition, was added.

Additionally, control vials prepared in the same conditions as the experimental ones but without PS were analyzed to account for the extent of AH in experiments i, ii and iv.

Batch experiments were prepared filling 40 mL EPA VOA glass vials with a mixture of PS or PSOX and TCM or CMs or CEs stock solutions to reach pre-established concentrations. The vials were filled without headspace to avoid partitioning of TCM/CMs/CEs between the aqueous and gas phases and were closed with PTFE-lined caps. The experiments were conducted at 23°C in the dark in a thermostatic chamber.

The oxidation reaction was stopped after different reaction times by replacing 7.5 mL of the experimental solution with a 1.5 M ascorbic acid (AA) solution, resulting in a molar ratio of AA:PS equal to 4:1, inducing a rapid dissociation of the PS [36]. At this molar ratio, any radical reacts rapidly with the AA, inhibiting further TCM degradation [36,37]. In experiment iv, the solution was previously filtered using a 0.45 µm nylon filter to separate the solid phase from the liquid samples, before the quenching procedure with AA. The 7.5 mL aliquots extracted from the experimental vials were used to measure the pH of the experiment with a pH probe (WTW pH SenTix pH 940 electrode). Duplicate samples were always collected for each reaction time and stored at 4°C in darkness until analysis.

2.2. Analytical methods

A detailed description of the analytical methods and equipment used for concentration and isotope ratio measurements is available in Appendix B. Briefly, CEs and CMs concentrations were measured by headspace gas chromatography-mass spectrometry (HS-GC-MS) as explained elsewhere [28]. Carbon isotope analysis was performed using a GC coupled to an Isotope Ratio Mass Spectrometer (GC-IRMS) at the Technological Centers of the University of Barcelona (CCiT-UB). Chlorine isotope analysis of CT, TCM, DCM, PCE and TCE was performed by GC-qMS at the CCiT-UB using the methodology described by [38], while cis-DCE was analyzed using a GC-IRMS at Isotope Tracer Technologies Inc. (Waterloo, Canada) as described in [39]. All samples were analyzed in duplicate and corrected for slight isotopic fractionation induced by the preconcentration technique (solid-phase micro extraction – SPME) relative to daily aqueous isotopic standards of the target compounds with known isotopic composition. These aqueous isotopic standards were prepared as the samples and measured in the same sequence. Precision (1σ) of the analysis was ≤ 0.5 ‰ for $\delta^{13}C$ on all compounds and ≤ 0.2 ‰ for $\delta^{37}Cl$ of cis-DCE, and ≤ 0.5 ‰ for $\delta^{37}Cl$ of PCE, TCE and the CMs. The presence of volatile byproducts generated in the degradation process was determined using the HS-GC-qMS system in the CCiT-UB, using the previously described configuration but in full scan mode.

2.3. Isotope data evaluation

The carbon and chlorine isotopic compositions are reported in delta notation (δ^hE, in ‰, Eq. 1), relative to the international standards VPDB (Vienna Pee Dee Belemnite) and SMOC (Standard Mean Ocean Chlorine) [40,41], respectively. The isotopic ratio of a sample and the standard of an element (E) (e.g., $^{13}C/^{12}C$, $^{37}Cl/^{35}Cl$) is denoted as R_{sample} and R_{std}, respectively:

$$\delta^h E = \left(\frac{R_{sample}}{R_{std}} - 1\right) \quad (1)$$

A simplified version of the Rayleigh equation in logarithmic form (Eq. 2) can be used to correlate changes in the isotopic composition of an element in a compound (R_t / R_0) with changes in its concentration for a given reaction ($f = C_t / C_0$), by using the corresponding isotopic fractionation (ε) [24,42]:

$$\ln\left(\frac{R_t}{R_0}\right) = \varepsilon \cdot \ln(f) \quad (2)$$

where R_t / R_0 can be expressed as $(\delta^hE_t + 1) / (\delta^hE_0 + 1)$ according to the δ^hE definition. For degradation to be considered significant, differences in isotope values in the field for both carbon and chlorine must be > 2 ‰ [43].

Finally, $\Lambda^{C\text{-}Cl}$ values for specific reactions can be defined under controlled laboratory conditions. The slope of the ordinary linear regression (OLR) in the dual C-Cl isotope plot [24] with uncertainty reported as the 95 % confidence interval (CI) is calculated. Since recent studies by [44,45] suggested using the York regression method instead of OLR to determine Λ and its uncertainty, a comparison between both approaches is also shown.

Statistical differences with previously reported values for the estimated isotope fractionation values (εCl and εC) and dual isotope slopes ($\Lambda^{C/Cl}$) were assessed using statistical two-tailed z-score tests [44,45]. Differences were considered statistically significant at the $\alpha = 0.05$ confidence level.

3. Results and discussion

3.1. Experiment i: effect of TCM:PS molar ratio

The commercial product PSOX used in experiment i kept the pH at 10.2 ± 0.2, independently of the used TCM:PS molar ratio. At this pH, the primary radicals driving the oxidation are expected to be $SO_4^{\cdot-}$ and $OH^{\cdot}$ [12,13]. Degradation of TCM was observed over time, reaching 98 % after 30 days at the molar ratio of 1:65 (experiment i.a, Table 1) and after 13 days at the molar ratio of 1:125 (i.b). In the control vials, the concentration of TCM remained unchanged for up to 35 days (see

Figure C.1 in Appendix C), discarding TCM degradation by AH and ruling out potential TCM losses due to other processes such as volatilization through the caps. Therefore, TCM degradation was attributed solely to chemical oxidation, which followed pseudo-first-order kinetics, as evidenced by the good linear correlation between $\ln(C/C_0)$ and time (Figure C.1). The results show that the rate of TCM degradation increases with higher relative PS concentrations, with pseudo-first-order rate constant (k'obs) values of 0.151 and 0.232 d^{-1} (Table 2), corresponding to half-lives of 4.6 and 3.0 days for TCM:PS molar ratios of 1:65 and 1:125, respectively.

Despite these differences in TCM:PS molar ratios and degradation rates, experiments i.a and i.b exhibited comparable enrichment in ^{13}C and ^{37}Cl, while isotopic changes in the controls were not statistically significant ($p > 0.05$) (Figures C.2 and C.3). The calculated εC values were -12 ± 1 and -11 ± 1 ‰, while for chlorine the obtained εCl values were much lower, -0.30 ± 0.05 and -0.4 ± 0.2 ‰, for experiments i.a and i.b, respectively (see Table 2 for all calculated εC, εCl and $\Lambda^{C\text{-}Cl}$ values). Since no systematic bias introduced by OLR was observed compared to York method [44,45], we used OLR values, but present York results in the SI (Appendix D). The determined $\Lambda^{C\text{-}Cl}$ values did not show a significant difference either ($p > 0.05$), being 33 ± 6 and 23 ± 10 for experiments i.a and i.b, respectively. Due to the notably higher carbon isotope fractionation compared to chlorine, both $\Lambda^{C\text{-}Cl}$ values exceeded any previously reported in the literature for TCM, showing that TCM oxidation by alkaline-activated PS at this pH (10.2) can be distinguishable from other degradation processes using 2D isotopic tools.

3.2. Experiment ii: effect of pH increase

Experiments ii.a and ii.b were conducted at pH 11.4 and 12.8, respectively, where both $SO_4^{\cdot-}$ and $OH^{\cdot}$ radicals were supposed to be present [46]. An important reduction in TCM concentration was observed over time, reaching degradation percentages of 92 % after 20 days in experiment ii.a and 98 % after 67 days in experiment ii.b. Interestingly, control experiments without PS also exhibited noticeable TCM degradation within the same time period, attributed to AH. In control ii.a (pH=11.4), a 10 % reduction in TCM was observed over 20 days, while in control ii.b (pH=12.8), TCM concentration decreased by 50 % after 30 days, reaching 87 % degradation after 78 days (Figure C.1). TCM degradation, under stronger alkaline conditions than experiment i, followed pseudo-first order kinetics in both the experimental and control vials (Table 2 and Figure C.1). The observed k'obs values were 0.12 ± 0.02 and 0.053 ± 0.009 d^{-1} for experiments ii.a and ii.b, and 0.006 ± 0.003 and 0.026 ± 0.001 d^{-1} for the corresponding controls (Table 2). These results indicated that the rate of TCM degradation decreases with increasing pH. This is likely due to the predominance of AH, which has significantly slower kinetics compared to oxidation. This hypothesis is further discussed below using the isotope data.

Isotopic analysis of experiments ii.a and ii.b revealed different εC values of -10.1 ± 0.7 and -25 ± 12 ‰, and also distinct εCl values of -0.40 ± 0.1 and -2.7 ± 0.3 ‰, respectively (Table 2), leading to $\Lambda^{C\text{-}Cl}$ values of 23 ± 7 and 9 ± 2, respectively. In contrast, control ii.b showed much higher carbon and chlorine isotopic fractionation values of εC = -59 ± 16 ‰ and εCl = -5 ± 2 ‰, with a $\Lambda^{C\text{-}Cl}$ value of 11 ± 1. The latter values are consistent with those reported for TCM degradation via AH [23,28]. Carbon and chlorine isotopic fractionation values could not be estimated for control ii.a because the limited data points (n = 3) and extent of degradation (10 %) resulted in a statistically not significant regression ($p > 0.05$) (Figures C.2 and C.3). The isotopic findings align with the observed trends in reaction kinetics: the isotopic results for experiment ii.a (pH 11.4) are similar to those observed at pH 10.2 (experiments i.a and i.b) (Table 2), pointing to oxidation as the predominant degradation mechanism. Conversely, the isotopic data from experiment ii.b (pH 12.8) indicated a substantial contribution of AH in TCM degradation, as evidenced by εC and εCl values that fall within the range typically associated with AH. This result could thus explain the lower degradation rates observed in the vials at higher pH.

3.3. Experiment iii: impact of CO_3^{2-} on the radical cascade

In experiment iii, where CO_3^{2-} anion was introduced to the alkaline-activated PS system, the scavenging of $SO_4^{\cdot-}$ and $OH^{\cdot}$ radicals and the resulting generation of $CO_3^{\cdot-}$ radical anion was hypothesized based on previous studies [7,14]. TCM degradation reached 96 % after 20 days at pH 11.3 (iii.a) and 97 % after 67 days at pH 12.8 (iii.b). Estimated k'obs values were 0.16 ± 0.02 d^{-1} for experiment iii.a and 0.05 ± 0.01 d^{-1} for experiment iii.b (Figure C.1 and Table 2). At pH 11.3, the presence of CO_3^{2-} anion slightly enhanced TCM degradation kinetics ($t_{1/2} = 4.5$ days) compared to experiment ii.a ($t_{1/2} = 5.8$ days). However, the kinetics of experiments ii.b and iii.b were almost identical ($t_{1/2} = 13.1$ and 13.3 days, respectively), indicating that at pH 12.8, the degradation was mainly driven by AH, regardless of the presence of CO_3^{2-} anion.

Experiments iii.a and iii.b showed significant differences in isotopic fractionation (Figures C.2 and C.3), with εC values of -7.0 ± 0.6 ‰ and -26 ± 11 ‰, and εCl values of -0.5 ± 0.2 ‰ and -3.7 ± 0.3 ‰, respectively (Table 2). While the obtained $\Lambda^{C\text{-}Cl}$ values of 11 ± 5 and 10 ± 4 for these experiments could initially indicate an AH mechanism for both experiments, the differences observed in kinetics and isotopic fractionation values of C and Cl suggest that the presence of CO_3^{2-} anion might alter the TCM degradation mechanism at moderate alkaline pH (iii.a). The low εCl is similar to that observed in previous oxidative degradations (exp. i.a, i.b, iia), but the εC value is significantly lower. This difference may be related to the presence of different oxidative radicals, possibly $CO_3^{\cdot-}$. However, the contribution of superoxide anion radical ($O_2^{\cdot-}$) to TCM degradation cannot be discarded [47,48]. Considering this, the $\Lambda^{C\text{-}Cl}$ value observed in experiment iii.a might reflect

Table 2
Results of TCM degradation kinetics (k'obs and $t_{1/2}$), isotopic fractionation (εC and εCl) and dual C-Cl slope ($\Lambda^{C\text{-}Cl}$) for each experiment (Exp) and their corresponding controls without PS (below). Isotopic fractionation and dual isotope slope values are stated together with their ± 95 % confidence intervals. N = number of points; n.s. = not statistically significant ($p > 0.05$).

	Exp	pH	k'obs (d^{-1})	R^2	$t_{1/2}$ (d)	εC (‰)	εCl (‰)	$\Lambda^{C\text{-}Cl}$	N
Experimental	i.a	10.2 ± 0.2	0.15	0.939	4.6	−12 ± 1	−0.30 ± 0.05	33 ± 6	11
	i.b	10.2 ± 0.2	0.23	0.819	3.0	−11 ± 1	−0.4 ± 0.2	23 ± 10	10
	ii.a	11.4 ± 0.4	0.12	0.914	5.8	−10.1 ± 0.7	−0.4 ± 0.1	23 ± 7	7
	ii.b	12.8 ± 0.1	0.05	0.901	13.1	−25 ± 12	−2.7 ± 0.3	9 ± 2	6
	iii.a	11.3 ± 0.4	0.16	0.933	4.5	−7.0 ± 0.6	−0.5 ± 0.2	11 ± 5	7
	iii.b	12.8 ± 0.1	0.052	0.956	13.3	−26 ± 11	−3.7 ± 0.3	10 ± 4	5
	iv.a	10.6 ± 0.6	0.28	0.927	2.5	−3 ± 2	−0.6 ± 0.4	5.5 ± 0.6	4
Control	i.a	10.2 ± 0.2	0.001	0.008	802	n.s.	n.s.	n.s.	10
	i.b	10.2 ± 0.3	0.001	0.004	481	n.s.	n.s.	n.s.	10
	ii.a	11.4 ± 0.1	0.006	0.828	120	n.s.	n.s.	5 ± 3	3
	ii.b	12.8 ± 0.1	0.026	0.997	26.2	−59 ± 16	−5 ± 2	11 ± 1	4
	iv.a	11.6 ± 0.7	0.010	0.921	72.4	n.s.	n.s.	16 ± 15	4

mixed oxidative (as seen in experiment i.a, i.b and ii.a) and reductive degradation mechanisms. This hypothesis is further discussed in Section 3.6.

3.4. Experiment iv: mimicking alkaline trench conditions

In the PS experiments conducted under alkaline trench conditions (pH 10.6), containing trench-sampled solids and alkaline water, TCM degradation reached 99.9 % after 27 days (Figure C.1). In contrast, control vials without PS (pH 11.6) exhibited slower degradation kinetics, consuming only 27 % of TCM within the same time period. The estimated k'obs for the vials with PS was 0.28 ± 0.05 d^{-1}, with a half-life of 2.5 days, while the control vials showed values of 0.010 ± 0.002 d^{-1} and a half-life of 72.4 days (Table 2, Figure C.1). Notably, TCM degradation in the presence of PS under alkaline trench conditions exhibited the fastest kinetics among all the experiments performed.

Experimental vials exhibited significant shifts to higher $\delta^{13}C$ and $\delta^{37}Cl$ values of TCM, resulting in isotopic fractionation values of $\varepsilon C = -3 \pm 2$ ‰ (Figure C.2) and $\varepsilon Cl = -0.6 \pm 0.4$ ‰ (Figure C.3), and a dual-element slope of 5.5 ± 0.6. In contrast, the control experiments yielded very different isotopic values; although εC and εCl could not be estimated because the linear regressions were not statistically significant ($p > 0.05$), a reliable $\Lambda^{C\text{-}Cl}$ value of 16 ± 6 was obtained.

These results indicate that in such a complex system, other processes may be influencing the removal of TCM in the control vials. One potential process is adsorption of organic compounds onto the solid phase, which may result in a reduction of the concentration of TCM without significantly changing its isotopic composition (see more details in Appendix E). In our study, the relatively high $\Lambda^{C\text{-}Cl}$ value obtained in the control experiments and the observed pH of 11.6 ± 0.7 are consistent with AH being the dominant process as already observed previously in similar conditions [28]. In addition, the AH process could be enhanced due to the equilibrium between the solid phase (containing concrete minerals such as portlandite, $Ca(OH)_2$) and the solution.

The experimental vials of experiment iv.a exhibited the lowest $\Lambda^{C\text{-}Cl}$ value (5.5 ± 0.6) among all the experiments, suggesting a minimal contribution of the AH mechanism, in agreement with the relatively moderate alkaline pH of 10.6. Similar $\Lambda^{C\text{-}Cl}$ values of 5.8 ± 0.4, 8 ± 2 and 6.7 ± 0.4 have been reported for abiotic reductive degradation of TCM by Fe(0) at neutral and alkaline pH [28,30] and by $CO_2^{\cdot-}$ radicals (via OS-SET), generated by thermal activation of PS and reaction with formate [35]. Although the initial CO_3^{2-} concentration in this experiment (95 mg/L) was similar to that in experiment iii.a (110 mg/L) (Table 2), the equilibrium with the solid phase in experiment iv.a resulted in a much higher final CO_3^{2-} concentration of approximately 300 mg/L. This suggests that there was sufficient CO_3^{2-} to scavenge hydroxide and sulphate radicals. In this scenario, superoxide radicals ($O_2^{\cdot-}$) might have contributed to TCM degradation, as ionic strength has been shown to enhance $O_2^{\cdot-}$ reactivity [8]. $O_2^{\cdot-}$ is known to act as both reducing and oxidizing agent [49]. In this case, given the low $\Lambda^{C\text{-}Cl}$ value determined for TCM in this experiment, $O_2^{\cdot-}$ radicals could drive TCM degradation primarily through a reductive mechanism. This suggest that the presence of PS and an excess of CO_3^{2-} could transform TCM degradation into an In Situ Chemical Reduction (ISCR) process rather than an ISCO. However, further evidence supporting this hypothesis is necessary.

Further insights into the potential reductive degradation of TCM were explored by comparing the results obtained for TCM with those for other CMs and CEs in experiments iv.a and iv.b, respectively (detailed in Appendix E). For CEs, PCE displayed low chlorine isotope fractionation ($\varepsilon Cl = -0.4 \pm 0.2$) and a $\Lambda^{C\text{-}Cl}$ value of 5 ± 3 (Table E.1). This value is similar to the $\Lambda^{C\text{-}Cl}$ range of 4.6–7 reported for abiotically mediated RD by corrinoids [50], but diverge from those obtained for reduction of PCE, TCE and cis-DCE via OS-SET in experiments with $CO_2^{\cdot-}$ radical anion, which are reported to approach infinity because of the negligible chlorine isotopic fractionation [35]. In line with these discrepancies, TCE and cis-DCE in our experiments showed $\Lambda^{C\text{-}Cl}$ values of 6 ± 4 and 2 ± 1, respectively, contrasting with the trends for OS-SET.

The $\Lambda^{C\text{-}Cl}$ values for TCE (6 ± 4) and cis-DCE (2 ± 1) are relatively similar to the values reported for Fe(0)-induced (5.2 ± 0.3 for TCE and 3.1 ± 0.2 for cis-DCE, [51]) and corrinoids-induced (3.7–4.5 for TCE, [50]) reductive degradation. On the other hand, the isotopic fractionation results would also be consistent with those for CEs degradation with oxidation reactants. First, obtained εC value for TCE (-3.3 ± 0.4 ‰, Table E.1) is close to those reported for degradation with Fe(0)-activated PS at acid pH, both with (-3.4 to −4.3 ‰, [52]) and without (-3.9 to −4.7 ‰, [53]) carbonates, driven by $SO_4^{\cdot-}$ radical. Unfortunately, chlorine isotope data are not available for comparison. Second, the εC value for TCE is similar to that reported for Fenton-like degradation of TCE (-2.9 ± 0.3 ‰), where it was assumed that $OH^{\cdot}$ radical predominated and secondary chlorine isotopic fractionation resulted in a $\Lambda^{C\text{-}Cl}$ value of 3.1 ± 0.2 [54].

Overall, these results suggest that reductive processes could play a role in CEs degradation in the alkaline-activated PS system in presence of carbonates, and the observable chlorine isotopic fractionation tends to dismiss a stepwise OS-SET mechanism for CEs, in contrast to the observations with $CO_2^{\cdot-}$ radicals [35].

For the other CMs, for which limited isotopic data are available in the literature compared to TCM, CT exhibited a $\Lambda^{C\text{-}Cl}$ value of 2.2 ± 0.4 in experiment iv.a (Table E.1), closer to the value reported for magnetite ($Fe^{2+}Fe_2^{3+}O_4$)-mediated reductive reactions than to the one for Fe(0)-induced reaction (2 ± 1 and 5.8 ± 0.4, respectively) at pH 12 [29]. A potential reductive degradation of CT via reaction with $O_2^{\cdot-}$ could also be possible in our experiments. The reductive degradation of CT by $O_2^{\cdot-}$ radical anion was reported in previous studies [47,48], however, isotope data is still not available for this reaction. DCM, on the other hand, showed no statistically significant chlorine fractionation (with or without PS) and no $\Lambda^{C\text{-}Cl}$ values could thus be obtained (see Annex E).

3.5. Precipitate formation and chlorinated byproducts in experiments ii and iii

During experiments ii.a and iii.a (at pH 11.4 and 11.3, respectively), the formation of precipitate aggregates was observed in the vials containing PS (see figure F.1), but not in the control vials (Table F.1). HS-GC-qMS analysis identified and quantified higher chlorinated hydrocarbons alongside the degradation of TCM in the ii.a and iii.a experimental vials, while such byproducts were not detected in the control vials. This suggests that their formation is linked to the radical cascade in the oxidation process. Unexpectedly, the degradation of TCM in these conditions led thus to the accumulation of higher chlorinated compounds than the original contaminant, with hexachloroethane (HCA) emerging as the primary byproduct, and CT also detected. These compounds have been previously reported in photocatalytic degradation reactors of TCM and TCE [55,56], but, to the best of our knowledge, have never been associated with alkaline activated PS treatments.

The accumulation of HCA suggests that $OH^{\cdot}$ radicals, rather than $SO_4^{\cdot-}$ radicals, likely drove TCM degradation in experiments ii.a and iii.a, as prior findings have shown that $SO_4^{\cdot-}$ initiate HCA degradation [57], whereas HCA shows low reactivity with $OH^{\cdot}$ [48]. The formation of HCA might be explained by a HAA mechanism, where TCM reacts with $OH^{\cdot}$, similar to the mechanism proposed for 1,1,1-trichloroethane [58,59]. As a result, the C-H bond cleavage would produce trichloromethyl radicals ($CCl_3^{\cdot}$), which would subsequently dimerize to form HCA via radical coupling [60,61]. The formation of HCA occurs thus after the first reaction step of TCM degradation and, therefore, it does not influence the determined isotopic fractionation values of TCM. In experiment iv.a, although precipitates could not be observed because of the presence of the solid materials, HCA was also detected (Table F.1).

Due to the low solubility of HCA (50 mg/L) [62], it is likely that the observed precipitates corresponded to HCA. Direct quantification of precipitated HCA was challenging due to its volatility, which made

filtration, drying, and weighing unreliable. Therefore, an indirect calculation of the solid HCA formed during the experiments was performed using a chlorine mass balance equation (Eq. 3).

$$Cl_{TOT} = Cl^-_{aq} + Cl_{TCM} + Cl_{CT} + Cl_{HCA(aq)} + Cl_{HCA(s)} \quad (3)$$

Since the experiments were conducted in deionized water, the only initial source of chlorine was TCM (690 mg/L). Therefore, the total chlorine content in each experimental vial comprises the chloride anion present in the aqueous phase (Cl^-_{aq}, measured by HPLC), chlorine atoms in the dissolved organic chlorinated compounds (Cl_{TCM}, Cl_{CT} and $Cl_{HCA(aq)}$), and chlorine precipitated as solid HCA ($Cl_{HCA(s)}$). Results for estimated $Cl_{HCA(s)}$ are detailed in Table F.2. After near-complete transformation of TCM in experiments ii.a and iii.a, approximately 55–65 % of the initial chlorine from TCM was converted into HCA, predominantly recovered as precipitate (Fig. 1).

3.6. Insights into TCM degradation from 2D-CSIA

Isotope data revealed that while changes in TCM:PS molar ratio influence degradation kinetics they do not affect the degradation mechanism itself. Additionally, strong alkaline conditions (pH > 12) lead to the predominance of TCM degradation by AH over the reaction with PS-derived radical species, resulting in slower degradation kinetics. Consequently, isotope data from experiments for which differences between their dual element isotope trends were not significant ($p > 0.05$) were merged to derive combined $\Lambda^{C\text{-}Cl}$ values (i.e., experiments i.a + i.b + ii.a and experiments ii.b + iii.b). Obtained results are summarized in Fig. 2, where three distinct isotopic trends can be observed: (i) $\Lambda^{C\text{-}Cl}$ of 29 ± 4 during TCM oxidation by alkaline-activated PS (experiments i.a + i.b + ii.a). Compared to the slope from thermally activated PS (17 ± 2) [28], where $SO_4^{\cdot-}$ radicals are formed, the different slope obtained in this study suggest the involvement of $OH^{\cdot}$ radicals; (ii) $\Lambda^{C\text{-}Cl}$ between 11 ± 1 (Ctrl ii.b) and 9 ± 1 (experiments ii.b and iii.b), accompanied by significantly higher carbon and chlorine isotopic fractionation values for AH, where degradation predominantly follows the $E1_{CB}$ mechanism; and (iii) $\Lambda^{C\text{-}Cl}$ of 5.5 ± 0.6 during TCM degradation by alkaline-activated PS in experiments reproducing alkaline trench field conditions with the presence of excess of CO_3^{2-} (iv.a), which exhibited the fastest kinetics. The CO_3^{2-} anion can scavenge $SO_4^{\cdot-}$ and $OH^{\cdot}$ radical species and it could give rise to the contribution of other radical species, such as $O_2^{\cdot-}$, on TCM transformation. The reaction of TCM with $O_2^{\cdot-}$ could proceed via a reductive mechanism [47,48], however, the obtained slope differs from that reported for an OS-SET mechanism [35].

The observed C-Cl slope of experiment iii.a likely reflects a mixture of parallel or competing processes, suggesting the co-existence of oxidative-reductive reactions: oxidation (mainly via reaction with $OH^{\cdot}$) and a probable reductive reaction (driven by $O_2^{\cdot-}$), as suggested in experiment iv.a. An estimation of the contribution of each process to TCM degradation is shown in Appendix G, in the SI.

However, the range of $\Lambda^{C\text{-}Cl}$ values observed in our experiments also suggests that distinguishing between the action of alkaline-activated PS and TCM reductive biodegradation in the field may not always be possible based solely on isotopic C-Cl data. The range of $\Lambda^{C\text{-}Cl}$ values for RD of TCM (2.8 ± 0.3–7 ± 1, [33,31,32,34]) overlaps with the slope obtained in the presence of an excess of carbonates (exp. iv.a). In such cases, a more comprehensive analysis, including detailed hydrogeochemical and biological molecular tools, may be required to fully characterize the degradation mechanisms.

4. Conclusions

The degradation of TCM by alkaline-activated PS was studied in batch experiments to determine whether different factors such as TCM: PS molar ratio, pH and the presence of radical scavengers may affect the assessment of the degradation process by 2D-CSIA in ISCO treatments. In addition, experiments were performed reproducing alkaline trench field conditions to identify the factors driving the contaminant degradation processes in a complex field application scenario.

The distinct $\Lambda^{C\text{-}Cl}$ values obtained in this study provide compelling evidence of the potential of 2D-CSIA to differentiate between AH and other TCM degradation mechanisms, probably involving different ROS (e.g., $OH^{\cdot}$, $SO_4^{\cdot-}$, $O_2^{\cdot-}$ and $CO_3^{\cdot-}$), during alkaline-activated PS treatment in TCM-contaminated sites. These findings establish a solid foundation for understanding the multiple processes, that may occur simultaneously, during ISCO with alkaline-activated PS in contamination plumes. Further research using advanced techniques such as electron paramagnetic resonance (EPR) spectroscopy is needed to fully elucidate the specific radical species driving TCM degradation under the different conditions investigated.

The different carbon isotope fractionation values obtained in the experiments performed in this study underscore the need for caution when applying CSIA for the quantification of TCM degradation in the field. Relying on εC values obtained from simplified, deionized water experiments, common in literature, could lead to a significant underestimation of degradation extent when assessing TCM transformation with PS.

To the best of the authors' knowledge, this is the first study to document the formation of highly chlorinated byproducts such as HCA and CT during the chemical oxidation of TCM by PS. The formation of these byproducts raises important environmental concerns, as both HCA and CT are toxic and persistent in the environment. Several factors need to be considered when translating these findings to field applications: (i) our experiments were conducted in a closed system, leading to elevated byproducts concentrations that may be mitigated by dilution in natural

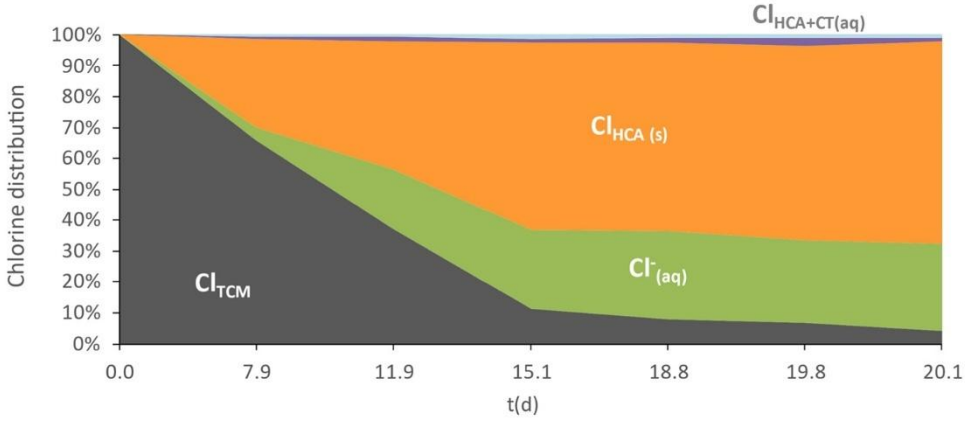

Fig. 1. Chlorine mass balance of experiment iii.a, showing quantified aqueous chloride and chlorine in dissolved TCM, CT and HCA, alongside the calculated chlorine precipitated as solid HCA.

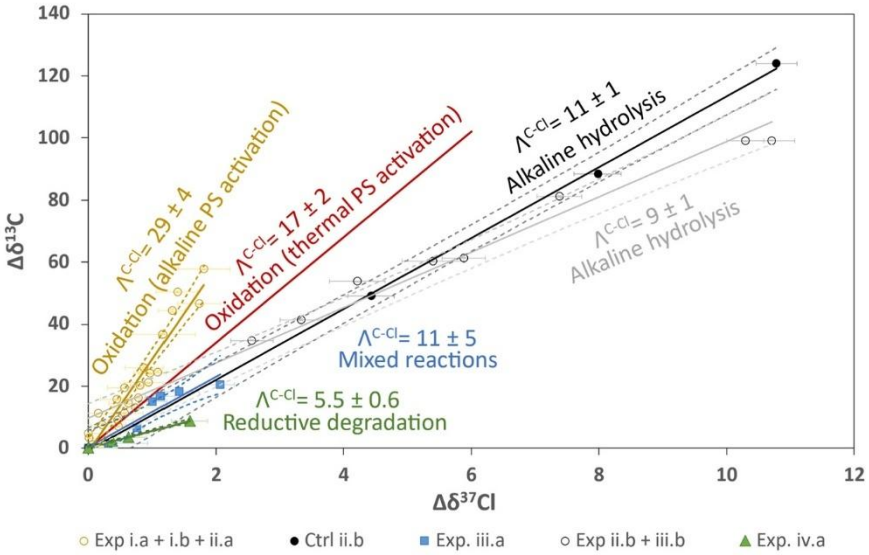

Fig. 2. Dual C-Cl isotope plot displaying results from different experiments with alkaline-activated PS (Exp) and control experiments without it (Ctrl), as well as the proposed TCM degradation mechanisms. Trends for thermally activated PS (in red) and alkaline hydrolysis ($\Lambda^{C\text{-}Cl}$ of 13.0 ± 0.8 at pH ~ 12, not shown) from [28] are shown for comparison. Data from some experiments was combined due to similarity ($p > 0.05$) (i.e., i.a + i.b + ii.a and ii.b + ii.b), yielding characteristic $\Lambda^{C\text{-}Cl}$ values. Dashed lines indicate the 95 % CI of the linear regression.

settings; (ii) the initial TCM concentration was 690 mg/L, which represents conditions near free-phase (DNAPL) zones or source areas of pollution, where PS treatments are often applied. Along the contamination plume, where the concentration of the contaminant is lower, expected generation of HCA would be reduced; (iii) processes such as volatilization and adsorption could reduce HCA concentrations in the field. Despite these considerations, the detection of HCA and CT in this study highlights the need for further investigation into the potential unintended consequences of PS-based ISCO techniques in TCM-contaminated sites. The results of this study might have thus important implications for the selection and evaluation of remediation strategies by decision-makers.

Environmental implications

TCM is one of the most prevalent contaminants in groundwater. ISCO using alkaline activated PS has gained increasing attention as a remediation method. This study demonstrates the potential of 2D-CSIA to differentiate between AH and other TCM degradation mechanisms, during alkaline-activated PS treatment in TCM-contaminated sites. Additionally, for the first time, hexachloroethane was observed as a byproduct of chloroform oxidation. These findings have important implications for the selection and evaluation of remediation strategies by decision-makers.

CRediT authorship contribution statement

Gil-Villalba Sergio: Writing – original draft, Visualization, Methodology, Investigation, Formal analysis, Data curation, Conceptualization. **Rosell Mònica:** Writing – review & editing, Visualization, Validation, Supervision, Methodology, Investigation, Formal analysis, Conceptualization. **Vinyes-Nadal Martí:** Writing – review & editing, Methodology, Investigation, Data curation, Conceptualization. **Torrentó Clara:** Writing – review & editing, Methodology, Investigation, Formal analysis, Conceptualization. **Palau Jordi:** Writing – review & editing, Validation, Supervision, Investigation, Conceptualization. **Soler Albert:** Validation, Supervision, Project administration, Methodology, Funding acquisition, Conceptualization.

Declaration of Competing Interest

The authors declare that they have no known competing financial interests or personal relationships that could have appeared to influence the work reported in this paper.

Acknowledgements

This study was financed through the following projects: PACE-ISOTEC (CGL2017–87216-C4–1-R) and REMECLOR (PDC2021–120861-C21), both funded by the Spanish Government and AEI/FEDER from the UE projects. This work was also supported by the Consolidate Research Group (2021SGR00308), funded by the AGAUR (Catalan Government). The experiments and work performed by S. Gil-Villalba were supported by the FPI2018/084979 contract. A small contribution for consumables was received from "Accions de Suport de l'Institut de Recerca de l'Aigua (IdRA) a la Recerca de Joves Investigadors" in 2021, 2022 and 2023. We thank all the technicians in MAiMA and CCiT-UB for their support. We thank two anonymous reviewers for their helpful comments that improved the quality of this manuscript.

Appendix A. Supporting information

Supplementary data associated with this article can be found in the online version at doi:10.1016/j.jhazmat.2025.137702.

Data availability

Data will be made available on request.

References

[1] ATSDR. (2023). *Substance Priority List [WWW Document]. Subst. Prior. List.* ⟨https://www.atsdr.cdc.gov/spl/index.html#2022spl⟩.
[2] Santos, A., Fernandez, J., Rodriguez, S., Dominguez, C.M., Lominchar, M.A., Lorenzo, D., Romero, A., 2018. Abatement of chlorinated compounds in groundwater contaminated by HCH wastes using ISCO with alkali activated persulfate. Sci Total Environ 615, 1070–1077. https://doi.org/10.1016/j.scitotenv.2017.09.224.
[3] Siegrist, R.L., Crimi, M., Brown, R.A., 2011. In: Siegrist, R.L., Crimi, M., Simpkin, T. J. (Eds.), In Situ Chemical Oxidation: Technology Description and Status BT - In Situ Chemical Oxidation for Groundwater Remediation. Springer New York, pp. 1–32. https://doi.org/10.1007/978-1-4419-7826-4_1.

[4] Tsitonaki, A., Petri, B., Crimi, M., Mosbk, H., Siegrist, R.L., Bjerg, P.L., 2010. In situ chemical oxidation of contaminated soil and groundwater using persulfate: a review. Crit Rev Environ Sci Technol 40 (1), 55–91. https://doi.org/10.1080/10643380802039303.
[5] Xu, J.C., Yang, L.H., Yuan, J.X., Li, S.Q., Peng, K.M., Lu, L.J., Huang, X.F., Liu, J., 2022. Coupling surfactants with ISCO for remediating of NAPLs: recent progress and application challenges. Chemosphere 303 (P1), 135004. https://doi.org/10.1016/j.chemosphere.2022.135004.
[6] Devi, P., Das, U., Dalai, A.K., 2016. In-situ chemical oxidation: principle and applications of peroxide and persulfate treatments in wastewater systems. Sci Total Environ 571, 643–657. https://doi.org/10.1016/j.scitotenv.2016.07.032.
[7] Li, W., Orozco, R., Camargos, N., Liu, H., 2017. Mechanisms on the impacts of alkalinity, pH, and chloride on persulfate-based groundwater remediation. Environ Sci Technol 51 (7), 3948–3959. https://doi.org/10.1021/acs.est.6b04849.
[8] Furman, O.S., Teel, A.L., Watts, R.J., 2010. Mechanism of base activation of persulfate. Environ Sci Technol 44 (16), 6423–6428. https://doi.org/10.1021/es1013714.
[9] Ike, I.A., Linden, K.G., Orbell, J.D., Duke, M., 2018. Critical review of the science and sustainability of persulphate advanced oxidation processes. Chem Eng J 338 (January), 651–669. https://doi.org/10.1016/j.cej.2018.01.034.
[10] Tian, K., Hu, L., Li, L., Zheng, Q., Xin, Y., Zhang, G., 2022. Recent advances in persulfate-based advanced oxidation processes for organic wastewater treatment. Chin Chem Lett 33 (10), 4461–4477. https://doi.org/10.1016/j.cclet.2021.12.042.
[11] Criquet, J., Leitner, N.K.V., 2009. Degradation of acetic acid with sulfate radical generated by persulfate ions photolysis. Chemosphere 77 (2), 194–200. https://doi.org/10.1016/j.chemosphere.2009.07.040.
[12] Furman, O.S., Teel, A.L., Ahmad, M., Merker, M.C., Watts, R.J., 2011. Effect of basicity on persulfate reactivity. J Environ Eng 137 (4), 241–247. https://doi.org/10.1061/(asce)ee.1943-7870.0000323.
[13] Liang, C., Lei, J., 2015. Identification of active radical species in alkaline persulfate oxidation. Water Environ Res 87 (7), 656–659. https://doi.org/10.2175/106143015x14338845154986.
[14] Lee, J., Von Gunten, U., Kim, J.H., 2020. Persulfate-based advanced oxidation: critical assessment of opportunities and roadblocks. Environ Sci Technol 54 (6), 3064–3081. https://doi.org/10.1021/acs.est.9b07082.
[15] Qi, C., Liu, X., Ma, J., Lin, C., Li, X., Zhang, H., 2016. Activation of peroxymonosulfate by base: Implications for the degradation of organic pollutants. Chemosphere 151, 280–288. https://doi.org/10.1016/j.chemosphere.2016.02.089.
[16] Ma, J., Yang, Y., Jiang, X., Xie, Z., Li, X., Chen, C., Chen, H., 2018. Impacts of inorganic anions and natural organic matter on thermally activated persulfate oxidation of BTEX in water. Chemosphere 190, 296–306. https://doi.org/10.1016/j.chemosphere.2017.09.148.
[17] Nie, M., Yang, Y., Zhang, Z., Yan, C., Wang, X., Li, H., Dong, W., 2014. Degradation of chloramphenicol by thermally activated persulfate in aqueous solution. Chem Eng J 246, 373–382. https://doi.org/10.1016/j.cej.2014.02.047.
[18] Buxton, G.V., Greenstock, C.L., Helman, W.P., Ross, A.B., 1988. Critical review of rate constants for reactions of hydrated electrons, hydrogen atoms and hydroxyl radicals (·OH/·O− in aqueous solution. J Phys Chem Ref Data 17 (2), 513–886. https://doi.org/10.1063/1.555805.
[19] Ji, Y., Wang, L., Jiang, M., Lu, J., Ferronato, C., Chovelon, J.M., 2017. The role of nitrite in sulfate radical-based degradation of phenolic compounds: an unexpected nitration process relevant to groundwater remediation by in-situ chemical oxidation (ISCO). Water Res 123, 249–257. https://doi.org/10.1016/j.watres.2017.06.081.
[20] Lian, L., Yao, B., Hou, S., Fang, J., Yan, S., Song, W., 2017. Kinetic study of hydroxyl and sulfate radical-mediated oxidation of pharmaceuticals in wastewater effluents. Environ Sci Technol 51 (5), 2954–2962. https://doi.org/10.1021/acs.est.6b05536.
[21] Canonica, S., Kohn, T., Mac, M., Real, F.J., Wirz, J., Von Gunten, U., 2005. Photosensitizer method to determine rate constants for the reaction of carbonate radical with organic compounds. Environ Sci Technol 39 (23), 9182–9188. https://doi.org/10.1021/es051236b.
[22] Liu, Y., Zhang, Y., Zhou, A., Li, M., 2021. Insights into carbon isotope fractionation on trichloroethene degradation in base activated persulfate process: the role of multiple reactive oxygen species. Sci Total Environ 800, 149371. https://doi.org/10.1016/j.scitotenv.2021.149371.
[23] Torrentó, C., Audí-Miró, C., Bordeleau, G., Marchesi, M., Rosell, M., Otero, N., Soler, A., 2014. The use of alkaline hydrolysis as a novel strategy for chloroform remediation: the feasibility of using construction wastes and evaluation of carbon isotopic fractionation. Environ Sci Technol 48 (3), 1869–1877. https://doi.org/10.1021/es403838t.
[24] Elsner, M., 2010. Stable isotope fractionation to investigate natural transformation mechanisms of organic contaminants: principles, prospects and limitations. J Environ Monit 12 (11), 2005–2031. https://doi.org/10.1039/c0em00277a.
[25] Lincker, M., Lagneau, V., Guillon, S., Wanner, P., 2022. Identification of chlorohydrocarbon degradation pathways in aquitards using dual element compound-specific isotope measurements in aquifers. Chemosphere 303 (P2), 135131. https://doi.org/10.1016/j.chemosphere.2022.135131.
[26] Palau, J., Jamin, P., Badin, A., Vanhecke, N., Haerens, B., Brouyère, S., Hunkeler, D., 2016. Use of dual carbon-chlorine isotope analysis to assess the degradation pathways of 1,1,1-trichloroethane in groundwater. Water Res 92, 235–243. https://doi.org/10.1016/j.watres.2016.01.057.
[27] Wiegert, C., Aeppli, C., Knowles, T., Holmstrand, H., Evershed, R., Pancost, R.D., Macháčková, J., Gustafsson, Ö., 2012. Dual carbon-chlorine stable isotope investigation of sources and fate of chlorinated ethenes in contaminated groundwater. Environ Sci Technol 46 (20), 10918–10925. https://doi.org/10.1021/es3016843.
[28] Torrentó, C., Palau, J., Rodríguez-Fernández, D., Heckel, B., Meyer, A., Domènech, C., Rosell, M., Soler, A., Elsner, M., Hunkeler, D., 2017. Carbon and chlorine isotope fractionation patterns associated with different engineered chloroform transformation reactions. Environ Sci Technol 51 (11), 6174–6184. https://doi.org/10.1021/acs.est.7b00679.
[29] Rodríguez-Fernández, D., Heckel, B., Torrentó, C., Meyer, A., Elsner, M., Hunkeler, D., Soler, A., Rosell, M., Domènech, C., 2018. Dual element (C-Cl) isotope approach to distinguish abiotic reactions of chlorinated methanes by Fe(0) and by Fe(II) on iron minerals at neutral and alkaline pH. Chemosphere 206, 447–456. https://doi.org/10.1016/j.chemosphere.2018.05.036.
[30] Asfaw, B.A., Sakaguchi-Söder, K., Schiedek, T., Michelsen, N., Bernstein, A., Siebner, H., Schüth, C., 2023. Isotopic evidence (δ13C, δ37Cl, δ2H) for distinct transformation mechanisms of chloroform: catalyzed H2-water system vs. zero-valent iron (ZVI). J Environ Chem Eng 11 (3). https://doi.org/10.1016/j.jece.2023.110005.
[31] Heckel, B., Phillips, E., Edwards, E., Sherwood Lollar, B., Elsner, M., Manefield, M. J., Lee, M., 2019. Reductive dehalogenation of trichloromethane by two different dehalobacter restrictus strains reveal opposing dual element isotope effects. Environ Sci Technol 53 (5), 2332–2343. https://doi.org/10.1021/acs.est.8b03717.
[32] Rodríguez-Fernández, D., Torrentó, C., Guivernau, M., Viñas, M., Hunkeler, D., Soler, A., Domènech, C., Rosell, M., 2018. Vitamin B12 effects on chlorinated methanes-degrading microcosms: dual isotope and metabolically active microbial populations assessment. Sci Total Environ 621, 1615–1625. https://doi.org/10.1016/j.scitotenv.2017.10.067.
[33] Heckel, B., Elsner, M., 2022. Exploring mechanisms of biotic chlorinated alkane reduction: evidence of nucleophilic substitution (SN2) with vitamin B12. Environ Sci Technol 56 (10), 6325–6336. https://doi.org/10.1021/acs.est.1c06066.
[34] Soder-Walz, J.M., Torrentó, C., Algora, C., Wasmund, K., Cortés, P., Soler, A., Vicent, T., Rosell, M., Marco-Urrea, E., 2022. Trichloromethane dechlorination by a novel Dehalobacter sp. strain 8M reveals a third contrasting C and Cl isotope fractionation pattern within this genus. Sci Total Environ 813. https://doi.org/10.1016/j.scitotenv.2021.152659.
[35] Heckel, B., Cretnik, S., Kliegman, S., Shouakar-Stash, O., McNeill, K., Elsner, M., 2017. Reductive outer-sphere single electron transfer is an exception rather than the rule in natural and engineered chlorinated ethene dehalogenation. Environ Sci Technol 51 (17), 9663–9673. https://doi.org/10.1021/acs.est.7b01447.
[36] Huling, S.G., Ko, S., Pivetz, B., 2011. Groundwater sampling at ISCO sites: binary mixtures of volatile organic compounds and persulfate. Ground Water Monit Remediat 31 (2), 72–79. https://doi.org/10.1111/j.1745-6592.2011.01332.x.
[37] Cao, M., Hou, Y., Zhang, E., Tu, S., Xiong, S., 2019. Ascorbic acid induced activation of persulfate for pentachlorophenol degradation. Chemosphere 229, 200–205. https://doi.org/10.1016/j.chemosphere.2019.04.135.
[38] Jin, B., Laskov, C., Rolle, M., Haderlein, S.B., 2011. Chlorine isotope analysis of organic contaminants using GC-qMS: method optimization and comparison of different evaluation schemes. Environ Sci Technol 45 (12), 5279–5286. https://doi.org/10.1021/es200749d.
[39] Shouakar-Stash, O., Drimmie, R.J., Zhang, M., Frape, S.K., 2006. Compound-specific chlorine isotope ratios of TCE, PCE and DCE isomers by direct injection using CF-IRMS. Appl Geochem 21 (5), 766–781. https://doi.org/10.1016/j.apgeochem.2006.02.006.
[40] Coplen, T.B., 1996. New guidelines for reporting stable hydrogen, carbon, and oxygen isotope-ratio data. Geochim Et Cosmochim Acta 60 (17), 3359–3360. https://doi.org/10.1016/0016-7037(96)00263-3.
[41] Kaufmann, R., Long, A., Bentley, H., Davis, S., 1984. Natural chlorine isotope variations. Nature 309 (5966), 338–340. https://doi.org/10.1038/309338a0.
[42] Coplen, T.B., 2011. Guidelines and recommended terms for expression of stable-isotope-ratio and gas-ratio measurement results. Rapid Commun Mass Spectrom 25 (17), 2538–2560. https://doi.org/10.1002/rcm.5129.
[43] Elsner, M., Hunkeler, D., 2008. Evaluating chlorine isotope effects from isotope ratios and mass spectra of polychlorinated molecules. Anal Chem 80 (12), 4731–4740. https://doi.org/10.1021/ac702543y.
[44] Ojeda, A.S., Phillips, E., Mancini, S.A., Lollar, B.S., 2019. Sources of uncertainty in biotransformation mechanistic interpretations and remediation studies using CSIA. Anal Chem 91 (14), 9147–9153. https://doi.org/10.1021/acs.analchem.9b01756.
[45] Ojeda, A.S., Phillips, E., Sherwood Lollar, B., 2020. Multi-element (C, H, Cl, Br) stable isotope fractionation as a tool to investigate transformation processes for halogenated hydrocarbons. Environ Sci: Process Impacts 22 (3), 567–582. https://doi.org/10.1039/C9EM00498J.
[46] Liang, C., Su, H.W., 2009. Identification of sulfate and hydroxyl radicals in thermally activated persulfate. Ind Eng Chem Res 48 (11), 5558–5562. https://doi.org/10.1021/ie9002848.
[47] Smith, B.A., Teel, A.L., Watts, R.J., 2006. Mechanism for the destruction of carbon tetrachloride and chloroform DNAPLs by modified Fenton's reagent. J Contam Hydrol 85 (3–4). https://doi.org/10.1016/j.jconhyd.2006.02.002.
[48] Teel, A.L., Watts, R.J., 2002. Degradation of carbon tetrachloride by modified Fenton's reagent. J Hazard Mater 94 (2), 179–189. https://doi.org/10.1016/S0304-3894(02)00068-7.
[49] Watts, R.J., Bottenberg, B.C., Hess, T.F., Jensen, M.D., Teel, A.L., 1999. Role of reductants in the enhanced desorption and transformation of chloroaliphatic compounds by modified Fenton's reactions. Environ Sci Technol 33 (19). https://doi.org/10.1021/es990054c.
[50] Renpenning, J., Keller, S., Cretnik, S., Shouakar-Stash, O., Elsner, M., Schubert, T., Nijenhuis, I., 2014. Combined C and Cl isotope effects indicate differences between corrinoids and enzyme (Sulfurospirillum multivorans PceA) in reductive

dehalogenation of tetrachloroethene, but not trichloroethene. Environ Sci Technol 48 (20), 11837–11845. https://doi.org/10.1021/es503306g.

[51] Audí-Miró, C., Cretnik, S., Otero, N., Palau, J., Shouakar-Stash, O., Soler, A., Elsner, M., 2013. Cl and C isotope analysis to assess the effectiveness of chlorinated ethene degradation by zero-valent iron: evidence from dual element and product isotope values. Appl Geochem 32, 175–183. https://doi.org/10.1016/j.apgeochem.2012.08.025.

[52] Liu, Y., Zhou, A., Gan, Y., Li, X., 2016. Variability in carbon isotope fractionation of trichloroethene during degradation by persulfate activated with zero-valent iron: Effects of inorganic anions. Sci Total Environ *548–549*. https://doi.org/10.1016/j.scitotenv.2016.01.011.

[53] Liu, Y., Zhou, A., Gan, Y., Li, X., 2018. Roles of hydroxyl and sulfate radicals in degradation of trichloroethene by persulfate activated with Fe2+ and zero-valent iron: Insights from carbon isotope fractionation. J Hazard Mater 344, 98–103. https://doi.org/10.1016/j.jhazmat.2017.09.048.

[54] Liu, Y., Gan, Y., Zhou, A., Liu, C., Li, X., Yu, T., 2014. Carbon and chlorine isotope fractionation during Fenton-like degradation of trichloroethene. Chemosphere 107, 94–100. https://doi.org/10.1016/j.chemosphere.2014.03.011.

[55] Cohen, L.R., Peña, L.A., Seidl, A.J., Chau, K.N., Keck, B.C., Feng, P.L., Hoggard, P. E., 2009. Photocatalytic degradation of chloroform by bis (bipyridine) dichlororuthenium(III/II). J Coord Chem 62 (11), 1743–1753. https://doi.org/10.1080/00958970802702254.

[56] Hung, C.-H., MariÑas, B.J., 1997. Role of chlorine and oxygen in the photocatalytic degradation of trichloroethylene vapor on TiO2 films. Environ Sci Technol 31 (2), 562–568. https://doi.org/10.1021/es960465i.

[57] Zhu, C., Zhu, F., Liu, C., Chen, N., Zhou, D., Fang, G., Gao, J., 2018. Reductive hexachloroethane degradation by $S_2O_8^{\bullet-}$ with thermal activation of persulfate under anaerobic conditions. Environ Sci Technol 52 (15), 8548–8557. https://doi.org/10.1021/acs.est.7b06279.

[58] Gu, X., Lu, S., Li, L., Qiu, Z., Sui, Q., Lin, K., Luo, Q., 2011. Oxidation of 1,1,1-trichloroethane stimulated by thermally activated persulfate. Ind Eng Chem Res 50 (19). https://doi.org/10.1021/ie201059x.

[59] Palau, J., Shouakar-Stash, O., Hunkeler, D., 2014. Carbon and chlorine isotope analysis to identify abiotic degradation pathways of 1,1,1-trichloroethane. Environ Sci Technol 48 (24). https://doi.org/10.1021/es504252z.

[60] Rodríguez-Chueca, J., Mediano, A., Pueyo, N., García-Suescun, I., Mosteo, R., Ormad, M.P., 2016. Degradation of chloroform by Fenton-like treatment induced by electromagnetic fields: a case of study. Chem Eng Sci 156. https://doi.org/10.1016/j.ces.2016.09.016.

[61] Tang, W.Z., Tassos, S., 1997. Oxidation kinetics and mechanisms of trihalomethanes by Fenton's reagent. Water Res 31 (5). https://doi.org/10.1016/S0043-1354(96)00348-X.

[62] Horvath, A.L., Getzen, F.W., Maczynska, Z., 1999. IUPAC-NIST solubility data series 67. Halogenated ethanes and ethenes with water. J Phys Chem Ref Data 28 (2), 395–627. https://doi.org/10.1063/1.556039.

Appendix 2. Additional information of CEs-EVO microcosm experiments

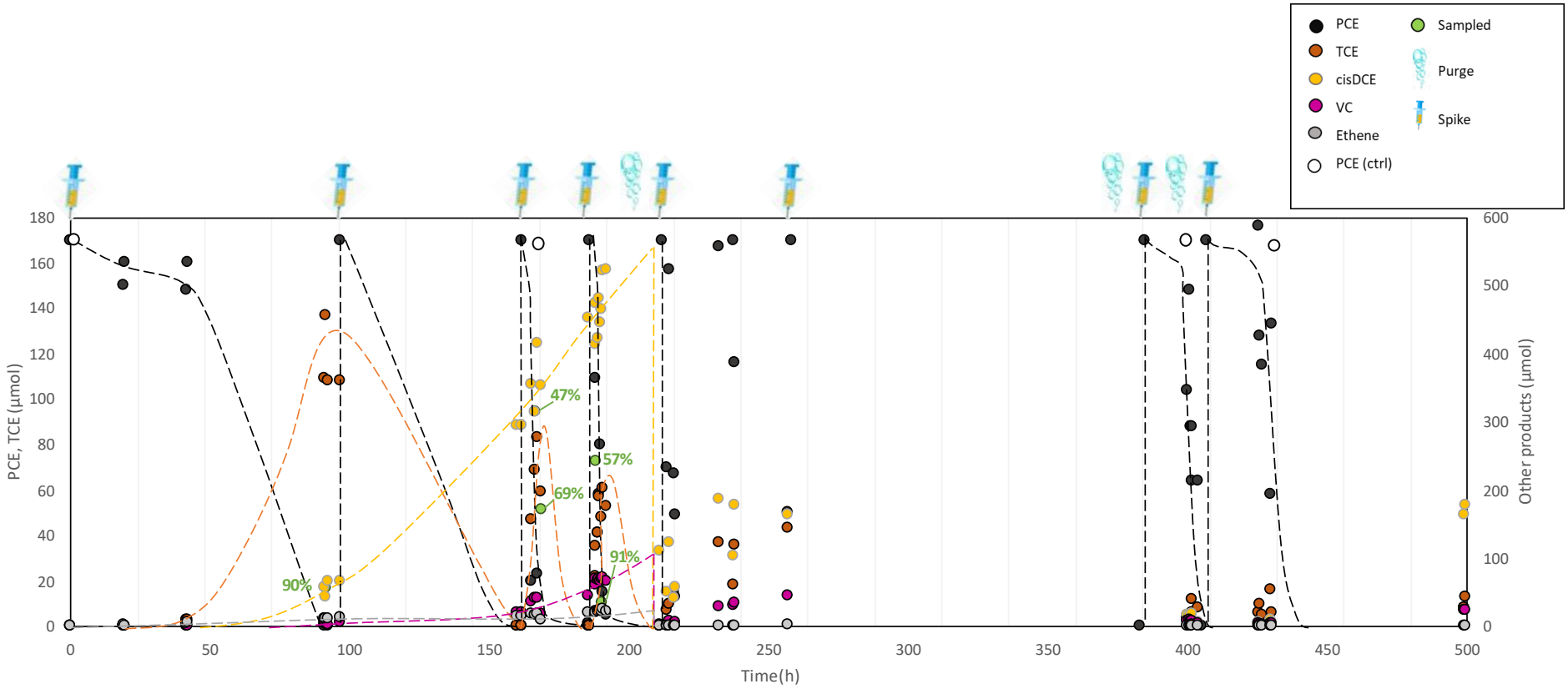

Figure A2.1. Evolution of moles of PCE and its degradation compounds in PCE microcosms. Note the rapid decay of PCE, which did not allow multiple samplings in the first spike, so re-spikes had to be done. Coloured circles correspond to single measurements of the respective CE by GC-FID. Green circles indicate the amount of PCE in samples that were stopped for the isotopic analysis. Biodegradation extent of PCE (in %) is indicated. On the top axis, re-spikes are indicated with a syringe symbol (7 in total), and purges are indicated with the bubble icon (three in total). Microcosm without lactate addition were included in this graph as experimental points. Control killed measurements added for reference.

138

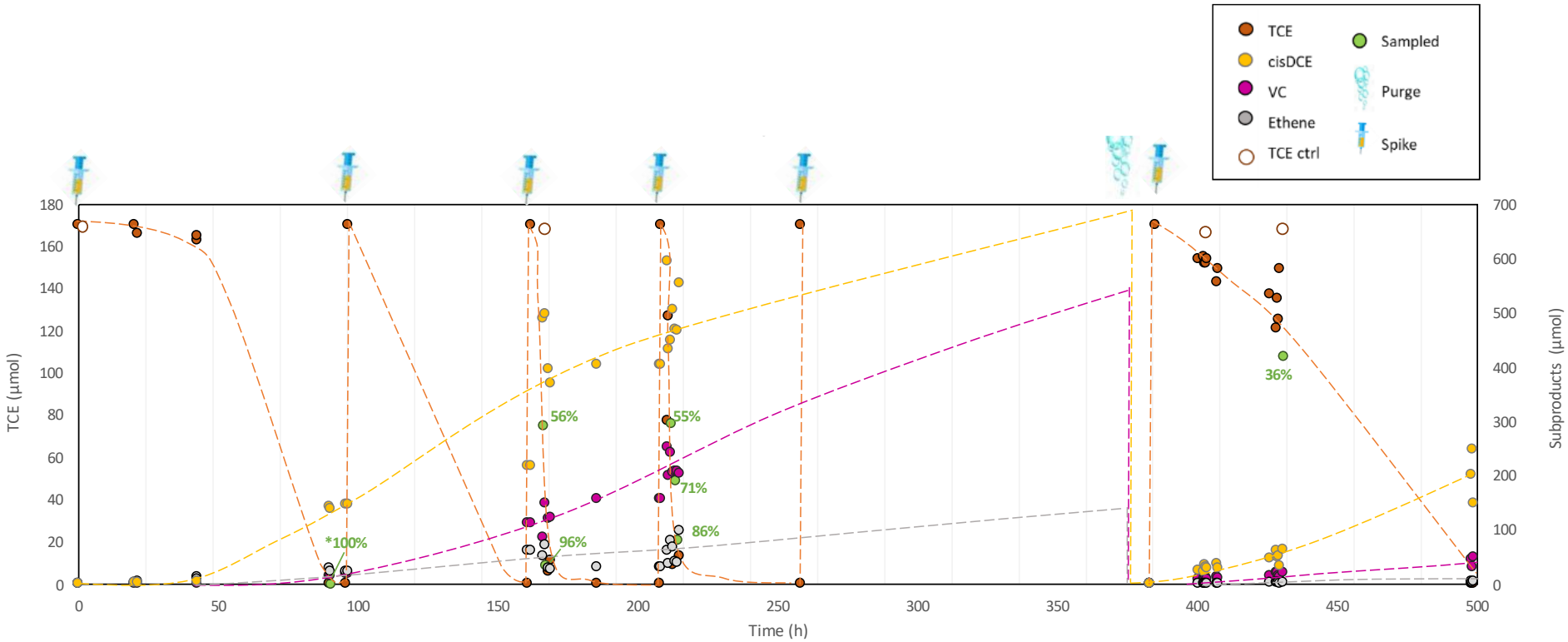

Figure A2.2. Evolution of moles of TCE and its degradation compounds in TCE microcosms. Note the rapid decay of TCE, which did not allow for sampling in the first spike, so re-spikes had to be done. Coloured circles correspond to single measurements of the respective CE by GC-FID. Green circles indicate the amounts of TCE in samples that were stopped for isotopic analysis. Biodegradation extent of TCE (in %) is indicated. On the top axis, re-spikes are indicated with a syringe symbol (5 in total), and the purges are indicated with the bubble icon (once). Microcosm without lactate addition were included in this graph as experimental points. Control killed measurements added for reference.

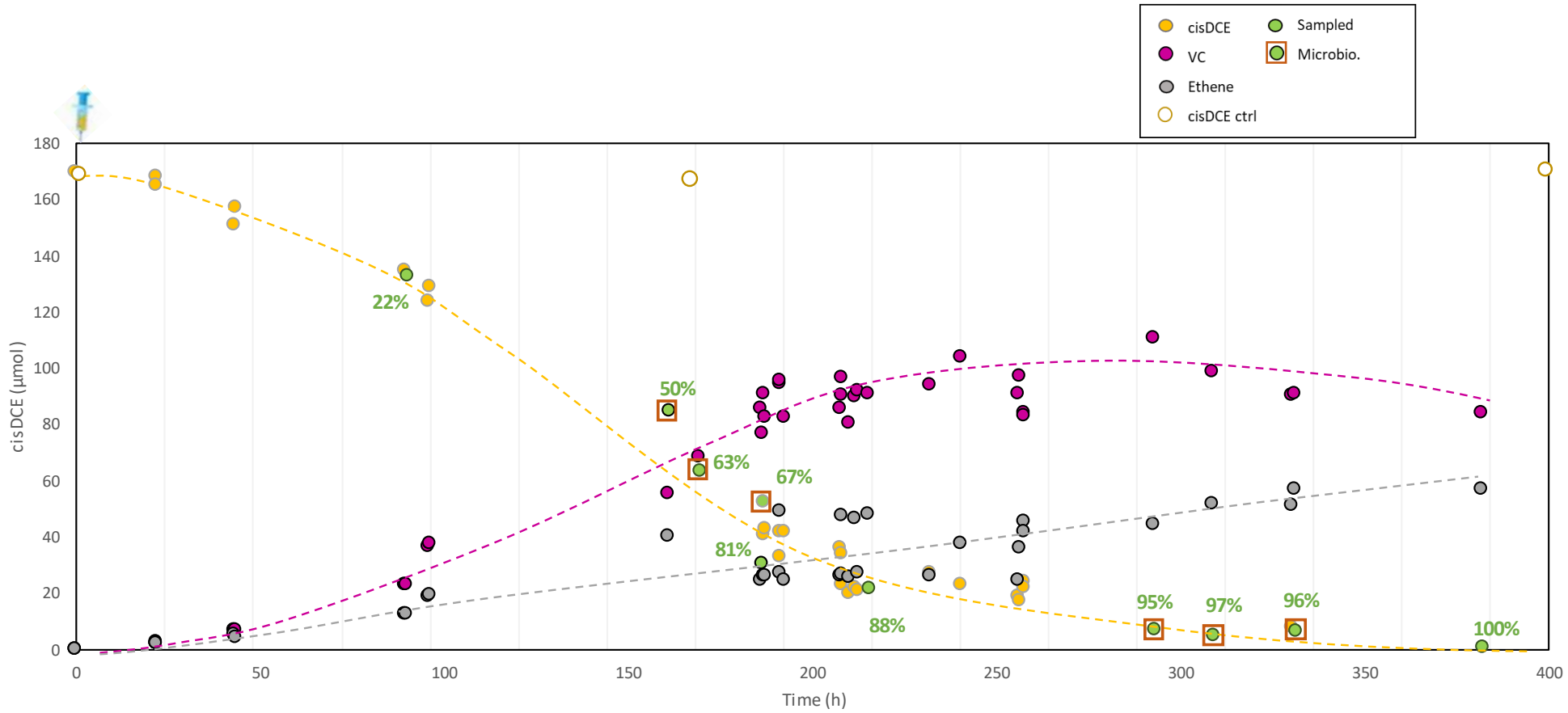

Figure A2.3. Evolution of moles of cis-DCE and its degradation compounds in cis-DCE microcosms. Coloured circles correspond to single measurements of the respective CE by GC-FID. Green circles indicate the amounts of cis-DCE in samples that were stopped for microbiologic and isotopic analysis. Squares indicate samples that were analysed for microbiology. Biodegradation extent of cis-DCE (in %) is indicated. Re-spikes and purges were not necessary for cis-DCE microcosmos due to its slower biodegradation kinetics. Microcosm without lactate addition were included in this graph as experimental points. Control killed measurements added for reference.

140

Table A2.1. Measured isotopic data in wells, including the $\delta^{13}C$ and $\delta^{37}Cl$, the measurement error and the fraction of vinyl chloride.

Sampling	Well	$\delta^{13}C$	SD	$\delta^{37}Cl$	SD	X_{VC}
1	W1	-24.31	0.10	4.68	0.46	0.00
1	W2	-34.09	0.02	3.13	0.22	0.00
1	W3	-16.84	0.05	4.75	0.37	0.00
1	W4	-28.68	0.21	4.41	0.29	0.04
1	W5	-20.63	0.34	5.15	0.90	0.00
1	W6	-23.64	0.61	6.76	0.21	0.00
1	W7	-25.37	0.29	2.72	0.50	0.01
1	W8	-26.91	0.12	4.55	0.38	0.02
1	W9	-21.19	0.05	6.47	0.54	0.00
1	W10	-14.95	0.89	4.62	0.20	0.00
1	W11	-17.71	0.20	4.62	0.19	0.00
2	W1	-25.37	0.08	4.89	0.22	0.08
2	W2	-22.66	0.09	5.75	0.29	0.02
2	W3	-27.15	0.31	5.77	0.00	0.10
2	W4	-27.10	0.10	4.49	0.16	0.24
2	W5	-26.78	0.14	6.11	0.59	0.09
2	W6	-20.91	0.04	6.42	0.28	0.49
2	W7	28.14	0.01	10.01	0.21	0.95
2	W8	-24.34	0.13	5.05	0.19	0.11
2	W9	-14.89	0.25	6.03	0.04	0.88
2	W10	-23.22	0.02	5.53	0.29	0.19
3	W1	-25.53	0.05	4.47	0.19	0.01
3	W2	-22.92	0.01	5.64	0.47	0.00
3	W3	-28.70	0.19	7.87	0.72	0.96
3	W4	-22.12	0.27	4.76	0.12	0.07
3	W6	11.21	0.41	9.79	0.31	0.22
3	W8	-24.21	0.09	6.27	0.16	0.02
3	W10	-20.74	0.13	4.41	0.02	0.09
4	W1	-1.10	0.44	6.67	0.45	0.61
4	W2	-17.63	0.22	6.12	0.16	0.39
4	W4	-17.08	0.20	5.77	0.05	0.62
4	W5	-7.06	0.01	6.20	0.15	0.00
4	W8	-9.28	0.41	8.62	0.40	0.56
5	W1	-9.09	1.69	10.62	0.54	0.94
5	W2	-10.60	0.11	6.84	0.62	0.42
5	W4	-9.30	0.04	6.20	0.02	0.71
6	W4	-9.28	0.31	10.31	0.76	0.91
6	W6	2.48	0.53	7.75	0.19	0.40

Appendix 3. Other publications derived from this thesis

48th International Association of Hydrogeology Congress – IAH 2021

Brussels, Belgium. September 2021

Poster presentation

Multi-isotopic assessment of potential chloroform remediation by a combined treatment of alkaline-activated persulphate in alkaline recharge water interception trenches

Gil-Villalba, S.; Vinyes-Nadal, M.; Torrentó, C.; Soler, A.; Palau, J.; Rosell, M.

Abstract

Chloroform (CF) is one of the highest-ranked halogenated volatile organic compounds in the most recent priority list of hazardous substances ATSDR, in 2019. Due to its extended use by the industry, accidental leakages or improper disposal, it is an ubiquitous environmental pollutant which can form Dense Non-Aqueous Phase Liquids (DNAPLs) at inaccessible parts of the subsoil. Persulphate (PS) injection-based In Situ Chemical Oxidation (ISCO) is a commonly applied technique for the remediation of such contaminated sites, but inducing a long-lasting alkaline activation of PS is challenging. In our contaminated site near Barcelona (NE Spain), these alkaline conditions have been already created by two recharge water interception trenches filled with concrete-based construction wastes and around 30% CF alkaline hydrolysis was previously proved by compound-specific stable isotope analysis (CSIA). The present study aims to evaluate the use of CF (13C and 37Cl) and sulphate as a degradation product of PS (34S and 18O) isotopic data for assessing i) the remediation efficiency and ii) the oxidant consumption, respectively, during an ISCO treatment by commercial alkaline-activated persulphate (i.e., PersulfOx®) in combination with the mentioned alkaline recharge water interception trenches before its application in the field. Firstly, laboratory batch experiments with distilled water allowed to determine the C and Cl isotopic fractionation (εC, εCl and Λ) of CF for the reaction with PersulfOx® and the isotopic pattern of sulphate produced. Secondly, the same but reproducing the field conditions, prepared with real contaminated infiltration water (e.g. containing geogenic sulphate) and crushed solid particles from the materials filling the interception trenches, allowed to investigate how the conditions of trench water could influence CF oxidation and other processes potentially interfering during the field application. Preliminary results showed a

significant difference between the CF dual C-Cl isotope slope (Λ) with PersulfOx® in distilled water and those available in the literature for CF oxidation with thermally-activated persulphate, alkaline hydrolysis, or reductive dechlorination. This fact would open its use to distinguish CF remediation by ISCO treatments against anaerobic biodegradation in field studies. However, unexpectedly, the CF Λ determined for the experiments resembling the field conditions differed from the first one and it was similar to Outer-Sphere Single Electron Transfer (OS-SET) or reductive dechlorination, suggesting that the hydrochemistry of the trenches might affect the radicals formation and therefore the CF degradation mechanisms in the field.

Multi-isotopic assessment of potential chloroform remediation by a combined treatment of alkaline-activated persulphate in alkaline recharge water interception trenches

Sergio Gil-Villalba✉, Martí Vinyes-Nadal, Clara Torrentó, Albert Soler, Jordi Palau, Mònica Rosell

✉sergiogilv@ub.edu

Motivation

In Situ Chemical Oxidation (ISCO) is a common treatment for groundwater pollution. However, in most cases it is not easy to differentiate the remediation efficiency from other processes, such as biodegradation or non-degrading processes as dilution or adsorption. As a result, it is common that the oxidant is applied in vast excess in field applications.

The aim of this study was to evaluate the suitability of multi-isotopic tools to measure the treatment efficiency and the oxidant consumption to gain control over the remediation process.

In this case, chloroform (CF) oxidation by a commercial alkaline-activated persulphate (i.e. PersulfOx®) was performed in laboratory batch experiments, reproducing field conditions of alkaline recharge water interception trenches installed in a contaminated site [1].

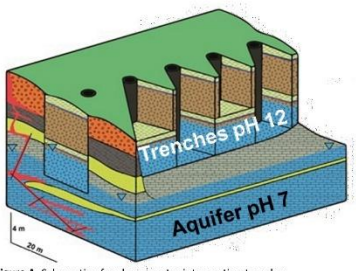

Figure A. Schematic of recharge water interception trenches.

CF remediation efficiency: $\delta^{13}C$ & $\delta^{37}Cl$

Preliminary results in distilled water experiments showed that CF oxidation with PersulfOx® (PS) generate results in a dual C-Cl isotope slope (Λ) that are significantly different to literature values for other CF degradation processes, such as oxidation with thermally-activated persulphate, alkaline hydrolysis, or reductive dechlorination [2].

This fact would open the use of Λ to distinguish CF remediation by ISCO treatments against anaerobic biodegradation or other degradation mechanisms in field studies.

However, unexpectedly, the Λ value for the experiments performed with trench water (simulating field conditions), differed from the results obtained for the experiments with distilled water, and it was similar to the values reported for Outer-Sphere Single Electron Transfer (OS-SET) and reductive dechlorination. This suggests that the hydrochemistry of the trench water might affect the radicals formation and therefore the CF degradation mechanisms in the field.

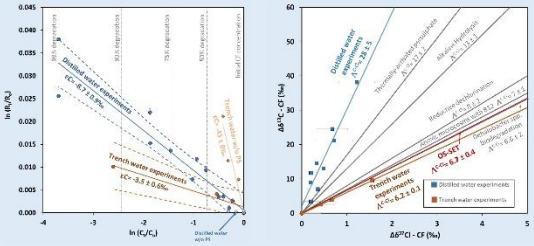

Figure B. Logarithmic Raleigh plot of C fractionation in oxidation experiments (left); C-Cl Isotopic dual plot for different CF degradation reactions (right).

CF degradation by $CO_2^{\cdot-}$ radical anions through an OS-SET reaction might be the result of the oxidation of formate by the $SO_4^{\cdot-}$ radicals generated from PS. Formate is a product of CF alkaline hydrolysis, which has been occurring in the interception trenches for years. This reaction of CF with the resulting $CO_2^{\cdot-}$ radical anions would explain the observed C and Cl isotope effects, which are similar to those reported by Heckel et al., 2017 [3].

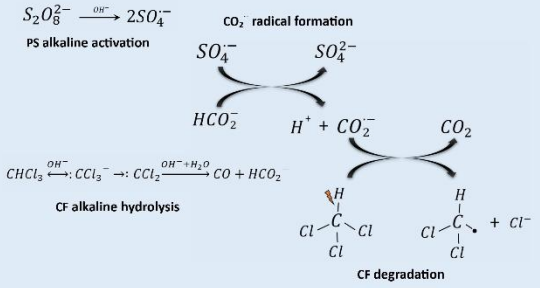

Conclusion: Lab experiments showed that previous CF alkaline hydrolysis could modify water hydrochemistry having an impact on the pathways of CF degradation with PS and on the resulting C and Cl isotopic fractionation. Further research is required before this dual isotope approach is used for assessing ISCO remediation efficiency in field studies.

Expected oxidation reaction under alkaline trench conditions:

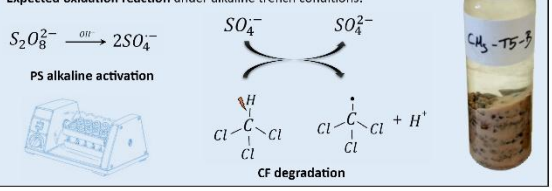

Oxidant consumption: $\delta^{34}S$ & $\delta^{18}O$

Sulphate is immediately generated by PS activation when dissolved in alkaline water. As PS is consumed in CF oxidation, more SO_4^{2-} is generated.

Therefore, three end-members have been identified for the sulphate isotopic values in the current oxidation experiments:

1. PersulfOx® sulphate isotopic composition [4]
2. Sulphate from the PS decomposition in water
3. Geogenic sulphate from groundwater in trench water experiments

In the current oxidation experiments the isotopic values of generated sulphate pointed to the second end-member. Even in control vials, where no additional CF was spiked, the sulphate concentration and isotopic signature changed in similar ways. This suggests that either PS is oxidating other compounds and/or organic matter in the trench water or that the prevalent process is sulphate generation from PS activation due to the alkaline conditions. Stoichiometric calculations indicated that only 4% of the initial PS was consumed by CF oxidation. Therefore, a higher PS consumption degree would be required to measure sulphate isotopic fractionation associated to CF oxidation.

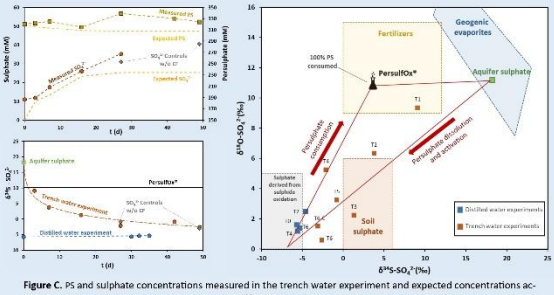

Figure C. PS and sulphate concentrations measured in the trench water experiment and expected concentrations according to the oxidation stoichiometry (top left); $\delta^{34}S$ of dissolved sulphate for both experiments (bottom, left); Dual S-O isotopic compositions for both experiments and processes description (right).

Conclusion: Sulphate isotope data is very sensitive to PS treatments. However, higher degradation extent are required to differentiate the effects of initial PS activation and the CF degradation. Further research is being conducted to reach higher degradation percentages that give insight of isotopic effects on field applications with advanced oxidant consumption.

References

[1] Torrentó, C., Audí-Miró, C., Bordeleau, G., Marchesi, M., Rosell, M., Otero, N., Soler, A., 2014. The use of alkaline hydrolysis as a novel strategy for chloroform remediation: the feasibility of using construction wastes and evaluation of carbon isotopic fractionation. Environ. Sci. Technol. 48:1869–1877.

[2] D. Rodríguez-Fernández, C. Torrento, M. Guivernau, M. Viñas, D. Hunkeler, A. Soler, C. Domènech, M. Rosell, Vitamin B12 effects on chlorinated methanes-degrading microcosms: dual isotope and metabolically active microbial populations assessment, Sci. Total Environ. 621 (2018) 1615–1625.

[3] Heckel, B., Cretnik, S., Kliegman, S., Shouakar-Stash, O., McNeill, K., & Elsner, M., 2017. Reductive outer-sphere single electron transfer is an exception rather than the rule in natural and engineered chlorinated ethene dehalogenation. Environ. Sci. & Tech., 51(17), 9663-9673.

[4] Vinyes-Nadal, M. (2019). Multi-isotopic assessment during chloroform oxidation by PersulfOx® in laboratory experiments for monitoring in-situ chemical oxidation applications. Master's Degree thesis. Universitat de Barcelona.

MAiMA ISÒTOPS ESTABLES I MINERALOGIA

UNIVERSITAT DE BARCELONA

About us

Our mission is to provide solutions for the management of contaminated sites, the authentication of food products and studies of mineral durability in civil construction. We apply the last technology in stable isotopes and mineralogy .

Location

Departament de Mineralogia, Petrologia i Geologia Aplicada. Facultat de Ciències de la Terra, Universitat de Barcelona
C/Martí i Franquès s/n, 08028 Barcelona, Spain

www.ub.edu/maima/

Acknowledgements

This research is supported by PACE (CGL2017-87216-C4-1-R) project financed by Spanish *Ministerio de Economía y Competitividad (MINECO)*. Gil-Villalba acknowledges a FPI grant of Spanish MINECO. *Facultat de Ciències de la Terra* of *Universitat de Barcelona* has financed the assistance to this congress.

Joint European Stable Isotope Users group Meeting – JESIUM

Kuopio, Finland. September 2022

Poster presentation

Combined isotopic (C-Cl) and molecular approach for the assessment of an EVO biostimulation treatment of an aquifer polluted with chlorinated ethenes

Gil-Villalba, S.; Rosell, M.; Soder-Walz, J.M.; Corregidor, J.; Vallecillo, M.A.; Shouakar-Stash, O.; Vinyas, M.; Palau, J.

Abstract

Bioremediation is a sustainable technology that has recently emerged as a cost-effective alternative to cleaning up aquifers polluted by chlorinated solvents compared to conventional physicochemical techniques. This biological approach uses the metabolism of bacteria to transform the contaminants and detoxify groundwater. In the last years, research has focused on understanding the physiology and biochemistry of such degrading mechanisms, however, its successful implementation in the field is still limited.

This research aims to assess and expand the knowledge of in-situ anaerobic biodegradation processes of chlorinated solvents. A biostimulation remediation treatment, using a commercial emulsified vegetable oil (EVO-EOSpro®), B12 vitamin, and lactate was applied to a sedimentary unconfined aquifer polluted with chloroethenes. A combined approach was used to identify the effectiveness of the treatment and the processes that occur in the field by dual C-Cl isotope analysis, hydrochemical data, and molecular analysis (*Dehalococcoides* 16S rRNA and functional genes) of the bacterial community.

First, microcosm experiments were carried out using the aquifer bacterial community. Sampled groundwater was initially purged to remove the original volatile compounds. Three parallel experiments were prepared in an anoxic chamber where PCE, TCE, and cisDCE were spiked separately and lactate was added to reproduce the biostimulation processes as they will occur at the site, characterize the corresponding C-Cl isotopic fractionation pattern, and assess bacterial growth.

Secondly, abiotic experiments were carried out to evaluate a possible isotopic fractionation during the oil-water phase distribution of the chloroethenes. A water solution with PCE, TCE, and cisDCE of known concentration and carbon isotopic composition was in contact, through a dialysis membrane, with EVO and sampled at 12 and 48 hours to assess possible changes.

Finally, the biostimulation treatment was applied at the contaminated site and monitored in eleven piezometers by one pre-injection sampling and five post-injection samplings. Concentration and C-Cl

isotopic composition were measured for the parental PCE and the degradation products TCE, cisDCE, and VC.

Preliminary results show a rapid decrease in PCE and TCE concentrations in the field. Isotopic data confirms that degradation to ethene is taking place after some months, as $\delta^{13}C$ enrichments over +30‰ were calculated from the isotopic balance, corresponding to a degradation efficiency over 95% in some piezometers. Dual C-Cl isotope slope (Λ) and molecular results will allow comparing in situ degradation process with the laboratory experiments and previously reported values, to understand the processes occurring in the field application.

Book of abstracts: https://www.jesium2022-kuopio.org/assets/jesium-2022---abstracts---2022-10-10_sec.pdf

Combined isotopic (C-Cl) and molecular approach for the assessment of EVO biostimulation treatment of an aquifer polluted with chlorinated ethenes

Sergio Gil-Villalba[1]✉, Mònica Rosell[1], Jesica M. Soder-Walz[2], Jordi Corregidor[3], Miguel A. Vallecillo[3], Andrea Tirado[3], Orfan Shouakar-Stash[4], Marc Viñas[5], Jordi Palau[1]

✉sergiogilv@ub.edu

Introduction and objectives

Bioremediation is a sustainable and cost-effective alternative to conventional physicochemical techniques for remediation of aquifers polluted by chlorinated solvents. This biological approach uses the metabolism of bacteria to transform the contaminants and detoxify groundwater.

This research aims to assess and expand the knowledge of in-situ anaerobic biodegradation processes of chlorinated solvents. A biostimulation remediation treatment, using a commercial emulsified vegetable oil (EVO-EOSpro®), B_{12} vitamin, and lactate was applied to a sedimentary unconfined aquifer polluted with chloroethenes (CEs). A combined approach was used to identify the effectiveness of the treatment and the degradative processes that occurred in the field by dual C-Cl isotope analysis, hydrochemical data, and molecular analysis of the bacterial community.

Analytical methods: $\delta^{13}C$ & $\delta^{37}Cl$

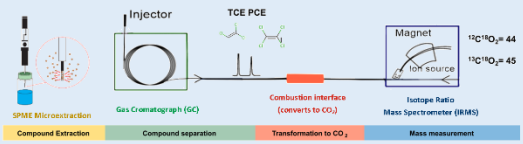

Figure A. Stable carbon isotope analysis were performed with an Agilent 6890 GC, coupled to a Delta V IRMS through a GC-Combustion III Interface (Thermo Finnigan). CEs were extracted from the aqueous sample by using headspace solid-phase microextraction (HS-SPME). Stable chlorine isotope analysis were performed with an Agilent 7890 GC, coupled to a Agilent 5975C qMS (for PCE and TCE) or a Thermo Finnigan MAT 253 IRMS (for cis-DCE).

Laboratory experiments

For the assessment of isotopic fractionation of CEs in the field, two processes caused by the EVO injection in the groundwater were previously investigated in laboratory experiments:

Sorption

Sorption of chlorinated hydrocarbons is a well-known abiotic process caused by the injection of a vegetable oil into the subsurface[1].

Partitioning experiments were performed with EVO and an aqueous solution of CEs separated by a dialysis membrane.

After 48 hours the sorption percentages for PCE, TCE and cis-DCE were 83%, 69% and 65% respectively. However, isotopic fractionation was not observed.

Reductive dechlorination (RD)

Microcosm experiments were carried out using the aquifer bacterial community to reproduce RD under controlled conditions, characterize the corresponding C-Cl isotopic fractionation pattern, and assess bacterial growth [2].

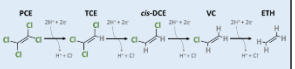

Figure B. CEs RD degradation pathway.

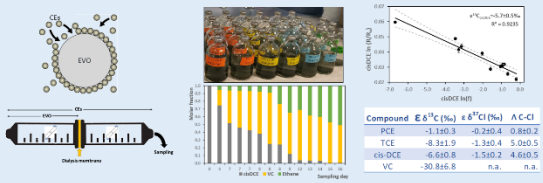

Compound	$\varepsilon\ \delta^{13}C$ (‰)	$\varepsilon\ \delta^{37}Cl$ (‰)	Λ C-Cl
PCE	-1.1±0.3	-0.2±0.4	0.8±0.2
TCE	-8.3±1.9	-1.3±0.4	5.0±0.5
cis-DCE	-6.6±0.8	-1.5±0.2	4.6±0.5
VC	-30.8±6.8	n.a.	n.a.

Figure C. Left: Schematic of CEs sorption to EVO (top), experimental design of partitioning experiments (bottom); Center: Microcosm bottles after preparation in an anoxic chamber, amended with different compounds (top), molar fraction of CEs and ethene in cis-DCE microcosms. Daughter compounds VC and ethene appear following the RD process. Right: Rayleigh plot for the calculation of the carbon isotopic fractionation factor (ε) of cis-DCE (top), ^{13}C, ^{37}Cl and dual C-Cl isotope fractionation values for analyzed CEs in microcosm experiments.

Field application

The biostimulation treatment was applied at the contaminated site and monitored periodically in eleven piezometers through five samplings during 12 months after the injection. Concentration and C and Cl isotopic composition were measured for all CEs.

Initially, a rapid decrease in PCE and TCE concentrations was observed while the overall molarity of CEs increased in 7 piezometers. This might be caused by contaminant mobilization after the injection. All sampling wells showed a reduction of CEs, which practically disappeared within 12 months.

Carbon isotopic balance confirms that degradation to ethene is taking place as enrichments in $\delta^{13}C$ over +30‰ were obtained using the isotopic balance (eq. below).

$$\delta^{13}C_{CEs} = \chi_{PCE} \cdot \delta^{13}C_{PCE} + \chi_{TCE} \cdot \delta^{13}C_{TCE} + \chi_{cisDCE} \cdot \delta^{13}C_{cisDCE} + \chi_{VC} \cdot \delta^{13}C_{VC}$$

Although Pz1 showed a rebound in CEs concentration in the last sampling, molar fraction and isotopic values indicate that RD is still going on. Hence, remediation is still working in this site after 12 months.

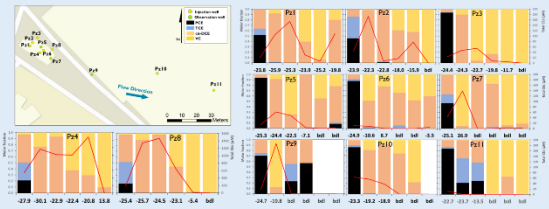

Figure D. Evolution of CEs molarity in monitoring wells (red line) shows an important decrease on CEs, note that piezometers 4 and 8 have a different vertical axis scale due to higher concentrations. Molar fractions (stacked columns) show a rapid transition from a PCE /TCE to a cis-DCE/VC dominated systems. Isotopic balance results (below each column) show an enrichment in ^{13}C values.

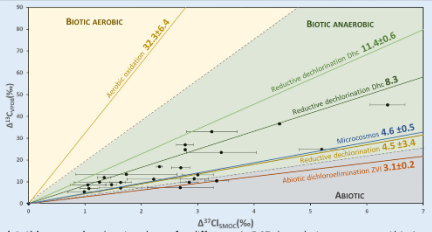

Figure E. Dual C-Cl isotope plot showing slopes for different cis-DCE degradation processes: Abiotic versus biotic aerobic and anaerobic as reported in the literature [3]. Both the results of the microcosms (blue line) and field values (black dots) are in the range of previously reported RD anaerobic degradative isotopic signature. This confirms the degradation mechanism taking place in the field.

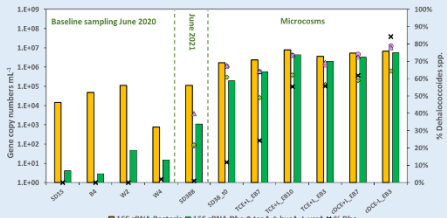

Figure F. Molecular analysis of *Dehalococcoides* 16SrRNA and functional genes was carried out by qPCR analysis. Bacterial growth was observed in the field after the EVO injection and along the microcosm experiments. The percentage of *Dehalococcoides* increased from 1% to 85% in microcosm experiments. Functional genes expressed for reductive dehalogenation processes also increased significantly.

Conclusions

A combined approach using isotopic and molecular results confirmed that the biostimulation of the aquifer bacteria was successful for over one year after the EVO injection. CEs degradation to non-toxic ethene was observed. *Dehalococcoides* population and functional genes increases matched with isotopic shifts towards positive values, and both confirmed that RD was the principal degradation mechanism of CEs. The lack of isotopic fractionation caused by sorption of CEs to EVO, suggested that all isotopic fractionation in field will be caused by biodegradation. The similar dual C-Cl isotope fractionation values for cis-DCE degradation in the microcosms and in the field indicates that the same transformation mechanism is taking place. Therefore, the ^{13}C enrichment factor determined in the microcosm experiments can be used to estimate the cis-DCE degradation extent at the contaminated site.

References

[1] Halloran, L. J. S., Vakili, F., Wanner, P., Shouakar-Stash, O., & Hunkeler, D. (2021). Sorption- and diffusion-induced isotopic fractionation in chloroethenes. *Science of the Total Environment*, *788*, 147826. https://doi.org/10.1016/j.scitotenv.2021.147826

[2] Blázquez-Palli, N., Shouakar-Stash, O., Palau, J., Trueba-Santiso, A., Varias, J., Bosch, M., Soler, A., Vicent, T., Marco-Urrea, E., & Rosell, M. (2019). Use of dual element isotope analysis and microcosm studies to determine the origin and potential anaerobic biodegradation of dichloromethane in two multi-contaminated aquifers. *Science of the Total Environment*, *696*, 134066. https://doi.org/10.1016/j.scitotenv.2019.134066

[3] Ojeda, A. S., Phillips, E., & Sherwood Lollar, B. (2020). Multi-element (C, H, Cl, Br) stable isotope fractionation as a tool to investigate transformation processes for halogenated hydrocarbons. *Environmental Science: Processes and Impacts*, *22*(3), 567–582. https://doi.org/10.1039/c9em00498j

Affiliations

1. MAIMA group, Mineralogia Aplicada, Geoquímica i Geomicrobiologia, Departament de Mineralogia i Petrologia Aplicada, Facultat de Ciències de la Terra. Institut de Recerca de l'Aigua (IdRA), Universitat de Barcelona (UB), Martí i Franquès s/n, 08028 Barcelona, Spain.
2. Departament d'Enginyeria Química, Biològica i Ambiental, Universitat Autònoma de Barcelona (UAB), Carrer de les Sitges s/n, Bellaterra, Spain
3. Environmental Resources Management Iberia SAU (ERM), Portal de l'Angel 36, 08002 Barcelona, Spain.
4. Isotope Tracer Technologies Inc., Waterloo, Ontario N2V 1Z5, Canada. Department of Earth and Environmental Sciences, University of Waterloo, Ontario N2L 3G1, Canada.
5. GIRO Joint Research Unit IRTA-UPC, IRTA, Torre Marimon, Caldes de Montbui E-08140, Spain.

Acknowledgements

This research is supported by INNOTEC (INNOTECRD19-1-0006) project, financed by ACCIO/Generalitat de Catalunya and PACE (CGL2017-87216-C4-1-R) project, financed by the Spanish *Ministerio de Economía y Competitividad* (MINECO). *Facultat de Ciències de la Terra of Universitat de Barcelona* has financed the assistance to this congress. IdRA research grants supported the financing of laboratory reactives. IAGC PhD Student Research Grant financed the isotopic analyses carried out in Waterloo (Canada). Gil-Villalba acknowledges a FPI grant of Spanish MINECO.

Congreso Ibérico de las Aguas Subterráneas

Albacete, Spain, October 2022

Oral presentation

Uso de los análisis isotópicos (13C, 37Cl) en etenos clorados para la evaluación de la biorremediación mediante la inyección de aceite vegetal emulsionado en un acuífero contaminado

Gil-Villalba, S.; Rosell, M.; Soder-Walz, J.M.; Corregidor, J.; Vallecillo, M.A.; Shouakar-Stash, O.; Soler, A.; Palau, J.

Resumen

La biorremediación es una alternativa económicamente viable para el tratamiento de aguas subterráneas contaminadas con disolventes clorados. Esta técnica utiliza la capacidad metabólica de determinadas poblaciones microbianas para transformar los contaminantes del agua subterránea. En los últimos años se ha investigado la fisiología y bioquímica de los mecanismos de biodegradación, principalmente a escala de laboratorio. Sin embargo, el estudio detallado de los procesos que ocurren durante la biorremediación in situ, a escala de campo, es aún limitado.

El presente estudio utiliza un enfoque múltiple para ampliar el conocimiento en procesos de bioestimulación de dehalogenación reductiva microbiana in situ de etenos clorados en condiciones anaerobias. Concretamente, este estudio se ha realizado durante un tratamiento de bioestimulación mediante la inyección de aceite vegetal emulsionado (EVO de sus siglas en inglés), vitamina B12 y lactato, en un acuífero libre detrítico contaminado con etenos clorados. La evaluación de la eficacia del tratamiento y la determinación de la vía de biodegradación se llevaron a cabo mediante un estudio multidisciplinar que incluyó: i) análisis isotópico de carbono y cloro en compuestos específicos (13C, 37Cl – CSIA, por sus siglas en inglés), ii) información hidroquímica y iii) análisis molecular de la comunidad bacteriana (cuantificación de Dehalococcoides totales y genes funcionales ligados a procesos de dehalogenación redutiva). El aceite vegetal emulsionado pretende incrementar la biodisponibilidad de ácidos orgánicos e H2 in situ, actuando como fuente de electrones a lo largo del tiempo, así como mantener unas condiciones reductoras en el agua subterránea a largo plazo, a diferencia de otros tratamientos utilizados frecuentemente donde las reinyecciones son a menudo necesarias, p.ej. lactato.

Simultáneamente a la aplicación del tratamiento de estimulación en el campo, durante este estudio se llevaron a cabo diferentes experimentos en el laboratorio. Se realizaron experimentos tipo “batch” con microcosmos, utilizando la comunidad bacteriana autóctona del acuífero. Se prepararon diferentes experimentos en paralelo, inyectando percloroetileno (PCE), tricloroetileno (TCE) o dicloroetileno (DCE), respectivamente, como contaminante inicial y lactato para reproducir las condiciones de biodegradación en el acuífero. Esto permitió caracterizar el patrón de fraccionamiento isotópico dual (C-Cl) y evaluar el crecimiento bacteriano asociado, siendo estos resultados de utilidad para evaluar los datos de campo. Además, se realizaron experimentos abióticos para evaluar el posible fraccionamiento isotópico asociado a la distribución de los etenos clorados entre la fase acuosa y la fase oleosa (EVO). Con este fin, una solución control con PCE, TCE y DCE se puso en contacto con EVO a través de una membrana de diálisis. Los cambios en la concentración y en la composición isotópica se midieron a las 12 y 48 horas. Resultados preliminares descartan cambios significativos en la composición isotópica del carbono asociados a la distribución de los contaminantes entre la fase acuosa y la fase oleosa.

La evaluación del tratamiento de bioestimulación in situ se realizó mediante el monitoreo de 11 piezómetros durante 12 meses (en 5 campañas de muestreo). Se analizaron los cambios en la concentración y composición isotópica C-Cl de los etenos clorados, en las poblaciones bacterianas y en los parámetros hidroquímicos. Los resultados preliminares muestran un rápido descenso en las concentraciones de PCE y TCE. El balance isotópico de los etenos clorados, PCE, TCE, DCE y cloruro de vinilo (VC), muestra un elevado enriquecimiento en el isótopo pesado (13C), alcanzando en algunos pozos cambios en valores δ13C superiores a +30‰. Estos resultados son consistentes con los análisis de concentración e indican un elevado grado de biodegradación. El análisis isotópico dual C-Cl sugiere que el mecanismo de biodegradación de los etenos clorados en el campo es el mismo que el observado en los experimentos con microcosmos, permitiendo a su vez el uso de los factores de enriquecimiento isotópico determinados en el laboratorio para la cuantificación de la biodegradación en el acuífero. Finalmente, el incremento de las poblaciones bacterianas totales, de Dehalococcoides sp. y de genes funcionales, confirman que la bioestimulación fue efectiva y específica a favor de procesos de dehalogenación reductiva. Los resultados muestran que la capacidad de biodegradación se mantiene 12 meses después de la inyección.

Book of abstracts: https://cias2022.webs.upv.es/wp-content/uploads/2022/11/LibroDeResumenes2.pdf

Catalan Water Partnership - Water Innovation Day (WID 2023)

Barcelona, Spain, February 2023

Oral presentation

Premi al millor projecte I+D dels 12 presentats

Proyecto: Eines isotòpiques per a la descontaminació sostenible amb oli vegetal emulsionat (EVO).

Gil-Villalba, S.

Abstract

L'objectiu general és desenvolupar solucions sostenibles per a la remediació d'aqüífers contaminats amb compostos orgànics volàtils (COVs) clorats. S'investigarà l'aplicació de tècniques isotòpiques innovadores com a eina de diagnosi dels tractaments de remediació amb oli vegetal emulsionat (EVO). L´EVO actua bioestimulant els microorganismes presents a l'aqüífer, capaços de degradar aquests contaminants. Aquest projecte inclou el desenvolupament de les tècniques isotòpiques al laboratori, i la seva validació al camp mitjançant una prova pilot en un emplaçament contaminat. L'ús d'EVO en els tractaments de bioestimulació és recent, i actualment hi ha poques experiències i publicacions científiques. Les eines isotòpiques permeten millorar significativament la monitorització dels tractaments de remediació. Aquest estudi multi-isotòpic (carboni i clor) suposa un avenç en l'estat de l'art i representa una innovació tant a nivell nacional com internacional.

V Jornades de joves investigadors de l'IDRA

Barcelona, Spain, June 2023

Oral presentation

Remediació d'aigua subterrània contaminada per compostos organoclorats volàtils i avaluació amb anàlisi isotòpic

Gil-Villalba, S.

Abstract

A Catalunya, aproximadament el 8% de les masses d'aigua subterrània estan contaminades per compostos orgànics clorats volàtils (CVOCs). Aquests han estat àmpliament utilitzats a la indústria com a dissolvents o precursors químics, arribant als aqüífers degut a abocaments accidentals o intencionats. Un cop arriben a les aigües subterrànies poden romandre durant dècades si no es donen les condicions adients per a la seva degradació i, sovint, requereixen d'algun tractament per recuperar la qualitat de les aigües.

A la ponència s'exposaran dues línies de recerca que s'estan desenvolupant per resoldre aquesta problemàtica:

- *In situ chemical oxidation* (ISCO): consisteix en la injecció d'un oxidant químic a l'aqüífer per degradar els compostos orgànics. El persulfat és un oxidant àmpliament utilitzat, però que, per a la seva activació, requereix un pH bàsic (pH>10) que no es dona de forma natural als aqüífers. Es proposa un tractament combinat, injectant el persulfat a través d'una barrera reactiva permeable (BRP) que garanteixi la seva activació i la oxidació dels CVOCs. Aquesta estratègia es posa en pràctica en diferents experiments de laboratori per obtenir els valors de fraccionament isotòpic i preveure potencials limitacions, per posteriorment portar-la a terme a un emplaçament contaminat per CVOCs on ja existeix aquesta BRP.

- Bioestimulació: consisteix en la injecció d'un donador d'electrons per potenciar la decloració reductiva dels CVOCs pels microorganismes anaerobis presents a un aqüífer.

La injecció d'un oli vegetal emulsionat comercial (EOS PRO EVO) es posa en pràctica a un aqüífer contaminat amb CVOCs i es reprodueixen experiments de laboratori per avaluar els diferents processos biòtics i abiòtics que poden generar fraccionament isotòpic i podrien afectar el càlcul d'eficiència a l'aplicació de camp.

S'explicarà quines eines isotòpiques s'utilitzen per identificar els processos de transformació i l'eficiència real dels tractaments per tal de millorar la gestió dels emplaçaments contaminats.

Workshop SiCon 2024 – Siti Contaminati

Taormina, Italy. February 2024

Oral presentation

Assessment of bioremediation of chlorinated ethenes with EVO using isotopic analysis

Gil-Villalba, S.; Rosell, M.; Soder-Walz, J.M.; Corregidor, J.; Vallecillo, M.A.; Shouakar-Stash, O.; Palau, J.

Abstract

Contamination of groundwater by organochlorides has become a pressing concern due to the environmental and human health risks that derive from it. Bioremediation has emerged as a sustainable and cost-effective alternative to cleaning up aquifers polluted by chlorinated solvents, compared to conventional physicochemical techniques. This biological approach uses the metabolism of bacteria to transform the contaminants and detoxify groundwater.

Our research aimed to assess and expand the knowledge of in-situ anaerobic biodegradation processes of chlorinated solvents. A biostimulation remediation treatment, using a commercial emulsified vegetable oil (EVO-EOSpro®) was applied to a sedimentary unconfined aquifer polluted with chloroethenes. Contrarily to highly soluble biostimulation substrates, the emulsified oil is supposed to provide a long-lasting carbon source, reducing remediation costs caused by recurrent injections. A combined approach was used to identify the effectiveness of the treatment and the degradative processes that occurred in the field using dual C-Cl isotope analysis, hydrochemical data, and molecular analysis of the bacterial community.

Microcosm experiments were carried out using the aquifer bacterial community. Three parallel experiments with sampled groundwater were prepared in an anoxic chamber where PCE, TCE, and cisDCE were spiked separately and lactate was added to reproduce the biostimulation processes as they will occur at the site, characterize the corresponding C-Cl isotopic fractionation pattern, and assess bacterial growth. Subsequently, the biostimulation treatment was applied at the contaminated site and monitored for 14 months in eleven piezometers by one pre-injection sampling and five post-injection samplings. Concentration and C-Cl isotopic compositions were measured for PCE and its degradation products TCE, cisDCE, and VC.

Results showed a rapid decrease in PCE and TCE concentrations after the injection while cis-DCE, and VC accumulated for several months. However, isotopic, hydrochemical and biological results confirmed that the biostimulation was still active 12 months after the injection. Furthermore, the carbon isotopic balance demonstrated that the accumulation of cis-DCE was overcome, degrading all chlorinated ethenes to non-toxic ethene. The dual C-Cl isotope slope measured for cis-DCE in field samples was equal to that found in microcosm experiments, confirming that anaerobic biodegradation was the major degradation pathway in the field. This allowed the calculation of the degradation efficiency, which was higher than 60% in all monitored points.

World Groundwater Congress – IAH 2024

Davos, Switzerland. September 2024

Oral presentation

Use of dual C-Cl isotope analysis of trichloromethane for the assessment of active radical species during alkaline persulfate activation

Gil-Villalba, S.; Rosell, M.; Torrentó, C.; Vinyes-Nadal, M.; Soler A.; Palau, J.

Abstract

Activated persulfate ($S_2O8$2-) has been increasingly applied in ISCO treatments of contaminated soil and groundwater due to its capacity to generate highly reactive and selective sulfate radicals (SO4·). Activated persulfate facilitates the degradation of multiple contaminants through the generation of various reactive oxygen species (ROS) including sulfate radicals (SO4·-), hydroxyl radicals (HO·), and superoxide radicals (O2·-). Different reactivity and/or reaction mechanisms of reactive oxygen species (ROS) with target contaminants would pose implications on the contaminant degradation rates, efficiencies, and intermediates and isotopic fractionation. Therefore, it is important to identify the dominant ROS and major degradation pathways in persulfate-based reactions in order to utilize the full potential of the ISCO processes treatment.

Laboratory experiments were conducted to evaluate the potential of isotopic $\delta^{13}C$ and δ37Cl values of trichloromethane (TCM) as a proxy for the identification of the active radical species during alkaline persulfate activation under field conditions. Batch experiments were designed to replicate the following conditions: i) different TCM:PS molar ratios to investigate potential variations associated with different dosages or sections of a contamination plume; ii) different pH values to assess the impact of alkalinity on persulfate activation; iii) absence and presence of CO32-, to assess the potential influence of this natural groundwater ion, known to act as a scavenger, on the radical cascade; iv) conditions simulating an alkaline interception trench, aiming to understand the processes that occur in this innovative TCM remediation strategy.

Our results reveal, for the first time, that dual isotopic analysis can be used as a proxy for the identification of active radical species in field applications of advanced oxidation processes such as alkaline-activated persulfate oxidation.

Journal of Hazardous Materials 488 (2025) 137447

Contents lists available at ScienceDirect

Journal of Hazardous Materials

journal homepage: www.elsevier.com/locate/jhazmat

Fate and degradation of methoxychlor in a contaminated aquifer: Insights from dual carbon-chlorine isotope analysis and isomeric fraction

Martí Vinyes-Nadal [a,*], Sergio Gil-Villalba [a], Mònica Rosell [a], Albert Soler [a], Neus Otero [a,b], Clara Torrentó [a,b]

[a] Grup MAiMA, SGR Mineralogia Aplicada, Geoquímica i Hidrogeologia (MAGH), Departament de Mineralogia, Petrologia i Geologia Aplicada, Facultat de Ciències de la Terra, Institut de Recerca de l'Aigua (IdRA), Universitat de Barcelona (UB), Martí i Franquès s/n, Barcelona 08028, Spain
[b] Serra Húnter Fellowship, Generalitat de Catalunya, Spain

HIGHLIGHTS

- C & Cl isotopic fractionation revealed methoxychlor degradation at field scale.
- Mobilization of less degraded methoxychlor to the water was detected using $\delta^{13}C$ data.
- Isotopic data allowed quantifying the extent of methoxychlor reductive dechlorination.
- Isomeric fraction revealed distinct environmental behaviour of methoxychlor isomers.

GRAPHICAL ABSTRACT

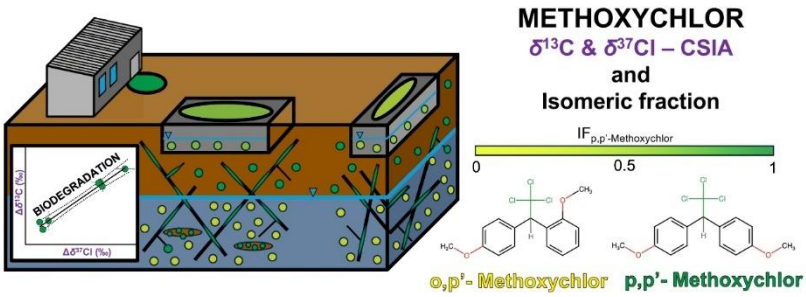

ARTICLE INFO

Keywords:
Pesticides
Methoxychlor
Isotopes
CSIA
Isomers

ABSTRACT

The combined use of isomeric fraction (IF) and multi-element compound-specific isotope analysis (ME-CSIA) was evaluated for the first time to assess the fate and degradation of methoxychlor in the environment. The concentration and carbon and chlorine isotope composition of methoxychlor and its transformation products were monitored in water and solid phases of a fractured aquifer. The results from the interception trenches water samples demonstrated that induced alkaline conditions promoted alkaline hydrolysis. Natural attenuation of methoxychlor isomers was evidenced by carbon and chlorine isotopic fractionation. The field C-Cl isotope slope ($\Lambda_{C/Cl} = 0.42 \pm 0.06$; $R^2 = 0.98$) was statistically indistinguishable ($p > 0.05$) from that obtained in a previous experiment (0.44 ± 0.14), confirming the occurrence of reductive dechlorination of methoxychlor isomers. P,p'-methoxychlor $\delta^{13}C$ values in groundwater samples revealed variations linked to rainfall patterns. The extent of p,p′-methoxychlor biodegradation was calculated to be greater than 89 % across the monitoring period. The combined use of CSIA and IF evidenced that alkaline hydrolysis and reductive dechlorination did not exhibit isomeric selectivity. Differences in IF values between slurry and water samples, as well as between upstream and downstream wells, suggested variations in the environmental behaviour of the p,p' and o,p'-isomers, likely due to differing water solubilities. Overall, ME-CSIA proved to be a valuable tool for identifying, quantifying, and tracing methoxychlor degradation in this aquifer. Additionally, IF provided insights into the distinct environmental behaviour of the p,p′- and o,p′-isomers. These tools offer crucial information, valuable for decision-makers in developing remediation strategies for methoxychlor-contaminated sites.

* Corresponding author.
E-mail address: martivinyesnadal@ub.edu (M. Vinyes-Nadal).

https://doi.org/10.1016/j.jhazmat.2025.137447
Received 12 November 2024; Received in revised form 27 January 2025; Accepted 28 January 2025
Available online 29 January 2025

1. Introduction

The insecticide methoxychlor (MET) (2,2,2-trichloro-1,1-bis (4-methoxyphenyl) ethane) is an organochlorine pesticide (OCP) widely used since the 1990s in animal feeds, agriculture, and gardens due to its high effectiveness against a wide variety of insects [1-3]. MET is a persistent compound in the environment that aware a considerable concern due to its estrogenic activity [4,5]. It is highly toxic to aquatic invertebrates and fish [6], and potentially harmful to human health, since it may induce ovarian cancer cells to grow [7]. Due to these risks, MET production and use have been phased out or banned in many countries since the early 2000s [8-10]. However, its persistence in soils continues to pose a challenge at several highly contaminated sites, especially at former pesticide manufacturing, formulation or storage facilities [11-13].

MET is an isomeric pesticide, consisting of two constitutional isomers: p,p'-MET and o,p'-MET. The pesticide activity primarily originates from the p,p'-isomer, which was the main product of commercial formulations [14]. Typically, commercially available MET consisted of 88 % pure p,p'-MET, while the remaining 12 % being primarily the constitutional isomer o,p'-MET and other reaction products [15,16]. As a result, most studies have concentrated on detecting p,p'-MET in the environment, with concentrations as high as 522 μg/g reported in soils [17]. Despite its low solubility (<0.05 mg/L at 24°C in water; [18]) and high partition coefficient (log K_{ow} > 5; [19]), p,p'-MET has also been found in drinking water sources, with levels reaching up to 56 μg/L [20]. A few studies have explored the environmental presence of o,p'-MET [21]. Given the harmful effects of MET on human health and ecosystems, it is crucial to thoroughly understand the environmental fate of both isomers.

Monitoring concentrations of parental and by-product compounds as indicators of degradation has some limitations. It can be challenging to determine whether pollutants are recalcitrant or if their degradation is too slow to be detected. Additionally, drawing proper conclusions is difficult when a compound acts as both a parent and a by-product, when a by-product can be derived from multiple parent compounds, or when the target by-product undergoes further degradation. Furthermore, variations in concentration may result from differential transport, sorption, desorption, or dilution events rather than actual degradation. Since it overcomes all these limitations, multi-elemental compound-specific isotope analysis (ME-CSIA) offers a valuable complementary tool to trace pesticide degradation [22-24]. Nevertheless, the use of pesticide CSIA at the field scale remains scarce [25-29], mainly due to conceptual and analytical limitations [30,31,22,23].

For isomeric pesticides, changes in isomeric fractions (IF) can help evaluating different processes that these contaminants undergo in the environment [32,33]. Additionally, integrating isomeric-specific analysis and CSIA provides opportunities to offer enhanced insights into pesticide transformation and fate [34,27,35]. This combined approach has been applied to OCPs such as hexachlorocyclohexane (HCH, [34,36, 28]) and dichlorodiphenyltrichloroethane (DDT, [27,37]), to phenoxy acid herbicides [38], and to systemic fungicides [26,35,39]. For chiral pesticides, which have enantiomers with identical physicochemical properties, the combination of enantiomeric fraction with CSIA allows differentiating between biotic and abiotic degradation processes [34,36, 38,28,35,37]. However, for diastereomeric or constitutional isomers, which may exhibit different physicochemical properties, the combined use of CSIA with IF has been scarcely explored. Recent studies have demonstrated the effectiveness of this approach in evaluating the degradation of the diastereomeric fungicide dimethomorph, as certain degradation processes exhibit diastereomeric selectivity [26,39]. In the case of constitutional isomers, the feasibility of using IF to evidence degradation remains uncertain, as various environmental processes may influence the isomeric composition [40]. While IF has primarily been used to determine the origin of DDT [27], its broader application in assessing environmental fate of OCPs is still limited.

To date, the applicability of ME-CSIA, whether combined with IF or not, for tracing the environmental fate of MET has not been assessed at field scale. We recently overcame the analytical limitations and established carbon ($^{13}C/^{12}C$) and chlorine ($^{37}Cl/^{35}Cl$) CSIA methods for p,p'-MET and its transformation products at environmentally relevant concentrations in both solid and liquid matrices [41]. Conceptually, we demonstrated at the laboratory scale that ME-CSIA is a powerful tool for identifying and quantifying the biotic reductive dechlorination of p, p′-MET, while also distinguishing it from abiotic processes such as alkaline hydrolysis or oxidation with alkaline-activated persulfate [42]. Specifically, significant carbon and chlorine isotopic fractionation during the reductive dechlorination of p,p′-MET to 1,1-Dichloro-2,2-bis (4-methoxyphenyl)ethane (p,p'-DMDD) in a field-derived microcosm under strictly anoxic conditions was observed ($\varepsilon_C = -0.9 \pm 0.3$ ‰ and $\varepsilon_{Cl} = -1.9 \pm 1.0$ ‰, $\Lambda_{C/Cl} = 0.4 \pm 0.1$). No significant carbon or chlorine isotopic fractionation was detected during dehydrochlorination of p, p'-MET to 1-[2,2-dichloro-1-(4-methoxyphenyl)ethenyl]-4-methoxybenzene (p,p'-MET-OLEF) via alkaline hydrolysis or oxidation with alkaline-activated persulfate. A scheme of the main transformation pathways and degradation products of methoxychlor may be found in Figure A1.

The aim of this research was to evaluate for the first time the use of C and Cl ME-CSIA for identifying and quantifying MET degradation at field scale. Furthermore, this work pioneers an exploration into the deeper insights that the integration of CSIA with IF may provide into the environmental fate of MET and its degradation products.

The field site selected for this study was a multi-polluted site in Òdena (Catalonia), expected to host various MET transformation processes. This site was highly contaminated with MET and other contaminants as a result of the activities of a former chemical plant manufacturing plant-protection products [43-45]. Twenty years ago, remediation efforts included removing contaminated soil from two pollution source areas and installing two interception trenches in the unsaturated zone to retain contaminants before they could infiltrate into the aquifer. These trenches were designed to induce alkaline conditions, promoting the degradation of certain compounds via alkaline hydrolysis [45]. In the aquifer, natural attenuation of chlorinated volatile organic compounds has been observed [43,44]. Previous experiments with slurry from one of the Òdena wells where anaerobic reductive biodegradation of chlorinated ethenes and methanes was evidenced, confirmed favorable conditions in the aquifer for reductive dechlorination of p, p'-MET [42]. However, the occurrence of MET degradation in the interception trenches or in the aquifer has not yet been explored.

2. Materials and methods

2.1. Site description

The study area is an unconfined bedrock aquifer located 50 km northwest of Barcelona, in Òdena (NE Spain), which has been heavily impacted by MET and other pesticides [46], as well as chlorinated ethenes, ethanes, methanes, chlorobenzenes and traces of BTEX [43-45]. The aquifer is primarily composed of Eocene blue-grey limestone, which has low permeability but contains fissures and fractures with high hydraulic conductivity.

Contamination at the site was originated from a chemical plant that operated between 1978 and 1985. When the chemical plant started operating, an underground wastewater tank, built without impermeabilization, was constructed to collect liquid waste. Closer to the closure of the chemical plant, a lagoon for the disposal of liquid wastes was excavated on the ground and left open to the atmosphere, allowing volatile compounds to evaporate. However, the liquid waste also easily infiltrated the soil. A few years after, the disposal lagoon was covered with Quaternary sediments. The exploration of the contamination started 20 years after the plant closure. Consistently with data of chlorinated volatile organic compounds [43-45], the highest levels of p,p'-MET were

detected in three specific areas: around the chemical plant building, near the area where the disposal lagoon was located, and around the wastewater tank. Therefore, pollution was attributed to these three contaminant sources: (1) abandoned barrels inside the chemical plant building, (2) the disposal lagoon, and (3) the wastewater tank [43] (Fig. 1).

In 2006, approximately 2000 t of polluted soil were removed from the pollution source areas, and two interception trenches were installed in the unsaturated zone where the polluted soil had been removed. These trenches, the "pit trench" in the disposal lagoon area and the "tank trench" in the wastewater tank area, were refilled with recycled concrete-based aggregates [45]. The aim of those trenches was to induce alkaline conditions (pH ~12) so that contaminants retained in the unsaturated zone can be lixiviated by rainwater and infiltrated to the trenches, where they can be degraded by alkaline hydrolysis. While alkaline hydrolysis of trichloromethane was confirmed [45], its impact on MET has yet to be studied. A detailed hydrological model of the trenches is provided in Torrentó et al. [45]. Briefly, trenches water discharges to the unsaturated zone following the main water flow direction, and the connection to the aquifer mainly occurs through fractures and following the contact between the detrital unit and the underlying carbonate layers.

Natural attenuation of chlorinated volatile organic compounds in the aquifer was extensively studied in previous studies [43,44]. Reductive pathways were evidenced in the aquifer, especially in the area of the former wastewater tank [44]. However, the potential for natural attenuation of MET at this site remains unexplored.

The existing monitoring network consists of several monitoring wells, some of them drilled along the interception trenches. For this study, wells L5 and L8 were used for sampling water from the tank and pit trenches, respectively (Fig. 1). To trace contamination in the aquifer, groundwater samples were also collected from two downstream wells (S3 and S1) located near each trench, and an upstream well (S8) situated closer to the chemical plant building (Fig. 1). Historical data of p,p'-MET concentrations at these monitoring points (L5, L8, S3, S1 and S8) are available from an annual monitoring program conducted by the Waste Agency of Catalonia between 2007 and 2019 (unpublished data) (Figure A2). However, o,p'-isomers and potential transformation products were not monitored on this site prior to the start of our study. Additional information about the contamination history of this site can be found in the Appendix A.

To enhance tracing capacity, new piezometers (S11, S12 and S13) were installed in June 2023 in the wastewater tank area (Fig. 1). Construction details of the newly drilled piezometers are provided in Figure A3.

2.2. Sample collection

Water and slurry samples were collected periodically for concentration (from September 2020 to June 2023) and isotopic (from December 2021 to June 2023) analyses of MET and its degradation products. Water samples for concentration measurements from wells L5 and L8 (trenches water), and from wells S3, S1 and S8 (groundwater) were collected in 500-mL amber glass bottles. Water samples for isotopic analyses were collected from wells L5, L8 and S3 using two 10-L glass bottles per sample. All the bottles were closed with PTFE-lined caps and samples were held at 4 °C in darkness until extraction, which was usually conducted within a week after sampling.

Bottom-well slurry samples for concentration measurements and isotopic analyses were collected from the bottom of the wells S3 and S8, using an electrical submersible pump, in 1 or 2.5-L amber glass bottles closed with PTFE-lined caps. Samples were centrifuged using 50-mL Falcon vials to separate the solid from the water and were held at 4 °C in darkness until its extraction that usually was conducted within a week after sampling.

Slurries from the newly drilled piezometers (S11, S12, S13) were collected during the drilling process from the fractured sandstone and altered marl layers of the cores, especially at depths where fractures were detected and in the contact between the detrital unit and the underlying carbonate unit (Figure A3). To collect these slurry-core samples, the wet, disaggregated material from the fractures was carefully extracted using a spatula and placed into polypropylene centrifuge tubes and stored at 4 °C in darkness. Pesticides extraction was conducted within one month after sampling.

2.3. Chemicals and materials

Analytical standards p,p'-MET (1-methoxy-4-[2,2,2-trichloro-1-(4-

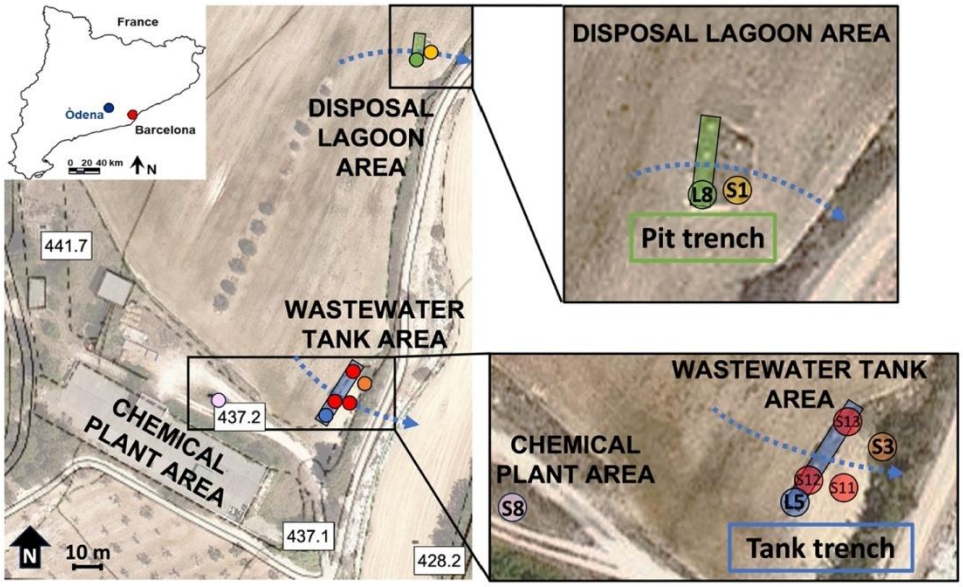

Fig. 1. Location of the former chemical plant, the trenches, and the monitoring points, which included wells for collecting water from the two trenches (L5 and L8), wells for collecting groundwater (S1, S3 and S8) and aquifer slurry samples (S3 and S8), and newly drilled piezometers (S11, S12 and S13) from which slurry-core samples were collected. The numbers indicate the altitude (m above sea level), and groundwater flow lines (blue dashed lines) suggested by Torrentó et al. [45] are also shown.

methoxyphenyl)ethyl]benzen, Pestanal® quality, 98 % purity) and p,p'-MET-OLEF (1-[2,2-dichloro-1-(4-methoxyphenyl)ethenyl]-4-methoxybenzene, standard quality) were purchased from Supelco®. The analytical standard o,p'-MET (1-methoxy-2-[2,2,2-trichloro-1-(4-methoxyphenyl)ethyl]benzene, 99.8 % purity) was purchased from Dr. Ehrenstorfer™. These standards were used for concentration analysis and as in-house working isotope standards. Stock solutions were prepared in hexane at 1 mg/mL and stored at −18 °C. As surrogate, p,p'-MET-d14 (100 µg/mL in acetone, Certified Reference Material), purchased from Dr. Ehrenstorfer™, was used.

For the extraction procedures, a DOA-P504-BN model Gast vacuum pump, a 12 port 5982–9110 model Agilent VacElut Cartridge Manifold and an IEC CL31R Multispeed ThermoFisher Scientific centrifuge were used. Cartridges used for Solid Phase Extraction (SPE) were purchased from Waters and the solvents used: hexane, dichloromethane (DCM), and ethyl acetate (EtAc), in SupraSolv® quality, and acetone and methanol (MeOH), in EMPROVE®ESSENTIAL quality, were purchased from Merck.

A well water level sounder (WL–500) purchased from Xylem was used for measuring piezometric levels. Water and bottom-well slurry samples were pumped from monitoring points using electrical submersible pumps (Royal Eijkelkamp) with polyethylene discharge tubing. The pH, Eh, conductivity, dissolved oxygen and temperature of the water samples were monitored in situ using a flow-through cell, to avoid contact with the atmosphere, and measured using a multiparametric probe (WTW Multi 3630 IDS) with pH (SenTix® ORP 940), redox (SenTix® ORP 900), conductivity (TetraCon® 925) and dissolved oxygen (FDO® 925) sensors that also measured temperature. The reference electrode potential at the water temperature was added to the Eh measurements to correct them to the standard hydrogen electrode system (UH).

2.4. Pesticide extraction methods

Samples were extracted using methods described previously [41]. Briefly, SPE, using Oasis HLB cartridges (Waters), was performed for water samples, whereas liquid-solid extraction (LSE) with a mixture of water, methanol, and hexane was used for slurry samples. Oasis HLB 500 mg cartridges were used to extract the 500-mL water samples for concentration measurements, whereas 6 g cartridges were used to extract the 20-L water samples for isotopic analyses. The SPE (mix of ethyl acetate and dichloromethane) and LSE (hexane) extracts were evaporated to dryness and reconstituted with appropriate volumes of hexane for injections into GC-MS, GC-IRMS, and GC-MC-ICPMS. The efficiency of both extraction methods and the carbon and chlorine isotope fractionation were previously evaluated [41].

2.5. Analytical methods

2.5.1. Pesticide quantification

Concentrations of p,p'-MET, o,p'-MET and p,p'-MET-OLEF were measured by Gas Chromatography Mass Spectrometry (GC-MS) following the method described previously [41]. Briefly, a Shimadzu QP2010 single quadrupole GC-MS and a SAPIENS-X5MS column (30 m × 0.25 mm × 0.25 µm, Teknokroma) were used. The oven program was as follows: initial temperature of 60 °C for 1 min, ramp at 6 °C/min to 270 °C and ramp at 40 °C/min to 300 °C (total run time: 36.75 min) and the mass spectrometer was operated in electron ionization mode (70 eV). Selected-ion monitoring (SIM) measurements were performed, and each analyte was quantified (external calibration) based on peak area using one quantifier and three qualifier ions (Table A1).

Due to the lack of authentic standards, semi-quantitative determination of p,p'-DMDD, o,p'-DMDD and o,p'-MET-OLEF was performed by the same method but under the assumption that their MS response factors were the same as those for p,p'-MET, o,p'-MET and p,p'-MET-OLEF, respectively.

2.5.2. Compound specific isotope analyses

C and Cl isotope measurements of p,p'-MET, o,p'-MET, p,p'-MET-OLEF, p,p'-DMDD and o,p'-DMDD were performed by gas chromatography coupled with isotope ratio mass spectrometry (GC-IRMS), and by gas chromatography coupled with multiple-collector inductively coupled plasma mass spectrometry (GC-MC-ICPMS), respectively, following the methods described previously [41]. Briefly, a Trace GC 1310 coupled to a MAT 253 Plus IRMS through a GC Isolink II and a Conflo IV interface (Thermo Fisher Scientific) was used for C isotope ratios determination and a Trace 1310 GC coupled to a NEPTUNE MC-ICPMS (Thermo Fisher Scientific) via an AE2080 transfer line (Aquitaine Electronique, France) was used for Cl-CSIA. Further instrumental and methodological details, including linearity, precision, reproducibility and instrumental limits, may be found in Vinyes-Nadal, Masbou, et al. [41].

C and Cl isotope values are reported using the delta notation (δ) relative to the international reference standards Vienna PeeDee Belemnite (V-PDB) and Mean Ocean Chloride (SMOC), respectively, and expressed in per mil (‰):

$$\delta^h E(‰) = \left[\frac{R_E}{R_{E,std}} - 1\right] \quad (1)$$

where E is the considered element (C or Cl), h is the atomic mass of the heavy isotope (13 for C and 37 for Cl), R_E and $R_{E,std}$ are the isotope ratios of the element E ($^{13}C/^{12}C$ for carbon and $^{37}Cl/^{35}Cl$ for chlorine) in the sample and the corresponding reference standard, respectively. The analytical uncertainty is given as the standard deviation of the values obtained from multiple injections of each sample: two injections for $\delta^{13}C$ and three injections for $\delta^{37}Cl$.

The minimum carbon and chlorine isotopic shift considered before p,p′-MET degradation can be concluded ($\Delta\delta^hE$) is estimated by error propagation for both water and slurry matrixes, following Alvarez-Zaldívar et al. [25]. Details can be found in the Appendix A.

The fraction of a compound remaining as result of degradation at time t (f) can be calculated using a linearized Rayleigh equation:

$$f = \left(\frac{\delta^h E_t + 1}{\delta^h E_0 + 1}\right)^{\frac{1}{\varepsilon_E}} \quad (2)$$

where δ^hE_0 and δ^hE_t are the isotope values of element E at the beginning (0) and at any given time (t), respectively, and ε_E is the isotopic fractionation of element E. Subsequently, the extent of degradation, D (%), can be calculated as D (%) = (1 - f). For the estimation of the extent of p,p′-MET reductive dechlorination in the present study, the isotopic fractionation values previously obtained in [42] ($\varepsilon_C = -0.9 \pm 0.3$ ‰, $\varepsilon_{Cl} = -1.9 \pm 1.0$ ‰, $\Lambda_{C/Cl} = 0.4 \pm 0.1$) were used. The uncertainty of D (%) is calculated by error propagation following Thullner et al. [47], as described in the Appendix A.

Dual-element isotope fractionation was determined by the York regression method in 2D-isotope plots ($\Lambda_{C/Cl} = \Delta\delta^{13}C/\Delta\delta^{37}Cl$) incorporating the error measurement in both variables [48]. The ^{13}C and ^{37}Cl most depleted values found in the field site were considered as the origin for $\Lambda_{C/Cl}$ calculations, assuming them to be the most similar to the original isotopic composition of the contamination source. The uncertainty of $\Delta\delta$ values was calculated by error propagation. The uncertainty of Λ is reported showing the 95 % CI of the slope in the graphs. Statistical differences with the previously reported $\Lambda_{C/Cl}$ value [42] were assessed using statistical two-tailed z-score tests [48]. Differences were considered statistically significant at the $\alpha = 0.05$ confidence level.

2.6. Isomeric fraction

Changes in the isomeric proportion were evaluated by using the isomeric fraction of the p,p'-isomer for each compound ($IF_{p,p'\text{-isomer}}$):

$$IF_{p,p'-isomer} = \left(\frac{[p,p' - isomer]}{[p,p' - isomer] + [o,p' - isomer]}\right) \quad (3)$$

where if there is the same concentration of both isomers, $IF_{p,p'-isomer} = 0.5$, if there is a greater concentration of the p,p'-isomer, $IF_{p,p'-isomer} > 0.5$, and if there is a greater concentration of the o,p'-isomer, $IF_{p,p'-isomer} < 0.5$.

3. Results and discussion

3.1. Hydrogeochemical conditions and MET distribution

In general, the measured concentrations of p,p′-MET from slurry and water samples were of the same order as those detected during the excavation of the contaminated soil in 2005 and water samplings recorded since wells were installed in 2006 (Figure A2), reaffirming that this site is still highly contaminated. According to the hydrological conceptual model [45], rainfall in the area appears to directly affect the concentrations of MET and its transformation products in the trenches

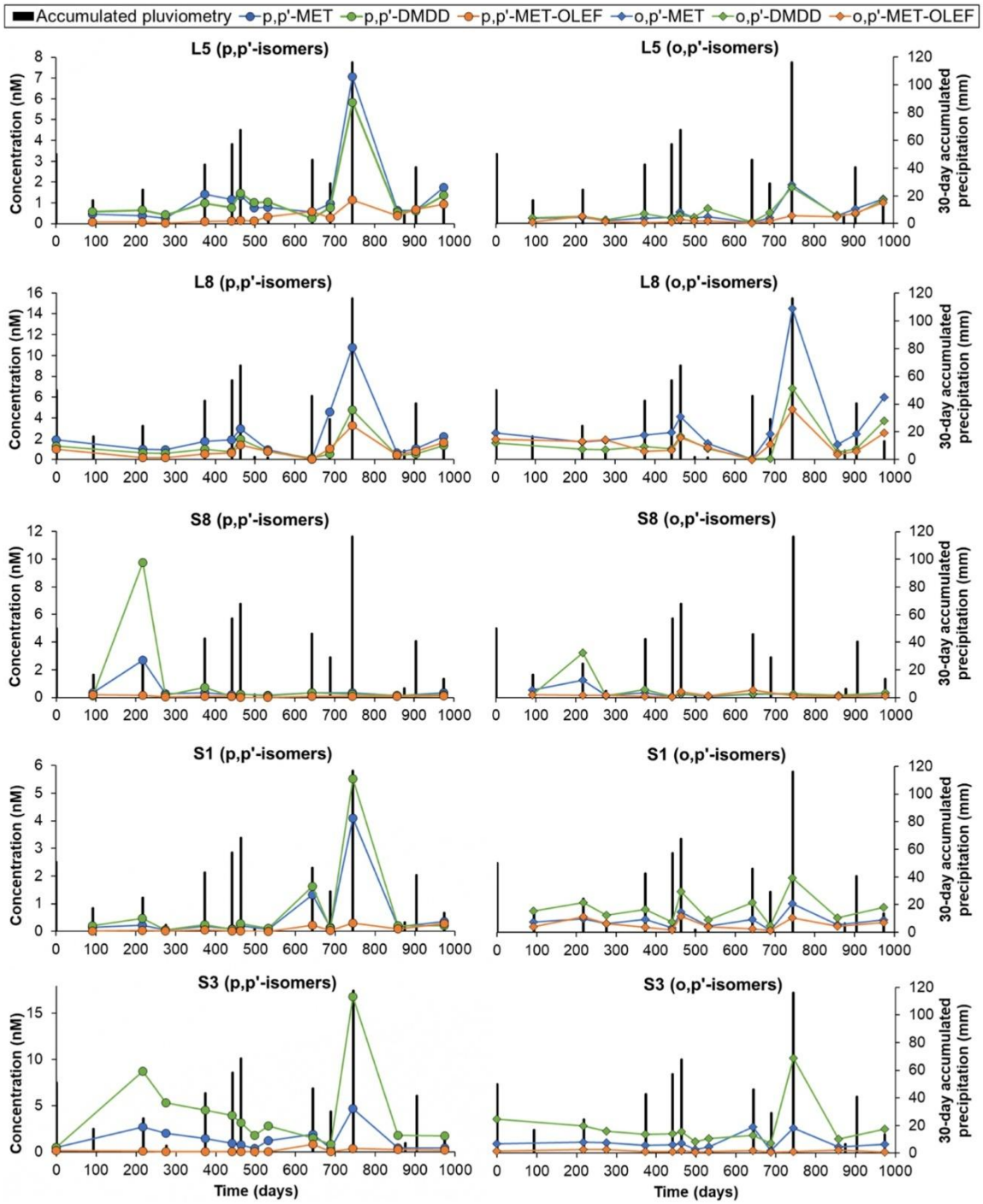

Fig. 2. Concentration of p,p'- (left panels) and o,p'- (right panels) isomers of MET (blue), DMDD (green) and MET-OLEF (orange) over time in water samples from wells L5, L8, S8, S1 and S3. Black vertical bars indicate the accumulated rainfall in mm during the 30-day before each sampling event.

and the aquifer water. Precipitation events mobilize MET and transformation products that, due to their affinity for the solid phase, primarily remain attached to the unsaturated part of the aquifer. This results in higher concentrations in the water phase after precipitation events (Fig. 2). The following discussion will be focused on the fate of MET isomers and transformation products, first in both trenches (L5 and L8 wells) and then in the aquifer, specifically within the influence zones of the three primary contamination sources: the chemical plant building (S8 well), the former disposal lagoon (S1 well) and the wastewater tank (S3 well and drilled piezometers S11, S12, and S13). Detailed information and further discussion can be found in the **Appendix A** (Tables A4 to A9).

3.1.1. MET fate in the interception trenches

The measured alkaline conditions in the trenches (pH = 11.3 ± 0.1 and 11.4 ± 0.1 in L5 and L8, respectively) are consistent with those observed between June 2010 and April 2013 by Torrentó et al. [45]. Both isomers of MET, and its transformation products, DMDD and MET-OLEF, were detected in the water of the trenches. Concentrations of the isomers of the transformation products were, in general, lower than those of MET isomers (Fig. 2). The concentrations of MET-OLEF isomers in L5 and L8, despite being lower than MET and DMDD concentrations, represent the highest levels of MET-OLEF detected in the site, pointing to the degradation of MET isomers through alkaline hydrolysis [42]. Low concentrations of MET-OLEF isomers are consistent with laboratory-scale experiments where p,p'-MET-OLEF was found to undergo further degradation through alkaline hydrolysis [42]. The detection of the two isomers of DMDD suggests mobilization from the unsaturated zone of the aquifer, since no microbial activity has been detected in the alkaline trench water.

3.1.2. MET fate in the aquifer

The physicochemical parameters of groundwater samples collected from well S8, in the chemical plant building area, and S1, in the former disposal lagoon area, suggest that oxidative conditions dominate in both wells, as previously suggested by Rodríguez-Fernández et al. [44]. In contrast, the lower dissolved oxygen and Eh values measured in well S3, in the wastewater tank area, indicate that reducing conditions are prevalent in this well. This aligns with the findings of Palau et al. [43] and Rodríguez-Fernández et al. [44].

Higher concentrations of the DMDD isomers than those of the MET isomers were detected in groundwater samples from the influence zones of the three primary contamination sources: the chemical plant building (S8 well), the former disposal lagoon (S1 well) and the wastewater tank (S3 well) (Fig. 2). In contrast, most of the slurry samples showed higher concentrations of MET isomers compared to DMDD isomers. This disparity in MET and DMDD concentrations between water and slurry samples aligns with laboratory-scale experiments, which demonstrated that DMDD (Log K_{ow} = 4.03, [49]) exhibits a greater affinity for the water phase, while MET (Log K_{ow} = 5.08, [19]) tends to partition into the solid phase [42].

The degradation of MET through reductive dechlorination accounts for the detection of DMDD in the wastewater tank area (S3 well and drilled piezometers S11, S12, and S13), where reducing conditions predominate. The presence of DMDD in groundwater and bottom-well slurry samples from wells S8 and S1 (Fig. 2), which exhibit predominantly oxidative conditions, can be explained by the fact that, as noted by Satsuma & Masuda [50], MET-degrading bacterial species do not always require strictly anoxic conditions for MET dechlorination into DMDD.

With regards to MET-OLEF, both p,p'- and o,p'-isomers, if detected, were found in lower concentrations compared to MET and DMDD. The presence of MET-OLEF in the water and slurry samples from the former disposal lagoon (S1 well) and the wastewater tank (S3 well and drilled piezometers S11, S12, and S13) areas can be attributed to the downstream proximity of these wells and piezometers to the pit and tank trench, respectively, where MET degradation via alkaline hydrolysis and higher concentrations of MET-OLEF were recorded. In contrast, it is unlikely that the MET-OLEF detected in the chemical plant building area (S8 well) originated from alkaline hydrolysis of MET, as the trenches are located downstream from this area. Instead, it is more plausible that the detected MET-OLEF in well S8 represents a residual contaminant. This interpretation is supported by evidence that p,p'-MET-OLEF, and to a lesser extent o,p'-MET-OLEF, are significant impurities in commercial p,p'-MET formulations, as described by West et al. [16].

Finally, regarding the drilled piezometers in the wastewater tank area (S11, S12, and S13), the highest concentrations of the isomers of MET and transformation products were detected at depths ranging from 3.9 to 8.6 m. Since the average piezometric level in this area was measured at 8.7 ± 0.5 m, the highest concentrations of the MET isomers were found in the unsaturated zone of the aquifer (Figure A3). Specifically, the highest contents were detected at the contact between the detrital and carbonate units, as well as in fractures within the carbonate unit, where the hydrological conceptual model suggest the occurrence of preferential water and contaminant flow.

3.2. Insights from CSIA on MET degradation and transport

Carbon and chlorine isotope data obtained from both water and slurry samples are detailed in Appendix A (Tables A10 and A11) and discussed as follows. Since samples from the original contamination sources were not available, the ^{13}C and ^{37}Cl most depleted values found in the field site, which were found in the slurry samples from the piezometers drilled in the wastewater tank area, were considered as the assumed isotopic signature of the contamination source in that area. Therefore, as discussed below, to quantify the extent of the p,p'-MET degradation through reductive dechlorination in the wastewater tank area samples, the most depleted $\delta^{13}C$-p,p'-MET value found in the area (-32.89 ± 0.03 ‰; S12 at 8.1 m depth) was used as the initial value.

3.2.1. MET alkaline hydrolysis in the interception trenches

As discussed in Section 3.1.1, the detection of p,p'- and o,p'-MET-OLEF, as well as the previous evidences for trichloromethane [45], pointed to degradation of p,p'- and o,p'-MET through alkaline hydrolysis in both interception trenches. Alkaline hydrolysis of p,p'-MET at a similar pH (11.0 ± 0.1) than that measured in the trenches was already demonstrated in a previous study [42], where C and Cl isotope effects associated with this degradation pathway were determined. Since no reliable isomeric-specific isotopic values were obtained from L5 water samples, due to the high chromatographic background, the discussion about CSIA results is focused only on the pit trench (L8).

Fig. 3 shows the evolution with time of $\delta^{13}C$ values of the p,p'- and o,p'-isomers of MET and DMDD in water collected from L8. According to the fact that neither carbon nor chlorine isotopic fractionation of MET is expected for alkaline hydrolysis [42], $\delta^{13}C$ and $\delta^{37}Cl$ values of the two isomers of MET slightly varied with time, with maximum shifts in $\delta^{13}C$ of $\Delta\delta^{13}C$ = 0.6 ± 0.4 ‰ and 0.4 ± 0.2 ‰ for p,p'- and o,p'-MET, respectively, and maximum $\Delta\delta^{37}Cl$ values of 0.2 ± 0.4 ‰ for p,p'-MET (Table A10). These variations fall within the isotopic extraction and analytical uncertainty range for carbon ($\Delta\delta^{13}C_{extraction}$ = ± 0.5 ‰) and chlorine ($\Delta\delta^{37}Cl_{extraction}$ = ± 0.7 ‰) associated with pesticide extraction, as determined during the method setup and tests described by Vinyes-Nadal, Masbou, et al. [41]. For p,p'-MET-OLEF, however, higher $\Delta\delta^{13}C$ values up to 1.3 ± 0.5 ‰ were observed. This might indicate that further degradation of MET-OLEF by alkaline hydrolysis induces C isotopic fractionation, although no experimental data are available to confirm this hypothesis.

The DMDD isomers detected in the trench water, which we attributed to the result of MET degradation in the unsaturated part of the aquifer and its subsequent mobilization into the trenches since no DMDD is generated from the alkaline hydrolysis of MET [42], showed $\Delta\delta^{13}C$ values up to 1.7 ± 0.3 ‰ and 1.0 ± 0.1 ‰ for p,p'- and o,p'-DMDD,

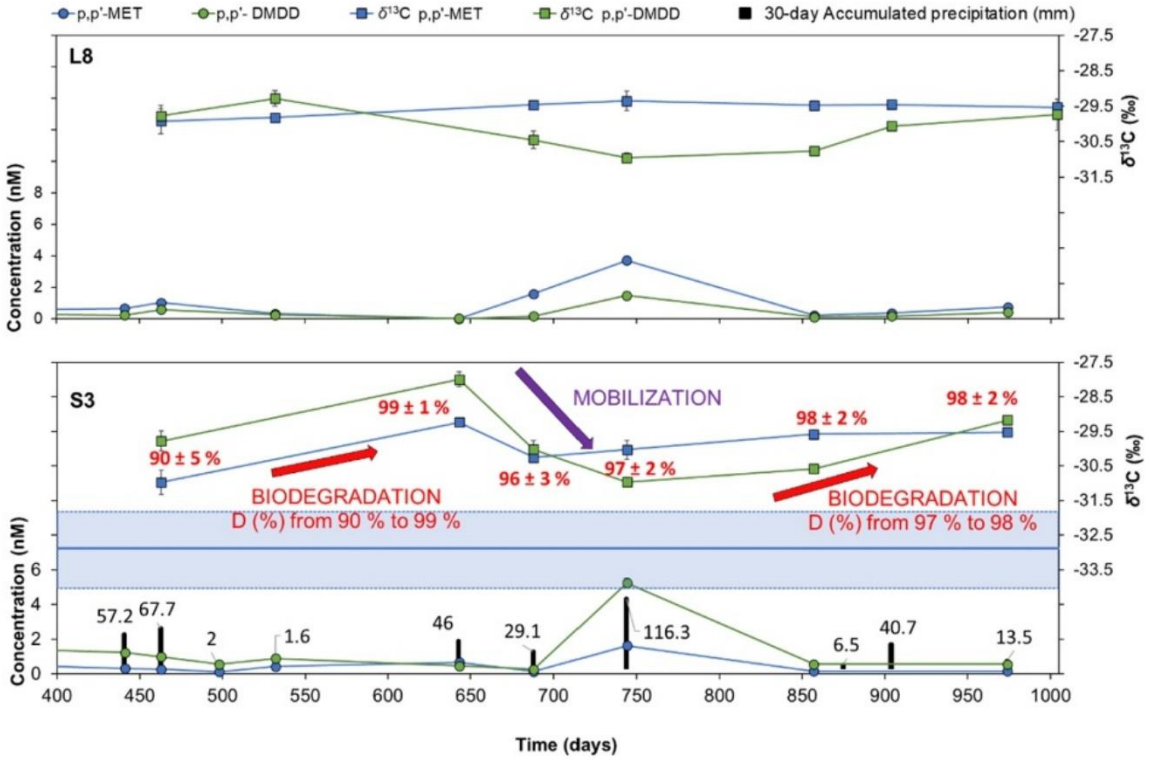

Fig. 3. Concentration and $\delta^{13}C$ values of p,p'-isomers of MET and DMDD with time in water samples from wells L8 (upper panel, pit trench water) and S3 (lower panel, wastewater tank area groundwater). Error bars display the uncertainty in concentration (5 % error) and $\delta^{13}C$ (calculated as the standard deviation of the values obtained from multiple injections) values. In most cases, error bars are smaller than the symbols. Black vertical bars indicate the accumulated rainfall in mm during the 30-day before each sampling event. For S3, the horizontal blue bar represents the assumed isotopic signature of the source (i.e., the most depleted $\delta^{13}C$-p,p'-MET value found in the area, −32.89 ± 0.03 ‰; S12 at 8.1 m depth, with an assumed uncertainty of ± 1 ‰). The extent of p,p'-MET degradation, D (%), was calculated following the linearized Rayleigh equation (Eq. 2) and using the carbon isotopic fractionation value ($\varepsilon_C = -0.9$ ‰) associated with p,p'-MET reductive dechlorination [42]. The uncertainty of D (%) was calculated by error propagation, following Thullner et al# [47], as described in the Appendix A.

respectively (Fig. 3). This variability might be attributed to isotopic fractionation due to potential DMDD hydrolysis in the alkaline trenches water, or to mobilization into the trench of DMDD with variable extents of reductive dechlorination [42].

3.2.2. *Unravelling and quantifying MET degradation pathways in the aquifer*

For groundwater samples collected from the chemical plant building area (S8) and the disposal lagoon area (S1), reliable isotopic values could not be obtained due to the low concentrations of MET and transformation products and/or a high chromatographic background. It was, however, possible to obtain a $\delta^{13}C$ value of p,p'-MET (-30.842 ± 0.003 ‰) from one of the S8 bottom-well slurry samples. In contrast, a more in-depth discussion of CSIA application is possible in the wastewater tank area, since reliable isotopic ratios were obtained from the slurry samples obtained from the newly drilled piezometers (S11, S12, S13), and from groundwater and bottom-slurry samples from well S3.

For the S3 bottom-well slurry samples, the obtained $\delta^{13}C$ value of p,p'-MET (-31.20 ± 0.02 ‰) was consistent with the one measured in the slurry from well S8 (-30.842 ± 0.003 ‰).

As detailed in Table A11, reliable carbon isotope ratios were obtained for the two isomers of MET and DMDD and for p,p'-MET-OLEF for most of the slurry-core samples from the drilling of piezometers S11, S12 and S13. However, $\delta^{37}Cl$ values were only obtained for p,p'-MET. Significant shifts in the $\delta^{13}C$ and $\delta^{37}Cl$ values of the target compounds were observed among the slurry samples. Considering the most negative values detected in the area (-32.89 ± 0.03 ‰; S12 at 8.1 m depth), maximum shifts in $\delta^{13}C$ for p,p'-MET and p,p'-DMDD were $\Delta\delta^{13}C = 3.1 \pm 0.1$ and 4.6 ± 0.1 ‰, respectively, while changes in $\delta^{13}C$ values of p,p'-MET-OLEF, o,p'-MET and o,p'-DMDD were up to 1.9 ± 0.3 ‰. Significant changes were also observed in $\delta^{37}Cl$ values of p,p'-MET, with a $\Delta\delta^{37}Cl$ value of up to 4.8 ± 0.5 ‰ (Table A9). Minimum isotopic shifts of $\Delta\delta^{13}C \approx 2.1$ ‰ and $\Delta\delta^{37}Cl \approx 1.4$ ‰ were considered before degradation can be concluded (Table A2), following Alvarez-Zaldívar et al. [25], as detailed in the Appendix A. Therefore, the observed shifts clearly indicated degradation processes.

Assuming a single source of p,p'-MET in the wastewater tank area, the isotopic values of p,p'-MET were plotted in a $\Delta\delta^{13}C/\Delta\delta^{37}Cl$ graph to further explore the MET degradation mechanisms (Fig. 4). The obtained $\Lambda_{C/Cl}$ value of 0.42 ± 0.06 ($R^2 = 0.98$) is statistically indistinguishable ($p > 0.05$) from the $\Lambda_{C/Cl}$ value of 0.44 ± 0.14 ($R^2 = 0.97$) obtained in the laboratory-scale reductive biodegradation experiment performed with bottom-well slurry from well S3 [42]. The evidence that p,p'-MET was undergoing reductive dechlorination is consistent with the detection of p,p'-DMDD. Considering the most negative detected $\delta^{13}C$ value (-32.89 ± 0.03; S12 at 8.1 m depth), the extent of p,p'-MET degradation for each slurry sample was estimated applying Eq. 2 and using the carbon isotopic fractionation value associated with p,p'-MET reductive dechlorination estimated in [42]. A degree of p,p'-MET degradation of up to 91 ± 3 % was estimated (Table A3), confirming the hypothesis of intense reductive dechlorination in this area.

The distribution of $\delta^{13}C$ and $\delta^{37}Cl$-p,p'-MET values with depth (Figure A4) indicates detection of degradation in both the saturated and unsaturated parts of the aquifer, since ^{13}C and ^{37}Cl-enriched isotopic values were detected below (e.g., sample collected from S12 at 12.4 m) and above (e.g., samples collected at depths of 3.9, 6.3 and 6.0 m from wells S11, S12 and S13, respectively) the average piezometric level of the area (8.7 ± 0.5 m). This finding might indicate that reductive dechlorination of MET isomers could occur in the unsaturated part of the aquifer followed by mobilization of the degraded compounds into the

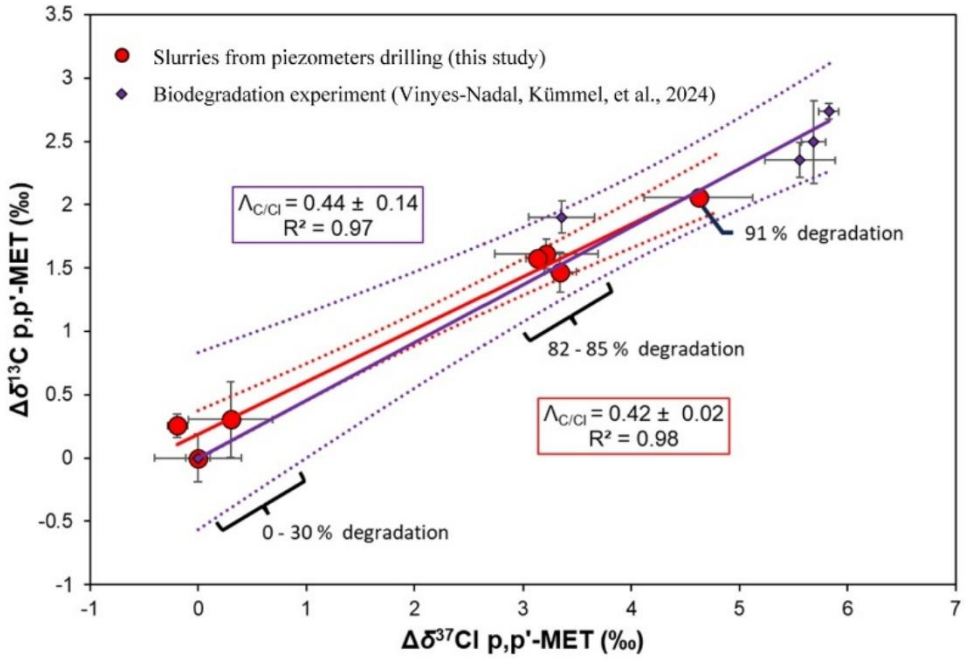

Fig. 4. Dual isotope plot ($\Delta\delta^{13}C$ vs. $\Delta\delta^{37}Cl$) of p,p'-MET in field samples in comparison with data from the biotic reductive dechlorination experiment performed with S3 bottom-well slurry [42]. Error bars display the uncertainty calculated by error propagation. The slope (Λ value) was calculated by the York regression method. The uncertainty (dashed lines) is shown as 95 % CI.

saturated zone, in alignment with the hydrological conceptual model. This would also be in accordance with the hypothesis of DMDD isomers mobilization from the unsaturated zone into the trenches. Furthermore, it aligns with the findings of Satsuma & Masuda [50] that bacterial species do not always require a strict anoxic environment for dechlorination of MET. Nevertheless, degradation likely also occurred in the saturated zone under anoxic conditions, as observed in the experiments with S3 bottom-well slurry [42]. Most of the $\delta^{13}C$ values of p,p'-DMDD were more enriched than the most negative $\delta^{13}C$-p,p'-MET value found in the area (-32.89 ‰; S12 at 8.1 m depth) (Figure A5). Assuming a single source of p,p'-MET in this area, this indicates further degradation of p,p'-DMDD. A similar pattern was observed for o,p'-MET and o,p'-DMDD, except in the sample collected from S13 at a depth of 6 m (Table A11).

Compared to the slurry-core samples, $\delta^{13}C$ values of p,p'-MET in the bottom-slurry samples (S3 and S8) were in general more enriched in ^{13}C (Figure A6), likely indicating a higher extent of degradation. In this sense, $\delta^{13}C$ values of p,p'-MET in groundwater samples from well S3, which ranged between −31.0 and −29.2 ‰ (Table A10), were even more enriched than those from all the slurry samples and similar to those obtained for the pit trench water (-29.9 to −29.4 ‰).

Fig. 3 illustrates the temporal evolution of $\delta^{13}C$ values of the p,p'-isomers of MET and DMDD in S3 groundwater samples, alongside the accumulated rainfall during the 30-day preceding each sampling event. Three distinct precipitation intervals were identified: two intervals with lower rainfall (the first from day 463 to day 643, with an average rainfall of 0.7 mm/day, and the second from day 744 to day 974, with an average rainfall of 0.6 mm/day), separated by a rainier interval (from day 643 to day 744, with an average rainfall of 1.7 mm/day). During the rainier interval, a trend with time towards more negative $\delta^{13}C$ values was observed for p,p'-MET ($\Delta\delta^{13}C = -0.8 \pm 0.3$ ‰) and p,p'-DMDD ($\Delta\delta^{13}C = -3.0 \pm 0.4$ ‰). On the contrary, during the lower rainfall periods, $\delta^{13}C$ values tended to become more positive, with maximum shifts in the first interval of 1.7 ± 0.2 and 1.8 ± 0.2 ‰ for p,p'-MET and p,p'-DMDD, respectively. Throughout the second lower rainfall interval, p,p'-MET and p,p'-DMDD $\delta^{13}C$ values increased 0.5 ± 0.3 and 1.8 ± 0.3 ‰, respectively. Similar but less pronounced shifts were detected for o,p′-MET and o,p′-DMDD (Table A10). These results indicate either the prevalence of degradation processes of MET isomers (^{13}C enrichment trends), or the prevalence of mobilization by rainwater of nondegraded MET, or with a lower extent of degradation (^{13}C depletion trends), likely retained in the fractures from the carbonate unit, where high concentration of MET with more negative $\delta^{13}C$ values were detected (Figure A4). Although no $\delta^{37}Cl$ data are available for discerning degradation mechanisms, MET isomers biodegradation through reductive dechlorination is assumed to occur releasing DMDD isomers, as it was observed in laboratory-scale experiments using slurry collected from well S3 [42]. Compared to the most negative $\delta^{13}C$ value detected in the area (-32.89 ± 0.03 ‰), shifts in $\delta^{13}C$ were clearly indicative of degradation, being higher than the minimum isotopic shift of $\Delta\delta^{13}C \approx 1.6$ ‰ considered before degradation can be concluded in water samples (Table A2). The extent of p,p'-MET biodegradation was therefore calculated, assuming again the lowest $\delta^{13}C$ value detected in the area (-32.89 ± 0.03 ‰) as the initial value for calculations. Despite the mobilization of less degraded p,p'-MET, the calculated extent of biodegradation was higher than 90 ± 3 % during all the monitoring period (Table A3 and Fig. 3). As observed in the slurry-core samples, most of the $\delta^{13}C$ values of p,p'-DMDD were more enriched than the most negative $\delta^{13}C$-p,p'-MET value found in the area (-32.89 ‰; S12 at 8.1 m depth), indicating further degradation of p,p'-DMDD.

3.3. Enhanced understanding of MET fate through IF integrated with CSIA

The ranges of $IF_{p,p'\text{-isomer}}$ values for MET, DMDD and MET-OLEF estimated for all water and slurry samples analyzed in this study are summarized in Fig. 5. Detailed data can be found in the Appendix A (Tables A5, A7, A8 and A9).

The highest average $IF_{p,p'\text{-MET}}$ values were detected in all slurry samples: the bottom-well slurry samples from the chemical plant (S8, 0.99 ± 0.01), and the bottom-well slurry samples (S3, 0.84 ± 0.07) and slurries collected during the drilling of piezometers (S11, S12 and S13, 0.80 ± 0.08) from the wastewater tank area. These results align with the $IF_{p,p'\text{-isomer}}$ range (0.81–0.94) estimated for MET from concentration

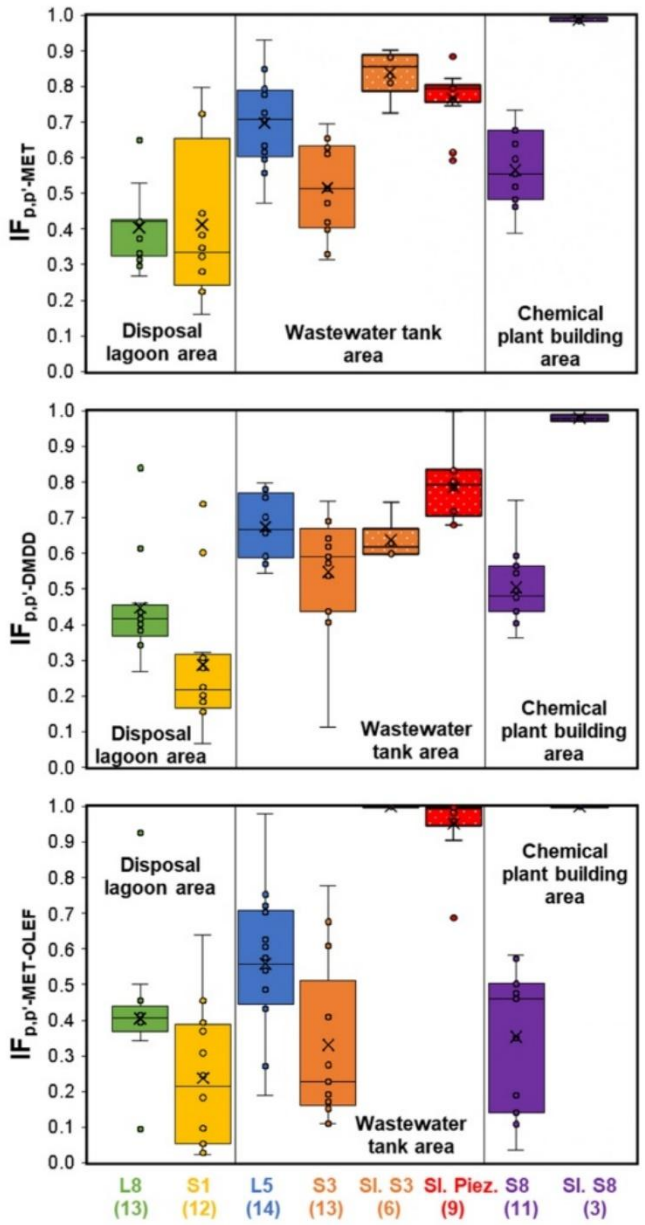

Fig. 5. Isomeric fraction ($IF_{p,p'\text{-isomer}}$) of MET (upper panel), DMDD (middle panel) and MET-OLEF (lower panel) from all the field samples, including water samples (L8, S1, L5, S3 and S8), bottom-well slurry samples (Sl. S3 and Sl. S8), and slurry samples from the newly drilled piezometers (Sl. Piez). For each group of samples, box shows inter-quartile range, black cross shows the average value, horizontal line shows the median, and whiskers show the data extent within 1.5 times the interquartile range, leaving the outliers (circles) out. The number of measurements for each group of samples is shown in parenthesis. Note that for some samples in which o,p'-MET-OLEF was below detection limit, a value of $IF_{p,p'\text{-MET-OLEF}} = 1.0$ was assigned.

data reported by [21] for sediment samples (up to 35 cm depth) collected from an industrial wastewater drainage in Berlin (Germany), near a chemical production plant that manufactured MET and other chlorinated pesticides until 1990. On the contrary, significantly lower $IF_{p,p'\text{ MET}}$ values were detected in groundwater samples from wells located in the same areas, with average values of 0.57 ± 0.11 and 0.52 ± 0.13 from the chemical plant (S8) and the wastewater tank (S3) areas, respectively. A similar tendency may be observed in the $IF_{p,p'\text{-isomer}}$ values for DMDD and MET-OLEF (Fig. 5).

Unlike enantiomers, which typically exhibit enantioselectivity only in biologically mediated processes due to isomers identical physical and chemical properties but differing enzyme interactions [51,52], constitutional isomers (e.g., p,p' and o,p'-MET, p,p'- and o,p'-DDT) may display selectivity in non-biological processes as well. Since these isomers often possess distinct physicochemical properties, variations in environmental behaviour might be expected, and thus processes such as transport, phase transfer, degradation, or environmental aging might influence the isomeric composition in the environment [53].

The differences in IF values for MET between the slurry and the water samples lead to the distinction of two differentiated groups of samples in IF vs. $\delta^{13}C$ plots for both isomers (Fig. 6). For the slurry samples from the wastewater tank area (S3 bottom-well and from piezometers drilling), changes in $\delta^{13}C$ values of p,p'-MET and o,p'-MET did not correlate with variations in $IF_{p,p'\text{-MET}}$ and $IF_{o,p'\text{-MET}}$ values. The same trend was observed for $IF_{p,p'\text{-MET}}$ vs. $\delta^{37}Cl$ (Figure A7). These results suggest that MET biodegradation through reductive dechlorination is not an isomeric-selective process. Accordingly, no remarkable differences were observed between average $IF_{p,p'\text{-isomer}}$ values of MET and DMDD (Fig. 5).

Once isomeric selectivity was discarded for biodegradation, the observed differences in IF point to isomeric fractionation, with enrichment of the o,p'-isomers of the three compounds, during contaminant transfer from solid to water phases. This preferential presence of o,p'-isomers in the water phase may be attributed to differences in the solubility of the isomers. Although specific data on the solubility of o,p'-MET, o,p'-DMDD and o,p'-MET-OLEF in water is not available in the literature, it is expected that the o,p'-isomers are more soluble than the p,p'-isomers based on the fact that symmetrical molecules tend to be less soluble than their asymmetrical counterparts [54,55]. In the p,p'-isomers, the methoxy groups (-OCH_3) are symmetrically positioned on the para (p) positions of the benzene rings, resulting in a more symmetrical molecule. Conversely, the methoxy groups in the o,p'-isomers are located asymmetrically, one in the ortho (o) position on one ring and the other in the para (p) position on the other ring, leading to a less symmetrical structure.

This isomeric fractionation during transfer processes has also been reported for DDT [40,53], for which it can be linked to differences in physicochemical properties between the two DDT isomers (solubility of 0.005 mg/L for p,p'-DDT, and 0.085 mg/L for o,p'-DDT, [56]), due to the different stereochemical orientation of the chlorine atoms at the phenyl rings. Similarly to our findings, terrestrial soil samples from the largest producer of DDT in Germany, located in the industrial mega-site of Bitterfeld–Wolfen, were found to be depleted in o,p'-DDT compared to the corresponding subaquatic sediments originated from the same riverine particulate matter [53].

Contrary to our findings, Kucher et al. [53] assumed isomeric selectivity for reductive dechlorination of DDT. This assumption is based on the remarkable differences in average IF values between DDT and the degradation product dichlorodiphenyldichloroethane (DDD) observed in fluvial sediments collected downstream from a discharge outlet of a former chemical production plant in Berlin [53]. However, those differences could also be explained by the fact that DDT isomers present important water solubility differences, as commented previously, while DDD isomers exhibit much similar water solubilities (0.09 mg/L for p,p'-DDD, and 0.10 mg/L for o,p'-DDD, [57]).

For DDT dehydrochlorination, Kucher et al. [53] assumed that it does not result in significant IF shifts. This is based on similar IF values between DDT and its degradation product dichlorodiphenyldichloroethylene (DDE) detected in marine sediments from a highly contaminated site in Palos Verdes, California, where dehydrochlorination was the dominant DDT transformation process. In this case, given the parallel differences in water solubility between the two DDE isomers (0.011 mg/L for p,p'-DDE, and 0.140 mg/L for o,p'-DDE, [56]) and between the two DDT isomers, it is unlikely that variations in IF between the parental compound and the transformation product are controlled by solubility differences alone. For MET, our results also support that dehydrochlorination does not result in significant IF shifts, based on the

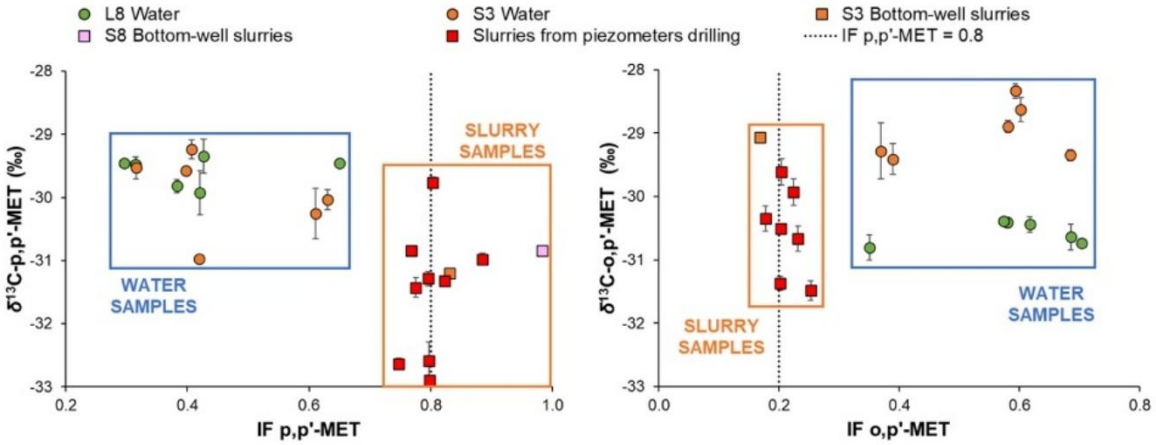

Fig. 6. Comparison of $\delta^{13}C$ values of p,p'-MET (left panel) and o,p'-MET (right panel) vs. $IF_{p,p'\text{-MET}}$ and $IF_{o,p'\text{-MET}}$, respectively, for the water and slurry field samples. Error bars display the uncertainty calculated as the standard deviation of the values obtained from multiple injections. The vertical lines show the average values of $IF_{p,p'\text{-MET}}$ and $IF_{o,p'\text{-MET}}$ from the slurry samples collected in the wastewater tank area (S3 bottom-well slurries and slurries collected during the drilling of piezometers S11, S12 and S13).

$IF_{p,p'\text{-isomer}}$ stability and absence of a clear trend in the tank and pit trenches (L5 and L8), where dehydrochlorination of MET through alkaline hydrolysis is occurring. Accordingly, no remarkable differences in the average $IF_{p,p'\text{-isomer}}$ values of MET and the transformation product MET-OLEF were detected (Fig. 5).

The preferential mobilization of o,p'-isomers over p,p'-isomers, likely due to higher solubility of the former, could also have resulted in isomeric fractionation during the contaminants transport from the upstream trenches (L5 and L8) to the downstream groundwater (S3 and S1). Indeed, average $IF_{p,p'\text{-isomer}}$ values for MET, DMDD and MET-OLEF in groundwater samples from wells located downstream of the tank and pit trenches (S3, 0.52 ± 0.13, 0.55 ± 0.17 and 0.33 ± 0.23; and S1, 0.41 ± 0.22, 0.29 ± 0.19 and 0.24 ± 0.20, respectively), were lower than those from the corresponding trench (L5, 0.70 ± 0.12, 0.67 ± 0.09 and 0.56 ± 0.20; and L8, 0.41 ± 0.10, 0.45 ± 0.14 and 0.56 ± 0.20, respectively) (Fig. 5).

The preferential mobilization of the o,p'-isomers versus the p,p'-isomers would also have resulted in increasing $IF_{p,p'\text{-isomer}}$ values with time. This fact would explain the differences in $IF_{p,p'\text{-isomer}}$ values of MET, DMDD, and MET-OLEF between pollution areas. Indeed, lower $IF_{p,p'\text{-isomer}}$ values were detected in the disposal lagoon area compared to those in the wastewater tank and chemical plant building areas (Fig. 5). Given that the construction of the disposal lagoon and, therefore the pollution of that area, occurred later than that of the wastewater tank and chemical plant areas, it can be hypothesized that the preferential mobilization of the o,p'-isomers in this area has been occurring for a shorter period of time, resulting in lower $IF_{p,p'\text{-isomer}}$ values. However, other processes could also have contributed to these differences. The disposal lagoon was exposed to the atmosphere for an uncertain period of time and, thus, processes like volatilization or photodegradation may have led to the observed isomeric fractionation. Furthermore, we cannot rule out the possibility that the initial composition of pollutants, including the proportions of isomers, differed between the contaminated areas.

Overall, although the use of IF combined with CSIA has enhanced our understanding of the fate of MET and its degradation products in the study site, the complexity of the site and the potential masking of IF values due to the differing physicochemical properties between isomers suggests that further laboratory experiments and systematic studies are necessary. These steps will help definitively link IF variations to specific processes, enabling a wider application of this combined approach for constitutional isomers as a tool for tracing environmental processes. Nonetheless, these results underscore the fundamental importance of considering the different physicochemical properties that constitutional isomers may have when its IF behaviour is interpreted and emphasizes the value of coupling CSIA with IF for improved comprehension of the behaviour of these compounds in the environment.

4. Conclusions

This study presents the first evaluation of combined use of IF and CSIA of MET and its transformation products from slurry and water samples collected over nearly three years, to improve the understanding of MET fate in the multi-polluted site in Òdena, Catalonia. Hydrogeochemical data evidenced the direct influence of rainfall on the MET isomers concentrations and their transformation products in the interception trenches and the aquifer. In the trenches water, the detection of MET-OLEF isomers as degradation products, along with minimal carbon (0.6 ± 0.4 ‰) and chlorine (0.2 ± 0.4 ‰) isotopic shifts, supported the occurrence of MET isomers degradation through alkaline hydrolysis [42].

In the aquifer, while oxidizing conditions dominated in the chemical plant and disposal lagoon areas, the wastewater tank area evidenced more reducing conditions. The detection of DMDD isomers suggested the occurrence of reductive dechlorination processes, which was corroborated by ME-CSIA data. Specifically, isotopic analysis of MET in slurry samples from the wastewater tank area, plotted on a $\Delta\delta^{13}C/\Delta\delta^{37}Cl$ graph, yielded a $\Lambda_{C/Cl}$ value (0.42 ± 0.06; $R^2 = 0.98$) statistically indistinguishable ($p > 0.05$) from laboratory-scale reductive biodegradation experiment results (0.44 ± 0.14; $R^2 = 0.97$) performed using slurry from the same area [42]. Reductive dechlorination was likely occurring in the three contamination areas, according to the fact that reductive dechlorination can occur under both oxic and hypoxic conditions [50].

Over time, $\delta^{13}C$ data from groundwater samples highlighted periods with intensified MET degradation versus those dominated by mobilization of non-degraded or less degraded MET under rainier conditions. This mobilization likely occurred through fractures in the carbonate unit, where the highest MET concentrations coupled to the most negative $\delta^{13}C$ values were recorded. Notably, the p,p′-MET concentrations measured in these fractures (up to 8411 nmol/g) are, to our knowledge, the highest ever reported in environmental soil samples. By applying the carbon isotopic fractionation value associated with p,p′-MET reductive dechlorination ($\varepsilon_C = -0.9$ ‰) obtained from previous laboratory experiments [42], the percentage of p,p′-MET degradation was calculated for both slurry and water samples. Despite the mobilization of non-degraded contaminant, the extent of natural attenuation of p,p′-MET exceeded 89 % throughout the study.

The combined use of CSIA and IF suggested that alkaline hydrolysis and reductive dechlorination of MET isomers are not isomer-selective processes. The observed differences in IF between slurry and water samples, and between upstream and downstream wells, pointed to varied environmental behaviours among isomers, likely due to differences in solubility between p,p'- and o,p'-isomers of MET, DMDD and MET-OLEF. These findings, consistent with previous studies for DDT [40,53], imply that isomeric-specific physicochemical properties, such as solubility, impact isomers environmental distribution.

These results underscore the importance of considering physicochemical differences between constitutional isomers to better understand their environmental fate. The integrated use of CSIA and IF offered insight into the behaviours of MET isomers, illustrating the significance of these tools for complex environmental systems. Overall, the combined application of ME-CSIA and IF proved valuable for tracking MET transformation processes in a complex fractured aquifer. These insights will assist decision-makers in developing targeted remediation strategies for sites contaminated with MET, advancing the field's understanding of environmental dynamics of isomeric pesticides.

Environmental implication

The organochlorine pesticide methoxychlor poses significant risks to the environment and human health due to its toxicity and potential bioaccumulation in the food chain. Understanding methoxychlor environmental behavior is essential for risk mitigation. This study demonstrates that the combined use of isomeric fraction and isotopic analysis effectively identifies and allows quantifying the extent of methoxychlor biodegradation in the field. Isotopic data also allowed distinguishing low rainfall periods dominated by biodegradation from wetter periods dominated by mobilization of less degraded methoxychlor. Finally, it was evidenced that the environmental behavior of methoxychlor constitutional isomers is influenced by their different physicochemical properties. This work provides decision-makers with crucial insights for effective remediation strategies.

CRediT authorship contribution statement

Torrentó Clara: Writing – review & editing, Writing – original draft, Supervision, Resources, Project administration, Methodology, Investigation, Funding acquisition, Formal analysis, Data curation, Conceptualization. **Soler Albert:** Writing – review & editing, Resources, Project administration, Funding acquisition. **Otero Neus:** Writing – review & editing, Supervision, Resources, Project administration, Funding acquisition. **Gil-Villalba Sergio:** Writing – review & editing, Investigation, Conceptualization. **Rosell Mònica:** Writing – review & editing, Investigation, Conceptualization. **Vinyes-Nadal Martí:** Writing – original draft, Visualization, Validation, Methodology, Investigation, Formal analysis, Data curation, Conceptualization.

Declaration of Competing Interest

The authors declare that they have no known competing financial interests or personal relationships that could have appeared to influence the work reported in this paper.

Acknowledgements

This study was supported by PACE (CGL2017-87216-C4-1-R), REMECLOR (PDC2021-120861-C21), and PASITO (CNS2022-135543) projects, all funded by MICIU/AEI/10.13039/501100011033 and by European Union NextGenerationEU/PRTR. Funding was also received from the ADVANCE4WATER-ISOTRACE (PID2022-139911OB-C4–01) project, funded by MICIU/AEI/10.13039/501100011033/FEDER,UE, and from the European Union's Horizon 2020 research and innovation programme under the Marie Sklodowska-Curie grant agreement No 837873. This work was also partly supported by the Generalitat de Catalunya through a Consolidate Research Group (2021SGR 00308). M. Vinyes Nadal received a PhD grant (FPU18/03862) from the "*Ayudas de Formación de Profesorado Universitario*" program of the Spanish Ministry of Universities and a small help for consumables from *Accions de Suport de l'Institut de Recerca de l'Aigua (IdRA) a la Recerca de Joves Investigadors* 2021, 2022 and 2023. The authors would like to thank the Technological Centers of the University of Barcelona (CCiT-UB) for the technical assistance. The authors are also thankful for the use of the analytical facilities of the Laboratories for Stable Isotopes (LSI) and the Centre for Chemical Microscopy (ProVIS) at UFZ Leipzig.

Appendix A. Supporting information

Supplementary data associated with this article can be found in the online version at doi:10.1016/j.jhazmat.2025.137447.

Data availability

Data will be made available on request.

References

[1] Basavarajappa, M.S., Craig, Z.R., Hernández-Ochoa, I., Paulose, T., Leslie, T.C., Flaws, J.A., 2011. Methoxychlor reduces estradiol levels by altering steroidogenesis and metabolism in mouse antral follicles in vitro. Toxicol Appl Pharmacol 253 (3), 161–169.
[2] Chen, G. (2014). Methoxychlor. Encyclopedia of Toxicology: Third Edition, 3, 254–255. https://doi.org/10.1016/B978-0-12-386454-3.00162-7.
[3] Harris, M.O., Miller, L.L., Little, S., McClure, P., Sutton, W., 2002. Toxicological profile for methoxychlor. ATSDR.
[4] Frye, C., Bo, E., Calamandrei, G., Calza, L., Dessì-Fulgheri, F., Fernández, M., Fusani, L., Kah, O., Kajta, M., Le Page, Y., 2012. Endocrine disrupters: a review of some sources, effects, and mechanisms of actions on behaviour and neuroendocrine systems. J Neuroendocrinol 24 (1), 144–159.
[5] Staub, C., Hardy, V.B., Chapin, R.E., Harris, M.W., Johnson, L., 2002. The hidden effect of estrogenic/antiandrogenic methoxychlor on spermatogenesis. Toxicol Appl Pharmacol 180 (2), 129–135.
[6] Anderson, R.L., DeFoe, D.L., 1980. Toxicity and bioaccumulation of endrin and methoxychlor in aquatic invertebrates and fish. Environ Pollut Ser A, Ecol Biol 22 (2), 111–121.
[7] Kim, J. Y., Yi, B. R., Go, R. E., Hwang, K. A., Nam, K. H., Choi, K. C., 2014. Methoxychlor and triclosan stimulates ovarian cancer growth by regulating cell cycle-and apoptosis-related genes via an estrogen receptor-dependent pathway. Environ Toxicol Pharmacol 37 (3), 1264–1274.
[8] ATSDR. (2022). ATSDR's Substance Priority List. ⟨https://www.atsdr.cdc.gov/spl/index.html#⟩.
[9] Stuchal, L.D., Kleinow, K.M., Stegeman, J.J., James, M.O., 2006. Demethylation of the pesticide methoxychlor in liver and intestine from untreated, methoxychlor-treated, and 3-methylcholanthrene-treated channel catfish (Ictalurus punctatus): evidence for roles of CYP1 and CYP3A family isozymes. Drug Metab Dispos 34 (6), 932–938.
[10] UN. (2023). Stockholm convention on persistent organic pollutants (POPS).
[11] Affum, A.O., Acquaah, S.O., Osae, S.D., Kwaansa-Ansah, E.E., 2018. Distribution and risk assessment of banned and other current-use pesticides in surface and groundwaters consumed in an agricultural catchment dominated by cocoa crops in the Ankobra Basin, Ghana. Sci Total Environ 633, 630–640.
[12] Cruzeiro, C., Rocha, E., Pardal, M.Â., Rocha, M.J., 2016. Seasonal-spatial survey of pesticides in the most significant estuary of the Iberian Peninsula–the Tagus River estuary. J Clean Prod 126, 419–427.
[13] Prajapati, S., Challis, J.K., Jardine, T.D., Brinkmann, M., 2022. Levels of pesticides and trace metals in water, sediment, and fish of a large, agriculturally dominated river. Chemosphere 308, 136236.
[14] Goodford, P.J., Hudson, A.T., Sheppey, G.C., Wootton, R., Black, M.H., Sutherland, G.J., Wickham, J.C., 1976. Physicochemical-activity relationships in asymmetrical analogues of methoxychlor. J Med Chem 19 (10), 1239–1247.
[15] IARC. (1972). Monographs on the Evaluation of the Carcinogenic Risk of Chemicals to Humans. ⟨https://monographs.iarc.who.int/monographs-available/⟩.
[16] West, P.R., Chaudhary, S.K., Branton, G.R., Mitchell, R.H., 1982. High performance liquid chromatographic analysis of impurities and degradation products of methoxychlor. J Assoc Anal Chem 65 (6), 1457–1470.
[17] Thiombane, M., Petrik, A., Di Bonito, M., Albanese, S., Zuzolo, D., Cicchella, D., Lima, A., Qu, C., Qi, S., De Vivo, B., 2018. Status, sources and contamination levels of organochlorine pesticide residues in urban and agricultural areas: a preliminary review in central–southern Italian soils. Environ Sci Pollut Res 25, 26361–26382.
[18] Verschueren, K., 2001. Handbook of environmental data on organic chemicals: Vol. 1, Issue Ed. 4. John Wiley and Sons, Inc.
[19] Karickhoff, S.W., Brown, D.S., Scott, T.A., 1979. Sorption of hydrophobic pollutants on natural sediments. Water Res 13 (3), 241–248.

[20] Oyekunle, J.A.O., Adegunwa, A.O., Ore, O.T., 2022. Distribution, source apportionment and health risk assessment of organochlorine pesticides in drinking groundwater. Chem Afr 5 (4), 1115–1125.
[21] Heim, S., Ricking, M., Schwarzbauer, J., Littke, R., 2005. Halogenated compounds in a dated sediment core of the Teltow canal, Berlin: time related sediment contamination. Chemosphere 61 (10), 1427–1438. https://doi.org/10.1016/j.chemosphere.2005.04.113.
[22] Elsner, M., Imfeld, G., 2016. Compound-specific isotope analysis (CSIA) of micropollutants in the environment – current developments and future challenges. Curr Opin Biotechnol 41 (Table 1), 60–72. https://doi.org/10.1016/j.copbio.2016.04.014.
[23] Hofstetter, T.B., Bakkour, R., Buchner, D., Eisenmann, H., Fischer, A., Gehre, M., Haderlein, S.B., Höhener, P., Hunkeler, D., Imfeld, G., 2024. Perspectives of compound-specific isotope analysis of organic contaminants for assessing environmental fate and managing chemical pollution. Nat Water 2 (1), 14–30.
[24] Höhener, P., Guers, D., Malleret, L., Boukaroum, O., Martin-Laurent, F., Masbou, J., Payraudeau, S., Imfeld, G., 2022. Multi-elemental compound-specific isotope analysis of pesticides for source identification and monitoring of degradation in soil: A review. Environ Chem Lett 20 (6), 3927–3942.
[25] Alvarez-Zaldívar, P., Payraudeau, S., Meite, F., Masbou, J., Imfeld, G., 2018. Pesticide degradation and export losses at the catchment scale: insights from compound-specific isotope analysis (CSIA). Water Res 139, 198–207. https://doi.org/10.1016/j.watres.2018.03.061.
[26] Gilevska, T., Payraudeau, S., Imfeld, G., 2023. Evaluating pesticide degradation in artificial wetlands with compound specific isotope analysis: a case study with the fungicide dimethomorph. Sci Total Environ 900, 165767.
[27] Guo, Z., Gao, X., Wang, C., Liu, S., Xu, C., Mao, S., Sun, X., Niu, L., Liu, W., 2024. Isomer, enantiomer and compound-specific stable isotope evidences for the transformation of dichlorodiphenyltrichloroethanes (DDTs) in soils from three typical paddy fields in China. J Hazard Mater 476, 135233.
[28] Liu, Y., Bashir, S., Stollberg, R., Trabitzsch, R., Weiß, H., Paschke, H., Nijenhuis, I., Richnow, H.H., 2017. Compound specific and enantioselective stable isotope analysis as tools to monitor transformation of hexachlorocyclohexane (HCH) in a complex aquifer system. Environ Sci Technol 51 (16), 8909–8916. https://doi.org/10.1021/acs.est.6b05632.
[29] Melsbach, A., Torrentó, C., Ponsin, V., Bolotin, J., Lachat, L., Prasuhn, V., Hofstetter, T.B., Hunkeler, D., Elsner, M., 2020. Dual-element isotope analysis of desphenylchloridazon to investigate its environmental fate in a systematic field study: a long-term lysimeter experiment. Environ Sci Technol 54 (7), 3929–3939. https://doi.org/10.1021/acs.est.9b04606.
[30] Bakkour, R., Wabnitz, C., Glöckler, D., 2024. Lack of selectivity in sample preparation-an achilles heel of compound-specific isotope analysis for environmental micropollutants. TrAC Trends Anal Chem, 117908.
[31] Blessing, M., Baran, N., 2022. A review on environmental isotope analysis of aquatic micropollutants: Recent advances, pitfalls and perspectives. TrAC Trends Anal Chem, 116730.
[32] Jin, B., Rolle, M., 2016. Joint interpretation of enantiomer and stable isotope fractionation for chiral pesticides degradation. Water Res 105, 178–186. https://doi.org/10.1016/j.watres.2016.08.057.
[33] Williams, G.M., Harrison, I., Carlick, C.A., Crowley, O., 2003. Changes in enantiomeric fraction as evidence of natural attenuation of mecoprop in a limestone aquifer. J Contam Hydrol 64 (3), 253–267. https://doi.org/10.1016/S0169-7722(02)00206-1.
[34] Badea, S. L., Danet, A., 2015. Enantioselective stable isotope analysis (ESIA) — a new concept to evaluate the environmental fate of chiral organic contaminants. Sci Total Environ 514, 459–466. https://doi.org/10.1016/j.scitotenv.2015.01.082.
[35] Masbou, J., Meite, F., Guyot, B., Imfeld, G., 2018. Enantiomer specific stable carbon isotope analysis (ESIA) to evaluate degradation of the chiral fungicide Metalaxyl in soils. J Hazard Mater 353 (March), 99–107. https://doi.org/10.1016/j.jhazmat.2018.03.047.
[36] Badea, S.-L., Vogt, C., Gehre, M., Fischer, A., Danet, A., Richnow, H., 2011. Development of an enantiomer specific stable carbon isotope analysis (ESIA) method for assessing the fate of α-hexachlorocyclo-hexane in the environment. Rapid Commun Mass Spectrom 25 (10), 1363–1372.
[37] Niu, L., Xu, C., Zhu, S., Bao, H., Xu, Y., Li, H., Zhang, Z., Zhang, X., Qiu, J., Liu, W., 2016. Enantiomer signature and carbon isotope evidence for the migration and transformation of DDTs in arable soils across China. Sci Rep 6 (December), 1–10. https://doi.org/10.1038/srep38475.
[38] Jammer, S., Voloshenko, A., Gelman, F., Lev, O., 2014. Chiral and isotope analyses for assessing the degradation of organic contaminants in the environment: Rayleigh dependence. Environ Sci Technol 48 (6), 3310–3318.
[39] Masbou, J., Payraudeau, S., Guyot, B., Imfeld, G., 2023. Dimethomorph degradation in vineyards examined by isomeric and isotopic fractionation. Chemosphere 313, 137341.
[40] Ricking, M., Schwarzbauer, J., 2012. DDT isomers and metabolites in the environment: an overview. Environ Chem Lett 10, 317–323.
[41] Vinyes-Nadal, M., Masbou, J., Kümmel, S., Gehre, M., Imfeld, G., Otero, N., Torrentó, C., 2024. Novel extraction methods and compound-specific isotope analysis of methoxychlor in environmental water and aquifer slurry samples. Sci Total Environ 931 (March). https://doi.org/10.1016/j.scitotenv.2024.172858.
[42] Vinyes-Nadal, M., Kümmel, S., Espín, Y., Gómez-Alday, J.J., Gehre, M., Otero, N., Torrentó, C., 2024. Dual C and Cl compound-specific isotope analysis and metagenomic insights into the degradation of the pesticide methoxychlor. J Hazard Mater, 135929.
[43] Palau, J., Marchesi, M., Chambon, J.C.C., Aravena, R., Canals, À., Binning, P.J., Bjerg, P.L., Otero, N., Soler, A., 2014. Multi-isotope (carbon and chlorine) analysis for fingerprinting and site characterization at a fractured bedrock aquifer contaminated by chlorinated ethenes. Sci Total Environ 475, 61–70. https://doi.org/10.1016/j.scitotenv.2013.12.059.
[44] Rodríguez-Fernández, D., Torrentó, C., Palau, J., Marchesi, M., Soler, A., Hunkeler, D., Domènech, C., Rosell, M., 2018. Unravelling long-term source removal effects and chlorinated methanes natural attenuation processes by C and Cl stable isotopic patterns at a complex field site. Sci Total Environ 645, 286–296. https://doi.org/10.1016/j.scitotenv.2018.07.130.
[45] Torrentó, C., Audí-Miró, C., Bordeleau, G., Marchesi, M., Rosell, M., Otero, N., Soler, A., 2014. The use of alkaline hydrolysis as a novel strategy for chloroform remediation: the feasibility of using construction wastes and evaluation of carbon isotopic fractionation. Environ Sci Technol 48 (3), 1869–1877. https://doi.org/10.1021/es403838t.
[46] Espinola, R., & Ben, L. (2007). Study of soil pollution in a site impacted by industrial activities at the municipality of Òdena, Catalonia (Spain).
[47] Thullner, M., Centler, F., Richnow, H.H., Fischer, A., 2012. Quantification of organic pollutant degradation in contaminated aquifers using compound specific stable isotope analysis–review of recent developments. Org Geochem 42 (12), 1440–1460.
[48] Ojeda, A.S., Phillips, E., Mancini, S.A., Lollar, B.S., 2019. Sources of uncertainty in biotransformation mechanistic interpretations and remediation studies using CSIA. Anal Chem 91 (14), 9147–9153.
[49] Lewis, K.A., Tzilivakis, J., Warner, D.J., Green, A., 2016. An international database for pesticide risk assessments and management. Hum Ecol Risk Assess: Int. J 22 (4), 1050–1064.
[50] Satsuma, K., Masuda, M., 2012. Reductive dechlorination of methoxychlor by bacterial species of environmental origin: evidence for primary biodegradation of methoxychlor in submerged environments. J Agric Food Chem 60 (8), 2018–2023. https://doi.org/10.1021/jf2048614.
[51] Arenas, M., Martín, J., Santos, J.L., Aparicio, I., Alonso, E., 2022. Enantioselective behavior of environmental chiral pollutants: a comprehensive review. Crit Rev Environ Sci Technol 52 (17), 2995–3034.
[52] Bidleman, T.F., Leone, A.D., Falconer, R.L., Harner, T., Jantunen, L.M.M., Wiberg, K., Helm, P.A., Diamond, M.L., Loo, B., 2002. Chiral pesticides in soil and water and exchange with the atmosphere. Sci World J 2 (1), 357–373.
[53] Kucher, S., Ricking, M., Schwarzbauer, J., 2019. The effect of environmental processes on the isomeric composition of DDT related compounds. Soil Sediment Contam: Int J 28 (3), 229–244.
[54] Gavezzotti, A., 1995. Molecular symmetry, melting temperatures and melting enthalpies of substituted benzenes and naphthalenes. J Chem Soc Perkin Trans 2 (7), 1399–1404.
[55] Brown, R.J.C., Brown, R.F.C., 2000. Melting point and molecular symmetry. J. Chem Educ 77 (6), 724.
[56] Zitko, V., 2003. Chlorinated pesticides: aldrin, DDT, endrin, dieldrin, mirex. Persistent Org Pollut 47–90.
[57] Biggar, J.W., & Riggs, R.L. (1974). Apparent solubility of organochlorine insecticides in water at various temperatures.